

Large Contraction Conducting Polymer Molecular Actuators

by

Patrick A. T. Anquetil

Diplom Ingenieur Maschinenbau ETHZ (1998)
Eidgenössische Technische Hochschule Zurich (ETH Zurich)
(M.Sc. Mechanical Engineering, Swiss Federal Institute of Technology, Zurich)

Submitted to the Department of Mechanical Engineering
in Partial Fulfillment of the Requirements for the Degree of

Doctor of Philosophy in Mechanical Engineering

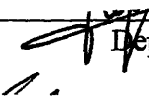
at the

MASSACHUSETTS INSTITUTE OF TECHNOLOGY


[February 2005]
OCTOBER 2004

© 2004 Massachusetts Institute of Technology
All rights reserved

Signature of Author _____

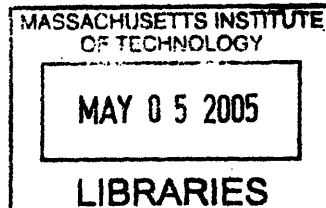

Department of Mechanical Engineering
October 8, 2004

Certified by _____


Ian W. Hunter
Professor of Mechanical Engineering and Biological Engineering
Thesis Supervisor

Accepted by _____


Lallit Anand
Chairman, Department Committee on Graduate Student



ARCHIVES

Large Contraction Conducting Polymer Molecular Actuators

by

Patrick A. T. Anquetil

Submitted to the Department of Mechanical Engineering
on October 8, 2004 in Partial Fulfillment of the
Requirements for the Degree of Doctor of Philosophy in
Mechanical Engineering

Abstract

The development of powerful and efficient artificial muscles that mimic Nature will profoundly affect engineering sciences including robotics and prosthetics, propulsion systems, and microelectromechanical systems (MEMS). Biological systems driven by muscle out-perform human-engineered systems in many key aspects. For example, muscle endows animals with a level of dexterity and speed that has yet to be emulated by even the most complex robotic system to date.

Conducting polymers were chosen for research as actuators, based on a review of the relevant properties of all known actuators and active materials. Key features of conducting polymer actuators include low drive voltages (1 - 2 V) and high active strength (10 – 40 MPa) but moderate active strains (2 %). Active strains of 20 %, which human skeletal muscle is capable of, are desirable for applications in life-like robotics, artificial prostheses or medical devices. This thesis focuses on two approaches to create large contraction in conducting polymer actuators.

The first strategy utilizes polypyrrole (PPy), a conducting polymer actuator material that contracts and expands based on a bulk ion swelling mechanism. Optimization of the polymer activation environment via room temperature ionic liquids enables PPy actuators to generate large contractions (16.3 % recoverable strain at 2.5 MPa, 21 % max) at slow speeds (0.4 %/s). In addition, cycle life can reach 10^5 cycles without significant polymer degradation. This thesis presents an in-depth characterization of the behavior of polypyrrole actuators in room temperature 1-butyl-3-methyl imidazolium tetrafluoroborate liquid salt electrolyte. The characterization includes the assessment of passive and electroactive mechanical properties as well as electrical and morphological properties.

Using Nature's actin-myosin molecular engine as a source of inspiration, the second approach uses molecular mechanisms to create motion. In this bottom-up approach molecules are rationally designed from the molecular level for specific actuation properties. Such active molecular building blocks include shape changing, load bearing, passively deformable or hinge-like molecular elements. Several novel materials based on contractile molecular design were synthesized and their active properties characterized.

Thesis Supervisor: Ian W. Hunter

Title: Hatsopoulos Professor of Mechanical Engineering and Biological Engineering

Acknowledgements

This thesis could not have been completed without the support of numerous individuals. Professor Ian Hunter has been an inspirational and resourceful advisor. He stimulated my passion for science and drew the best from me. I'll never forget that learning is a life-long process, and that one should take on a new field "from scratch" from time to time. I am extremely grateful to his kindness and the level of trust he entrusted me with during my later years in the laboratory as the leader of the conducting polymer subgroup. The BioInstrumentation Laboratory that Ian leads at MIT is composed of wonderful state-of-the-art resources, instruments and computer controlled manufacturing machines which made this thesis both enjoyable and an addiction to work on.

Great thanks also go to my exceptional thesis committee composed of Professor Timothy Swager (MIT Chemistry) and Dr. Shuguang Zhang (MIT Center for BioEngineering). Their time and attention allowed me to extend the scope of this work. Tim introduced me to chemistry and to molecular design. Shuguang's passion for looking at Nature as a source of inspiration was quite contagious.

I am extremely grateful to all the members of the conducting polymer subgroup at the MIT BioInstrumentation Laboratory, both former and present. The Madden brothers: John and Peter, have been a source of great support and offered me their friendship when I joined the lab. John originally inspired part of this work and motivated me to explore the exciting new field of conducting polymers. Peter Madden always had a patient way to answer all my questions and to offer great advice. Both allowed me to grow and to take on their legacy as their work in the lab drew to an end. I enjoyed a great connection with Nate Vandesteeg. His passion for what he does is tremendous, be it the "problem of the polymer excluded volume" or how to improve your Golf swing. Rachel Pytel was my first summer student and I am thrilled that we could attract her to continue her work in our laboratory. Special Thanks also go to S. Naomi Davidson and Bryan Schmid who both dared to move into a field away from ordinary mechanical engineering. I tremendously enjoyed helping them make their mark in the conducting polymer work and thinking how we could commercialize this technology. Finally I would like to thank all the UROPS, senior thesis students and summer students who helped me carry the work presented in this thesis: Derek Rinderknecht, Terry Gaige, Angela Chen, Nicaulas Powley, and Marie-Eve Aubin.

A great thanks goes to all members of the Bioinstrumentation Lab, especially to Dr. Colin Brenan for showing me "the ropes" when I first came to MIT in the spring of 1999 and for (re)shaping part of my scientific thought process. Dr. Tanya Kanigan showed me how to manage the chemistry area. Finally I learned from Dr. Serge Lafontaine how one can quickly and efficiently assemble a scientific instrument to perform key experimental measurements.

Very warm memories go to Bryan Crane, Steve Buerger, Max Berniker, Keng Lim, and Luke Sovsowski. The six of us would spend long nights "in desk formation" in the lab's mezzanine working on problem sets. The collegiality of this group made the initial years at MIT a joyful experience.

I also would like to take an opportunity to thank my professors from my undergraduate years for shaping my mind as a young scientist. Professor Rudolf Kalman, and Professor Mahir Sayir of the ETH Zurich as well as Professor Tomomasa Sato of the University of Tokyo have all helped me become the scientist I am today.

Dear thanks go to my fiancée Nitasha Manchanda for her unconditional love, support, companionship and delicious cooking. Her calm and up beat personality made it a delight being home, especially during the last weeks of writing the present thesis.

Finally very warm and special thanks go to both my parents for giving me the opportunity to pursue all my dreams outside of France. Their support allowed me to study in Switzerland (ETH Zurich), Japan (University of Tokyo) and in the USA (MIT).

This manuscript was extensively corrected by Peter Madden and Nitasha Manchanda who spent many hours of their personal time making sure that this work was not misspelled.

Contents

CHAPTER 1	INTRODUCTION.....	1
1.1	MUSCLE LIKE ACTIVE MATERIALS	2
1.2	PROBLEM STATEMENT.....	6
1.2.1	<i>Top-down Approach: PPy System Optimization.....</i>	7
1.2.2	<i>Bottom-Up Approach: Molecular Mechanisms</i>	10
1.3	THESIS OBJECTIVES AND TARGET SPECIFICATIONS	13
1.4	STRUCTURE OF THE THESIS	14
1.5	REFERENCES	16
CHAPTER 2	MOLECULAR ACTUATION IN NATURE AND SYNTHETIC SYSTEMS BASED ON CONDUCTING POLYMERS	18
2.1	INTRODUCTION.....	18
2.2	BIOLOGICAL MOLECULAR ACTUATORS	19
2.2.1	<i>Linear motion.....</i>	19
2.2.2	<i>Rotation.....</i>	23
2.2.3	<i>Other mechanisms.....</i>	26
2.2.4	<i>Nature’s Energy Source and Methods of Manufacturing</i>	28
2.3	DE NOVO SYNTHETIC MOLECULAR ACTUATORS.....	29
2.3.1	<i>Shape-changing backbone single molecule actuators</i>	30
2.3.2	<i>Supramolecular actuator systems</i>	32
2.3.3	<i>Systems Adapted from Biology.....</i>	35

2.4	MOLECULAR ACTUATORS DEVELOPED WITHIN THIS THESIS	38
2.4.1	<i>Design principles for molecular actuators</i>	38
2.4.2	<i>π-stacked single molecule actuators</i>	39
2.4.3	<i>Shape-changing backbone single molecule actuators</i>	42
2.5	SUMMARY AND CONCLUSION ON MOLECULAR ACTUATION	45
2.6	REFERENCES	48
CHAPTER 3	THEORY OF CONDUCTING POLYMER ACTUATORS.....	51
3.1	CONDUCTING POLYMERS	51
3.1.1	<i>Structure and Conductivity</i>	51
3.1.2	<i>The doping process</i>	54
3.2	PROPERTIES OF CONDUCTING POLYMERS	56
3.3	THEORETICAL EVALUATION OF CONDUCTING POLYMER ACTUATORS.....	59
3.3.1	<i>Limit in Strain Rate (Speed): Polymer Capacitance</i>	59
3.3.2	<i>Limit in Strain</i>	65
3.3.3	<i>Stored Energy Density and Efficiency</i>	66
3.4	ANALYSIS OF POLY(CALIX[4]ARENE BIS-BITHIOPHENE) AS AN ACTUATOR	68
3.4.1	<i>π-π Dimerization as Molecular Actuation Driving Force</i>	68
3.4.2	<i>Theoretical Performance Analysis of Poly(calixBBT)</i>	73
3.5	CONCLUSION.....	75
3.6	REFERENCES	76
CHAPTER 4	EXPERIMENTAL METHODS FOR POLYMER CHARACTERIZATION	78
4.1	METHODOLOGY	78
4.2	ELECTROCHEMICAL SYNTHESIS METHODS	81
4.2.1	<i>Electrochemical Cells</i>	81
4.2.2	<i>Electrochemical Characterization: Potential Sweep - Cyclic Voltammetry (CV)</i>	84
4.2.3	<i>Electrochemical Synthesis</i>	85
4.2.4	<i>In Situ Conductivity Measurement via Interdigitated Microelectrode</i>	87
4.2.5	<i>In situ EPR (Electron Paramagnetic Resonance) Experiment</i>	89
4.3	PARALLEL SYNTHESIS AND COMBINATORIAL TECHNIQUES.....	92
4.4	CHARACTERIZATION METHODS	95
4.4.1	<i>Bulk Conductivity Measurements</i>	95
4.4.2	<i>Electrochemical Quartz Crystal Microbalance (EQCM)</i>	96
4.4.3	<i>Passive mechanical testing; PE DMA 7e</i>	98

4.4.4	<i>Active mechanical testing: Construction of an electrochemical dynamic mechanical analyzer</i>	99
4.4.5	<i>Temperature Characterization: Thermal / Infrared Camera</i>	103
4.5	CONCLUSION	103
4.6	REFERENCES	104

CHAPTER 5 ELECTROCHEMICAL SYNTHESIS OF POLYPYRROLE ACTUATOR FILMS
..... 105

5.1	ELECTRODEPOSITION SYNTHESIS PROCESS	105
5.2	SYNTHESIS OF HIGH QUALITY CONDUCTING POLYMER FILMS	109
5.2.1	<i>Overview</i>	109
5.2.2	<i>Synthesis Results</i>	113
5.3	MASS PRODUCTION: CONTINUOUS DEPOSITION AND FIBER DEPOSITION	118
5.3.1	<i>Continuous Deposition</i>	119
5.3.2	<i>Continuous Fiber Production</i>	121
5.4	DISCUSSION OF RESULTS AND CONCLUSIONS	124
5.5	REFERENCES	124

CHAPTER 6 THERMAL TREATMENT OF POLYPYRROLE ACTUATOR FILMS 126

6.1	OVERVIEW OF THE EXPERIMENTAL PROCEDURE	126
6.2	EXPERIMENTAL PROCEDURE	127
6.3	THERMAL RELAXATION IN ELECTROLYTE (0.05 M TEAP IN PC)	127
6.4	DYNAMIC MECHANICAL ANALYSIS OF THERMAL RELAXATION IN AIR	130
6.5	THERMAL RELAXATION IN VACUUM	132
6.5.1	<i>Effect on Film Mass and Electrical Properties</i>	132
6.5.2	<i>Effect on Mechanical Properties</i>	134
6.5.3	<i>Post Treatment Analysis: Exposure to 90 °C Cycles in a DMA in Air</i>	138
6.5.4	<i>Post Treatment Analysis: Expansion Due to Ion “Re-swelling”</i>	139
6.6	THERMAL PROPERTIES	143
6.6.1	<i>Destructive Heating of PPy</i>	143
6.6.2	<i>Specific Heat Capacity of PPy</i>	146
6.6.3	<i>Coefficient of Thermal Expansion</i>	146
6.7	CONCLUSION	148
6.8	REFERENCES	148

CHAPTER 7	EXPERIMENTAL CHARACTERIZATION OF POLYPYRROLE ACTUATORS IN IONIC LIQUIDS	149
7.1	IMIDAZOLIUM-BASED ROOM TEMPERATURE LIQUID SALTS.....	149
7.2	EXPERIMENTAL PROCEDURE.....	151
7.3	PASSIVE MECHANICAL PROPERTIES OF PPY IN IONIC LIQUIDS.....	151
7.4	ACTIVE LOW FREQUENCY ISOMETRIC ACTUATOR TESTING	155
7.4.1	<i>Overview</i>	155
7.4.2	<i>Long vs. short activation cycles</i>	157
7.4.3	<i>Effects of Load on Active Strain</i>	163
7.4.4	<i>Creep Effects during Activation in Ionic Liquids</i>	164
7.4.5	<i>Cycle Life</i>	167
7.5	CONCLUSION.....	170
7.6	REFERENCES	171
CHAPTER 8	SYNTHESIS AND CHARACTERIZATION OF POLY(CALIX[4]ARENE <i>BIS</i>- BITHIOPHENE) AND POLY(QUARTERTHIOPHENE)/S-PHE ACTUATORS	172
CHAPTER 9	NOVEL POLYMER ACTUATOR SYSTEMS BASED ON MOLECULAR ACTUATING BUILDING BLOCKS.....	196
9.1	POLY(THIANTHRENE <i>BIS</i> -BITHIOPHENE).....	196
9.2	POLY(PHENYLENE-EDOT)	199
9.3	POLY(VANADYL-EDOT).....	201
9.4	CONCLUSION.....	204
CHAPTER 10	CONCLUSIONS AND OUTLOOK	206
10.1	THESIS CONCLUSIONS	206
10.2	CHALLENGES AND FUTURE WORK.....	212
10.3	CONTRIBUTIONS TO KNOWLEDGE.....	214
10.3.1	<i>Conference Proceedings</i>	215
10.3.2	<i>Talks</i>	215
10.3.3	<i>Patents</i>	216
10.3.4	<i>Theses Co-Supervised</i>	217
10.3.5	<i>Press Coverage</i>	217
10.4	REFERENCES	218

APPENDIX A	NATURE'S ENERGY SOURCES AND METHODS OF MANUFACTURING	219
A.1	SOURCES OF ENERGY FOR NATURE'S MOLECULAR MOTORS	219
A.2	NATURE'S METHODS OF MANUFACTURING	221
A.3	REFERENCES	222
APPENDIX B	THEORETICAL PERFORMANCE ESTIMATION OF POLY(CALIX[4]ARENE BIS-BITHIOPHENE)	223
APPENDIX C	ILABNOTEBOOK: A DIGITAL LABORATORY NOTEBOOK.....	226
APPENDIX D	ELECTROCHEMICAL DEPOSITION CONTROL WITH A TABLET PC	233
APPENDIX E	CURRICULUM VITAE.....	236

Chapter 1

Introduction

The development of powerful and efficient artificial muscles that mimic Nature will profoundly affect engineering sciences including robotics and prosthetics, propulsion systems, and Microelectromechanical systems (MEMS). Biological systems driven by muscle out-perform human-engineered systems in many key aspects. For example, muscle endows animals with a level of dexterity and speed that has yet to be emulated by even the most complex robotic system to date.

Conducting polymers¹ were chosen for research as actuators, based on a review of the relevant properties of all known actuators and active materials [Hunter I.W. and Lafontaine S. 1992], [Madden J.D. et al. 2004]. Key features of conducting polymer actuators include low drive voltages and high strength. They undergo moderate dimensional changes and have high energy storage capacity. In addition to actuators, electronic components (transistors, capacitors, diodes, etc.) and sensors (force, displacement, chemical, optical) can also be made

¹ A polymer is a class of macromolecules consisting of regularly repeating building blocks called monomers joined together to form a chain molecule

from conducting polymer materials, thus offering for the first time the possibility to construct systems from the same material via a co-fabrication process².

The aim of this doctoral research work is to develop an artificial actuator that matches or exceeds the performance of mammalian skeletal muscle in key figures of merit, including strain, stress, stiffness, strain rate, power to mass, and efficiency. The actuator is to be electrically powered and low in cost.

The strategy employed to achieve these goals is to optimize actuator performance through molecular design and system optimization. At the core of this approach lies the principle that achievable actuator strain can be increased by designing polymers that undergo large deformations along their backbone upon oxidation and reduction. This approach is implemented by a research feedback-loop methodology where design and synthesis of novel monomers and polymers is followed by rigorous mechanical, electrochemical, spectroscopic and structural investigations which directly feed back into the next generation of molecular design leading to novel materials.

1.1 Muscle Like Active Materials

Human skeletal muscle exhibits combined performance characteristics of active strain, active stress, active strain rate, power to mass ratio and efficiency which man-made actuator technologies do not match [Hunter I.W. and Lafontaine S. 1992]. Yet the active stress developed by skeletal muscle is actually moderate (0.35 MPa). Several actuator technologies have emerged as possible candidates for artificial muscle technology. These include older engineering materials such as piezo-ceramics, giant magnetostrictive materials and shape memory alloys (SMA) as well as novel electroactive polymers (or so called EAPs). The EAP family of actuators includes gel polymers, ionic polymer metal composites (IPMC), electrostrictive polymer artificial muscle (EPAM), ferroelectric polymers, liquid crystal elastomers, and conducting polymers (CP).

² Co-fabrication, refers to a manufacturing process, where elements are not separately manufactured and then assembled together as is done in classical engineering, but rather *grown* from the same basic set of material building blocks [Madden P.G. 2003; Madden P.G. et al. 2001].

An ideal actuator combines the following characteristics: large stress, large dimensional changes (strain), high activation rate, large numbers of cycles, large power to mass ratios and energy densities, efficient energy conversion to mechanical energy, electrical control and low activation voltages. In the following paragraphs we briefly present some current active materials. An up to date in depth review of all actuator technologies is given by Madden and colleagues [Madden J.D. and others 2004].

Piezoelectric ceramic materials change dimensions upon incorporation of charge into their crystal lattice. Typically large voltages are required to draw charges into the material, producing small strains (0.1 %/kV). On the other hand, these materials produce large stresses (>100 MPa) at high frequencies above hundreds of kilohertz. Similarly **giant magnetostrictive materials** offer little strain capability (0.1 %/T) but fast switching. The limited strain of these two engineering materials coupled with their high rigidity limits their use as artificial muscles.

Shape Memory Alloys such as Nickel-Titanium (NiTi - better known as Nitinol) use a thermally activated austenite-martensite transition to generate work [Buehler W.J. et al. 1963], [Funakubo H. (ed.) 1987]. Because of their gigantic stress generating capabilities (200 MPa), fast strain rates (300 %/s), moderate strains (5 %), reasonable cost and an electrical resistivity that easily lends itself to Joule heating (passing of an electrical current to generate heat), SMAs were viewed as the ideal actuator material [Hunter I.W. et al. 1991], [Hunter et al. 1990]. However their poor efficiency due to thermal activation (0.1 %) and the difficulty of controlling their length has limited their use to date.

Gel actuators are based on the work of Tanaka from MIT [Tanaka T. 1978], where gels undergo large volume changes when the solvent concentration is changed. A polymer such as polyacrylamide is processed into a gel when diluted in a mixture of solvent such as acetone and water, collapses when exposed to addition of extra acetone. The resulting sudden material volume change can be as high as 1000 times. The initial polymer network swelling is due to charges (ions) separating from the polymer backbone creating a net osmotic pressure on the whole network. Acetone acting as a bad solvent dramatically reduces this ionic interaction. Other triggering stimuli include tiny changes in temperature and light. While the strains in these actuators are gigantic, these materials produce weak forces and are difficult to control. However, as the collapse of polymer network is so

sensitive to the presence of small charges in the environment they may prove useful as sensors.

Ionic Polymer Matrix Composite (IPMC) made from sandwiching a thin layer of polymeric electrolyte between two metal electrodes produces large strains in a bending configuration, while offering limited force generation. For example a typical, 20 mm long, 5 mm wide and 200 μm thick IPMC actuator can bend over an angle of 180° but only produces 15 mN of force [Shahinpoor M. and Kim K.J.]. At the heart of the actuation mechanism of IPMC actuators is the shuttling of ions from one electrode to another upon application of an electric field between the electrodes.

Electrostrictive Polymer Artificial Muscle (EPAM) elastomer films expand and contract when a large voltage is applied to the material via large electrodes placed on its surfaces. As the volume of the material remains constant, electrostatic forces pulls (or pushes) the electrodes together (or apart), thus inducing expansion of the material in the perpendicular direction. While EPAMs offer impressive active properties such as peak strains of 215 %, stresses of 2.4 MPa and responses up to 1 kHz, they are mainly limited by the large voltages that need to be applied to the material (10 to 100 kV), making these materials impractical for many applications (lightweight actuation, medical devices, etc.) [Pelrine R. et al. 2000].

Liquid crystal elastomers have a mechanism of actuation that is based on a thermal phase transition occurring in liquid crystals. In this particular case, the liquid crystals are attached to an elastomeric matrix, thus forming a compliant material. The best performances achieved by this actuation technology are strains up to 40%, stresses of 140 kPa and response times as high as 1 to 13 Hz [Brand H.R. 1989], [Thomsen D.L. et al. 2001], [Camacho-Lopez M. et al. 2004]. Similar to polymer gels and IPMC, liquid crystal elastomers offer large strains but only produce 1/3 of the force per cross-section that is achieved by human skeletal muscle.

Ferroelectric polymers attempt to reduce the amount of voltage needed for actuation in electrostrictive material by clever design of high dielectric constant material additives. Advances made by Zhang [Zhang Q. et al. 2002] led to activation voltages below 1 kV. Resulting strains are up to 5% at stresses as high as 45 MPa and responses up to 100 kHz.

Zhang's novel approach is promising as it attempts to understand the fundamental limits of the active material and to correct shortcomings starting at the molecular level.

Finally **Conducting Polymers**, a class of materials first developed as synthetic metals by Shirakawa, Heeger and MacDiarmid, offer a high degree of freedom for the construction of novel, active materials similar to Nature's proteins. Applications for these materials not only include artificial muscles but also sensors (strain, light, chemical, etc.), logic & computation, energy storage, wires for information delivery or energy delivery. A whole artificial biomimetic system could be constructed from this whole class of materials. The importance of this research was recognized by the Nobel Committee in 2000 and Shirakawa, Heeger and MacDiarmid were awarded the Nobel Prize in Chemistry for their discovery of Conducting Polymer materials [Nobel 2000].

In 1991, Baughman proposed the use of Conducting Polymers as artificial muscles [Baughman R.H. et al. 1991], while Marque and Roncali recognized that mechanical energy could be produced by these polymers upon electrochemical oxidation and reduction in 1990 [Marque P. and Roncali J. 1990]. The class of materials based on conducting polymers is very large. Similar to proteins³, new materials can be built by association of building blocks. To date only a very small number of conducting polymers have been synthesized out of this large class of materials. A few of them are commercially available. These include variations of polyaniline, polypyrrole (PPY), polyEDOT and poly(p-phenylenevinylenes). Polypyrrole and polyaniline have been the most successful for artificial muscle applications. Polypyrrole-based actuators, for example, generate forces per cross-sectional area that are up to two orders of magnitude greater than human muscle (40 MPa) with comparable power to mass ratios (150 W/kg), using low actuation voltages (~ 1 V). However the use of this first-generation conducting polymer in devices and applications is mainly limited by their moderate active strain (1 – 2 %) and active strain rate (1 %/s) [Madden J.D. et al. 2001].

³ Proteins are Nature's bricks for building all living systems. Each protein in Nature's organisms (from trees to humans) is made from a set of 20 amino acid building blocks. These blocks are combined into a linear chain and upon completion, fold into a 3D structure based on the molecular forces due to interactions between the amino acids and their environment. To see the power of such a building technique, imagine a chain of 50 amino acids (a very short protein also called peptide). To build this chain there would be about 20^{50} possibilities. There is a possibility that conducting polymers upon combination could offer similar huge degrees of freedom.

Table 1.1 summarizes the properties of 2002 polypyrrole synthesized at MIT's BioInstrumentation Laboratory and compares them with mammalian skeletal muscle.

Properties	Mammalian skeletal muscle [Hunter I.W. and Lafontaine S. 1992]	2002 Polypyrrole [Madden J.D. et al. 2002]
Displacement (Strain)	20 %	1 – 2 % (7 % irreversible)
Active Stress (Load)	0.35 MPa	40 MPa
Velocity (Strain Rate)	>100 %/s	3 %/s
Power to mass	50 –100 W/kg	150 W/kg
Efficiency	30-35 %	1 % (18 % with energy recovery scheme)
Cycle Life	>10 ⁹	10 ⁵ (at 0.3 % displacement)

Table 1.1: Comparison of mammalian skeletal muscle with 2002 Polypyrrole. Note how poorly polypyrrole performs in the amount of strain it is capable of generating compared to skeletal muscle.

1.2 Problem statement

While conducting polymers offer muscle-like properties that are very desirable for the construction of actuators, they are unable to produce strains on the order of 20 % and strain-rates of 100 %/s achieved by human skeletal muscle (Table 1.1). Large strain generation at high speed and high stresses is a desirable characteristic for applications in life-like robotics, artificial prostheses or medical devices. Note that stresses greater than mammalian muscle are also an important feature and that most actuator technologies presented in Section 1.1 have that characteristic. Consider an exoskeleton application of polypyrrole, where the

actuator's role is to enable an old person to lift a large weight. If the amount of stress⁴ is 100 times larger than muscle then only 1/100th of the active cross-sectional area is needed to generate the same amount of force. It is then conceivable that an elderly person could wear a lightweight suit made of this material to assist her in her daily tasks.

There are two approaches to achieve the ambitious goal of creating a muscle-like actuator capable of generating large strains. First, the top down approach is to optimize current conducting polymer technology such as polypyrrole, where different parts of the system such as the electrolyte or the material microstructure show great room for improvements. The second, bottom-up approach, consists of designing the artificial muscle from the molecular level up, where force and displacement generation comes from chemically engineered molecule units changing shape upon the application of an electrical stimulus. Hence the designation for this new class of materials: "Conducting Polymer **Molecular** Actuators"

1.2.1 Top-down Approach: PPy System Optimization

Polypyrrole (PPy) is a mature conducting polymer-based actuator technology that is already at a state where the material itself can be repeatedly synthesized into a mechanically robust and electrically active film. In the quest of large contraction actuators it is sensible to also build a strategy where lessons can be learned from materials already in an "actuator-ready" state. Polypyrrole actuators are electrochemical systems composed of different parts such as the active material and its molecular and microstructure, an electrolyte onto which the contractile material is placed, and a counter electrode that closes the electrochemical circuit. All these different parameters are currently not optimized for large actuation. Conducting research on polypyrrole materials allows one to directly test the effect of varying these system parameters on a material that is already existing and in a stable form instead of waiting for a new material to be developed.

Actuation in *traditional* conducting polymers such as polypyrrole or polyanilines is based on the reversible diffusion and intercalation of ions into the polymer bulk film upon

⁴ Stress is defined as the amount of force per cross-sectional area

electrochemical oxidation [Baughman R.H. and others 1991]. This ionic intercalation process arises to maintain electro-neutrality during the oxidation process, leading to bulk volume changes (Figure 1.1). Accommodation of these ions and their associated solvated species is favored by the weak polymer interchain interactions and limited by the high modulus along each polymer molecular backbone [Baughman R. H. 1996]. As a result strains on the order of 2 % are produced upon electroactivation.

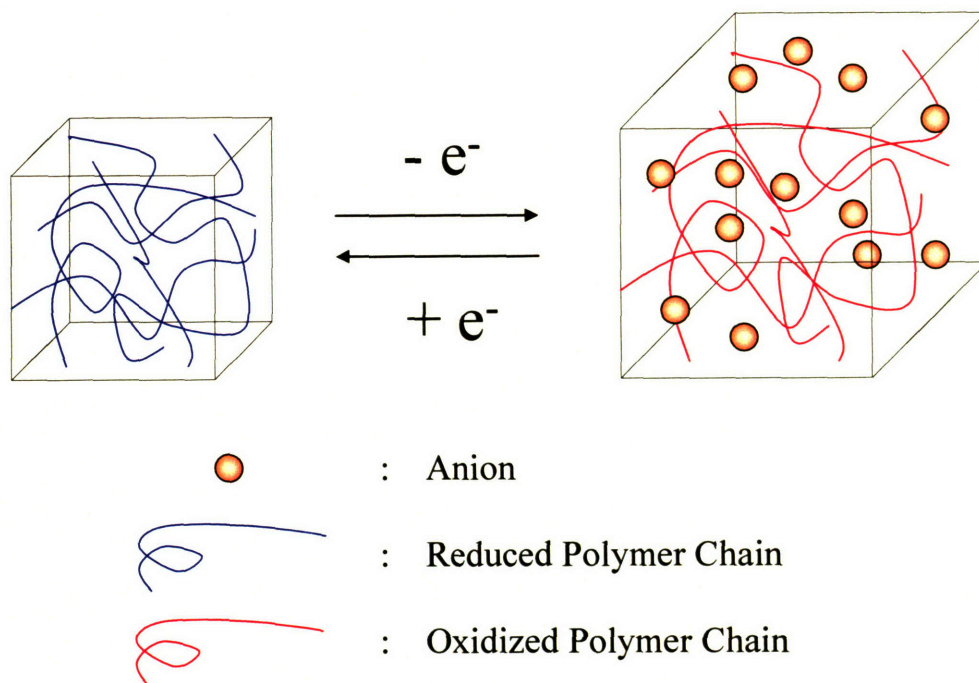


Figure 1.1: Schematic illustration of the actuation mechanism in classical conducting polymer actuators. To maintain charge neutrality, ions flow in and out of the conducting polymer bulk upon oxidation and reduction.

The ion swelling mechanism is triggered by changing the oxidation state of the material. This can be done by various types of stimuli: optical, chemical and electrochemical. As we desired to control these materials with a voltage or a current, this thesis will only focus on electrochemical means of actuation. To activate PPy in an electrochemical cell, both an electrolyte and a counter electrode are needed to close the electrical circuit (Figure 1.2). Typically a solution of propylene carbonate (PC) containing 0.1 M tetraethylammonium

hexafluorophosphate (TEAP) ions is used as electrolyte. Hexafluorophosphate ions (PF_6^-) are then moved in and out of the material upon electroactivation.

As the electrolyte is both the environment within which the active material is constantly in contact as well as the source of ions for actuation, its crucial role for electroactivation becomes obvious. A bad selection leads to poor active properties and even material degradation. A new class of electrolyte compatible with conjugated polymer systems has recently emerged as a possible improvement for classical conducting polymer based actuators. These electrolytes are room temperature ionic liquids, pioneered by Wallace and colleagues [Lu W. et al. 2002] on actuator systems. Early results have shown the great potential of these liquid salts to improve actuator performance. Key advantages come from their pure ionic nature which limits the exposure of the polymer to degrading agents upon electroactivation.

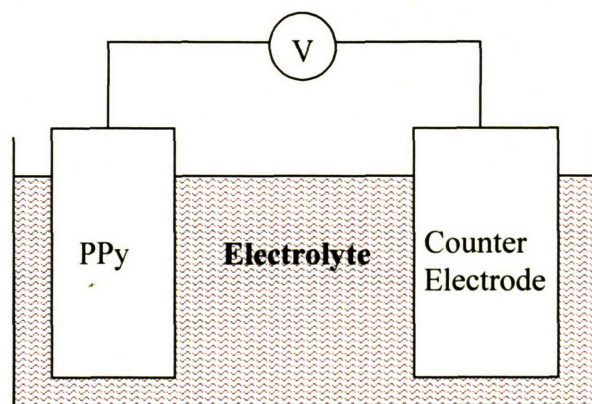


Figure 1.2: Electrochemical cell typically used to activate conductive polymer actuator materials.

Typical actuation limitations such as achievable strain, strain-rate and ultimately cycle degradation result from electrochemical material degradation due to the application of an excessively large potential to the material. The measure of actuator electrochemical robustness is assessed by the polymer potential window. For PPy in propylene carbonate, for example, the typical maximal potential applicable without degradation is about 0.4 V (versus the Ag/Ag^+ reference electrode). Using ionic liquids based on 1-butyl-3-methyl imidazolium cations allows extending the electrochemical potential of PPy up to 4.0 V [Lu W. and others

2002]. A system with a large potential window translates into faster actuator performance and enhanced cycle life. In addition maximum strain can be increased.

In this thesis we will present further advances where not only strain performance (up to 16.3 % - see Chapter 7) but also cycle life can be dramatically improved. Figure 1.3 shows schematically two room temperature ionic liquids that were used extensively in this thesis: 1-butyl 3-methyl imidazolium (BMIM) ionic liquids with hexafluorophosphate (PF_6^-) and BMIM with tetrafluoroborate counter ions (BF_4^-).

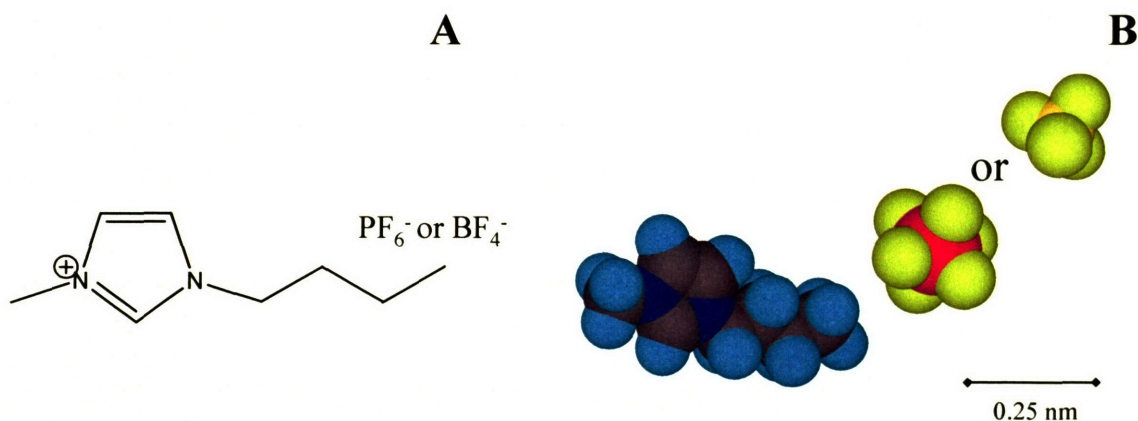


Figure 1.3: Schematic (A) and space filling structure (B) of 1-butyl 3-methyl imidazolium (BMIM) ionic liquids with hexafluorophosphate (PF_6^-) or tetrafluoroborate (BF_4^-) counter ions. Note that the BMIM moiety is about 2.7 times bigger than the PF_6^- counter ion.

1.2.2 Bottom-Up Approach: Molecular Mechanisms

As presented in the previous section, actuation in *traditional* conducting polymers is based on an ion swelling mechanism that is triggered by changing the oxidation state of the material. Accommodation of ions and their associated solvated species into the polymer is favored by the weak polymer interchain interactions but limited by the high modulus along each polymer molecular backbone [Baughman R. H. 1996]. As a result reversible strains are produced upon electroactivation. It is conceivable that ultimately the maximum strain achievable in these “classical” conducting polymer actuators is going to be limited by the inability of the polymer molecular backbone to significantly change length to accommodate further ions.

On the other hand Nature has solved the actuation problem by using a whole variety of molecular motors, ratchets and proteins exhibiting reversible transitions at the molecular level. These protein-based molecular machines are mostly powered by ATP but also by other energy sources such as light or pH gradients [Mao C. et al. 1999]. Interestingly, Nature's muscles are built using manufacturing based on bottom-up construction, co-fabrication, and self assembly. A beautiful example of such complex machinery is found in muscle cells, in which the sliding (walking) of myosin dimers along an actin protein guiding filament generates force and displacement (work) leading to muscle cell contraction. Energy is converted from ATP into protein motion using a molecular conformational change strategy, moving the actin filament by a 10 nm step increment (Figure 1.4) [Vale R.D. and Milligan R.A. 2000].

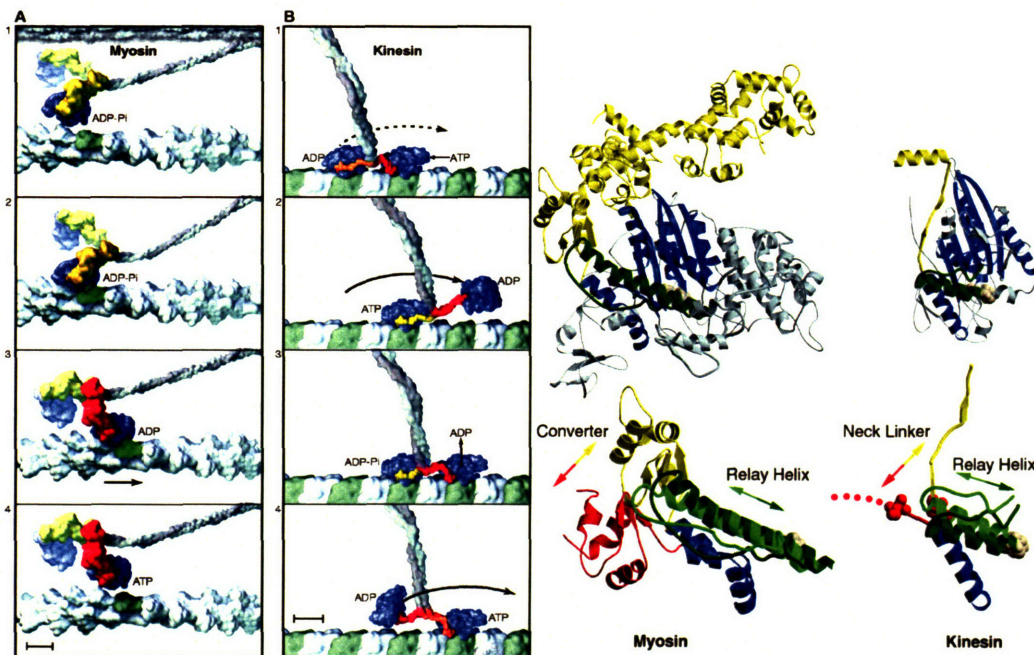


Figure 1.4: Mechanical model and protein structure of myosin and kinesin or microtubule. Both work from a similar principle where a motor protein (myosin or kinesin) “walks” onto an actin or microtubule filament protein [Vale R.D. and Milligan R.A. 2000].

Using Nature as a source of inspiration [Vale R.D. and Milligan R.A. 2000], [Mao C. and others 1999], [Mahadevan L. and Matsudaira P. 2000], a more powerful approach to design

synthetic contractile materials with muscle like characteristics is to incorporate chemically driven shape changing units in the conducting polymer molecular backbone. These building blocks are conceived to change conformation in response to electrically induced variation in oxidation state, leading to large volume changes. Advances in synthetic organic chemistry enable the design and synthesis of such molecules that mimic natural mechanisms. These include molecules that distort from bent to planar structures, materials that undergo volume changes due to stacking of redox units and molecular scaffolds that behave as “mechanical hinges” which, combined with the redox stackable units, creates accordion-like structures capable of being switched between an extended and a tightly folded molecular conformation (Figure 1.5).

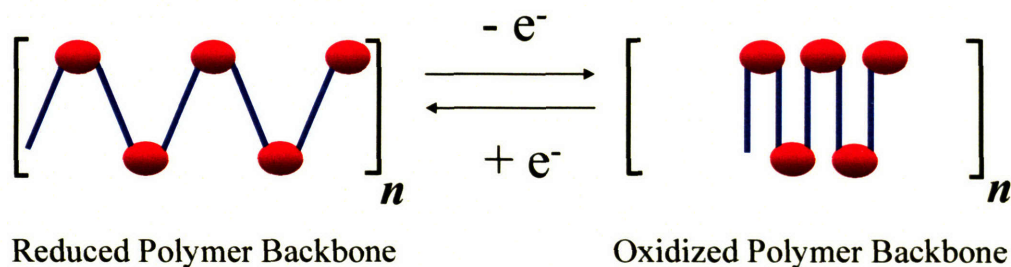


Figure 1.5: Schematic illustration of molecular actuation. Upon oxidation or reduction each polymer molecule changes shape, thus generating large contractions or expansions.

A material that can efficiently convert an applied external stimulus such as electrical current, light, or heat into mechanical work from the molecular level is highly desirable and presents a radical and exciting area of research. There are also many challenges that need to be overcome before one has a working molecular actuator material at hand from these molecular designs. First the molecule needs to be synthesized into a monomer form and then polymerized into a mechanically robust polymer film that has outstanding electromechanical properties. Each step involves a long and tedious screening and optimization process which this thesis intends to address. In this thesis, several molecules that possess the appropriate active properties are carefully selected, built into new materials and then characterized.

1.3 Thesis Objectives and Target specifications

The aim of this doctoral thesis is to develop large contraction actuators based on conducting polymers via optimization of polypyrrole-based actuator technology and to explore how incorporation of molecular contracting elements into a polymer can help achieve this goal. This novel actuator system should be capable of large strains on the order of 20 % at moderate strains (> 0.5 MPa).

The following specifications were selected as ambitious but realistic performance expectations for the new large contraction molecular actuator materials aimed at replacing “traditional” conducting polymer actuators. The targets presented in Table 1.2 are chosen as requirements to achieve muscle-like behavior from artificial actuators. Mammalian skeletal muscle performance as well as the 2002 version of the BioInstrumentation lab’s polypyrrole material are shown for evaluation purposes.

Properties	Mammalian skeletal muscle [Hunter I.W. and Lafontaine S. 1992]	2002 Polypyrrole [Madden J.D. and others 2002]	Target for Large Contraction Actuators
Displacement (Strain)	20 %	1 – 2 % (7 % irreversible)	15 - 20 %
Active Stress (Load)	0.35 MPa	40 MPa	0.5 MPa
Velocity (Strain Rate)	>100 %/s	3 %/s	20 %/s
Operating Voltage	-	1 – 5 V	1 – 5 V
Power to mass	50 –100 W/kg	150 W/kg (at 5 MPa)	50 W/kg
Conductivity	-	4.5×10^4 S/m	50 S/m
Cycle Life	$>10^9$	10^5 (at 0.3 % displacement)	10^5

Table 1.2: Targets set for large contractile muscle-like behavior with contractile polymer actuators.

The most important feature in achieving muscle-like actuation is to increase contractile strains to 15 - 20 % and maintain an achievable stress level greater than human skeletal muscle (0.5 MPa). No actuator technology exists that can combine these features at low activation voltage. Conducting polymers are activated by a voltage that is below 5 V; it is important to be able to retain this feature for incorporation in battery operated devices. Conductivity plays a crucial role in determining how efficiently these contractile materials can be activated (Chapter 3). Polypyrrole can achieve high conductivities 4.5×10^4 S/m for a conducting polymer. A conductivity of 50 S/m was set as a minimum to achieve moderate charge delivery into the novel materials. Finally life cycle is important for real applications. A cycle life of 10^5 cycles was set as a minimum, and is only two orders of magnitude less than muscle. Nature, however, uses a clever mechanism of constantly replacing the components of the human body. Muscle cells are thus continuously regenerated [Alberts B. et al. 1994]. Assuming a contraction rate of 1 Hz and a cell replacement rate of 3 month for complete muscle overhaul, the actual cycle life that muscle exhibits reduces to 10^7 cycles.

This thesis intends to study means to achieve higher contraction in conducting polymer actuators. A systematic protocol to synthesize and test the physical properties relevant to actuation of novel materials is established. As a result, for the first time, novel functional materials rationally designed at the molecular level are synthesized and characterized.

1.4 Structure of the Thesis

The thesis focuses on three main themes: instrumentation, optimization of PPy-based actuators and finally on the discovery of novel actuator systems based on molecular actuating units.

Chapter 2 gives an overview of molecular actuators found in nature and intends to go beyond the scope of this thesis to trigger the imagination to think of things possible but not yet exploited by mankind. The Chapter ends with an overview of current conducting polymer materials and the early attempt by various groups to design actuators with molecular contractile elements.

In **Chapter 3** theoretical limits of current actuators based on polypyrrole are evaluated and contrasted with performance projections of the novel molecular actuators. Models and

values for passive mechanical and electrical properties, active strain generation, energy storage and efficiency are presented.

Chapter 4 presents an overview of the techniques that were used in this thesis to study novel conducting polymer materials. These include electrochemical methods, conductivity measurement techniques, passive and active mechanical analysis as well as quartz crystal microbalance studies.

Chapter 5 is devoted to the synthesis of polypyrrole films. Optimal synthesis conditions are presented and analyzed. The importance of this Chapter is to understand what makes a good polymer film and what lessons can be transposed to the novel molecular-based active materials. The Chapter ends with two methods to move materials into a mass-production stage.

Chapter 6 focuses on the analysis of passive mechanical properties of polypyrrole films. These properties are reversibly modifiable depending on the solvent environment of the material and via thermal treatment. Thermal treatment is used to study the processing possibilities of PPy at the post-synthesis stage.

In **Chapter 7** the active performance enhancement properties of room-temperature ionic liquids are examined. Recoverable strains as high as 16.3 % in this electrolyte environment are presented and analyzed in terms of increased strain and cycle life.

Chapter 8 is devoted to the synthesis of poly(quarterthiophene) and poly(calix[4]arene bis-bithiophe), two novel active materials based on rational molecular design. The mechanism of contraction of this molecule is based on π - π dimer formation between quarterthiophene units. The active properties of composites of poly(quarterthiophene) polymers with a sulfated poly- β -hydroxy ether (S-PHE) are analyzed. The S-PHE serves as matrix to enhance the mechanical properties of poly(quarterthiophene).

Chapter 9 presents the synthesis and characterization of three other conducting polymer material candidates based on rational molecular design. These include:

- Butterfly-like molecules: poly(thianthrene);
- Transition metal-embedded materials: poly(VanadylEDOT);
- Twisting backbone molecules: poly(phenyleneEDOT);

Finally, conclusions and directions for future research are presented in **Chapter 10**.

1.5 References

- Alberts B. et al., "Molecular Biology of the Cell", 3rd ed. New York: Garland Publishing, (See Chapter 22): pp. 1139-1193, (1994).
- Baughman R. H. "Conducting Polymer Artificial Muscles", *Synthetic Metals*, Vol. 78, pp. 339-353, (1996).
- Baughman R.H., Shacklette S.W., Plichta E.J. and Becht C., "Electromechanical Actuators Based on Conducting Polymers", *Molecular Electronics*, pp. 267-289, (1991).
- Brand H.R., "Electromechanical Effects in Cholesteric and Chiral Smectic Liquid-Crystalline Elastomers ", *Makromolekulare Chemie*, Vol. 10, (9): pp. 441-445, (1989).
- Buehler W.J., Griffith J. and Wiley K., *Journal of Applied Physics*, Vol. 34, pp. 1465, (1963).
- Camacho-Lopez M., Finkelmann H., Palffy-Muhoray P. and Shelley M., "Fast Liquid-Crystal Elastomer Swims Into the Dark", *Nature Materials*, Vol. 3, pp. 307-310, (2004).
- Funakubo H. (ed.), "Shape Memory Alloys", *Gordon and Breach, New York*, (1987).
- Hunter I.W. and Lafontaine S., "A Comparison of Muscle with Artificial Actuators", *Technical Digest IEEE Solid State Sensors and Actuators Workshop*, pp. 178-185, (1992).
- Hunter I. W., Lafontaine S., Hollerbach J. M. and Hunter P. J., "Fast reversible NiTi fibers for use in microrobotics", *Proceedings IEEE Micro Electro Mechanical Systems*, Vol. 3, pp. 2156-2161, (1990).
- Hunter I.W., Lafontaine S., Hollerbach J.M. and Hunter P.J., "Fast Reversible NiTi Fibers For Use In MicroRobotics", *IEEE Symposium, Japan*, pp. 166-170, (1991).
- Lu W., Fadeev A.G., Qi B., Smela E., Mattes B.R., Ding J., Spinks G.M., Mazurkiewicz J., Zhou D., Wallace G.G., MacFarlane D.R., Forsyth S.A. and Forsyth M., "Use of Ionic Liquids for pi-Conjugated Polymer Electrochemical Devices", *Science*, Vol. 297, pp. 983-987, (2002).
- Madden J.D., Madden P.G. and Hunter I.W., "Polypyrrole Actuators: Modeling and Performance", *Smart Structures and Materials 2002: Electroactive Polymers Actuators and Devices, Yoseph Bar-Cohen, Editor, Proceedings of the SPIE*, (2001).
- Madden J.D., Madden P.G. and Hunter I.W., "Conducting Polymer Actuators As Engineering Materials", *Smart Structures and Materials 2002: Electroactive Polymers Actuators and Devices, Yoseph Bar-Cohen, Editor, Proceedings of the SPIE*, Vol. 4695, pp. 176-190, (2002).
- Madden J.D., Vandesteeg N., Anquetil P.A., Madden P.G., Takshi A., Pytel R., Lafontaine S.R., Wieringa P.A. and Hunter I.W., "Artificial Muscle Technology: Physical Principles and Naval Prospects", *to appear in IEEE Journal of Ocean Engineering*, (2004).
- Madden P.G., "Development and Modeling of Conducting Polymer Actuators and the Fabrication of a Conducting Polymer Based Feedback Loop", *MIT Ph.D. Thesis*, (2003).
- Madden P.G., Madden J.D., Anquetil P.A., Yu H.-h., Swager T.M. and Hunter I.W., "Conducting Polymers as Building Blocks For Biomimetic Systems", *Proceedings of the 2001 Symposium on Unmanned Untethered Submersible Technology (UUST'01)*, (2001).
- Mahadevan L. and Matsudaira P., "Mobility Powered by Supramolecular Springs and Ratchets", *Science*, Vol. 288, pp. 95-99, (2000).
- Mao C., Sun W., Shen Z. and Seeman N., "A Nanomechanical Device Based on B-Z Transition of DNA", *Nature*, Vol. 397, pp. 144-146, (1999).

Marque P. and Roncali J., "Structural Effect on the Redox Thermodynamics of Poly(thiophenes)", *Journal of Physical Chemistry*, Vol. 94, pp. 8614-8617, (1990).

Nobel 2000, <http://nobelprize.org/chemistry/laureates/2000/>

Pelrine R., Kornbluh R., Pei Q. and Joseph J., "High-Speed Electrically Actuated Elastomers with Strains Greater than 100%", *Science*, Vol. 287, pp. 846-839, (2000).

Shahinpoor M. and Kim K.J., "Ionic Polymer-Metal Composites: I. Fundamentals", *Smart Structures and Materials 2001: Electroactive Polymers Actuators and Devices*, Yoseph Bar-Cohen, Editor, *Proceedings of the SPIE*,

Tanaka T., "Collapse of Gels and the Critical Endpoint", *Physical Review Letters*, Vol. 40, (12): pp. 820-823, (1978).

Thomsen D.L., Keller P., Naciri J., Pink R., Jeon H., Shenoy D. and Ratna B.R., "Liquid Crystal Elastomers with Mechanical Properties of a Muscle", *Macromolecules*, Vol. 34, (17): pp. 5868-5875, (2001).

Vale R.D. and Milligan R.A., "The Way Things Move: Looking Under the Hood of Molecular Motor Proteins", *Science*, Vol. 288, pp. 88-95, (2000).

Zhang Q., Li H., Poh M., Xia F., Cheng Z.-Y., Xu H. and Huang C., "An All-Organic Composite Actuator with a High Dielectric Constant", *Nature*, Vol. 416, pp. 284-286, (2002).

Chapter 2

Molecular Actuation in Nature and Synthetic Systems based on Conducting Polymers

2.1 Introduction

Molecular motors are a blossoming field at the intersection of physics, chemistry, engineering and biology that have recently triggered great interest [Soong R.K. et al. 2000], [Astumian R.D. 2001], [Ballardini R. et al. 2001], [Collin J.P. et al. 2001]. A variety of biological molecular machines such as the ATP synthase, and kinesins have been studied extensively. Synthetic non-conducting polymer molecules embedding metal complexes that exhibit electron-induced (redox) chirality have been created [Zahn S. and Canary J.W. 2000]. Molecular (robotic) grippers made from resorcin[4]arene have been demonstrated [Yamakoshi Y. et al. 2001] and a possible mechanism of molecular actuation using cyclooctatetrathiophene conducting polymers has also been investigated by Marsella [Marsella M.J. and Reid R.J. 1999], to cite just a few. Both biological and synthetic molecular actuators share the characteristic of performing work from the molecular level up, leading to displacement and performance at the microscopic to macroscopic level.

This Chapter gives an overview of molecular actuators found in nature and shows how they can be used as a source of inspiration to create synthetic actuators. A review of early attempts by various groups to design actuators with molecular contractile elements is presented at the end of the Chapter followed by an overview of the proposed molecular mechanisms studied in this thesis. Finally, Table 2.1 at the end of the Chapter summarizes all the key mechanical properties of the molecular actuators surveyed herein.

2.2 Biological Molecular Actuators

Nature employs a whole variety of molecular rotational motors, motor proteins, ratchet-like structures and proteins exhibiting reversible transitions at the molecular level to move, translate and rotate things. The diversity of molecular actuators found in Nature comes from the polyvalence of constructing those using polypeptides, i.e. the long strings of coupled amino acids. Interestingly, protein-based molecular machines are built using a bottom-up construction approach, co-fabrication and self assembly. This manufacturing scheme enables the creation of different protein structures having various functions. Note that in protein engineering, structure equals function. In addition, energy is provided in the form of a chemical source. ATP, which is an energy storage molecule, is catalyzed through enzymes to allow specific interaction of motor proteins. There are two basic types of movements that are created by Nature using motor proteins: linear motion and rotation, where the latter is typically achieved by a combination of sliding and ratcheting mechanisms.

2.2.1 Linear motion

Motor proteins are biological machines converting chemical energy (ATP) into movement. Proteins exhibiting linear motion can be classified into three categories: the myosins, the kinesins and the dyneins. The myosins are mainly responsible for muscle contraction but have also been found to enable cell motility (via projections). The kinesins on the other hand are the transport workhorse of a cell, conveying diverse cellular materials such as vesicles and protein waste. As for the dyneins, they are the largest family of motor proteins and are presented here below.

2.2.1.1 Dyneins

Dyneins are not only responsible for the underlying mechanism powering cilia and flagella, but also for achieving the transport of proteins, organelles and membranes. It is still a mystery how dyneins generate force at the nano-mechanical level. A recent article by Burgess and colleagues proposes that the origin of dynein movement arises from conformational changes within the dynein. The dynein structure has a stalk separated from a stem by the AAA ring protein (Figure 2.1). Upon consumption of ATP, the stem changes conformation which allows it to rotate relative to the stalk by 24° , creating an impressive linear movement of 15 nm [Burgess S.A. et al. 2003]. Note that the dynein molecule alone has a total length of about 45 nm.

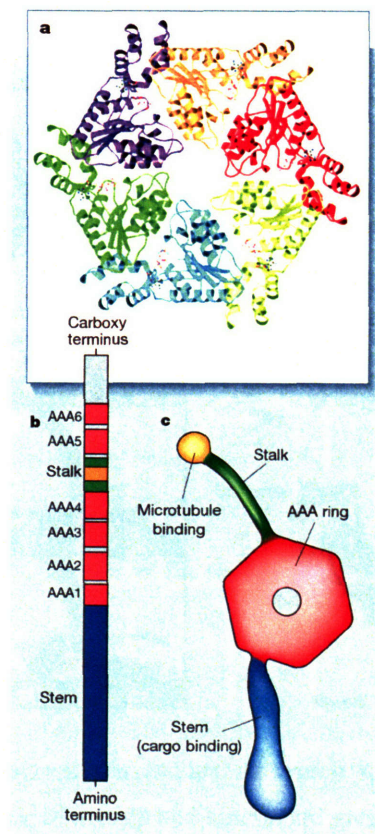


Figure 2.1: Dynein structure. Source: [Vallee R.B. and Hook P. 2003].

2.2.1.2 Muscle - Myosin

At the molecular level, the mechanism of muscle contraction can be crudely described as the interaction of two large proteins: actin and myosin. Muscle contraction is driven by ATP consumption and mediated by the sliding of interdigitated myosin and actin filaments. The thick myosin filaments have a diameter about 15 nm, whereas the thin actin filaments have a diameter about 9 nm. Under contraction, the thick filaments ratchet along the thin filaments. The length of both filaments remains constant during contraction. This motion is achieved by a complex molecular machinery transforming the free energy of ATP hydrolysis into a molecular conformational change of the myosin head, leading the myosin molecular motor to literally “walk”/ratchet along the actin filament. The crystal structure of myosin and the mechanical model of the actin/myosin contraction are shown in Figure 2.2.

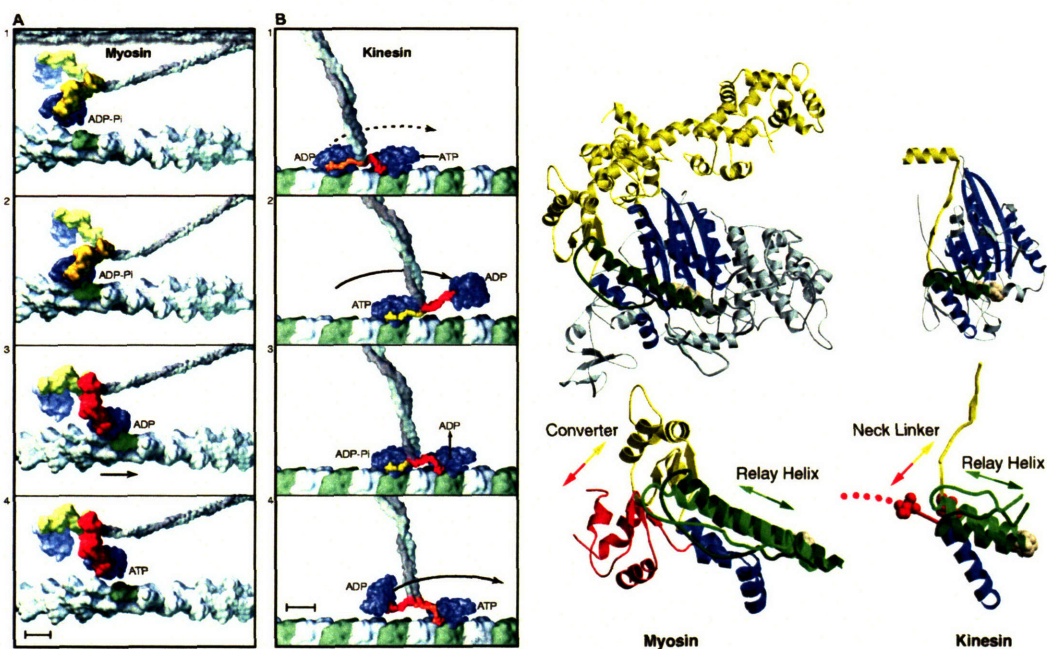


Figure 2.2: Comparison of the mechanical model and the protein structure of myosin and kinesin. Both the mechanical model of the actuation cycle of myosin and kinesin are given (left) as well as their crystal structure (right). Source: [Vale R.D. and Milligan R.A. 2000].

As muscle is activated, phosphate is first released from the hydrolysis of ATP, followed by the crucial conformational change of the myosin heads and finally ADP dissociation. During this power stroke, the myosin heads tilt by $\sim 45^\circ$ thus moving the thick (myosin) filament by ~ 12 nm. High velocities are achieved by consuming more ATP. For example the peak velocity of $2 \mu\text{m/s}$ is reached by “burning” 5 ATPs per myosin head [Hunter I.W. and Lafontaine S. 1992]. There are about 300 myosin heads per thick filament. As ATP is consumed, each myosin head ratchets continuously on the actin filament creating a smooth linear motion at the macro scale.

Muscle amplifies movement by a clever hierarchical structure of the muscle cell, where material organization is achieved at different levels. Fernandez et al. recently showed how much specialized function is actually built even down to single protein domains. Titin, for example, which is a protein that gives cardiac muscle its passive elasticity, has built-in domains that act as a buffer protecting sarcomeres from being exposed to high forces [Li H. et al. 2002]. In other words, muscle is not only nanostructured but it is also microstructured and macrostructured and each level of organization achieves a specific function.

2.2.1.3 Kinesin

Another beautiful molecular mechanism used by nature is the sliding (walking) of kinesin dimers along a protein guiding filament (microtubule). The kinesin molecular motor is used in intracellular material transport and cell division.

The structure and function of kinesin is very similar to the actin/myosin motor responsible for muscle contraction (described above). It has been shown recently that these two motor proteins share a common core structure and mode of function, where they convert energy from ATP into protein motion using a similar conformational change strategy [Vale R.D. and Milligan R.A. 2000]. Muscle myosin and conventional kinesin are dimers with two identical motor heads, which are anchored to rigid coiled coil lever arm proteins. With respect to Figure 2.2, the catalytic core of one myosin motor head binds weakly to actin

(Figure 2.2A-1,2), which causes phosphate¹ release from the active site (Figure 2.2A-3). The lever arm then swings forward, moving the actin filament by 10 nm (Figure 2.2A-3). After the stroke (Figure 2.2A-4), ADP dissociates from the active site and ATP binds to it, which rapidly reverts the catalytic core to its weak binding active state. As for kinesin locomotion, unlike myosin, the two heads of the kinesin dimer work in a coordinated manner (like two walking feet) to move progressively along the microtubule track protein. Each of these strokes produces about 7 to 10 pN of active force (from a 10 nm stroke) [Kojima H. et al. 1997]. Note that

2.2.1.4 RNA polymerase

The enzyme RNA polymerase is one of the most sophisticated linear motors found in Nature. Its role consists of transcribing a DNA template into messenger RNA (mRNA) for building proteins. Interestingly enough, the energy needed to drive movement along the DNA template is drawn from the nucleotide condensation reaction. Measurements show that the RNA polymerase can produce huge forces ranging between 21 and 27 pN [Wang M.D. et al. 1998].

2.2.2 Rotation

2.2.2.1 The F_1 -Adenosine Triphosphatase

The ATP synthase is a 10 nm rotational molecular motor found in mitochondria, bacteria and chloroplasts, and used by these living systems to synthesize ATP. Energy stored in the form of a transmembrane ion gradient is used to produce an amount of work, equivalent to $60 k_B T$ per rotation². Much like the potential energy of water stored in a dam is used to propel a turbine to generate electricity, the ion gradient is forced into the ion channel of the

¹ The phosphate comes from the ATP to ADP hydrolysis.

² Note that k_B is Boltzmann's constant and T is the absolute temperature; at room temperature $1 k_B T$ is roughly 4.1×10^{-21} J.

ATP synthase thus rotating the catalytic sites of the protein, which then “mechanically” reattaches a phosphate onto the ADP to regenerate ATP.

With reference to Figure 2.3, the F_0 portion of the ATP Synthase protein contains the proton channels, whereas the F_1 portion contains the three catalytic sites. The free energy generated by the difference in proton concentration across both sides of the membrane is sufficient to produce three ATPs per rotation while only 12 protons are used [Elston T. et al. 1998]. Interestingly, a group in Japan [Yasuda R. et al. 1997] showed that this motor is reversible, and can be used to convert the motor’s rotations into a proton pump. In a more recent paper, the same group showed how this molecular motor was not only using a chemical source of energy (hydrolysis of ATP) to pump protons, but also using the release of hydrolysis products to generate rotation [Yasuda R. et al. 2001].

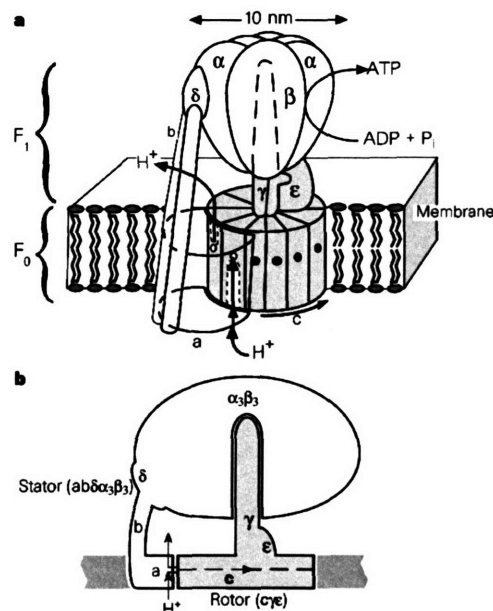


Figure 2.3: Structure of F_0F_1 ATP synthase. Source: [Elston T. and others 1998].

The F_1 -adenosine triphosphatase is also found in the bacterial flagella motor. Motile bacteria such as the *Escherichia coli* are propelled by a number of flagella several micrometers long. The source of power for these flagella is a membrane bound rotary motor that is powered by a proton gradient running the F_1 -ATPase molecular motor. Yasuda et al. [Yasuda R. and others 2001] measured recently that these motors are able to produce a

maximum amount of work equivalent to 80×10^{-21} J. [Mehta A.D. et al. 1999]. This motor system is quite exceptional. It contains equivalents of shafts and bearings, comparable to human engineered systems at the macro scale.

2.2.2.2 DNA packaging motor

During the viral replication cycle, the $\phi 29$ bacteriophage needs to package its newly created DNA into copied virus entities so that it can inject it into host cells. Such packaging is done by an ATP driven motor. During this operation, the bending, entropic and electrostatic energy of DNA must be overcome. Recent experiments by Smith et al. [Smith D.E. et al. 2001] have shown that the $\phi 29$ bacteriophage portal motor can package DNA against a force as large as 57 pN, which is the largest reported to date for a molecular motor. If we assume that DNA has a diameter of about 2 nm, [Branden C. and Tooze J. 1998] a maximum force of 57 pN then corresponds to 18.1 MPa stress.

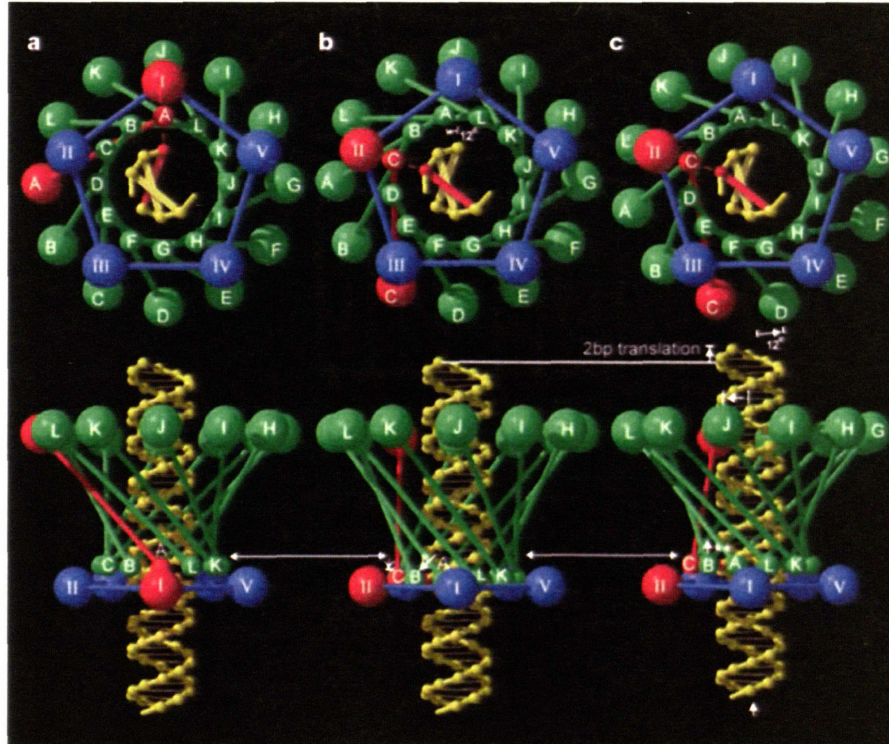


Figure 2.4: Structure of the DNA packaging motor in the $\phi 29$ bacteriophage. Source: [Simpson A. et al. 2000].

The DNA packaging mechanism of the $\phi 29$ bacteriophage is quite complex. Figure 2.4 shows one cycle of the packaging mechanism that rotates the connector and translates the DNA into the head of the bacteriophage.

2.2.3 Other mechanisms

Nature also employs sophisticated mechanisms that are not based on linear or rotational motion. It is interesting to note that all biological movements are not necessarily caused by molecular motors as described above. The following mechanisms make use of biochemical driving forces to achieve motion.

2.2.3.1 Springs

Just as human machines use spring and ratchets to store and release energy, Nature uses equivalent biological springs and ratchets. Biological supramolecular springs, for example are driven by the hydrolysis of a nucleotide or the binding of a ligand (typically an ion). Biological ratchets, on the other hand, are powered by Brownian movement of polymerizing filaments. The forces of contraction that can be generated by such mechanisms are on the order of 10 nN, while their power is typically about 100 pJ/s, which is enormous for such small systems [Mahadevan L. and Matsudaira P. 2000].

An example of a spring-loaded actuator found in Nature is the spasmoneme spring of the Vorticellid, a unicellular organism that typically attaches to leaves via a long 2 to 3 nm long slender stalk (Figure 2.5). Upon application of a stimulus the stalk shrinks at speeds as high as 80 mm/s, leading to a 40 % contraction. The cause of this rapid contraction of the spasmoneme is due to aligned helical rodlike organelles that are quickly collapsed upon exposure to calcium (Figure 2.5).

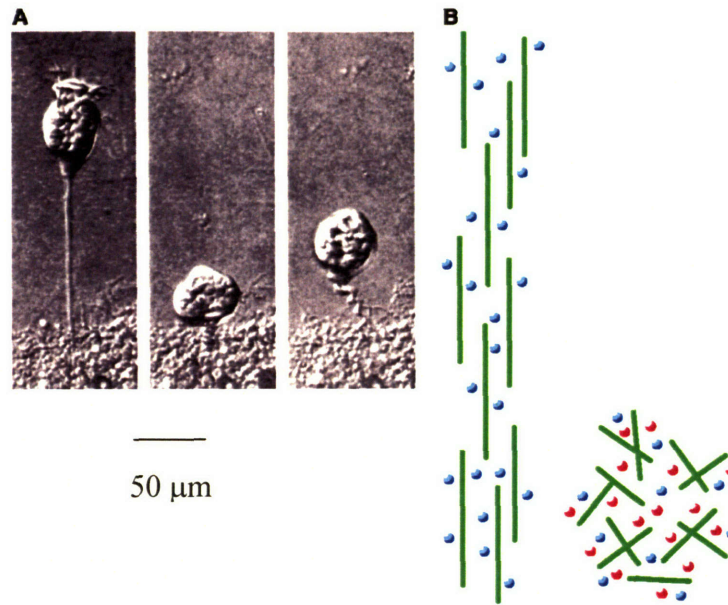


Figure 2.5: Contraction mechanism of the spasmoneme: (A) Micrographs, (B) The extended state (left) consists of aligned filaments held apart by negative charges (blue). Calcium (red) neutralizes the charge, and the filaments condense (right) into a rubberlike material. Source: [Mahadevan L. and Matsudaira P. 2000].

2.2.3.2 Actin Polymerization

Cell motility is necessary for tissue generation during embryonic development and used by viruses to spread during infection. Such motility is enabled by an actin polymerization-based engine which leads to a dynamic rearrangement of polymers composing the cytoskeletal structure. This polymerization is orchestrated by the addition of ATP-actin subunits at one end of the cell, projecting the cell's cytoskeleton in the direction of the cell's movement and de-polymerizing actin filaments at the other end, thus providing a net displacement purely due to "growth" (Figure 2.6). Crosslinking and bundling of different polymerized actin filament together leads to the highest power per unit mass reported for a natural molecular engine (100 kW/kg) {Mahadevan L. & Matsudaira P. 2000 #790} {Cory G.O.C. & Ridley A.J. 2002 #2090}.

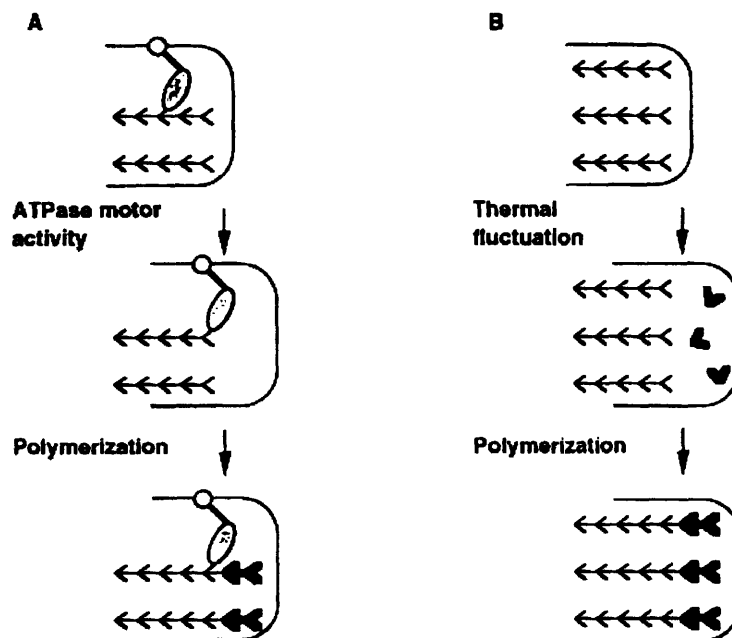


Figure 2.6: Mechanism of actin polymerization. In the motor model: (A) forward movement of the membrane tip is driven by a motor protein (e.g., myosin I) moving forward the filament barbed ends. Polymerization then fills in the resulting gap. In the thermal ratchet model (B), gaps between the protruding membrane and the barbed ends of actin filaments are created by thermally driven movements. Polymerization then fills in the gap, preventing backward movement of the membrane. Source: [Mitchison T.J. and Cramer L.P. 1996].

2.2.4 Nature's Energy Source and Methods of Manufacturing

To complete the description of actuator systems employed by Nature, a short overview of energy sources and manufacturing methods is presented in Appendix A.

2.3 De Novo Synthetic Molecular Actuators

We are currently entering the Materials Designer age (quoting Shuguang Zhang of MIT [Cook G. 2001]). Using Nature as a source of inspiration, several groups around the world are studying and creating de novo synthetic materials actuating from the molecular level up [Mao C. et al. 1999], [Vale R.D. and Milligan R.A. 2000], [Mahadevan L. and Matsudaira P. 2000], [Soong R.K. and others 2000], [Astumian R.D. 2001], [Ballardini R. and others 2001], [Collin J.P. and others 2001]. Advances in synthetic organic chemistry and molecular biology enable the design and synthesis of such molecules that mimic natural mechanisms.

In this new age, conducting polymers play an important role. The inherent conductive nature of these molecules allows control of their behavior down to the molecular scale via charge or voltage. Similar to the approach taken in this thesis, Marsella et al. [Marsella M.J. and Reid R.J. 1999] have moved away from a traditional materials survey strategy towards a materials designer approach where novel conducting polymer materials are created by incorporating property-designed molecular building blocks. Such molecular building blocks may include shape changing, load bearing, passively deformable or hinge-like molecular elements combined with precise control of the material morphology at the nanometer scale. The vision is that unprecedented actuating materials will be created by a bottom-up approach where specific molecular designs are incorporated into a material to achieve specific properties.

Within the framework of molecular actuation, chemically engineered units that are believed to change their molecular shape and produce force and displacement upon the application of an electrical stimulus are presented in the following section. These materials utilize a variety of molecular mechanisms such as the *cis-trans* transition, and the π - π molecular dimerization mechanism, to cite a few. Complex supramolecular systems are also presented.

2.3.1 Shape-changing backbone single molecule actuators

2.3.1.1 Photochemical actuation: Stilbene

One of the early examples of single molecule actuation, first presented in 1985, is the *cis-trans* photoactivated isomerization of the Stilbene photochrome [Zimmermann E.K. and Stille J.K. 1985]. This active molecule can then be incorporated into a larger polymer for characterization. Stille and Zimmermann incorporated this active unit into a photoresistive polyquinoline and demonstrated that exposure to radiation would induce 4.8% contraction of the polymer bulk.

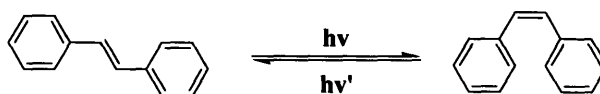


Figure 2.7: Mechanism of the *cis-trans* isomerization of the Stilbene photochrome.

Recently, Gaub and coworkers synthesized a polymer based on a modification of the Stilbene unit: azobenzene [Hugel T. et al. 2002]. The active azobenzene molecule was in turn embedded into a 47mer polyazobenzene-peptide and covalently bonded to both an AFM probe and a glass substrate. Attachment to the AFM cantilever allows probing the force and the displacement generated by the polymer when it is cycled between the *cis* and *trans* conformation induced by the optical stimulus. Photoactivation of an azobenzene unit leads to a 0.25nm contraction. By applying a load of 205 pN to the molecule via their AFM cantilever, Gaub and coworkers showed that each azobenzene unit could generate 4.5×10^{-20} J of work. The upper limit of the efficiency of the photomechanical coupling, however, is only about 10%.

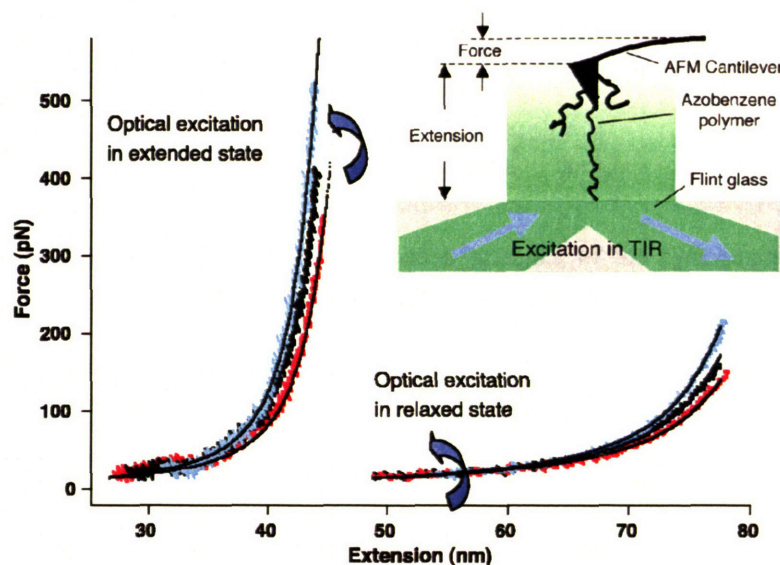


Figure 2.8: Data and schematic presentation of measuring the force and extension of a single polymer chain composed of azobenzene units using AFM techniques. Source: [Hugel T. and others 2002].

2.3.1.2 Electrochemical actuation: Cyclooctatetrathiophene

Cyclooctatetrathiophene (thiophene-fused [8]annulene) molecules exhibiting molecular switchable conformational changes have been proposed by Marsella and coworkers to produce molecular actuators. Similarly, polymers made of these active moieties have been synthesized. The molecular actuation mechanism of cyclooctatetraene is based on a switchable transition from a boat conformation to a planar conformation upon injection of electrons by an electrochemical stimulus. Polymerizing the cyclooctatetraene unit into conducting polymers leads to a system theoretically undergoing actuation by applied potential [Marsella M.J. and Reid R.J. 1999]. Theoretical quantum calculations show that a homodimer of thiophene-fused [8]annulenes can yield a maximum redox-induced dimensional change of 5.92% [Marsella M.J. et al. 2002].

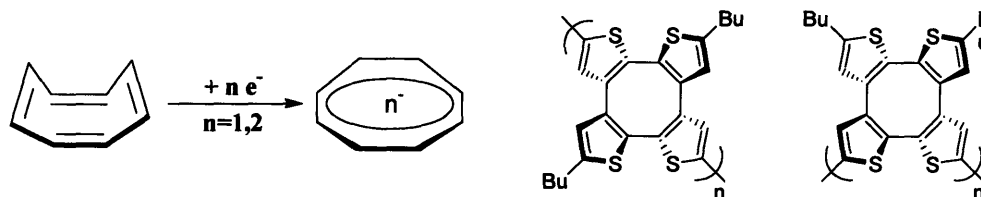


Figure 2.9: Schematic representation of the actuation principle of the cyclooctatetraene unit and its incorporation into polymers, [Marsella M.J. and others 2002].

2.3.2 Supramolecular actuator systems

2.3.2.1 Molecular unidirectional rotary motion

Kelly and colleagues demonstrated in 1998 that an artificial Brownian motor can be implemented at the molecular level [Kelly T.R. et al. 1998], [Kelly T.R. et al. 1999]. A tryptycene-substituted [3]-[4] helicene was synthesized such that it can act as a mechanical ratchet, where the tryptycene serves as the ratchet wheel and the helicene as the pawl and spring (Figure 2.10).

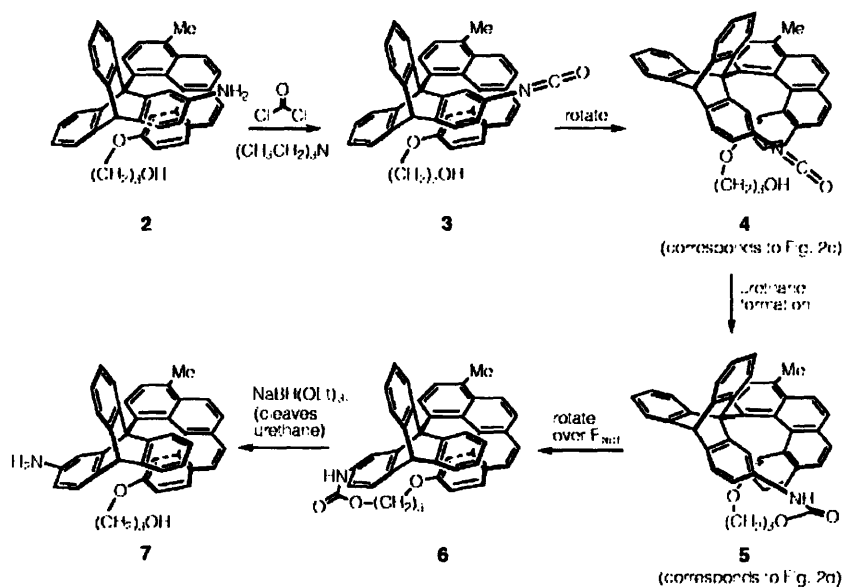


Figure 2.10: Kelly's tryptycene-substituted [3]-[4] helicene and its mechanism of actuation. Source: [Kelly T.R. and others 1999].

The estimated energy barrier to rotation of the tryptycene moiety around the tryptycene/helicene bond is about $\Delta G=25$ kcal/mol, whereas a typical rotation around C-C bond would be around 3-5 kcal/mol. Hence the helicene pawl can be regarded as stiff. The rotation is triggered by a clever chemical reaction powered by carbonyl dichloride. This reaction brings the system's energy very close to the rotation barrier energy and only a small amount of thermal energy is then required to reach the summit of the rotation energy barrier and get the tryptycene molecule to rotate. Once the molecule's energy has reached this summit, the tryptycene unit rotates and releases 25 kcal/mol of thermal energy. This energy immediately diffuses through the system and is thus not available to drive the back rotation. The rotation around the tryptycene/helicene single bond was confirmed by H-NMR studies.

2.3.2.2 A sliding molecule system

One of the most complex supramolecular actuators mimicking the sliding filament model has been built by Sauvage and coworkers around a rotaxane dimer [Jimenez M.C. et al. 2000]. The design utilizes different coordination between phenanthroline and terpyridine moieties. Binding with different metal ions leads to both strings moving along one another thus contracting this dimer theoretically by 22 %.

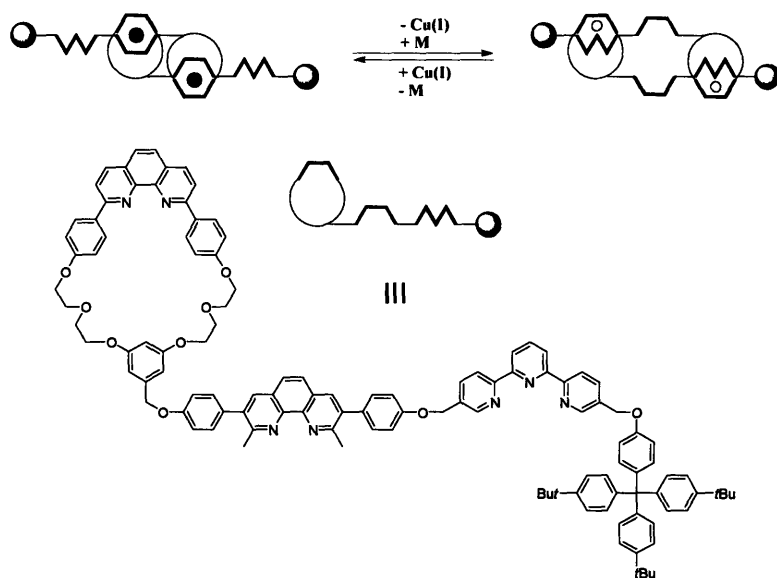


Figure 2.11: A linear rotaxane dimer simulating the sliding filament model, [Jimenez M.C. and others 2000].

2.3.2.3 Liquid Crystalline Materials

The reversible orientation properties of liquid crystalline material can be used to convert electrical energy into mechanical energy. Lehmann and colleagues [Lehmann W. et al. 2001] created a novel, stabilized liquid crystalline actuator material based on three moieties: an active liquid crystal polymer based on polysiloxane, a flexible connecting alkyl polymer $(-\text{CH}_2)_{11}-$ and crosslinkable units. First, they remove the inherent liquidity of the liquid crystalline moiety by attaching polymer mesogenic units to the flexible alkyl spacers which in turn are crosslinked with one another. In turn the second side of the mesogenic unit is attached to crosslinkable units. The length of these mesogenic units is 4nm. The average degree of polymerization is $n=108$, which means that there are a total of $108 \times 2 = 216$ mesogenic repeat units. Films made of this material are quite thin (<100 nm) and exhibit an elastic modulus of 3 MPa. Active strain generation occurs in the lateral direction of the film. This actuator is activated by an electric field and exhibits 4% strain at 1.5 MV/m (1.5 V/mm). The structure and mechanism of actuation of these liquid crystal actuators is shown below:

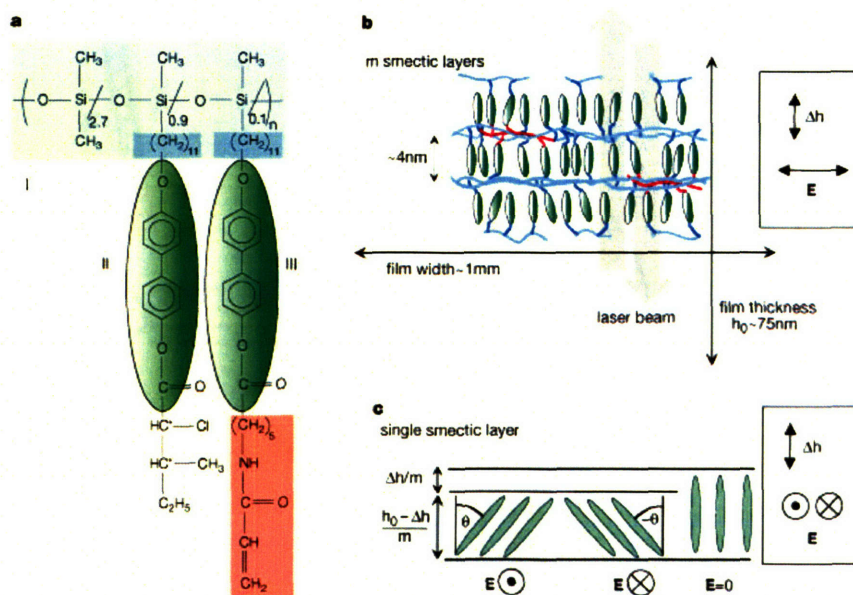


Figure 2.12: Structure and mechanism of actuation of the liquid crystalline polymer. Source: [Lehmann W. and others 2001].

2.3.3 Systems Adapted from Biology

The aim of this sub-section is to describe several man-made molecular machines that, unlike the *de novo* systems presented above, are assembled from biological building blocks. As seen in the first part of this Chapter, Nature has created sophisticated systems at the molecular level. Convergence of molecular biology with organic chemistry will lead to a new class of machines operating at the nano scale.

2.3.3.1 Molecular Grippers

Recent results reported from Bell Labs [Yurke B. et al. 2000] make use of DNA as a building block for *de-novo* molecular machines. This polymer can be used as a structural building block, as template material to organize the self assembly of other entities such as colloidal particles or semi-conductor nanocrystals, and for the construction of active devices such as switches and even fuel (Figure 2.13).

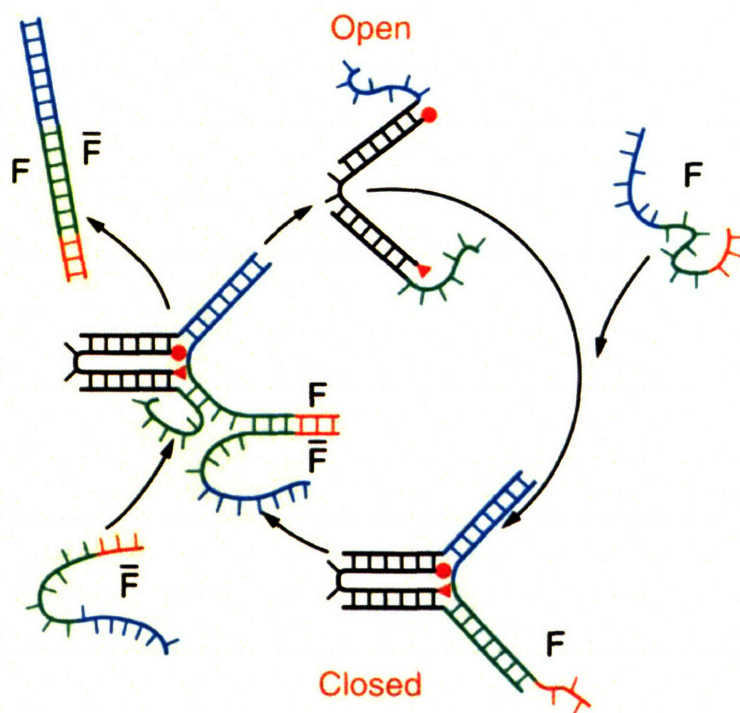


Figure 2.13: DNA grippers and cycle of activation. Source: [Yurke B. and others 2000].

The underlying principle of the DNA tweezers uses molecular recognition between complementary strands of DNA due to hydrogen-hydrogen interaction of matching base pairs. The average energy released when complementary bases assemble (hybridize) is 1.25×10^{-20} J (1.8 kcal/mol or ~ 3 $k_B T$) at room temperature (20 °C) and the separation between 2 bases pairs is 0.43nm. Dividing the amount of hybridization energy by the base pair separation leads to an average closing force of 15 pN. A full closing and opening cycle takes 34 seconds.

The machine presented by Yurke and colleagues has the form of a pair of tweezers. It is formed by 3 strands of DNA and is opened and closed by a 4th strand of DNA acting as “energy source”. Each cycle produces a duplex DNA waste product coming from the hybridization of the fuel molecule responsible for opening the tweezers and the one for closing them.

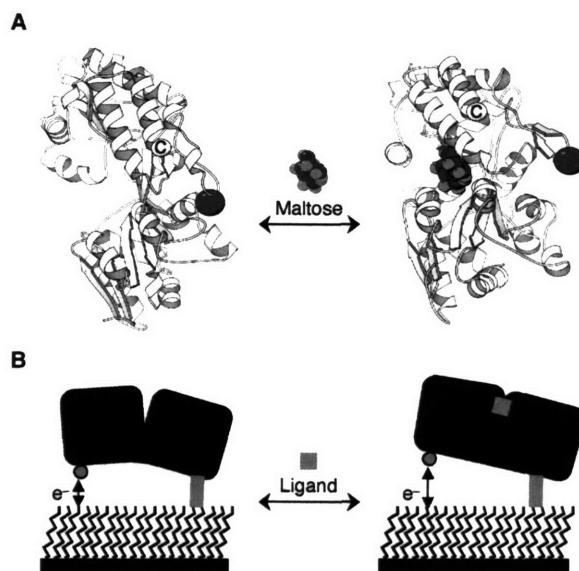


Figure 2.14: (A) Ligand-induced protein conformational changes in ruthenium-labeled maltose binding protein (MBP). (B) Upon ligand binding (square), the changes in the protein conformation [open (left) \rightarrow closed (right)] alter the interaction between the cofactor and electrode surface, and hence the observed current flowing between these two components. Source: [Benson D.E. et al. 2001].

2.3.3.2 Hinge Bending Motions in Proteins and pH sensitive molecular transitions

As we have seen, proteins naturally exhibit conformational transitions. Such molecular transitions can be engineered as chemical sensors. A group at the Chemical Department of Duke University [Benson D.E. and others 2001] exploited ligand-mediated hinge-bending protein motions, which they then characterized by electrochemical methods. This approach allows the development of bioelectronic interfaces that can sense minute quantities of diverse analytes (in this particular case maltose), while giving an electrical signal (Figure 2.14).

2.3.3.3 Molecular Switches

A class of *de-novo* molecular actuators is based on “molecular switch” peptides. DAR16-IV, for example, a 16 amino acid-long peptide undergoes a rapid collapse from an β -sheet (5 nm) conformation to a α -helix structure (2.5 nm) [Altman M. et al. 2000; Zhang S. and Rich A. 1997]. This change is triggered either by a thermal stimulus or a change in pH. Interestingly, this transformation occurs with no intermediary structure, making this class of protein a true 2 state or binary molecular switch.

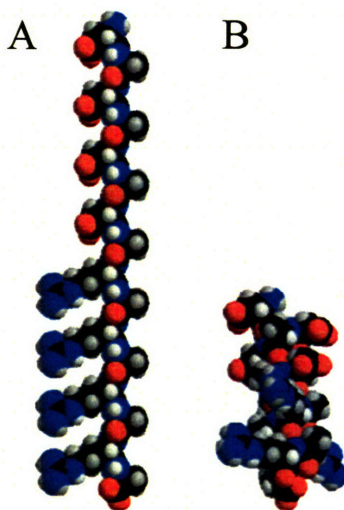


Figure 2.15: DAR16-IV in the β -sheet (A) and α -helix forms (B). Source: [Altman M. and others 2000]

2.4 Molecular Actuators developed within this Thesis

Four different (never synthesized before) conducting polymer materials based on molecular design are presented in this section. All the molecules shown below were designed by Professor Timothy Swager of MIT and synthesized into monomers by the members of the Swager laboratory. A goal of this Ph.D. thesis was to take these monomers and to polymerize them into robust and electroactive muscle films. For further information on the synthesis of these novel monomer molecules please refer to the works of Hiao-hua (Bruce) Yu [Yu H.-h. 2003], Michael Bueschel, Brad Holyday and Jocelyn Nadeau (unpublished).

2.4.1 Design principles for molecular actuators

The target molecules that this thesis focuses on are classified by different actuation mechanisms: π -stacking dimerization, backbone twisting, and molecular stacking. The general design consists of linking individual actuating unit through a thiophene backbone as shown in Figure 2.16. The use of thiophene-based elements assures good material conductivity and easy access to various polymerization methods, while the molecular mechanism provides the desired molecular conformational changes.

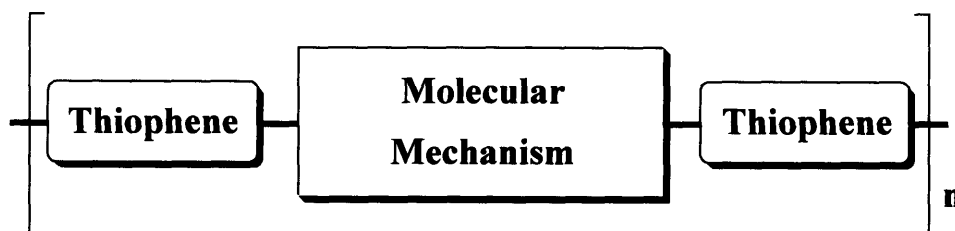


Figure 2.16: Schematic design for creating conducting polymer backbones with molecular actuating units.

In addition thiophenes offer many chemical degrees of freedoms. Manipulations of the properties of polythiophenes are possible by changing the primary structure (i.e. choice of monomer), the secondary structure (i.e. type of coupling between monomer units) and finally the tertiary structure (i.e. morphology).

2.4.2 π -stacked single molecule actuators

2.4.2.1 Dimer formation: molecular contraction via π - π stacking in poly(quarterthiophene)

The first novel conducting polymer actuator based on molecular designs is poly(quarterthiophene) (poly(QT)). This monomer is an oligomeric form of thiophene (quarterthiophene or four thiophenes) that is then polymerized into a polymer. When oxidized, quarterthiophenes attract each other into a stacked structure (Figure 2.17). The molecular driving force bringing the two quarterthiophene units together is referred to as π -dimerization or π - π stacking. This molecular mechanism makes use of wavefunction overlap in π -conjugated polymers, where it is more favorable for π orbitals to align (due to Pauli's exclusion principle) and share their electrons. The π -dimerization is attractive in the oxidized state (electron deficient) and repulsive in the reduced state (filled electronic levels) [Kingsborough R.P. and Swager T.M. 1999].

The π -stacked structure is typical of oxidized thiophene oligomers and has been studied experimentally by means of X-ray diffraction, Scanning Tunneling Microscopy (STM), Electron Paramagnetic Resonance Spectroscopy (EPR), as well as theoretical calculations [Kingsborough R.P. and Swager T.M. 1999; Azumi R. et al. 1999; Brocks G. 2000; Graf D.D. et al. 1996; Sirringhaus H. et al. 1999].

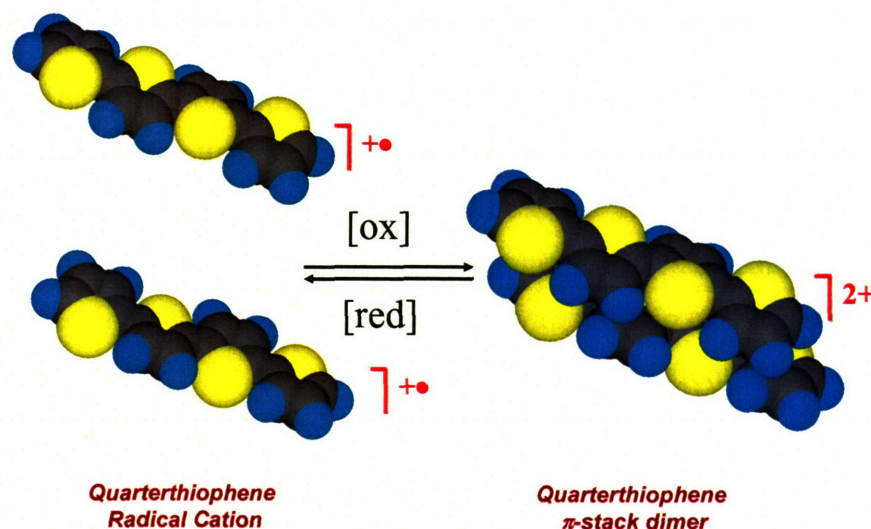


Figure 2.17: π - π stacking molecular contraction mechanism between oxidized quarterthiophenes.

A simple mixing diagram can be constructed to understand the interaction between the oxidized quarterthiophene linkage molecules. As shown in Figure 2.18, oxidation of two adjacent quarterthiophene molecules creates two radical cations with partially occupied Highest Occupied Molecular Orbitals (HOMO) which then mix to produce a new doubly occupied molecular orbital at lower energy (Figure 2.18, bottom).

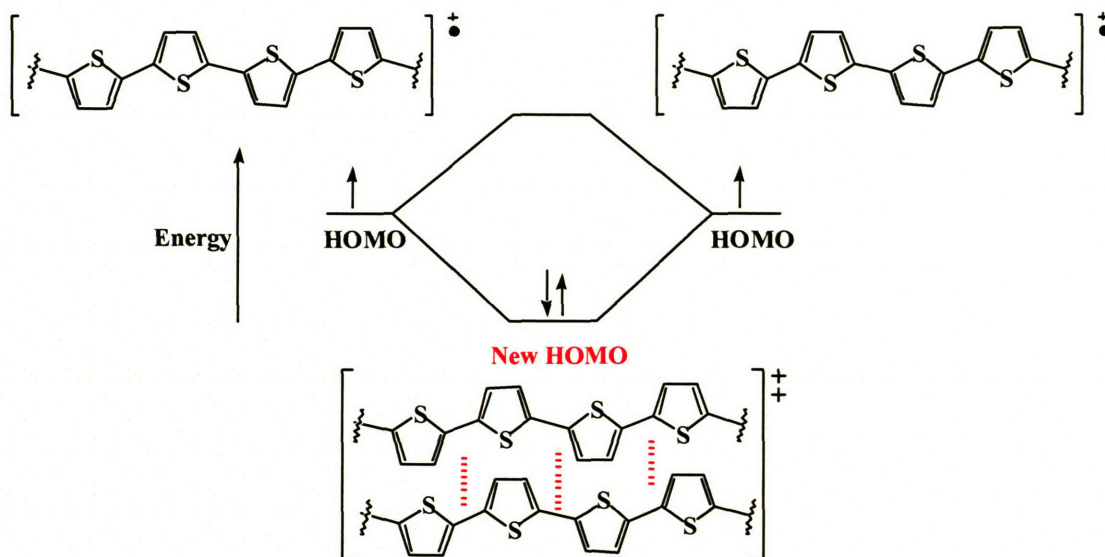


Figure 2.18: Mixing diagram for quarterthiophene

2.4.2.2 Molecular hinge systems: poly(calix[4]arene bis-bithiophene)

Poly(calix[4]arene bis-bithiophene) (poly(calixBBT)), employs passive hinge molecules (calix[4]arene) interconnected by conducting rigid rods (quarterthiophene). The cone conformation of the calix[4]arene scaffold allows the formation of an accordion-like molecule upon monomer polymerization. Unlike poly(QT) presented in the previous section, the π -dimerization in poly(calixBBT) is channeled with the help of the passive calix[4]arene molecular hinge linkers. The molecule can thus be switched from an accordion-like open structure to a collapsed configuration upon change of oxidation state.

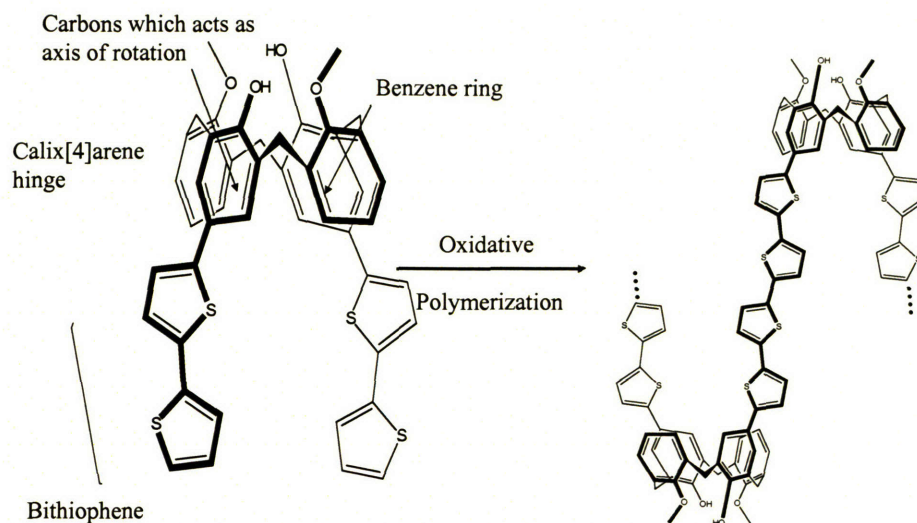


Figure 2.19: Polymerization of the calix[4]arene *bis*-bithiophene monomer

Poly(calixBBT) is a promising actuating material. Key features of this material include the deformable calix[4]arene scaffold and the redox active quarterthiophene units. The initial polymer displays an equilibrium conformation that has the quarterthiophene groups in a non-aggregated state. The proposed actuation mechanism and a 3-dimensional space-filling model are shown conceptually in Figure 2.20.

Polymer Backbone

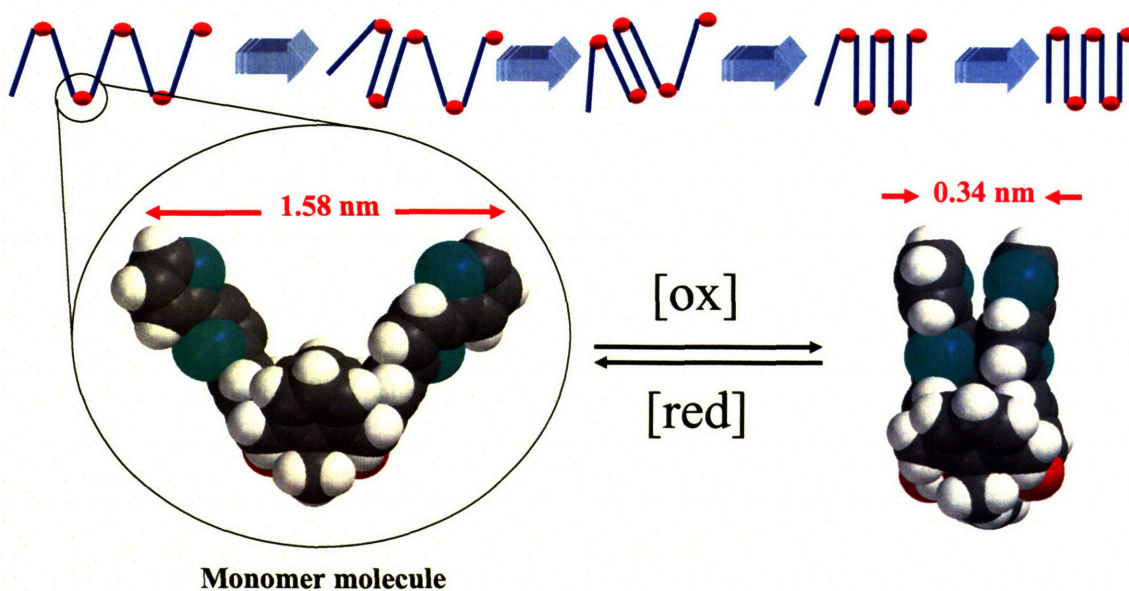


Figure 2.20: Schematic actuation mechanism and 3-dimentional space filling model of poly(CalixBBT).

Upon oxidation the quarterthiophene groups have a strong tendency to aggregate into a π -stacked structure (as presented in the previous section). Simple inspection of the space-filling model in Figure 2.20 suggests that one dimensional changes as large as a factor of 8.3 are possible for Poly(calixBBT).

2.4.3 Shape-changing backbone single molecule actuators

2.4.3.1 Butterfly-like and robust molecule: poly(thianthrene)

Thianthrene is a molecule that is composed of two benzene rings fused together by two *ortho*-sulfide bridges. Due to the tetrahedral orbital environment around the sulfur atoms the ring system is bent in its ground state forming a 128° angle (Figure 2.21). Upon oxidation to the radical cation state, the π -system delocalizes across the entire ring system and the molecule becomes planar. This behavior is well known and highly-reversible, but has never been used as an actuating mechanism. Expansion of the thianthrene compound leads to a 7% lengthening of the molecule. Bulk electrochemically stimulated materials can be built by assembling several thianthrene repeat units together or by combining them via thiophene conductive rods.

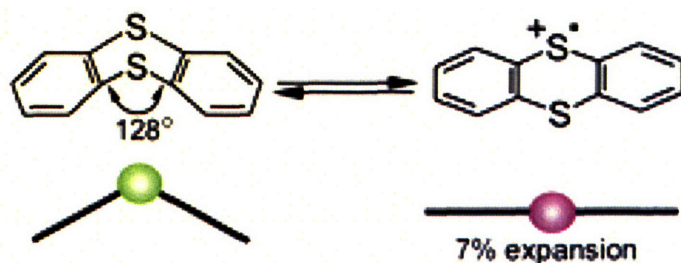


Figure 2.21: Thianthrene-based polymer actuator.

2.4.3.2 Twisting backbone molecule: poly(phenyleneEDOT)

The conformational change exhibited by poly(phenyleneEDOT) is based on yet another mechanism of molecular motion, where the molecular backbone unfolds from a twisted to a

planar structure upon oxidation. Such active backbone molecular transitions, if aligned, would lead to a highly anisotropic contractile polymer material.

This polymer is formed by a combination of phenylene and ethylenedioxythiophene (EDOT) units. What makes poly(phenyleneEDOT) an unusual candidate, though, is how material properties can be changed and optimized for actuation by changing the monomer side chains (R groups in Figure 2.22). The interaction between the sulfur and the nearby oxygen atoms is responsible for the molecular actuation driving force. In the neutral form, electrostatic interactions between these 2 groups of atoms lead to steric interactions, creating a twisted molecular backbone. Upon oxidation these groups have fewer electrons to share, leading to a molecular reorganization that translates into a flat structure.

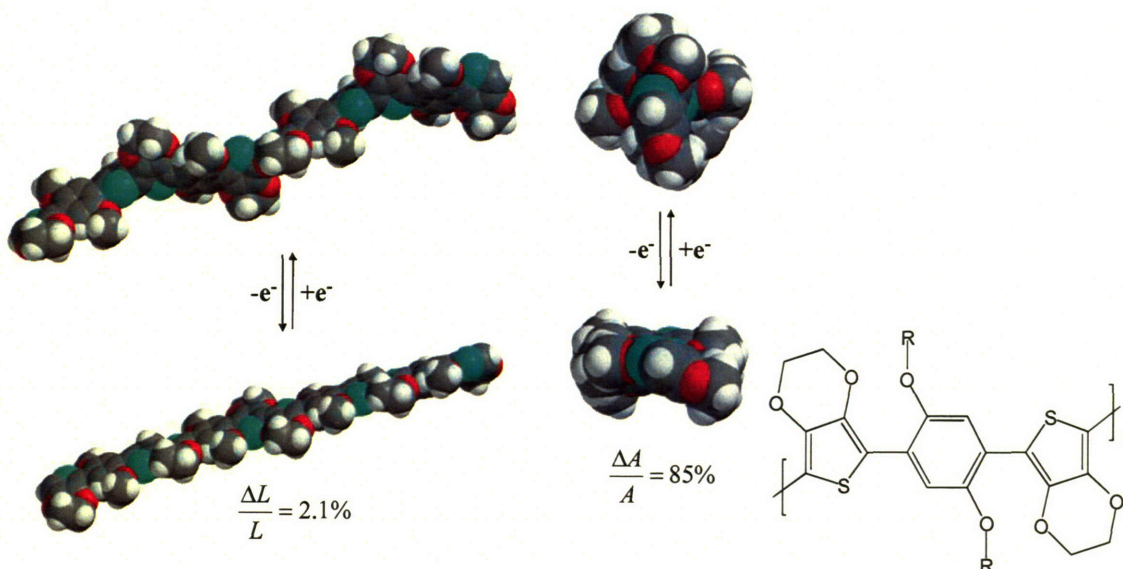


Figure 2.22: Actuation mechanism and molecular structure of poly(phenyleneEDOT).

Figure 2.22 shows our initial AM1 simulation³ of a 4mer of poly(phenyleneEDOT) subjected to charge removal (oxidation) and charge injection (reduction). The polymer is calculated to have a non-planar conformation in its neutral state and a twisted structure in its

³ AM1: Austin Model 1 molecular simulation.

oxidized form, exhibiting 2.1 % strain along its backbone, but more than 85% change in its cross-sectional area.

2.4.3.3 Stackable transition metal-complex polymers: poly(vanadyLEDOT)

The conducting polymer actuator materials based on molecular actuating elements presented above only contain organic molecules. Adding a metal transition complex such as vanadyl to the conducting polymer backbone can lead to surprising properties. The vanadyl-EDOT monomer for example incorporates a vanadyl transition metal compound with the well studied poly(EDOT) polymerizable group. The vanadyl moiety of this molecule is responsible for creating supramolecular ordering of the molecule into stacks (Figure 2.23). In addition it is designed to undergo a conformational change based on its redox switchable state. While the poly(EDOT) moiety assures good conductivity throughout the molecule, the vanadyl part assures the robustness and supramolecular conformation of the molecule.

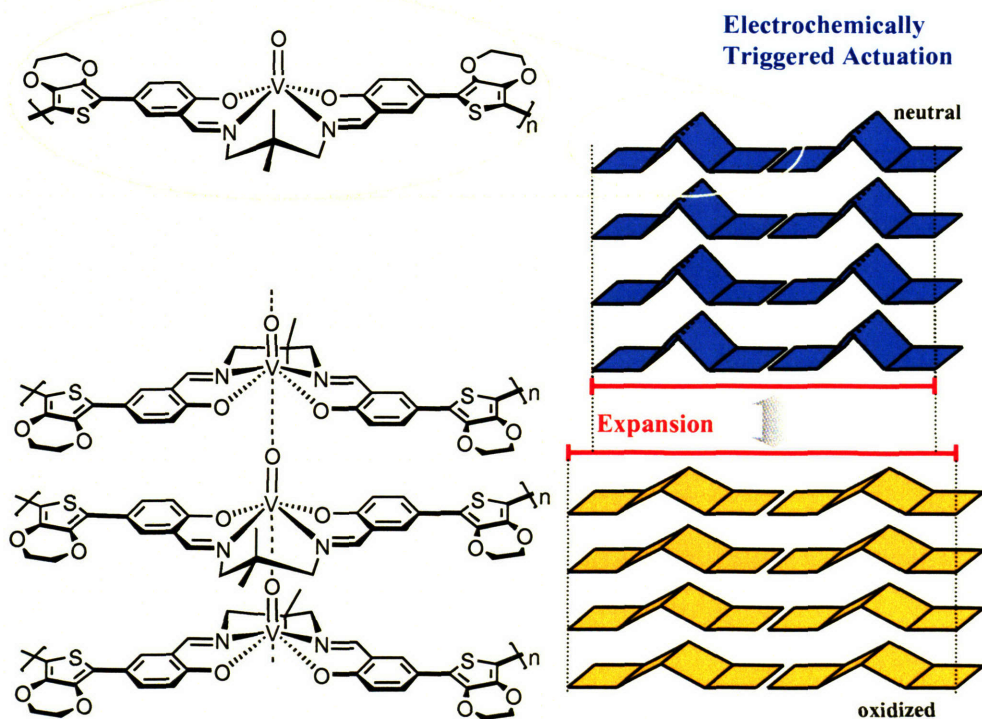


Figure 2.23: The VanadylEDOT monomer and its supramolecular stacking characteristics. The mechanism of actuation of this molecule is shown on the right. Diagram: courtesy of Professor Swager.

2.5 Summary and Conclusion on molecular actuation

In this Chapter we presented various molecular actuators, both naturally occurring and man made. These molecular motors have complex mechanisms for converting chemical or electrical energy into mechanical work. Table 2.1 summarizes the characteristic properties of some of the molecular actuators presented herein and orders them in decreasing order of specific power.

Biologically inspired molecular systems will lead to the creation of a new generation of engineering devices and materials. For example, advances in molecular motors might enable precise control of manufacturing processes at the nanoscale. Note that while some of these actuators have tremendous properties, retention of the properties when the molecular motor is incorporated into a supramolecular to macroscopic assembly remains a challenge in the discovery of novel active materials.

2. Molecular Actuation in Nature and Synthetic Systems based on Conducting Polymers

	Specific Power (W/kg)	Max Force (pN)	Displacement or Strain	Speed ($\mu\text{m/s}$)	Work (J)
kT (thermal energy)	-	-	-	-	4×10^{-21}
Actin Polymerization [Kahn s. and Sheez M.P. 1997; Mahadevan L. and Matsudaira P. 2000; Mogilner A. and Oster G. 2003]	100,000	10	5.4 nm step size	1	54×10^{-21}
Myosin II [Hunter I.W. and Lafontaine S. 1992; Mahadevan L. and Matsudaira P. 2000]	50,000	10	12 nm	2	12×10^{-21}
Kinesins [Kojima H. and others 1997]	7,000	7 – 10	8 nm	1	56×10^{-21}
Spasmoneme in Vorticellia [Mahadevan L. and Matsudaira P. 2000]	4,000	10,000	40 %	80,000	-
RNA polymerase [Wang M.D. and others 1998]	-	21 – 27	-	5000	-
Combustion Engine [Hunter I.W. and Lafontaine S. 1992]	1,000	-	-	-	-
Bacteriophage portal motor [Smith D.E. and others 2001]	100	57	rotation	100 Hz	39×10^{-21}
Muscle [Hunter I.W. and Lafontaine S. 1992]	50 - 200	-	20%	2	-
Poly(calix[4]arene bis-bithiophene) [Anquetil P.A. et al. 2002]	50	92	1.39 nm 80% (contraction)	-	1.3×10^{-19}
Sliding rotaxane [Jimenez M.C. and others 2000]	-	-	22 %	-	-
Poly(thianthrene)	-	-	7 %	-	-
Cyclooctatetrathiophene [Marsella M.J. and others 2002]	-	-	5.92 %	-	-
Poly(phenyleneEDOT)	-	-	2.1 % linear 85 % cross-section	-	-

Table 2.1: Summary of characteristic properties of the molecular actuators presented herein.

2.6 References

- Altman M., Lee P., Rich A. and Zhang S., "Conformational behavior of ionic self-complementary peptides", *Protein Science*, Vol. 9, pp. 1095-1105, (2000).
- Anquetil P.A., Yu H.-h., Madden J.D., Madden P.G., Swager T.M. and Hunter I.W., "Thiophene-Based Conducting Polymer Molecular Actuators", *Smart Structures and Materials 2002: Electroactive Polymers Actuators and Devices*, Yoseph Bar-Cohen, Editor, *Proceedings of the SPIE*, Vol. 4695, pp. 424-434, (2002).
- Astumian R.D., "Making Molecules into Motors", *Scientific American*, Vol. July, pp. 57-64, (2001).
- Azumi R., Goetz G. and Baeuerle P., "Self-Assembly of Alkylsubstituted Oligothiophenes", *Synthetic Metals*, Vol. 101, pp. 569-572, (1999).
- Ballardini R., Balzani V., Credi A., Gandolfi M.T. and Venturi M., "Artificial Molecular-Level Machines: Which Energy to Make them Work?", *Accounts of Chemical Research*, Vol. 34, pp. 445-455, (2001).
- Benson D.E., Conrad D.W., de Lorimier R.M., Trammell S.A. and Hellinga H.W. "Design of Bioelectronic Interfaces by Exploiting Hinge-Bending Motions in Proteins", *Science*, pp. 1641-1644, (2001).
- Branden C. and Tooze J., "Introduction to Protein Structure", *Second Edition*, Garland Ed. (1998).
- Brocks G., " π -dimers of oligothiophene cations", *Journal of Chemical Physics*, Vol. 112, (12): pp. 5353-5363, (2000).
- Burgess S.A., Walker M.L., Sakakibara H., Knight P.J. and Oiwa K., "Dynein Structure and Power Stroke", *Nature*, Vol. 421, pp. 715-718, (2003).
- Collin J.P., Dietrich-Buchecker C., Jimenez-Molero M.C. and Sauvage J.P., "Shuttles and Muscles: Linear Molecular Machines Based on Transition Metals", *Accounts of Chemical Research*, Vol. 34, pp. 477-487, (2001).
- Cook G., "No Assembly Required for these Tiny Machines", *Boston Globe*, (2001 Oct 16).
- Cory G.O.C. and Ridley A.J., "Braking Waves", *Nature*, Vol. 418, pp. 732-733, (2002).
- Elston T., Wang H. and Oster G., "Energy Transduction in ATP Synthase", *Nature*, Vol. 391, pp. 510-513, (1998).
- Graf D.D., Campbell J.P., Miller L.L. and Mann K.R., "Single-Crystal X-ray Structure of the Cation Radical of 3',4'-Dibutyl-2,5"-diphenyl-2,2'-terthiophene: Definitive Evidence for π -Stacked Oxidized Oligothiophenes", *Journal of the American Chemical Society*, Vol. 118, pp. 5480-5481, (1996).
- Hugel T., Holland N.B., Cattani A., Moroder L., Seitz M. and Gaub H.E., "Single-Molecule Optomechanical Cycle", *Science*, Vol. 296, pp. 1103-1106, (2002).
- Hunter I.W. and Lafontaine S., "A Comparison of Muscle with Artificial Actuators", *Technical Digest IEEE Solid State Sensors and Actuators Workshop*, pp. 178-185, (1992).
- Jimenez M.C., Dietrich-Buchecker C. and Sauvage J.P., "Towards Synthetic Molecular Muscles: Contraction and Stretching of a Linear Rotaxane Dimer", *Angewandte Chemie International*, Vol. 39 No. 18, pp. 3284-3287, (2000).

2. Molecular Actuation in Nature and Synthetic Systems based on Conducting Polymers

- Kahn s. and Sheez M.P., "Force Effects on Biochemical Kinetics", *Annual Review of Biochemistry*, Vol. 66, pp. 785-805, (1997).
- Kelly T.R., De Silva H. and Silva R.A., "Unidirectional Rotary Motion in a Molecular System", *Nature*, Vol. 401, pp. 150-153, (1999).
- Kelly T.R., Sestelo J.P. and Tellitu I., "New Molecular Devices: "In search of a Molecular Ratchet"", *Journal of Organic Chemistry*, Vol. 63, pp. 3655-3665, (1998).
- Kingsborough R.P. and Swager T.M., "Polythiophene Hybrids of Transition-Metal Bis(salicylideneimine): Correlation between Structure and Electronic Properties", *Journal of the American Chemical Society*, Vol. 121, (38): pp. 8825-8834, (1999).
- Kojima H., Muto E., Higuchi H. and Yanagida T., *Biophysical Journal*, Vol. 73, pp. 2012, (1997).
- Lehmann W., Skupin H., Tolksdorf C., Gebhard E., Zentel R., Kruger P., Losche M. and Kremer F., "Giant Electrostriction in Ferroelectric Liquid-Crystalline Elastomers", *Nature*, Vol. 410, pp. 447-450, (2001).
- Li H., Linke W.A., Oberhauser A.F., Carrion-Vazquez M., Kerkvliet J.G., Lu H., Marszalek P.E. and Fernandez J.M., "Reverse Engineering of the Giant Muscle Protein Titin", *Nature*, Vol. 418, pp. 998-1002, (2002).
- Mahadevan L. and Matsudaira P., "Mobility Powered by Supramolecular Springs and Ratchets", *Science*, Vol. 288, pp. 95-99, (2000).
- Mao C., Sun W., Shen Z. and Seeman N., "A Nanomechanical Device Based on B-Z Transition of DNA", *Nature*, Vol. 397, pp. 144-146, (1999).
- Marsella M.J. and Reid R.J., "Toward Molecular Muscles: Design and Synthesis of an Electrically Conducting Poly[cyclooctatetrathiophene]", *Macromolecules*, Vol. 32, pp. 5982-5984, (1999).
- Marsella M.J., Reid R.J., Estassi S. and Wang L.-S., "Tetra[2,3-thienylene]: A Building Block for Single Molecule Electromechanical Actuators", *Not known - in review*, (2002).
- Mehta A.D., Rief M., Spudich J.A., Smith D.A. and Simmons R.M., "Single-Molecule Biomechanics with Optical Methods", *Science*, Vol. 283, pp. 1689-1695, (1999).
- Mitchison T.J. and Cramer L.P., "Actin-Based Cell Motility and Cell Locomotion", *Cell*, Vol. 84, (3): pp. 371-379, (1996).
- Mogilner A. and Oster G., "Force Generation by Actin Polymerization II: The Elastic Ratchet and Tethered Filaments", *Biophysical Journal*, Vol. 84, pp. 1591-1605, (2003).
- Simpson A., Tao Y., Leiman P.G., Badasso M.O., He Y., Jardine P.J., Olson N.H., Morais M.C., Grimes S., Anderson D.L., Baker T.S. and Rossmann M.G., "Structure of the Bacteriophage ϕ 29 DNA packaging motor", *Nature*, Vol. 408, pp. 745-750, (2000).
- Sirringhaus H., Brown P.J., Friend R.H., Nielsen M.M., Bechgaard K., Langeveld-Voss B.M.W., Spierling A.J.H., Janssen R.A.J., Meijer E.W., Herwing P. and de Leeuw D.M., "Two-Dimensional Charge Transport in Self-Organized, High-Mobility Conjugated Polymers", *Nature*, Vol. 401, pp. 685-689, (1999).
- Smith D.E., Tans S.J., Smith S.B., Grimes S., Anderson D.L. and Bustamante C., "The Bacteriophage ϕ 29 Portal Motor Can Package DNA Against a Large Internal Force", *Nature*, Vol. 413, pp. 748-752, (2001).
- Soong R.K., Bachand G.D., Neves H.P., Olkhovets A.G., Craighead H.G. and Montemagno C.D., "Powering an Inorganic Nanodevice with a Biomolecular Motor", *Science*, Vol. 290, pp. 1555-1558, (2000).
- Vale R.D. and Milligan R.A., "The Way Things Move: Looking Under the Hood of Molecular Motor Proteins",

2. Molecular Actuation in Nature and Synthetic Systems based on Conducting Polymers

Science, Vol. 288, pp. 88-95, (2000).

Vallee R.B. and Hook P., "A Magnificent Machine", *Nature*, Vol. 421, pp. 701-702, (2003).

Wang M.D., Schnitzer M.J., Yin H., Landick R., Gelles J. and Block S. M. "Force and Velocity Measured for Single Molecules of RNA Polymerase ", *Science*, Vol. 282, pp. 902, (1998).

Yamakoshi Y., Schlitter R.R., Gimzewski J.K. and Diederich F., "Synthesis of Molecular-Gripper Type Dynamic Receptors and STM-imaging of Self-Assembled Monolayers on Gold", *Journal of Materials Chemistry*, Vol. 11, pp. 2895-2897, (2001).

Yasuda R., Noji H., Kinosita K., Motojima F. and Yoshida A., "Rotation of the γ subunit in F_1 -ATPase; Evidence that ATP Synthase Is a Rotary Motor Enzyme ", *J Bioenerg. Biomem.* Vol. 29, pp. 207-209, (1997).

Yasuda R., Noji H., Yoshida M., Kinosita K. and Itoh H., "Resolution of Distinct Rotational Substeps by Submillisecond Kinetic Analysis of F_1 -ATPase", *Nature*, Vol. 410, pp. 898-904, (2001).

Yu H.-h., "Molecular Actuators: Design, Syntheses and Applications toward Actuation and Sensory Materials", *MIT Ph.D. Thesis, Department of Chemistry*, (2003).

Yurke B., Turbfield A.J., Mills Jr. A.P., Simmel F.C. and Neumann J.L., "A DNA-Fuelled Molecular Machine", *Nature*, Vol. 406, pp. 605-608, (2000).

Zahn S. and Canary J.W., "Electron-Induced Inversion of Helical Chirality in Copper Complexes of N,N-Dialkylmethionines", *Science*, Vol. 288, pp. 1404-1407, (2000).

Zhang S. and Rich A., "Direct conversion of an oligopeptide from a β -sheet to an α -helix: A model for amyloid formation", *Proceedings of the National Academy of Science*, Vol. 94, pp. 23-28, (1997).

Zimmermann E.K. and Stille J.K., "Photoresponsive Polyquinolines", *Macromolecules*, Vol. 18, (321-327): (1985).

Chapter 3

Theory of Conducting Polymer Actuators

This Chapter presents a general introduction to conducting polymers and explains the limitations of using current materials as actuators. Considerations for creating novel systems based on specific molecular design for enhanced actuation are presented followed by the estimation of maximal theoretical performance in these novel materials.

3.1 Conducting Polymers

3.1.1 *Structure and Conductivity*

Polymers, e.g. plastics, are a commodity of modern life. Their use is ubiquitous from low tech, high volume consumer products such as packaging materials, tubing or furniture to high tech specialized products such as medical implants or technical garments. Typically one thinks of polymers as electrical insulators. Indeed, a typical polymer such as polyethylene (PE) has a conductivity of 10^{-16} S/m, which is 22 orders of magnitude smaller than copper (5.9×10^6 S/m). This common picture however changed in 1977 when Alan MacDiarmid, Alan Heeger and Hideki Shirakawa made the first discovery of a conducting polymer, polyacetylene: $(CH)_x$. By adding doping elements such as Br_2 , I_2 , AsF_5 to polyacetylene they discovered that this relatively insulating polymer (typically about 10^{-6} S/m) could be either n- or p-doped and ultimately show high intrinsic conductivities (up to 10^7 S/m) [Ito T. et al.

1974], [Shirakawa H. et al. 1977], [Basescu N. 1987]. This discovery led to a rapid growth and intensive study of a novel class of organic materials: Synthetic Metals.

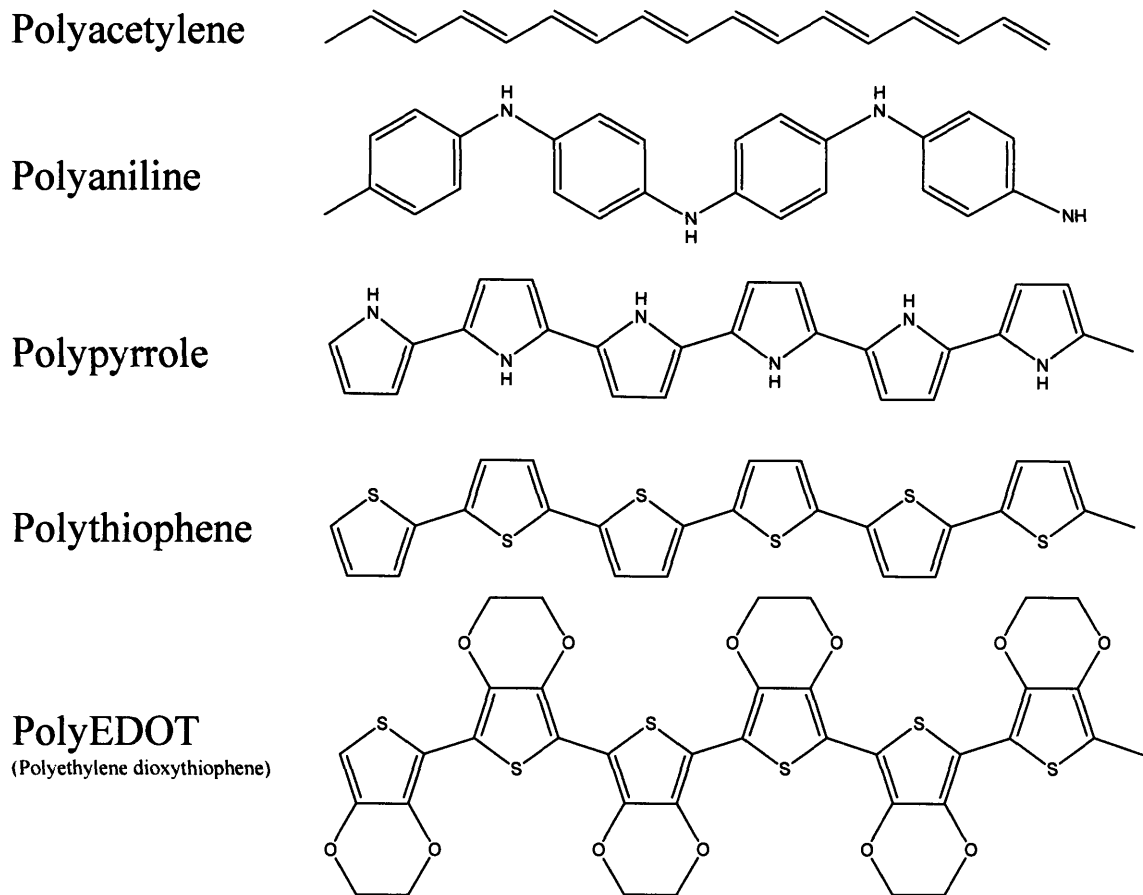


Figure 3.1: Common Conducting Polymers. Note the alternation of single and double bonds along the polymer backbone.

The surprising property of synthetic metals is that their conductivity can show metallic behavior, although they contain no metallic element. On the contrary, the inherent conductivity of these materials is the result of the conjugated structure of their molecular backbone. The bonds between carbon atoms that form the conjugated polymer backbone are alternating single and double bonds. As a result, these are composed of both strong σ bonds as well as delocalized π bonds which exhibit a weaker molecular force. Figure 3.1 shows common conducting polymers commercially available: polyacetylene, polyaniline, polypyrrole, polythiophene and polyethylene dioxythiophene. It is important to note that

Figure 3.1 represents only a tiny fraction of the members of the conducting polymer class of materials, most of which have yet to be synthesized. This thesis focuses on a number of novel conducting polymers whose structures have been optimized for actuation.

Addition of a charged molecule, a dopant, allows displacing the weakly bound π electrons from the backbone and ultimately leads to the conduction properties of these plastic materials. As dopants are added to the polymer, electrons or holes¹ have to be injected to maintain charge neutrality. Charge transport inside the polymer takes place both along the backbone (intrachain transfer) as well as from chain to chain (interchain transfer), both via a so called hopping mechanism [Roth S. 1995]. Recent studies by Bredas and colleagues [Beljonne D. et al. 2002] using quantum mechanical theory calculations backed by ultra fast spectroscopy indicate a two-step mechanism for intrachain energy transfer with hopping along the conjugated chains as the rate-limiting step (in the range of 1 ns^{-1}); the higher efficiency of the interchain transfer process, they argue, is mainly due to larger electronic coupling matrix elements between close lying chains. A goal in the conducting polymer community has been to develop polymers with stronger π - π interacting building blocks, thus creating higher motilities and, possibly a truly delocalized transport regime similar to metals [Sirringhaus H. et al. 1999].

Since the discovery by Shirakawa it has been found that conducting polymers not only feature unusually high conductivities, but also are excellent materials for energy storage (high energy density batteries and supercapacitors), energy/information shunting (transistors), displays (LEDs and electrochromic devices), sensors (strain gauges, photo-detectors and chemical sensors) and actuators. Conducting polymers offer the designer a greater range of capabilities than silicon. It is possible that in the future integrated electro-chemo-opto-mechanical devices will be constructed entirely from conducting polymers, at very low cost.

¹ A hole is an abstract charge, which corresponds to a position where an electron is missing.

3.1.2 The doping process

The extended π -system of conjugated compounds is ultimately responsible for the generation of mobile carriers. In the states shown in Figure 3.1 the charge carrier delocalization is incomplete and the polymers are hence semiconductors. The oxidation levels have to be changed to lead to the creation of states between the conduction and valence bands. Note that in several polymers, the band gap can be completely eliminated upon full oxidation.

As mentioned in the previous Chapter the polymer oxidation states can be changed via doping, analogous to traditional semi-conductors such as silicon and germanium. The doping process may be achieved chemically, electrochemically, and by photon absorption. Of high interest to this work is that the doping level and hence the conductivity can be chemically and electrochemically switched. In the case of electrochemical doping, the material's oxidation state (doping level) can be switched continuously from a semiconductor to a metal via an electrical signal. This process is schematically depicted in Figure 3.2. Note that doping is typically reversible, and hence polymer transistors can be built which have electrochemically controllable resistance. A number of other properties change with doping level, including color and volume. The volumetric changes are made use of in traditional actuators such as polypyrrole (PPy) and polyEDOT.

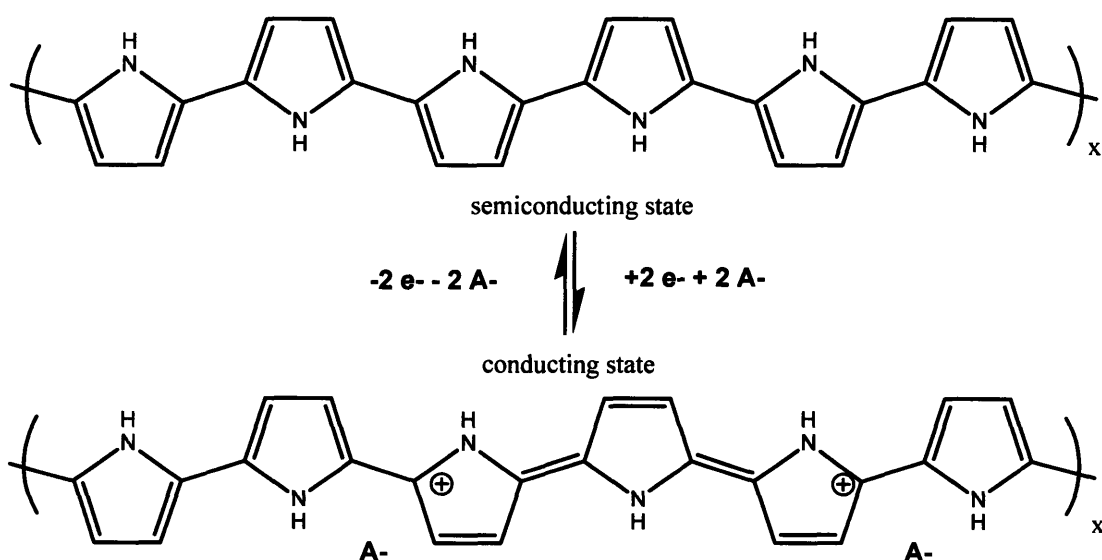


Figure 3.2: Electrochemical red-ox cycle for polypyrrole. A^- represents anions, and e^- electrons.

Ideally the extensions and contractions of actuators are electrically controlled. This allows interfacing with man made control systems and making use of the wealth of information processing tools that engineers possess². Electrochemical doping and undoping offers a means of switching the oxidation state of the artificial muscle and thus to control it electrically. Each potential versus a reference³ corresponds a different position or force that the artificial muscle can generate.

In an electrochemical configuration the conducting polymer material acts as a working electrode. There are two other electrodes in an electrochemical cell. First the counter electrode, which allows closing the electrical circuit and offers a second interface for charge transfer between electrons (charges in the electrical wires) and ions (charges in the solution); and second the reference electrode³ providing a reference against which the potential of the working electrode is measured and controlled via a potentiostat⁴. Note however two important points. First the counter electrode can also be another conducting polymer electrode/actuator. Second there is not necessarily a need for a reference electrode to activate the conducting polymer actuator. The actuator material can also be controlled in a two cell system in which the counter electrode acts as a reference electrode [Lewis T.W. et al. 2001].

During electrochemical activation, the polymer electrode is first supplied with electrical charges. To compensate for this process and maintain the electroneutrality of the material ions diffuse into the polymer from the nearby electrolyte. The doping level is then precisely determined by the potential between the working (polymer) and counter electrode at electrochemical equilibrium, which is ideal for electrical control. Polymer-film displacements can be adjusted via potential or charge control. Electrochemical doping has also the advantage of assuring homogeneous doping of the material in comparison with

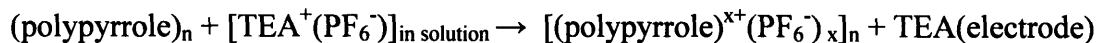
² Note that similarly muscles are controlled by electrical signals traveling through nerves.

³ A typical reference used is a so called reference electrode. These reference electrodes utilize the potential of a redox couple such as Ag/Ag^+ or K/K^+ as a reference point against which the potential of another electrode can then be measured. Ideally the reference electrode is assumed not to drift.

⁴ A potentiostat is a three terminal power supply. Two of the electrical terminal are comparable to a plus and minus of a classical power supply. The third terminal connects to the reference electrode. The potentiostat measures the potential of the working electrode via the reference electrode and controls this potential by adjusting the potential of the counter electrode. For more information on potentiostats including an electrical diagram the reader is referred to the works of Bard [Bard and Faulkner 1980].

chemical doping. Below is a schematic illustration of the red-ox doping mechanism in conducting polymers such as polypyrrole:

p-type doping mechanism:



n-type doping mechanism:



where TEA symbolizes tetraethylammonium and PF_6^- is hexafluorophosphate.

The discussion of the physical properties of conducting polymers will be further developed in the next section, where both passive and active properties will be presented.

3.2 Properties of Conducting Polymers

The supramolecular structure of conducting polymers is amorphous with substantial disorder. It is composed of an assembly of pseudo one dimensional conjugated chain molecules. Doping further increases the amorphous character of these materials. Material morphology has an impact on the performance. For example, conductivity is a property of the solid and thus a function of morphology: highly ordered packing of molecules typically leads to higher conductivities as electrons can move along one chain or hop from chain to chain while encountering fewer defects.

Two factors make conducting polymers an interesting class of materials. First as described in Chapter 2, they offer a very large degree of freedom in terms of synthesis possibilities. By assembling a combination of different building blocks many novel functional materials can be created. Second, the switchable nature of some of the physical properties of conducting polymers makes them very attractive, leading to the potential creation of whole biomimetic systems from the same material. Not only can actuators be created from these materials, but also sensors (chemical – nose, optical – retina), wires for energy or information delivery, to name a few.

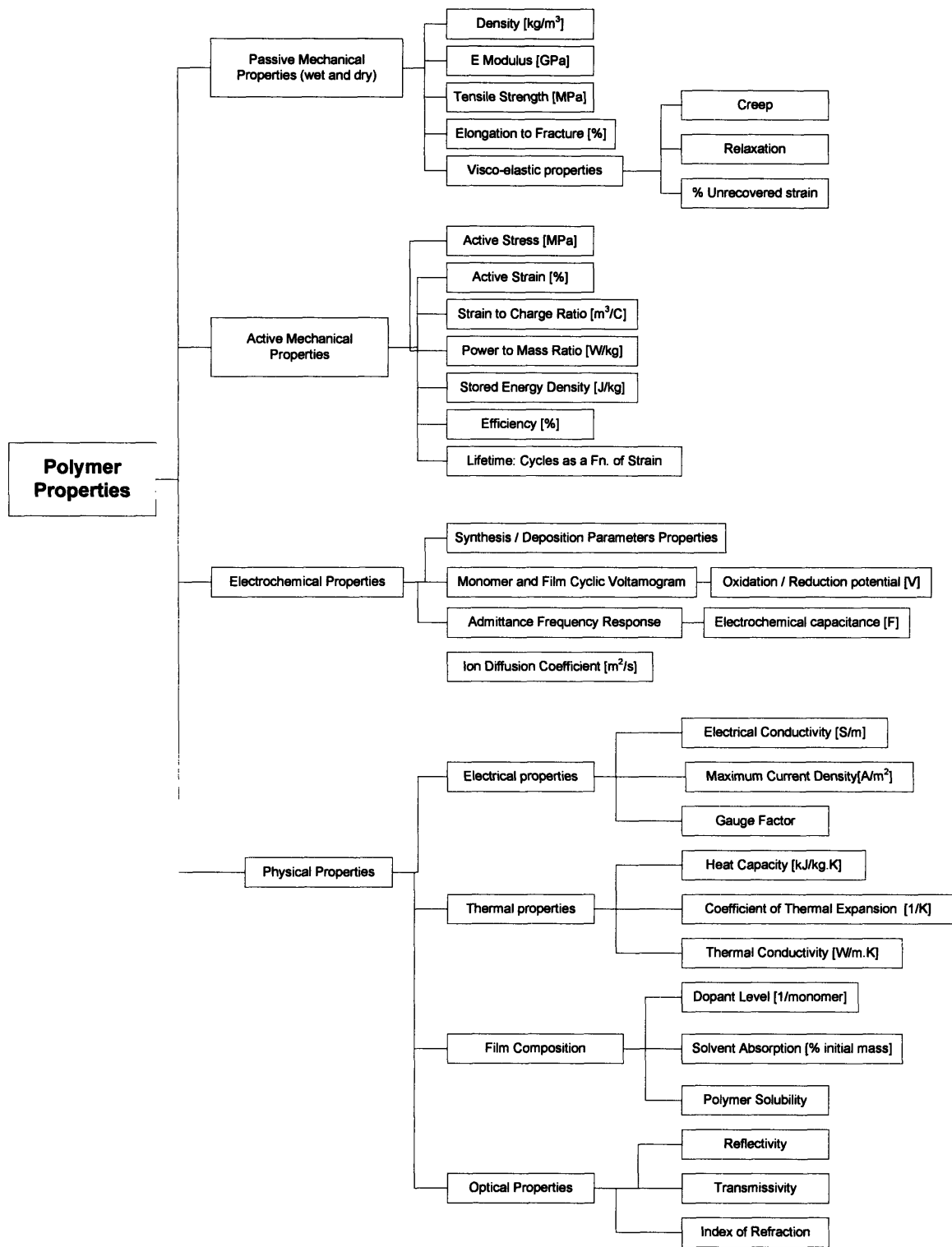


Figure 3.3: Overview of all conducting polymer properties relevant for the creation of actuators and all-polymer biomimetic systems.

Figure 3.3 shows an overview of all important properties of conducting polymers for the creation of such biomimetic systems. These are divided into passive and active mechanical properties, electrochemical properties as well as physical properties. Note that they are not all necessarily relevant for actuation. In this thesis, a plan is drawn up for creating large contraction conducting polymers via optimization of current contractile materials and synthesis of novel ones. These materials are then tested for active and passive mechanical properties.

3.3 Theoretical Evaluation of Conducting Polymer Actuators

Conducting polymer actuators need to convert electrical energy into mechanical energy to perform work when activated. Various models have been derived by previous workers to describe the electrical to mechanical energy conversion during actuation [Madden J.D. et al. 2000; Baughman R. H. 1996; Madden J.D. et al. 2002; Osada Y. and De Rossi D. 1999; Otero T.F. et al. 1995].

In this section the fundamental limits of current polypyrrole-based conducting polymer actuators are presented and the direction in which they shall be optimized derived. The subsequent subChapter shows how a material with optimal molecular design can theoretically have better performance in terms of active strain-rate, active strain, power output and efficiency.

3.3.1 *Limit in Strain Rate (Speed): Polymer Capacitance*

Based on a model describing the conducting polymer response to a command voltage, this section shows that the strain rate (i.e. the speed at which the polymer can contract and expand) is limited by the polymer electrical capacitance.

The electrochemical behavior of the polymer actuator in an electrolyte is modeled by a series of impedances and capacitances connected together in an electrical circuit (Figure 3.4). This model includes various resistances (contact, electrolyte and polymer resistances) as well as two types of capacitances: the double layer and bulk capacitances. When the polymer is initially activated, and the electrical circuit show in Figure 3.4 is closed, a charge double layer forms at the interface between charges at the polymer electrode (electrons) and charges in the solution (ions)⁵. This double layer effectively acts as a capacitor and is represented as the double layer capacitance in Figure 3.4.

Once the double layer capacitor is fully charged, it becomes more favorable for ions to diffuse from the ion-rich double layer into the polymer material. Ions will diffuse from the

⁵ Note that a double layer also forms at the counter electrode, but it is assumed not to be rate limiting via appropriate counter electrode design.

ion rich double layer into the polymer where they are stored between polymer chains. As a result, electrochemically activated conducting polymers effectively behave as three dimensional capacitors where charge is stored in the bulk polymer material and not at the surface of the electrode as is the case for electrolytic capacitors. [Baughman R. H. 1996].

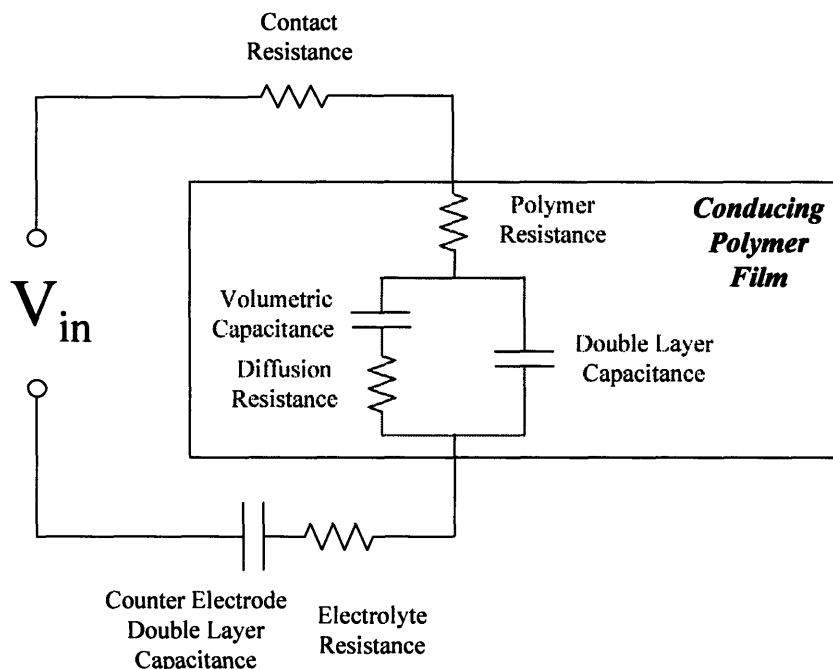


Figure 3.4: Circuit describing the electrochemical behavior of conducting polymer actuators.

The Helmholtz model for a parallel plate capacitor relates the double layer thickness δ to the double layer capacitance C_{dl} :

$$C_{dl} = \frac{\epsilon \cdot A}{\delta}, \quad (3.1)$$

where ϵ is the solvent dielectric constant and A the area. For example, propylene carbonate, a solvent used for electrochemical activation has a dielectric constant of 69. The double layer capacitance per unit area is typically between 0.1 and 0.4 F/m² [Bard and Faulkner 1980].

Let's define the specific capacitance of the polymer C_V (F/m³) as the ratio between the total volumetric capacitance, C and the polymer volume, V . The constitutive equation that relates the charge stored within the polymer to the applied potential is:

$$U_V = \frac{q}{C_V \cdot V}, \quad (3.2)$$

where U_V is the electrochemical potential at the polymer double layer, q is the charge stored in the polymer, C_V is the specific volumetric capacitance, and V is the polymer volume. The specific volumetric capacitance is determined by the ion concentration in the polymer double-layer, which depends on the size of the ions and the applied potential. In the potential range that most conducting polymers operate the specific volumetric capacitance can be considered constant.

$$C_V = \frac{q}{U_V \cdot V} \quad (3.3)$$

In his Ph.D. thesis, John D. Madden developed the diffusive elastic model, describing the electrical to mechanical behavior of a thin film of conducting polymer in the frequency domain [Madden J.D. and others 2000]. This model accurately predicts the behavior of conducting polymer actuators in electrolytes over 8 orders of magnitude in frequency, from 10⁻³ Hz to 10⁵ Hz.

The assumptions of the diffusive elastic model are:

- The polymer allows ions to diffuse in and out via its inherent porosity;
- No electron transfer (Faradaic reaction) takes place between the electrolyte and the polymer;
- Mass transport in the polymer is assumed to be slower than in the electrolyte;
- The potential throughout the thickness of the polymer is assumed to be constant;
- No mechanical visco-elastic properties of the polymer are accounted for;
- All processes are linear and time invariant.

The diffusive elastic model expresses the admittance⁶ of a conducting polymer film activated in an electrolyte as a function of the frequency [Madden J.D. 2000]:

$$Y(s) = \frac{s}{R} \cdot \frac{\frac{1}{\sqrt{\tau_{diff_dl}}} \cdot \tanh(\sqrt{s \cdot \tau_D}) + \sqrt{s}}{\frac{\sqrt{s}}{\tau_{RC_dl}} + s^{3/2} + \frac{s}{\sqrt{\tau_{diff_dl}}} \cdot \tanh(\sqrt{s \cdot \tau_D})}, \quad (3.4)$$

$$\text{with } I(s) = Y(s) \cdot U(s), \quad (3.5)$$

where s is the frequency domain variable, R is the total in-series resistance of the circuit (mostly dominated by the solution's resistance), C is the total volumetric capacitance, D is a coefficient characterizing the speed of diffusion of ions into the polymer, δ is the width of the double layer, and t is the thickness of the polymer. $I(s)$, the current output is related to the potential input $U(s)$ via the admittance transfer function $Y(s)$. The admittance transfer function results from the solution of the Fick diffusion equation [Bard & Faulkner] for a free standing film. From this equation the dynamic limitations of the polymer actuator become apparent and are associated with three time constants:

1. The charging of the double layer: $\tau_{RC_dl} = R \cdot C_{dl}; \quad (3.6)$

2. The diffusion of ions through the double layer thickness: $\tau_{diff_dl} = \frac{\delta^2}{D}; \quad (3.7)$

3. The diffusion of ions into the polymer: $\tau_D = \frac{t^2}{4 \cdot D} = \frac{1}{2 \cdot \pi \cdot f}; \quad (3.8)$

⁶ Admittance is the inverse of electrical resistance (Ω)

where t is the thickness of the polymer film, and f is the bandwidth of the ion diffusion process.

These three factors limit the rate of charge transfer into the polymer, leading to actuation. The first time constant, τ_{RC_dl} describes the RC charging of the double layer at the polymer/electrolyte interface. Notice that no charge transfer into the polymer (actuation) can occur until this double layer is charged. Madden showed how resistance compensation can sensibly reduce the double layer RC charging time constant, however at the expense of efficiency.

Once the double layer is charged, the next step involves the diffusion of ions through the double layer into the polymer. This process is characterized by τ_{diff_dl} (Equation 3.6). As the double layer thickness δ is typically very small (~ 1 nm), this process typically occurs very fast and is the theoretical ultimate limit of the activation speed of the polymer actuator. Assuming a diffusion constant $D = 7 \cdot 10^{-12} \text{ m}^2 \cdot \text{s}^{-2}$ [Madden J.D. 2000] leads to a maximal contraction bandwidth of 10^5 Hz.

Finally, the ions need to diffuse into the polymer bulk to charge it. This last step ultimately is the one that is physically responsible for actuation. This diffusion charging time constant τ_D is a function of the square of the thickness of the polymer. For a 20 μm thick polymer film, and assuming a diffusion constant $D = 7 \cdot 10^{-12} \text{ m}^2 \cdot \text{s}^{-2}$ [Madden J.D. 2000], τ_D is about 14 s. On the other hand, for a 2 μm thick film, the time constant for a full contraction decreases to 140 ms. Note that the charge and discharge rates in the kilohertz range have been demonstrated in 20-50 nm thick electrochemically driven conducting polymer transistors and electrochromic windows.

Note that there is also a volumetric RC charging time associated with the diffusion of ions into the bulk polymer. Indeed, conducting polymers have a very large capacitance per unit volume $C_v \sim 1.8 \cdot 10^8 \text{ F/m}^3$. A first order abstraction for the time constant for the volumetric RC charging is expressed by:

$$\tau_{RC} = \frac{d}{\sigma \cdot w \cdot t} \cdot C_v \cdot V, \quad (3.9)$$

where σ is the polymer's electrical conductivity, w the width, t the thickness and V the total volume of the polymer. The parameter d characterizes the longest pathway between a point on the polymer surface to the electrical contact point. For a long polymer film clamped and electrically connected at both ends, $d = \frac{l}{2}$, where l is the total length of the polymer film. In addition, if ions can diffuse into the polymer from both sides of the film, the effective thickness of the polymer becomes: $w = \frac{w_{film}}{2}$. For this case, Equation 3.9 becomes:

$$\tau_{RC} = \frac{l^2}{\sigma} \cdot C_V, \quad (3.10)$$

Example: for a 20 mm long, 2 mm wide and 20 μm thick film with an inherent conductivity of $4 \cdot 10^4$ S/m, τ_{RC} is 1.8 s. On the other hand, if the polymer film is deposited onto a conducting surface, Equation 3.8 becomes:

$$\tau_{RC} = \frac{t^2}{\sigma} \cdot C_V, \quad (3.11)$$

For the same polymer as the one presented in the example above, but where the entire polymer surface is connected onto a conducting electrode, τ_{RC} becomes $1.8 \cdot 10^{-6}$ s. For in depth analysis of the polymer charging and its modeling as a transmission line the reader is referred to Peter Madden's Ph.D. thesis [Madden P.G. 2003].

Table 3.1 summarizes the different values of the four different time constants for a typical film of polypyrrole with 20 mm length, 2 mm width and 20 mm thickness and connected electrically at both ends.

Based on the analysis of the four time constants governing the polymer actuator activation, strategies to increase actuator speed include:

- Reduction of the polymer thickness t to minimize τ_D and τ_{RC} . As was presented in this section decreasing the polymer thickness by a factor two results in a four times increase in polymer speed.

- Improvement of diffusion constant D for ions diffusing into the polymer to minimize τ_D . The diffusion constant is related to materials property. Rational polymer design can address the improvement of this property.

- Minimization of series resistance R (which includes polymer, polymer/wire contacts and electrolyte conductivity) to minimize τ_{RC_dl} and τ_{RC} . Polymer conductivity is an important parameter for actuation that is also addressed via molecular design and synthesis. In addition the electrolyte resistance can be compensated via a shaped potential activation waveform (Madden waveform [Madden J.D. and others 2000]).

- Minimization of the double layer thickness δ by decreasing the dielectric constant ϵ of the electrolyte. As is presented in this thesis, the conducting polymer actuators are multi-component electrochemical systems, where not only material properties, but also the counter electrode, the electrolyte and the activation input have to be optimized.

Time constants	Value	Remarks
Diffusion of ions in polymer: τ_D	14 s	Dominant rate limiting factor
RC charging of polymer: τ_{RC}	1.8 s	
Double layer charging: τ_{RC_dl}	$4 \cdot 10^{-4}$ s	100 Ω solution resistance
Diffusion of ions through the double layer: τ_{diff_dl}	$1.4 \cdot 10^{-7}$ s	Ultimate limit with a 1 nm thick double layer

Table 3.1: Summary of the time constants associated with each process involved during actuation for a 20 mm long, 2 mm wide and 20 μm thick film.

3.3.2 Limit in Strain

From the model presented in the previous section, we know that actuation is achieved and governed by the diffusion of ions into the polymer upon electrochemical charge buildup at the polymer electrode. Ion concentration at the electrode is controlled by the potential

applied to the electrode. Diffusion of ions into the polymer leads actuator volume change. For a long and slender film, most of the volume change will be apparent along the length of the film. Linear strain is defined as the change in length of the polymer:

$$\varepsilon = \frac{\Delta l}{l} = \frac{l - l_{contracted}}{l}, \quad (3.12)$$

where l is the total length of the film and $l_{contracted}$ its contracted length. For small strains, it can be experimentally demonstrated that strain ε is linearly proportional to charge ratio ρ [Madden J.D. 2000]. This proportionality constant is the strain to charge ratio α (m³/C). The strain to charge ratio is thus the parameter that characterizes the electrical to mechanical energy conversion in the polymer film. For a long polymer film, held at a constant stress σ , the overall strain response becomes:

$$\varepsilon(\rho) = \frac{\sigma}{E} + \alpha \cdot \rho, \quad (3.13)$$

where σ is the applied stress, E is Young's modulus, ρ is the input charge per unit volume and α is strain to charge ratio. $\frac{\sigma}{E}$ represents the passive response to a load, while $\alpha \cdot \rho$ is the active response.

It becomes clear that one strategy to improve the strain response of conducting polymer actuators is to improve their strain to charge ratio by rational material design at the molecular level. An alternative way to improve active strain which is not directly represented by Equation 3.13 is to increase the amount of charge that a polymer can accept. Molecular design can also be of help to address material stability under high charging.

3.3.3 Stored Energy Density and Efficiency

The electrochemical energy stored in the EAP actuator is readily obtained from Equation 3.2. The electrical potential energy is found by integrating potential with respect to charge while assuming constant volume:

$$E_{elec} = \int U_V(t) \cdot I(t) \cdot dt \quad (3.14)$$

The stored elastic energy density in the polymer actuator is expressed by:

$$E_{elast} = \int \sigma \, d\varepsilon = \frac{1}{2} E \cdot \varepsilon^2, \quad (3.15)$$

Incorporating the strain to charge ration, (3.15) becomes:

$$E_{elast} = \int \sigma \cdot \alpha \cdot I(t) \cdot dt. \quad (3.16)$$

The expression for the electrical to mechanical efficiency η is given by:

$$\eta = \frac{\int \sigma \cdot \alpha \cdot I(t) \cdot dt}{\int U_v(t) \cdot I(t) \cdot dt} \quad (3.17)$$

Equation 3.17 then reduces to:

$$\eta = \frac{\sigma \cdot \alpha}{U_v}. \quad (3.18)$$

The expression for the electrical to mechanical efficiency is maximized at large loads, high strain to charge ratios α and for small activation voltages U_v . For a polypyrrole actuator at a typical load of 2.5 MPa, a strain to charge ratio of $1.3 \cdot 10^{-10} \text{ m}^3/\text{C}$, and at an activation voltage of 0.5 V, the efficiency becomes: $\eta = 0.65 \%$.

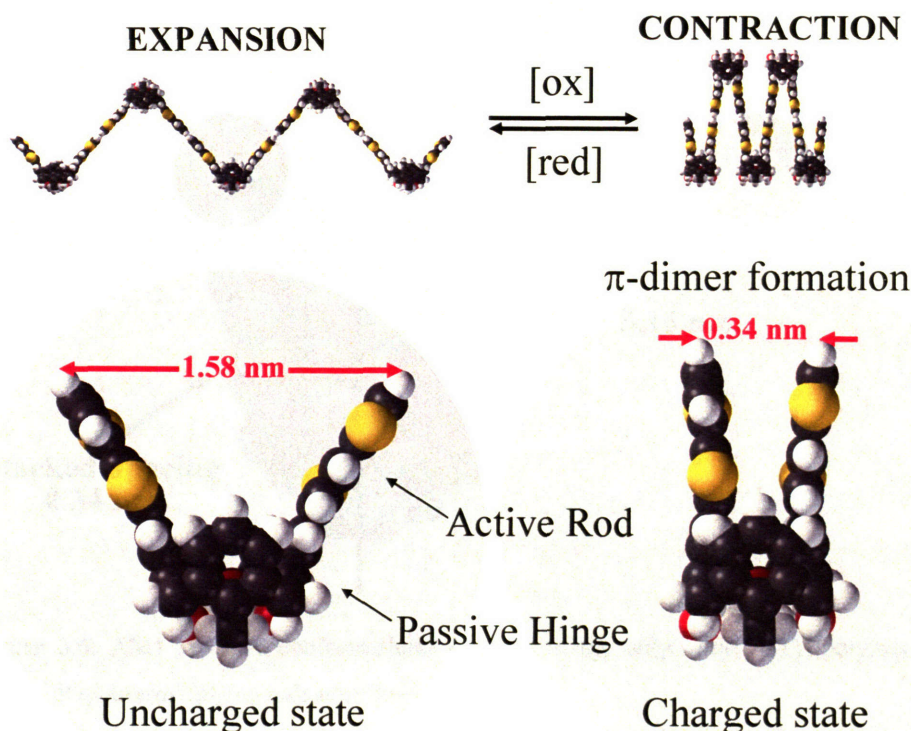
In the case of polypyrrole actuators the low electrical to mechanical coupling is clearly defined by the low strain to charge ratio parameter. Note that most of the electrical energy is not converted to mechanical work, but rather stored in the large electrical capacitance of the material as charge. Methods to recover the stored charge to improve efficiency have also been proposed by Madden [Madden J.D., 2000]

The small degree of electromechanical coupling in polypyrrole actuators leads to the need to design molecules that maximize energy transduction. Molecules presented in the following section intend to address this point.

3.4 Analysis of Poly(calix[4]arene *bis*-bithiophene) as an Actuator

3.4.1 π - π Dimerization as Molecular Actuation Driving Force

In this section, the actuation principle of poly(calix[4]arene *bis*-bithiophene) (poly(calixBBT)) and the theoretical prediction of its performance are presented. Poly(calixBBT) is a promising novel molecule. It employs passive hinge molecules (calix[4]arene) interconnected by conducting rigid rods (quarterthiophene). The cone conformation of the calix[4]arene scaffold allows the formation of an accordion-like molecule upon monomer polymerization.



Yu H.-h., Xu B., Swager, *J. Am. Chem. Soc.* **2003**, 125, 1142-1143
MIT Technology Review, October **2002**.

Figure 3.5: Schematic presentation of calix[4]arene-based hinge actuators.

Calix[4]arenes are known to be macromolecular structures with a flexible backbone, capable of undergoing passive conformational changes. As shown in Figure 3.5 the calix[4]arene scaffold serves as a hinge linking two conducting polymer rods together

(quarterthiophenes). In the neutral state, the system is relaxed and the distance between the two distal positions of the rods is 3.15 nm (obtained from AM1 calculations⁷) Figure 3.6. Upon oxidation π -dimers / π -stacks form among the quarterthiophene rods. Under the most optimal circumstances, the distance between the quarterthiophene rods reduces to 0.34 nm, resulting in a large polymer backbone deformation.

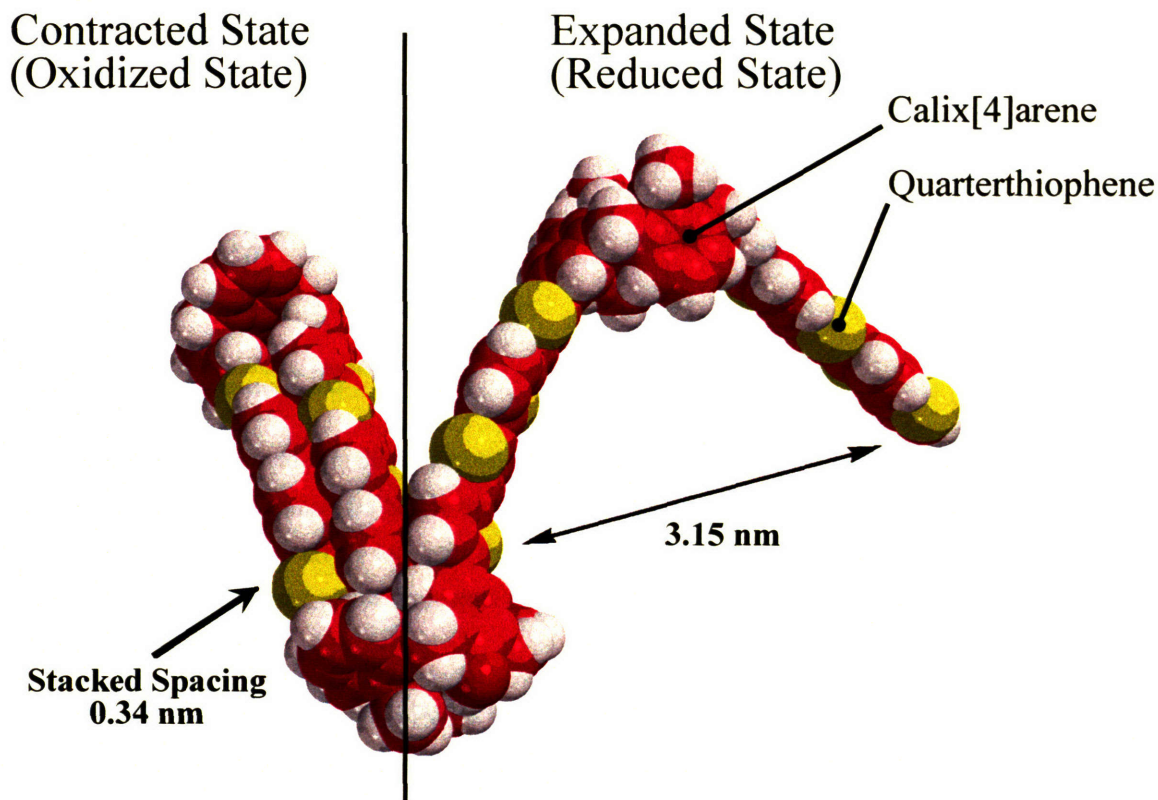


Figure 3.6: AM1 modeled conformational changes of the poly(calix(BBT)) polymer. Note that in this model the full quarterthiophene rods are shown.

The π -stacked structure is typical of oxidized thiophene oligomers and has been studied experimentally (by means of X-ray diffraction, STM) as well as theoretically [Azumi R. et al. 1999; Brocks G. 2000; Graf D.D. et al. 1996; Kingsborough R.P. and Swager T.M. 1999; Sirringhaus H. and others 1999].

⁷ Austin Model 1.

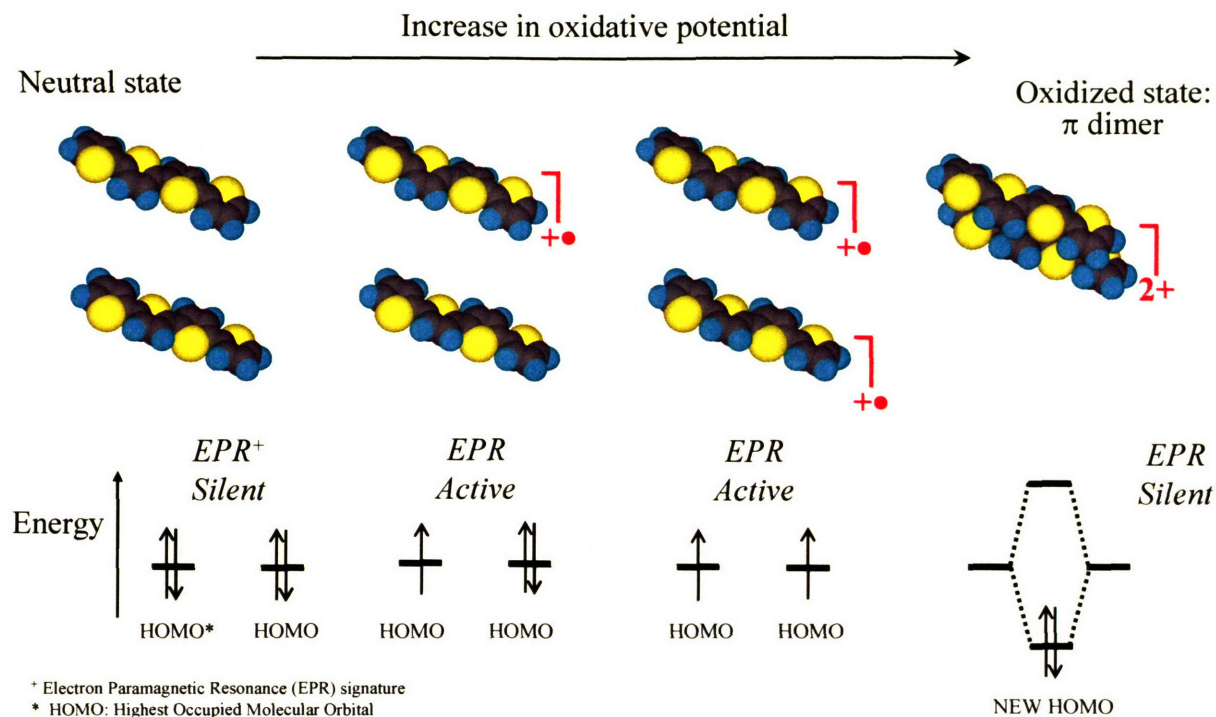


Figure 3.7: Mechanism of π - π dimer formation in quarterthiophene. The corresponding EPR spectroscopic signature is schematically represented below the 3D space filling molecular model. Each arrow represents the spin of an electron. A double arrow indicates that the Highest Occupied Molecular Orbital (HOMO) is fully occupied (EPR silent). A single arrow represents an unpaired spin or radical cation that is observable by EPR spectroscopy (EPR active).

As shown in Figure 3.7, oxidation of two adjacent quarterthiophene molecules creates two radical cations with slightly occupied Highest Occupied Molecular Orbitals (HOMOs). The spin of this state is observable by means of EPR spectroscopy due to the presence of an unpaired electron in the π -system of both oxidized molecules (EPR active). With further oxidation, both HOMO orbitals mix to produce a new doubly occupied molecular orbital at lower energy. The formation of this new molecular orbital provides stabilization of the π -dimer as the electronic energy of the charged quarterthiophene groups has been lowered. Unlike the singly occupied molecular orbitals, the π -stacked structure is EPR silent due to the electron spin pairing. This process is reversible and described in Equation 3.19.



where QT describes a quarterthiophene molecule.

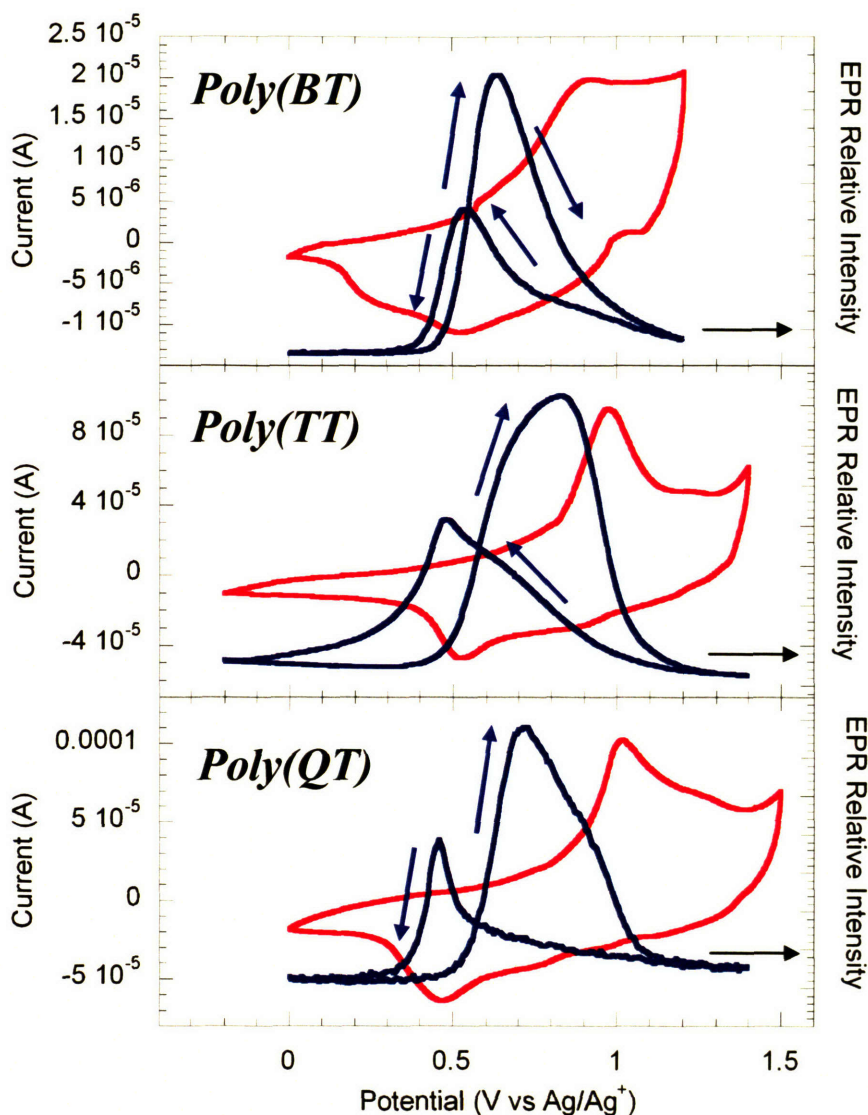


Figure 3.8: Cyclic voltammetry (at 100 mV/s) / *in situ* EPR combined experiments for various thiophene-based polymers polymerized from the following monomers: bithiophene (poly(BT)), terthiophene (poly(TT)) and quarterthiophene (poly(QT)). Data courtesy of Hsiao-hua (Bruce) Yu.

Evidence of a reversible transformation between π -stacked and un-stacked conformations as oxidation state is altered is obtained using EPR spectroscopy. Figure 3.8 shows the difference of the EPR signal during a 100 mV/s swept cyclic potential (0 V to 1.5 V vs. Ag/Ag⁺) for polymers polymerized from the monomers: bithiophene (poly(BT)), terthiophene (poly(TT)) and quarterthiophene (poly(QT)). Interestingly, the degree of π -stack stability in polythiophene is a function of the type of thiophene monomer used for

polymerization. Note the degree of the hysteresis that the EPR graph exhibit when poly(QT) is switched from its oxidized form to its reduced form during the reverse sweep (from 1.5V back to 0 V). Such hysteresis is barely observed for poly(BT) and poly(TT) whereas it spans 0.5 V for poly(QT).

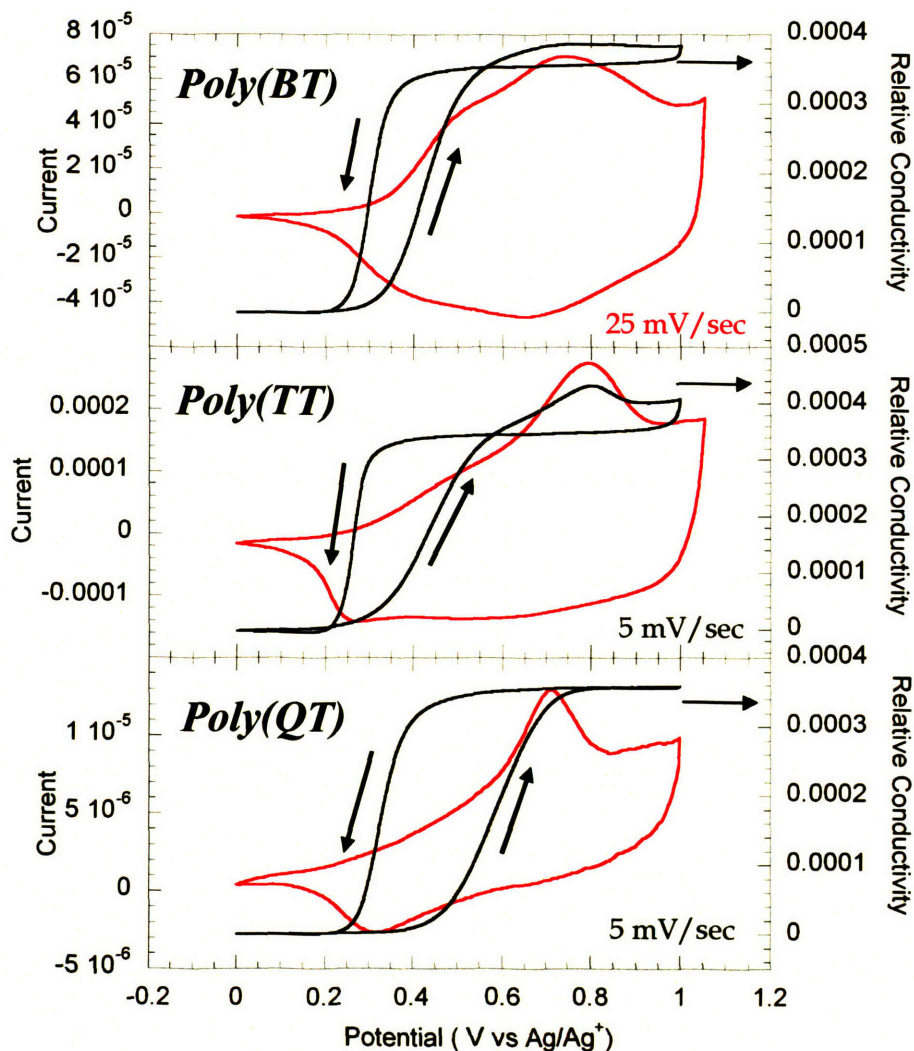


Figure 3.9: Cyclic voltammetry (100 mV/s) / *in situ* conductivity combined experiments for various thiophene-based polymers polymerized from the following monomers: bithiophene (poly(BT)), terthiophene (poly(TT)) and quarterthiophene (poly(QT)). Data courtesy of Hsiao-hua (Bruce) Yu.

The hysteresis effects during π -dimerization of poly(QT) are also easily observable by combined means of electrochemical cyclic voltammetry and *in situ* conductivity measurement. Interdigitated microelectrodes allow the measurement of film conductivity *in*

situ as a function of oxidation state. Films of poly(BT), poly(TT) and poly(QT) were cycled at 5 mV/s and 25 mV/s at potentials between 0 V and 1 V vs. Ag/Ag⁺ and their conductivity measured against a bias of 40 mV. Note the increase in the hysteresis in the relative conductivity graph in Figure 3.9 as a function of number of thiophenes used in the monomer (BT, TT or QT) prior to polymerization. The hysteresis observed during the reduction of poly(BT) to reverse it from an oxidized (conductive) state to a reduced state (insulated) requires 0.37 V whereas it requires almost twice as much to revert poly(QT) (0.5 V).

Such a large hysteresis indicates that more energy is required to switch poly(QT) from its oxidized state to its reduced state and vice versa, giving strong evidence that a more stable structure (possibly the π -dimer) has been formed as a result to the initial anodic potential sweep in which the quarterthiophene groups were oxidized. In other words, the higher stability of the π -dimer in poly(QT) makes the aggregated state harder to reduce, causing the large hysteresis in the current voltammogram. Such a behavior could be also attributed to electrochemical kinetic limitations such as electron transport or ion diffusion. However, the film relative conductivity is high over the entire potential range of the reduction sweep, indicating that such kinetic limitations do not take place.

3.4.2 Theoretical Performance Analysis of Poly(calixBBT)

In this section the upper-bound of the contraction energy of a repeat unit of calixarene bis-quarterthiophene (Figure 3.6) is analyzed. It is assumed that the π - π dimer formation of quarterthiophenes redox units is the driving force for actuation. For a detailed account of the calculations presented below, the reader is referred to Appendix B

Quantum Mechanical computer modeling and experiments shows that the barrier of dissociation of π -stacks for quarterthiophenes is about 3.6 kcal/mol ($2.5 \cdot 10^{-20}$ J, 0.16 eV) [Marzari N. and Scherlis D.A. 2003], [Brocks G 2001; Yamamoto T. et al. 1998]. It is also equivalent to $6.1 k_B T$ (where k_B is Boltzmann's constant and T is the absolute temperature; at room temperature $1 k_B T$ is $4.1 \cdot 10^{-21}$ J). Note that this energy value of is slightly larger than the Van der Waals bonding energy (~ 1 kcal/mole). Hence the π -dimer is considered to be an electro-reversible "low-energy" chemical bond. It is interesting to note that molecular

actuators found in nature operate within the same energy range (Chapter 2). The ATP synthase, for example - which is a 10 nm rotational ATP synthesizing molecular motor found in mitochondria, bacteria and chloroplasts - produces $20 k_B T$ of work per ATP synthesized (1/3 of rotation) [Elston T. et al. 1998]. Similarly, single actin-filament/myosin-head interaction in human skeletal muscle produces between 3 and $15 k_B T$ of work.

Quantum mechanical modeling also show that the quarterthiophene ends of poly(calix[4]arene-bithiophene) molecular actuator can theoretically contract by 2.81 nm upon oxidation (3.15 – 0.34 nm). Dividing the amount of work generated per monomer unit: $2.5 \cdot 10^{-20}$ J by the active molecular displacement (2.81 nm), it is estimated that a single molecule of calix[4]arene-quarterthiophene will produce at most 8.9 pN of average active force. Note that the poly(calixBBT) polymer can theoretically contract by 90% of its initial length in the direction of the polymer backbone

Likewise, the theoretical maximal efficiency of the calix[4]arene-quarterthiophene single actuating unit can be estimated. From the cyclic voltammogram of poly(calixBBT) (Figure 3.9), the difference between the oxidation and reduction potential is 0.5 V. Assuming that the removal of one electron is needed for two quarterthiophenes to form a π -stack we can estimate that the input energy to trigger actuation is $8 \cdot 10^{-20}$ J. Dividing the mechanical output energy by the input electrical energy allows one to estimate the efficiency of energy conversion to be 31 %.

Finally, the poly(calix[4]arene-bithiophene) is considered as a bulk material, to estimate the theoretical maximal average stress. This is computed, using the relationship the work per unit volume as stress times strain. Assuming that the actuator contracts by 20% strain on average, that it has a bulk density of 1400 kg/m^3 , a molecular weight of 1110 g/mole and that the energy for π - π stacking of 3.6 kcal/mol, the maximal average stress is found to be 95 MPa.

Polycalix(BBT) is material that shows theoretically great promise. Its theoretical performance combines large strains (up to 90 % along the polymer backbone), large stress (95 MPa at 20 % strain) and high efficiency (31 %). In the next Chapters the synthesis and experimental analysis of thiophene-based conducting polymer actuators will be presented.

3.5 Conclusion

The theoretical limitations of polypyrrole as an actuator were presented in this Chapter in terms of strain rate, maximal strain, stress and efficiency. Rational design of molecules such as the poly(calixBBT) that can be tailored at the molecular level theoretically leads to superior material performances. Upper theoretical bounds of the average performance properties of poly(calixBBT) were discussed. In the next section instruments needed to experimentally characterize conducting polymer actuators are discussed.

3.6 References

- Azumi R., Goetz G. and Baeuerle P., "Self-Assembly of Alkylsubstituted Oligothiophenes ", *Synthetic Metals*, **Vol. 101**, pp. 569-572, (1999).
- Bard, Allen J. and Faulkner, Larry R. *Electrochemical Methods, Fundamentals and Applications*. 1 ed. New York: Wiley; (1980).
- Basescu N. Liu Z. X. Moses D. Heeger A. J. Naarmann H., "High electrical conductivity in doped polyacetylene", *Nature*, **Vol. 327**, pp. 403-405, (1987).
- Baughman R. H. "Conducting Polymer Artificial Muscles", *Synthetic Metals*, **Vol. 78**, pp. 339-353, (1996).
- Beljonne D., Pourtois G., Silva C., Hennebicq E., Herz L.M., Friend R.H., Scholes G.D., Setayesh S., Muellen K. and Bredas J.L., "Interchain vs. Intrachain Energy Transfer in Acceptor-Capped Conjugated Polymers", *Proceedings of the National Academy of Science*, **Vol. 99**, (17): pp. 10982-10987, (2002).
- Brocks G., " π -dimers of oligothiophene cations", *Journal of Chemical Physics*, **Vol. 112**, (12): pp. 5353-5363, (2000).
- Brocks G, "Charged Oligothiophene Dimers and π -stacks: the Bipolaron Revisited", *Synthetic Metals*, **Vol. 119**, pp. 253-254, (2001).
- Elston T., Wang H. and Oster G., "Energy Transduction in ATP Synthase", *Nature*, **Vol. 391**, pp. 510-513, (1998).
- Graf D.D., Campbell J.P., Miller L.L. and Mann K.R., "Single-Crystal X-ray Structure of the Cation Radical of 3',4'-Dibutyl-2,5"-diphenyl-2,2'-terthiophene: Definitive Evidence for π -Stacked Oxidized Oligothiophenes", *Journal of the American Chemical Society*, **Vol. 118**, pp. 5480-5481, (1996).
- Ito T., Shirakawa H. and Ikeda S., "Simultaneous Polymerization and Formation of Polyacetylene Film on Surface of Concentrated Soluble Ziegler-Type Catalyst Solution ", *Journal of Polymer Science, Part A: Polymer Chemistry*, **Vol. 12**, (1): pp. 11-20, (1974).
- Kingsborough R.P. and Swager T.M., "Polythiophene Hybrids of Transition-Metal Bis(salicylideneimine): Correlation between Structure and Electronic Properties", *Journal of the American Chemical Society*, **Vol. 121**, (38): pp. 8825-8834, (1999).
- Lewis T.W., Spinks G.M., Wallace G.G., Mazzoldi A. and De Rossi D., "Investigation of the Applied Potential Limits for Polypyrrole when Employed as the Active Components in a Two-Electrode Device", *Synthetic Metals*, **Vol. 122**, (2): pp. 379-385, (2001).
- Madden J.D., Cush R.A., Kanigan T.S. and Hunter I.W., "Fast Contracting Polypyrrole Actuators", *Synthetic Metals*, **Vol. 113**, pp. 185-192, (2000).
- Madden J.D., Madden P.G. and Hunter I.W., "Conducting Polymer Actuators As Engineering Materials", *Smart Structures and Materials 2002: Electroactive Polymers Actuators and Devices*, Yoseph Bar-Cohen, Editor, *Proceedings of the SPIE*, **Vol. 4695**, pp. 176-190, (2002).
- Madden P.G., "Development and Modeling of Conducting Polymer Actuators and the Fabrication of a Conducting Polymer Based Feedback Loop", *MIT Ph.D. Thesis*, (2003).
- Marzari N. and Scherlis D.A., *MIT*, *Private Communications*, (2003).

- Osada Y. and De Rossi D., "Polymer Sensors and Actuators (Macromolecular Systems, Materials Approach)", *Springer-Verlag Telos*, (1999).
- Otero T.F., Grande H. and Rodriguez J., "A new model for electrochemical oxidation of polypyrrole under conformational relaxation control", *Journal of Electroanalytical Chemistry*, Vol. 394, pp. 211-216, (1995).
- Roth S., "One-Dimensional Metals: Physics and Material Science", *VCH, Weinheim; New York; Basel; Cambridge; Tokyo*, pp. 111-148, (1995).
- Shirakawa H., Louis E.J., MacDiarmid A.G., Chiang C.K. and Heeger A.J., "Synthesis of Electrically Conducting Organic Polymers - Halogen Derivatives of Polyacetylene", *Journal of the Chemical Society - Chemical Communications*, Vol. 16, pp. 578-580, (1977).
- Sirringhaus H., Brown P.J., Friend R.H., Nielsen M.M., Bechgaard K., Langeveld-Voss B.M.W., Spierling A.J.H., Janssen R.A.J., Meijer E.W., Herwing P. and de Leeuw D.M., "Two-Dimensional Charge Transport in Self-Organized, High-Mobility Conjugated Polymers", *Nature*, Vol. 401, pp. 685-689, (1999).
- Yamamoto T., Kamarudin D., Arai M., Lee B.-L., Suganuma H., Asakawa N., Inoue Y., Kubota K., Sasaki S., Fukuda T. and Matsuda H., "Extensive Studies of π Stacking of Poly(3-alkylthiophene-2,5-diyl)s and Poly(4-alkylthiazole-2,5-diyl)s by Optical Spectroscopy, NMR Analysis, Light Scattering Analysis, and X-ray Crystallography", *Journal of the American Chemical Society*, Vol. 120, pp. 2047-2058, (1998).

Chapter 4

Experimental Methods for Polymer Characterization

4.1 Methodology

One goal of this thesis is to study, for the first time, novel functional materials that are optimized for efficient electrical to mechanical energy conversion. Within this framework, a feedback loop methodology for novel materials discovery was implemented. This loop is multidisciplinary and makes use of advances in mathematics, organic chemistry, synthesis and processing, and finally instrumentation. In return, discoveries made through the primary feedback loop contribute to advances in all these disciplines. The feedback loop methodology for new materials discovery is divided into four steps, schematically summarized in Figure 4.1:

1. *Monomer Design and Synthesis:*

Materials are first designed at the molecular level and synthesized into monomers using advances in molecular organic chemistry. This step was carried out by members of the Swager laboratory at the MIT Department of Chemistry, in particular by Hsiao-hua (Bruce) Yu, Michael Bushel, Brad Holiday and Jocelyn Nadeau.

2. *Synthesis (polymerization) of mechanically strong free standing film or fiber:*

Conducting polymer actuators are typically used in the form of thin (20 μm) film. The creation of a mechanically strong freestanding polymer film from a monomer created in step 1 is the first crucial step in studying muscle-like actuators. Note that without this first step, no mechanical properties (passive or active) can be tested.

3. *Characterization of passive and active (contractile) mechanical properties of the novel polymer films:*

Once good quality films are obtained, the third step of the methodology comprises characterizing these novel contractile films, where relevant mechanical, electrical, and electrochemical properties relevant to actuation are being assessed. As a result, a conducting polymer actuator testing protocol, seeking the relevant physical properties of these materials, was developed in this thesis.

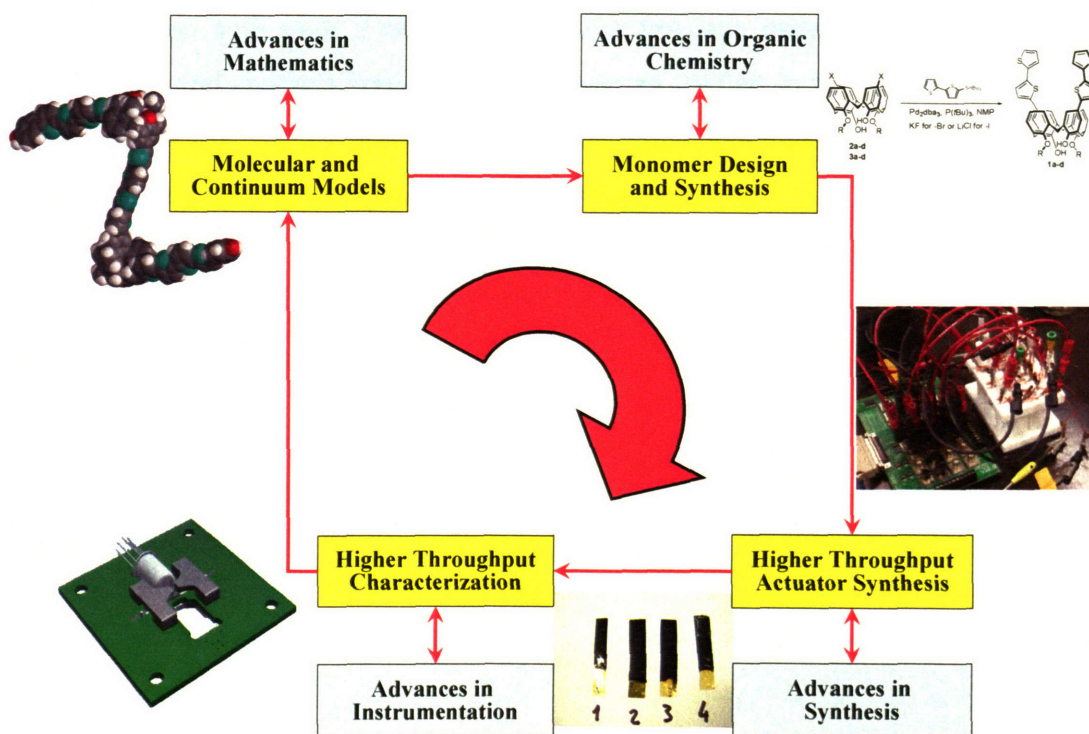


Figure 4.1: Conducting polymer molecular actuator research methodology and its multidisciplinary implications. The higher throughput fiber characterization apparatus on the bottom left of the figure is courtesy of Michael Garcia-Webb of the MIT BioInstrumentation Laboratory.

4. *Actuator modeling*

Following actuator testing is the actuator modeling step, whose goal is to reveal important material parameters, allowing predictions of actuator behavior. Modeling also enables material optimization for the next generation of molecular design, thus closing the design-synthesis-characterization feedback loop (Figure 4.1). Ideally, actuator modeling takes place both at the molecular and mesoscopic level.

This Chapter outlines the experimental methods and apparatus used to determine fundamental conducting polymer properties, relevant to actuation (Figure 3.3, Chapter 3). These include active properties such as active stress, active strain, strain rate, power to mass ratio, life cycle, and efficiency, and passive mechanical and physical properties such as tensile strength, Young's modulus, elongation to break, and conductivity. The emphasis of this thesis is laid on both steps 2 and 3 of the novel polymer material discovery loop, i.e. polymer synthesis and characterization. The monomers studied in this work were designed and synthesized by the Swager group at MIT. Molecular modeling of these materials was performed in-part by the Marzari group (MIT Material Science).

4.2 Electrochemical Synthesis Methods

As stated in Chapter 3, conducting polymer actuators are activated electrochemically using electrons as the source of energy. To study these active materials, electrochemical methods are employed. Cyclic voltammetry, for example, a dynamic electrochemical method, reveals the response of the conducting polymer actuator under a cycled (saw tooth pattern) potential. Data obtained from these electrochemical techniques provide kinetic and thermodynamic information about the nature of the electrochemical processes occurring within a polymer film or any electroactive species in solution. In this thesis, a wide variety of traditional and newly developed electrochemical methods were utilized. These techniques as well as their background and experimental details are summarized in this section.

4.2.1 Electrochemical Cells

A typical cyclic voltammetric experiment is performed in a three-electrode cell as shown in Figure 4.2. It is composed of one working electrode (WE), one counter electrode (CE), and one reference electrode (RE) in an aqueous or non-aqueous solution containing electrolyte.

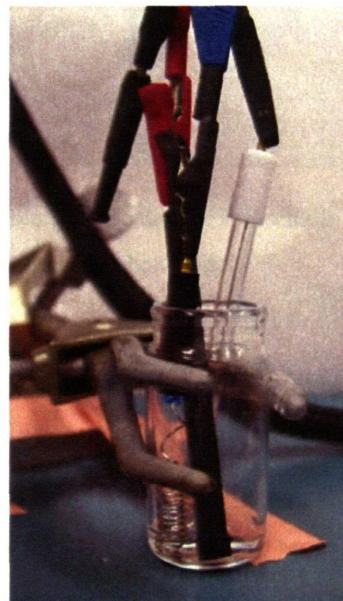
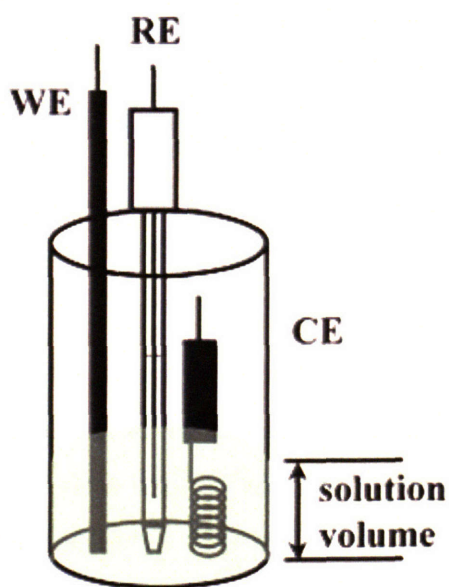


Figure 4.2: Schematic and photograph of a three electrode electrochemical cell, consisting of a working electrode (WE), a counter electrode (CE) and a reference electrode (RE).

4.2.1.1 Working Electrodes

Different materials and shapes can be used as working electrodes (WE) depending on the purpose of the experiment. Button electrodes as shown in Figure 4.2 are commonly used in standard cyclic voltammetry. They generally employ platinum (Pt), gold (Au), or glassy carbon, as the electrical material for the conducting surface. In a typical CV experiment, the CE should possess at least double the surface area of the WE in order to ensure that charge balancing issues at the counter electrode will not influence the reaction taking place at the working electrode that the CV technique is attempting to reveal. This requirement is easily met while using the button electrodes that have small surface areas. Button electrodes also require less electroactive material, critical when the material of interest is rare or difficult to synthesize.



Figure 4.3: Electrochemical cell designed to handle disposable gold-coated PET electrode films (left) and resulting conducting polymer (black film) resulting from a deposition (right-hand side).

To produce freestanding films for mechanical measurements, gold and stainless steel substrates are found to be suitable. As shown in Figure 4.3, gold can be thermally evaporated onto glass with an adhesive layer of Al or Cr. Typical thickness is 10 nm of adhesion layer and about 100 nm of evaporated gold. A conductive layer can also be evaporated onto flexible poly(ethylene terephthalate) (PET) films. This technique has the benefit that the electrodes are disposable and thus a fresh non-contaminated electrode can be used for each experiment. This is very relevant for the precise characterization of novel

polymers such as quarterthiophene or poly(calix[4]arene *bis*-bithiophene) where contaminants on the electrode may distort the electrochemical response of the polymer film under study.

In order to maintain a desired cell geometry, holders made of Teflon were created. These allow maintenance of a parallel alignment of the WE relative to the CE. The Teflon spacer also allows varying the distance between the two electrodes (Figure 4.4).

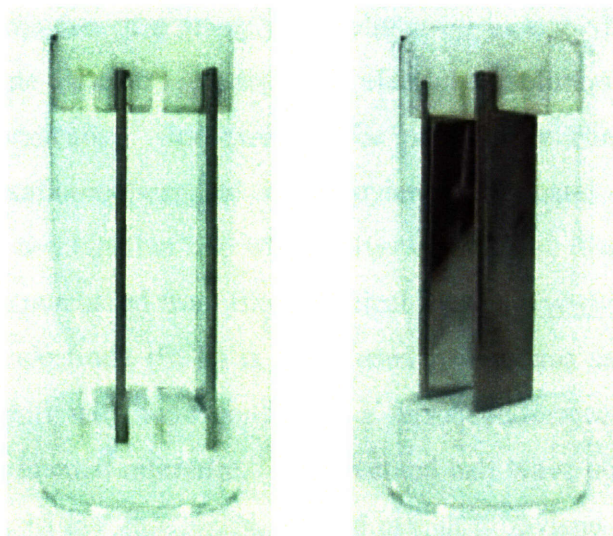


Figure 4.4: Electrochemical cell for precise control of the WE / CE spacing.

Another type of electrode for electrochemical study of conducting polymer is the interdigitated microelectrode (IME, Figure 4.6) which allows study of the conductivity of the polymer *in situ* as a function of oxidation potential. Note that conductivity is very relevant in the study of conducting polymers as these materials can be switched from a highly conductive to an insulator form as a function of their oxidation state. These electrodes are further discussed in Section 4.2.4.

Finally, platinum wires can be used as working or counter electrodes. For example, platinum wires were used as the working electrodes for *in situ* conductivity and *in situ* EPR experiments described in section 4.2.5.

4.2.1.2 Reference Electrodes (RE)

Reference electrodes use the potential of an arbitrary redox couple as a reference against which other electrochemical potentials are measured. Typically, all electrochemical reactions are referenced against the H/H^+ couple, called the standard hydrogen electrode. For practical reasons, however, as the standard hydrogen electrode is difficult to construct and to utilize, other reference electrodes are assembled from different redox couples. The most common reference electrode for non-aqueous solutions makes use of the Ag/Ag^+ redox couple. The electrode consists of a silver wire submerged in a mixture of 0.01 M silver nitrate or silver perchlorate dissolved into the same electrolyte solution used for the reaction to be studied electrochemically. For example for polypyrrole characterized in 0.1 M tetraethylammonium hexafluorophosphate in propylene carbonate, one would use the identical solvent and salt combination into which silver crystals are dissolved. Non-aqueous reference electrodes were purchased from BioAnalytical Systems (www.bioanalytical.com).

A saturated calomel electrode (SCE) is often used in aqueous solution. Because the Ag/Ag^+ reference can shift with time condition, a ferrocene/ferrocenium (Fc/Fc^+) redox couple can be used as an internal reference. The accepted half wave potentials of Fc/Fc^+ are *ca.* +225 mV in CH_2Cl_2 , +5 mV in CH_3CN , and +8 mV in propylene carbonate (PC). The Ag/Ag^+ reference electrode can then be easily referenced against Fc/Fc^+ .

4.2.1.3 Counter Electrodes (CE)

The typical material for the counter electrode is platinum in the form of a coil or gauze. Large stainless steel plates can also be used and offer a cheaper means of constructing large counter electrodes. The important point to remember is that the surface area of the counter electrode needs to be at least double that of the working electrode to ensure that the reaction one studies at the working electrode is not limited at the counter electrode.

4.2.2 Electrochemical Characterization: Potential Sweep - Cyclic Voltammetry (CV)

Cyclic Voltammetry (CV) is one of most frequently used methods to characterize electrochemically active species. In this experiment, a triangular-wave potential is applied to

an electrochemical cell (Figure 4.2). The potential of the working electrode is swept linearly between positive and negative voltages with respect to a reference electrode. The rate of the sweep can also be varied and allows the dynamics of the electrochemical system to be probed.

A typical reversible solution-phase cyclic voltammetric experiment results in “goose-head” shaped curves. The dynamics of the diffusion processes that occur during a CV experiment are well developed and extensively discussed in Bard & Faulkner work [Bard and Faulkner 2000].

4.2.3 *Electrochemical Synthesis*

Electrochemical synthesis of conducting polymers can occur via constant potential (potentiostatic), constant current (galvanostatic) and via potential sweep depositions. Potentiostatic depositions allow precise control of the deposition potential at the working electrode, thus preventing overoxidation of the polymer and monomer. On the other hand, galvanostatic deposition allows precise control of the rate of deposition of the polymer, while letting the potential at the working electrode rise as more film is deposited and the resistance of the whole film rises. Galvanostatic depositions typically lead to high quality films, but the final potential has to be limited in order to prevent overoxidation of the newly-formed polymer film. Finally, sweep potential techniques (potentiodynamic) in which the film is cycled between an oxidative and reductive potential as it is synthesized leads to homogenous conducting polymer films. Cycling the deposition potential leads to an homogenous molar composition of salt and monomer solution at the working electrode. A problem of potentiodynamic techniques, though, is that the current is not precisely controlled and ultimately limited as the resistance of the synthesized film rises. As a result, films of high thickness ($> 10 \mu\text{m}$) are difficult to synthesize. Such limitations are addressed by galvanodynamic techniques pioneered by Vandesteeg [Vandesteeg N. 2003].

Chapter 5 extensively discusses the synthesis of conducting polymer films. As polymers are synthesized, it is important to digitally record deposition parameters into synthesis databases so that a fingerprint of each film synthesized can be stored. These parameters

typically include: deposition current, deposition potential and temperature as a function of time.

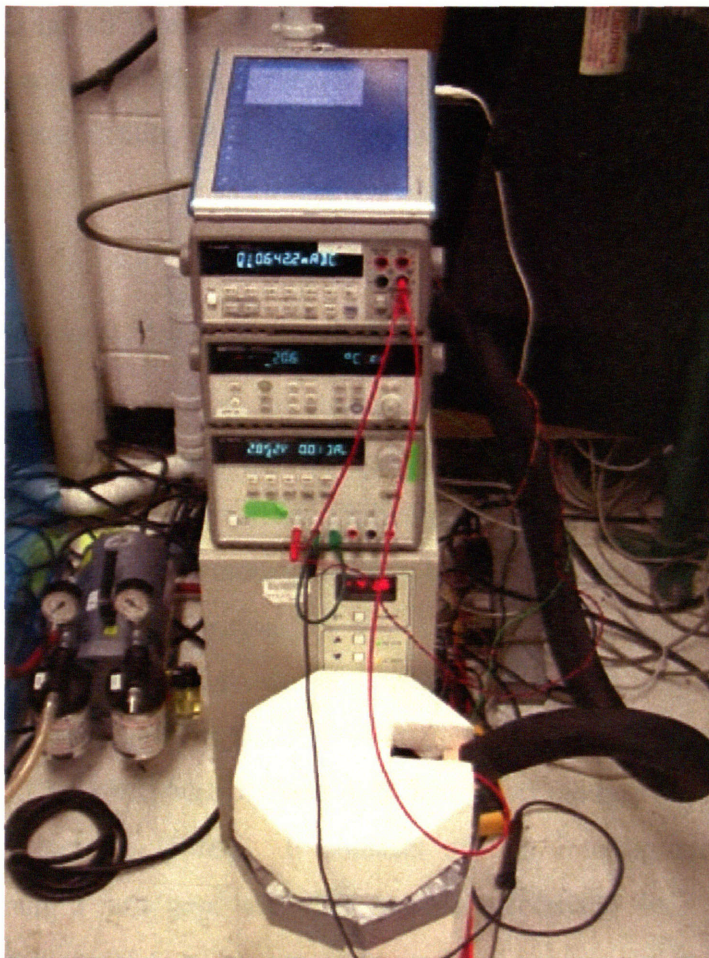


Figure 4.5: Scientific instruments controlled by tablet PC (from top to bottom: Agilent 34401A Digital Multimeter, Agilent 34970A Data Acquisition Switch with 34901A multiplexer card, and Agilent E3631A Power Supply).

Connection to synthesis instruments is made via the Agilent T&M Toolkit (www.agilent.com) allowing a USB to IEEE 488 computer to instrument connection. Instruments are then controlled via an interface programmed in Microsoft Visual Studio .NET (www.microsoft.com) allowing potential, deposition current and temperature to be accessed. Figure 4.5 shows the three scientific instruments used to record deposition parameters. These include from top to bottom: the Agilent 34401A digital multimeter, the

Agilent 34970A data acquisition switch with 34901A multiplexer card, and the Agilent E3631A power supply, all connected to a tablet PC laboratory notebook, the iLabNoteBook (<http://bioinstrumentation.mit.edu>). The Agilent IntuiLink connectivity allows data to be inserted directly into an MS Word laboratory notebook page of the iLabNoteBook Tablet PC, thus creating a dynamic laboratory notebook. Appendix C, presents the concepts of the iLabNoteBook in greater details, while Appendix D shows a sample program used to control instruments via a Tablet PC during electrodeposition.

4.2.4 *In Situ Conductivity Measurement via Interdigitated Microelectrode*

There are multiple ways to measure conductivities of bulk materials. The four-point probe method is considered the most accurate (section 4.4). However, this technique cannot be performed easily on films under various applied potentials in an electrochemical cell. As the conductivity of conductive polymers varies as a function of oxidation state, it is important to be able to probe this parameter *in situ*.

In-situ cyclic voltammetric methods developed by Wrighton and coworkers allow to assess the conductivity of films as a function of applied potential [Kittlesen G.P. et al. 1984; Kittlesen G.P. and others 1984; MacDiarmid A.G. 2002]. At the heart of this technique is the interdigitated microelectrode (IME). It consists of two interdigitated electrode-halves separated by a small 5 μm gap, and that behave effectively like multiple two-point conductivity probes (Figure 4.6). They are composed of a substrate plate, a conducting layer (Pt, Au, or ITO) deposited through a shadow mask for creating the interelectrode spacing (5 μm) and an insulating layer (silicon nitride) covering the surface of the electrode except the contacts and the active interdigitated electrode regions. The IMEs were purchased from Abtech (www.abtechsci.com) and can be cleaned and used repeatedly.

The first step of the *in-situ* conductivity experiments consists of depositing a conducting polymer film onto interdigitated microelectrodes (Figure 4.6). Initially, the potential of the two halves of the interdigitated microelectrodes is set to the same value such that the device behaves as a normal working electrode. As a result, the potential difference V_D between the two halves of the microelectrodes is initially zero. Polymer films are then typically deposited

onto this electrode via potentiodynamic deposition (cyclic voltammetry) in a typical three-electrode electrochemical cell.

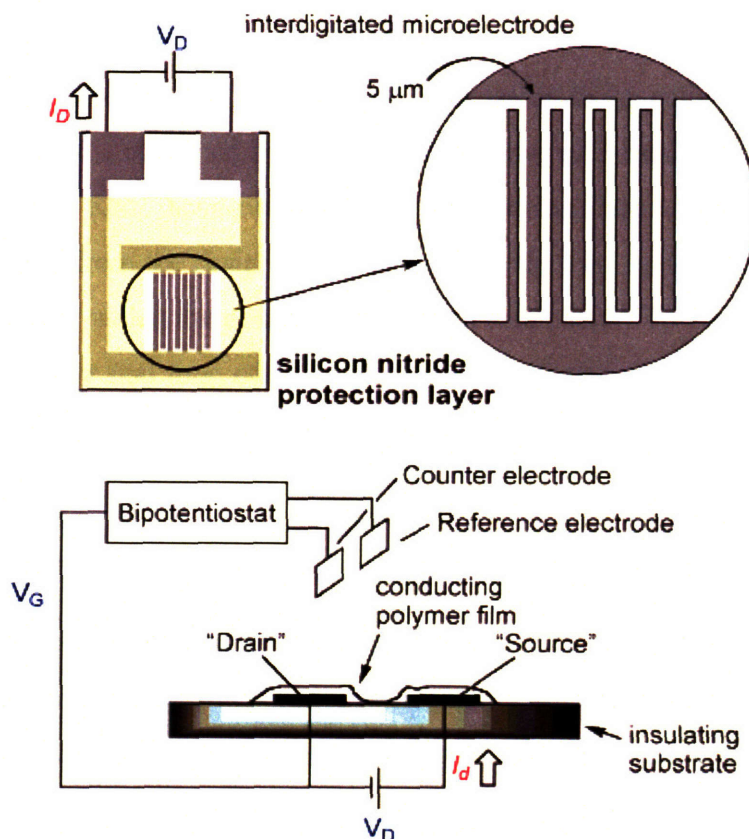


Figure 4.6: Top and side views of an interdigitated microelectrode used for *in situ* conductivity measurements [Kittlesen G.P. et al. 1984; Kittlesen G.P. and others 1984; MacDiarmid A.G. 2002]. Diagram courtesy of the MIT Swager Laboratory.

When performing conductivity experiments (as shown in Figure 4.6), a fixed potential difference, V_D (usually 40 mV), is applied between the two adjacent interdigitated electrodes, creating a potential difference across the polymer film. A bipotentiostat allows swiping of the potential of each half of the IME relative to an auxiliary reference electrode changing the oxidation state of the polymer while keeping V_D constant. When the polymer is in its conductive form, a current, I_D , flows between the source and drain electrodes and this is termed the drain current in early literature. The drain current obtained is proportional to the conductivity of the polymer, which can be easily determined by the following equation:

$$\sigma = \frac{i_D}{V_D} \cdot \frac{D}{n \times T \times L} \cdot A \quad (4.1)$$

where T is the polymer film thickness, D the size of the gap, n the number of gaps, L the electrode length, and A is a normalization factor.

The data obtained via the *in situ* experiment needs to be calibrated and interpreted carefully. Typically, it is corrected by an external standard of 3-methyl thiophene exhibiting a conductivity of $6 \cdot 10^3$ S/m. Scan-rate variation allows dissociation of the Faradaic response (scan rate dependent) from the drain current i_D between the two microelectrode halves (scan rate independent) from which the conductivity is then calculated. This method is very useful for obtaining qualitative real time conductivity values; however accurate quantitative data is difficult to obtain.

4.2.5 *In situ* EPR (Electron Paramagnetic Resonance) Experiment

During the electrochemical oxidation or reduction of a conducting polymer backbone, unpaired electrons are generated as positive or negative polarons. The nature and number of these radical cations or anions can be probed by *in situ* EPR spectroscopy.

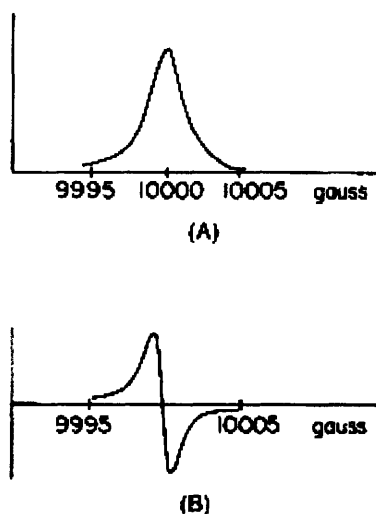


Figure 4.7: (A) A typical EPR signal and (B) its first derivative.

Like NMR, the EPR signal comes from stimulating a sample via an external magnetic field and recording its response. The basic experiment is performed by placing the sample in a microwave resonator between the poles of a magnet and adjusting the field strength until the sample absorbs microwaves. As the external field is swept, data is recorded typically as the first derivative of the number or intensity of the spins (Figure 4.7). The peak position of the EPR signals is generally reported as the g -value and is measured to an external standard. The most common standard is diphenylpicrylhydrazide (DPPH - $g = 2.0037$).

In order to minimize the absorption of microwaves by the solvent an EPR tube with a flat area containing a small volume of solvent is used in place of the normal quartz EPR tube (Figure 4.8). In the flat part of the EPR tube a working platinum wire electrode functionalized with a polymer film and the counter electrode are placed. The reference electrode is placed just above the flat portion of the cell. In this experiment, the extent of doping in the polymer is precisely controlled while the EPR signal intensity is recorded.

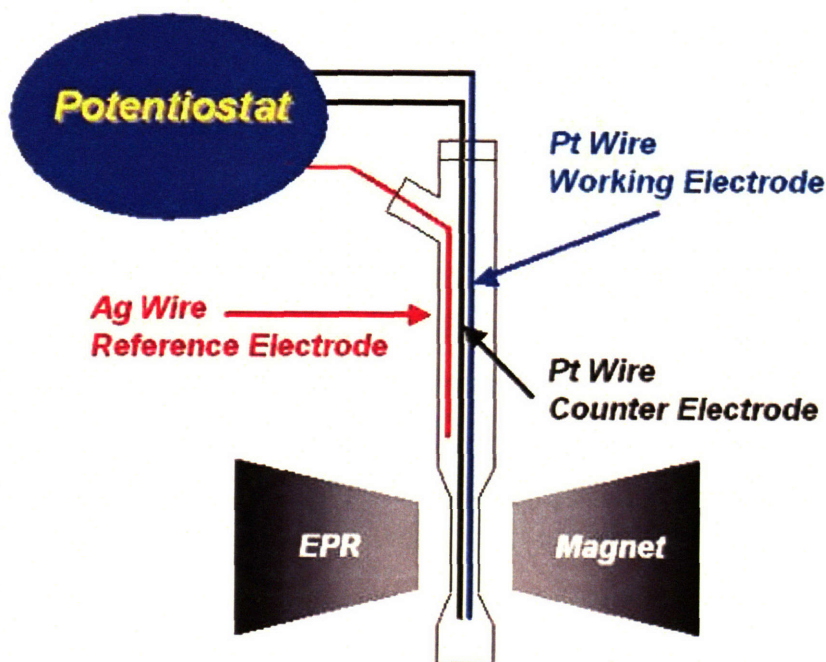


Figure 4.8: Experimental setup for *in situ* EPR spectroscopy on polymer film. Diagram courtesy of Dr. Bruce Yu of the MIT Swager Laboratory.

The actual EPR measurement can be performed by one of two methods. The *real-time* method can be used in cases where the g -value and peak width do not vary with the oxidation

level. The magnetic field is set to a corresponding high EPR signal amplitude which can be then followed as a function of time. As the potential is scanned between oxidizing and reducing voltages the EPR intensity is collected in the time-domain as shown in Figure 4.9a.

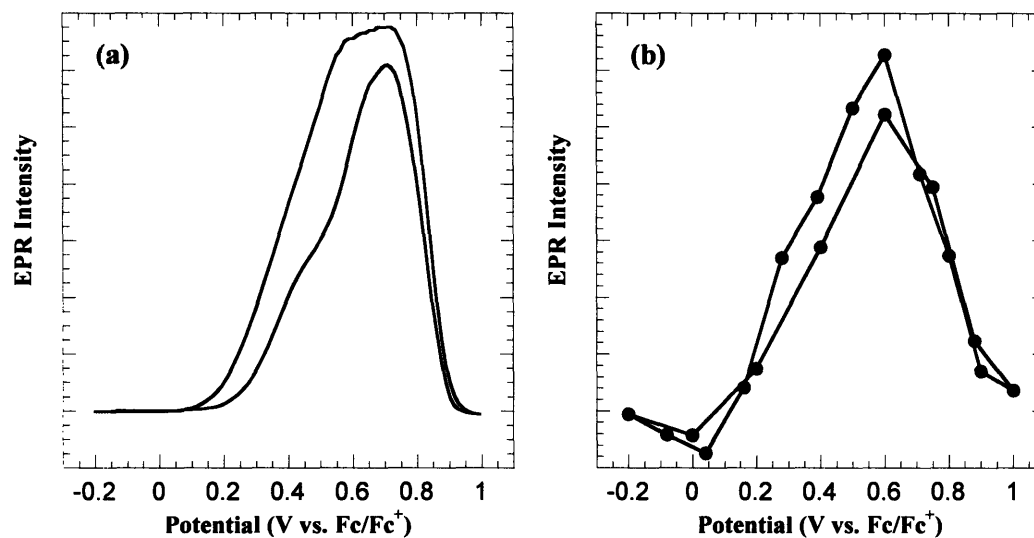


Figure 4.9: Comparison of (a) *real-time* and (b) “*stop-and scan*” EPR methods for a calix[4]arene-based conducting polymer film.

If the g -value or peak width vary upon doping, the “*stop and scan*” method must be used. The applied potential is held at a dialed voltage for a few minutes to equilibrate before a full EPR spectrum is taken. For each potential increment (typically 0.2 V), a whole EPR spectrum is taken. The spin count (intensity) is then derived by double integration of the EPR signal over a fixed field range and plotted versus applied potential as shown in Figure 4.9b.

4.3 Parallel Synthesis and Combinatorial Techniques

While the monomers presented in this thesis are rationally designed, determining their optimal electrochemical polymerization conditions requires an empirical dragnet, trial and error approach. A common method adopted in the pharmaceutical industry to solve such a problem, where a large synthesis parameter space has to be systematically explored, has been to use a combinatorial approach. The use of high throughput synthesis instrumentation has become a new and viable strategy to develop novel drugs against a specific target.

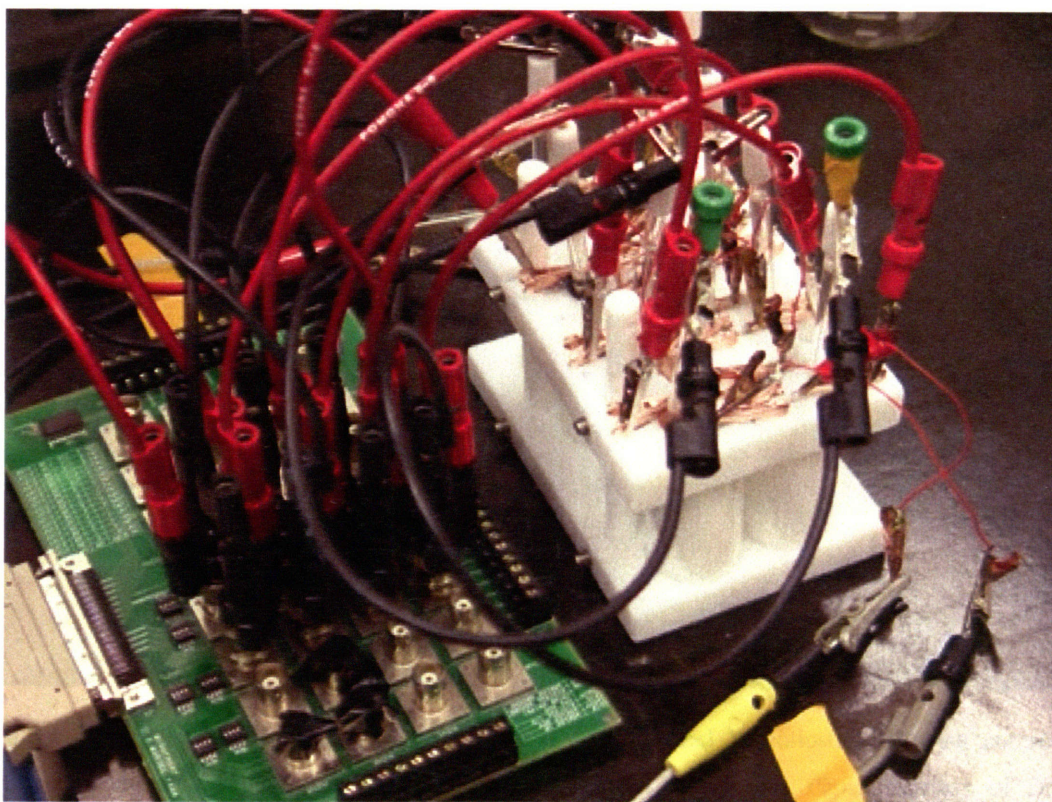


Figure 4.10: Prototype parallel characterization apparatus. Eight cells are connected to the 16 AD channels of the Allios Data acquisition card, performing eight *in-situ* current analysis of various conducting polymers.

Similarly, attempts were made to find new synthesis (polymerization) conditions for novel materials with optimal actuation properties were made by adopting a higher throughput, parallel synthesis and characterization approach. These methods allow the

systematic search for optimal synthesis conditions, while reducing synthesis time. The production of a single polymer film may take up to 5 hours of deposition time. In contrast, these high-throughput synthesis techniques enable accelerated material discovery. In addition, such techniques are designed to require only a very small amount of monomer [Madden P.G. et al. 2001]. Practically, this means that only minimal quantities of precious monomers are needed to complete experiments with this system.

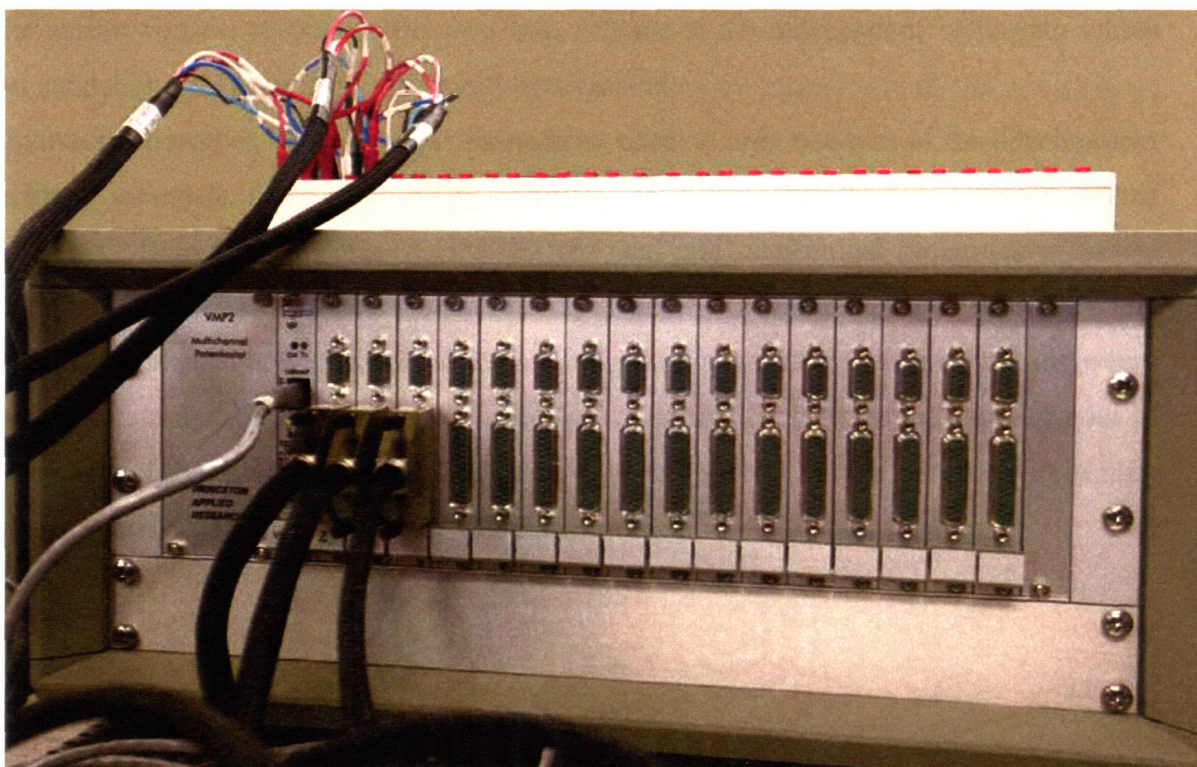


Figure 4.11: Princeton Applied VW2 16 Channel Multichannel Potentiostat, allowing control of 16 independent electrochemical cells, all via T-base 100 Ethernet connection. Photo courtesy of Dr. Serge Lafontaine of the MIT BioInstrumentation Laboratory.

An early prototype of the parallel deposition system, shown in Figure 4.10, is based on a specially designed eight-well plate. Each well contains up to 5 mL of synthesis solution and is electrochemically probed by working, counter and reference electrodes. The three electrodes in turn are connected to a 16 channel Allios data acquisition board (<http://bioinstrumentation.mit.edu>), allowing application of a synthesis waveform and to

record potential and current. In this apparatus, eight independent experiments can be performed simultaneously.

In a later prototype of the higher throughput synthesis apparatus, the Allios data acquisition board was replaced with a 16 channel multichannel potentiostat, allowing the control of 16 independent electrochemical cells (Figure 4.11). Digital computer connection is made via T-base 100 Ethernet connection, thus several computers can log onto the instrument at the same time to control or access the synthesis data. This doubles the capacity of the earlier version of the parallel synthesis scheme to 16 independent wells into which novel conducting polymer films are rapidly synthesized.

Synthesis, however, even at higher throughput rates, is only one part of the development of actuator materials. Once synthesis is complete, characterization of the materials formed takes place. Being able to characterize the physical and mechanical properties of newly synthesized conducting polymer films (ideally while the film is grown) in a fast and combinatorial manner is highly desirable. An integrated polymer high-throughput discovery machine, combining both synthesis and mechanical characterization is an ongoing goal of development at the MIT Bioinstrumentation lab. Such a system will be very helpful in fully evaluating candidate molecules in a rapid manner.

4.4 Characterization Methods

4.4.1 Bulk Conductivity Measurements

The conductivity of bulk conducting polymer actuator films is of importance as it affects both their speed of contraction (charge injection) as well as their efficiency (iR losses). As presented in Chapter 3, conductivity in conducting polymers is achieved by insertion of dopant anions such as hexafluorophosphate into the material.

To achieve a universal measurement of conductivity, the dimension of the film must be removed from the measurement. Equation 4.2 below shows a method to calculate a universal measure of conductivity σ expressed in S/m (Siemens per meter, where $1 \text{ S} = 1 \Omega^{-1}$):

$$\sigma = \frac{1}{R} \cdot \frac{l}{w \cdot t}, \quad (4.2)$$

where R is the measured resistance, l the film length, w its width and t its thickness.

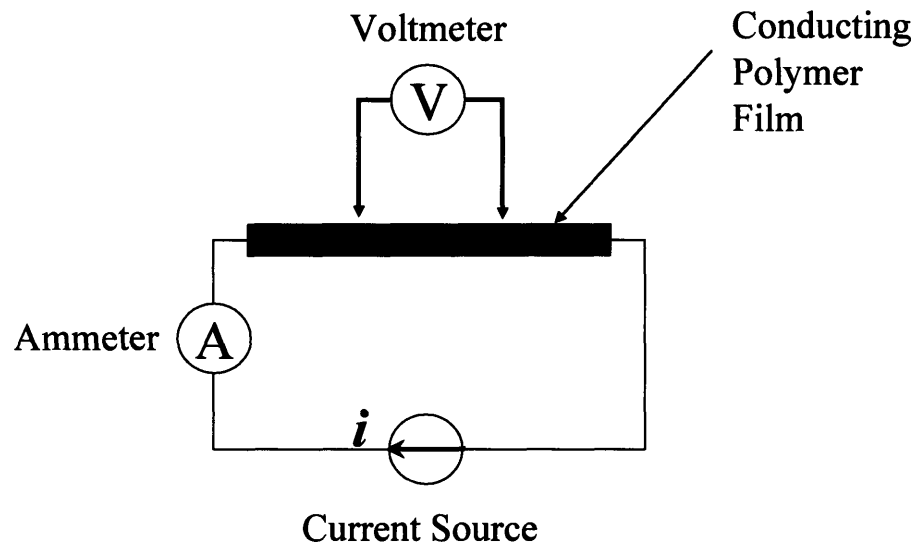


Figure 4.12: Circuit diagram to measure the conductivity of a conducting polymer film via the four point probe measurement

In addition, as the conducting polymer films are highly conductive, care must be taken not to measure other resistances that are in series with the digital multimeter making the measurement. Such resistances include the probe leads and the contact resistance between the film and the probes. The four point probe conductivity measurement allows one to only measure the resistance of the film and is considered the most accurate for highly conductive materials.

Figure 4.12 shows schematically how four point probe measurements are made. A known current i is applied to a sample via a current source and measured by an ammeter. The potential drop caused by the application of this current along the film is then measured by a voltmeter, upon which the resistance R can be measured.

An interesting variation of the four point probe measurement is the Van der Pauw technique [Van der Pauw L.J. 1958] which reduces the three geometric parameters in Equation 4.2 (l, w, t) to only one. As Equation 4.2 assumes that the film dimensions are known via measurement, errors can be induced. In the case of the Van der Pauw technique, only one measurement, the thickness of the film, is needed to compute the conductivity of the film. A disadvantage of this technique, though, is that the film must be cut in precise square.

Bulk conductivity measurements were conducted on a custom-built four point measurement apparatus connected to a multimeter (Keithley, model 2001, www.keithley.com) which can instantaneously compute the resistance measurement from the four probes. Four platinum wires, placed in parallel onto a machined Delrin (www.dupont.com) support plate served as the four point probes. This configuration allows one to lay the polymer film flat onto the platinum wires to perform a measurement.

4.4.2 Electrochemical Quartz Crystal Microbalance (EQCM)

As conductive polymers are synthesized, it is of interest to know the dynamics and the rate of mass deposition onto the working electrode. The quartz crystal microbalance is an extremely sensitive mass sensor capable of measuring small mass changes in the $0.1 \mu\text{g}/\text{m}^2$ (ng/cm^2) range with a wide dynamic range. Sauerbrey was the first to recognize the potential of using the change in resonance frequency of a quartz microcrystal to measure very small mass changes. As mass is added to the quartz crystal, its resonance frequency shifts and

becomes smaller. The results of his work are embodied in the Sauerbrey equation, which relates the mass change per unit area at the QCM electrode surface to the observed change in oscillation frequency of the crystal:

$$\Delta f = -C_f \cdot \Delta m, \quad (4.3)$$

where Δf is the observed frequency change in Hz, Δm is the change in mass per unit area, in kg/m^2 , and C_f is the sensitivity factor of the crystal in Hz. For example, an SRS 5 MHz quartz crystal at room temperature has a C_f factor of $5.66 \cdot 10^{-3} \text{ Hz} \cdot \mu\text{g}^{-1} \cdot \text{m}^2$ (<http://www.srsys.com>).

A Stanford Research System SRS QCM100 – Quartz Crystal Microbalance was used to perform microbalance studies (<http://www.srsys.com>). The advantage of using a commercial system is that it is already calibrated.



Figure 4.13: SRS QCM100 Quartz Crystal Microbalance control unit (left) and crystal holder (right) used to dynamically study mass transport to the working electrode. Source: <http://www.srsys.com/>

In addition to allowing the study of polymer deposition / synthesis at the working electrode, the EQCM instrument also enables us to probe *in situ* the dynamics of oxidation and reduction of a synthesized conducting polymer. As ions diffuse into the polymer film, mass is added to or removed from the bulk polymer material. Such small mass changes can be recorded *in situ* by the EQCM and allow probing the dynamics of ion diffusion into the polymer system as a function of oxidation potential. Furthermore, it is conceivable that such a technique could be easily parallelizable and incorporated into the higher throughput synthesis and deposition.

4.4.3 *Passive mechanical testing; PE DMA 7e*

The use of the novel polymer films as active elements in devices requires a material that can bear loads. It is thus essential to determine passive mechanical properties of the actuator as these set limits to performance. Passive mechanical properties of the novel film materials also include visco-elastic characteristics such as creep and stress relaxation. Tensile tests may reveal excessive creep and stress relaxation in the new polymers. This may lead to a reformulation of the molecular design, an increased desired degree of cross-linking, or additional post-processing.



Figure 4.14: Photograph of the digitally controlled Perkin Elmer DMA 7e used in this thesis to characterize the passive properties of conducting polymer actuator films.

A Perkin Elmer (PE) Dynamic Mechanical Analyzer (DMA) 7e was used extensively to probe the passive properties of novel conducting polymer films. Typical film dimensions used were 20 mm length, 2 mm width and 20 μm thickness. The PE DMA 7e allows

applications of forces ranging from 1 mN to 50 N and record displacements from 0.1 μm to 27 mm. In addition, dynamic loads can be applied (from 0.1 Hz to 50 Hz), which permits probing of the visco-elastic properties of materials.

Dynamic mechanical analysis enables one to extract both the real and the imaginary component of the complex modulus of the material tested. The real part of the amplitude of the complex modulus is referred to as the dynamic modulus E' while its phase δ is characterized by the $\tan \delta$ value. Both the dynamic modulus E' and the $\tan \delta$ give an appreciation of a material's viscoelastic behavior. Note, however, that this technique is a linear technique, where the properties of the film are revealed using a sinusoidal input. The drawback is that this technique is not appropriate for non-linear materials. Such materials should be probed with non linear system identification (system ID) techniques utilizing Wiener and Hammerstein cascades or Volterra kernels [Hunter I.W. and Korenberg M.J. 1986; Korenberg M.J. and Hunter I.W. 1996].

4.4.4 Active mechanical testing: Construction of an electrochemical dynamic mechanical analyzer

Measurements of active mechanical properties are made under two conditions: constant strain (isometric) and constant stress (isotonic) and at different frequencies. Current and voltage are applied to the electroactive material and recorded under digital control using a custom build DMA (Figure 4.15), thereby allowing contractile properties to be related to charge transfer. The strain to charge ratio represents the most important figure of merit of actuator performance as it relates input energy to output displacement. Equation 4.4 shows the relationship between the strain ε and the applied charge per unit volume ρ via the strain to charge ratio α :

$$\varepsilon = \frac{\sigma}{E} + \alpha \cdot \rho, \quad (4.4)$$

where σ is the stress and E is the elastic modulus [Madden J.D. et al. 2001]¹. Both a high strain to charge ratio and a high stress to charge ratio are desirable as they relate to high degree of electromechanical coupling efficiency. Note that these properties can be measured directly by performing strain to current-density frequency response measurements. This technique has the benefit of also assessing actuator linearity and electrochemical behavior.

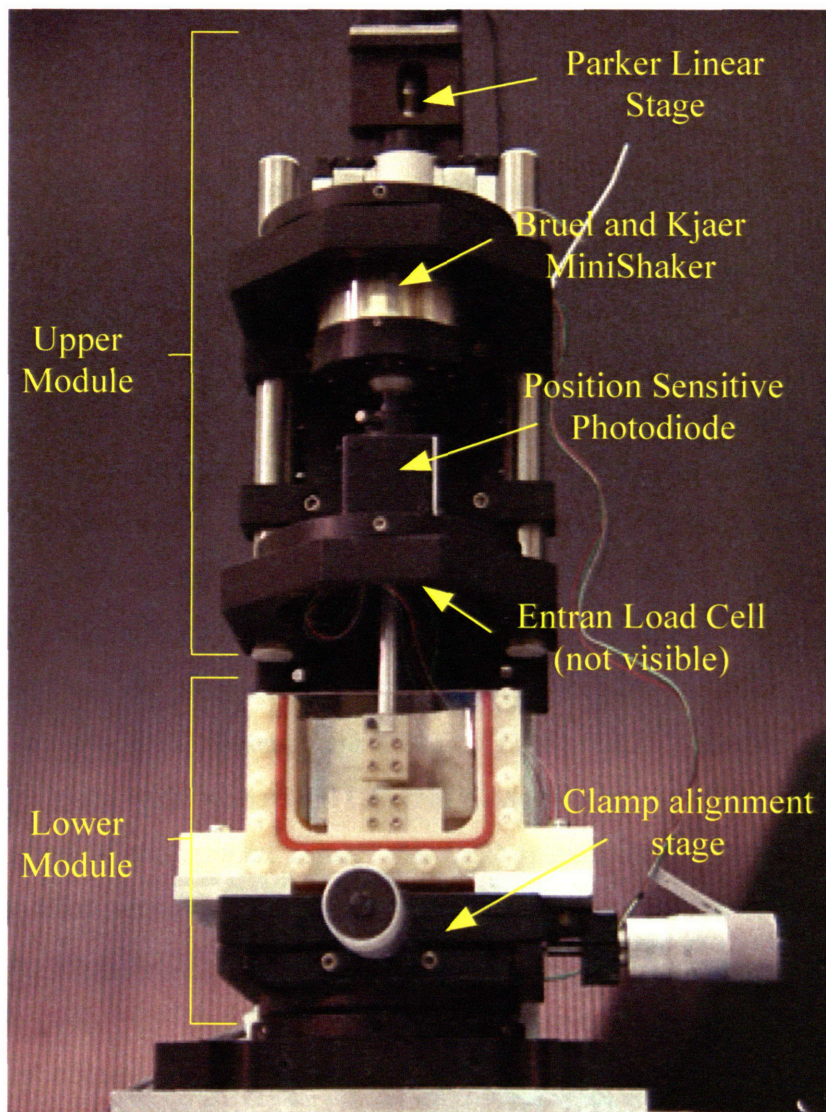


Figure 4.15: Custom-build electrochemical DMA developed to study the active linear strain of conducting polymer actuators.

¹ Note however, that Equation 4.4, which describes accurately the behavior of polypyrrole at low actuation voltages may no longer be valid at the large strains that are expected with the new materials presented herein.

Key parameters describing the active mechanical properties of the conducting polymer actuator including maximum active stress and strain, power to mass, stored energy density, efficiency and cycle life can be measured as a function of applied load. In addition methods typically used in muscle physiology such as the force-loop method or force velocity curves can be programmed with this instrument, allowing comparison of our artificial actuator technology with nature's muscle under common conditions [Full R.J. and Meijer K. 2001].

Active testing of polypyrrole was performed by an in-house-designed scientific instrument [Rinderknecht D.G. 2002]. No commercial tensile testing device exists that adequately combines mechanical testing with electrochemical excitation and monitoring. As a result, an Electrochemical Dynamic Mechanical Analyzer (E-DMA) testing apparatus was designed and constructed for performing isotonic, isometric and high frequency stress-strain measurements.

This custom made instrument is composed of two modules. The top half comprises force and displacement sensors as well as actuators, all connected to the upper sample clamp and probe. The bottom module hosts the lower sample clamp and electrochemical bath. A picture of the custom-build E-DMA is presented in Figure 4.15. Thin film samples are held vertically between two clamps within an electrochemical bath. Force is applied to the sample via a voice coil actuator (Bruel and Kjaer minishaker Model 4810, www.bkhome.com). A lightweight aluminum rod connects the voice coil actuator to the upper clamp. In series with the clamp is a low drift S-beam load cell (Futek L2357 S-beam 1 N load cell, <http://www.futek.com>, with Vishay 2311 Signal Conditioning Amplifier www.vishay.com), allowing recording of the applied force. An LED placed along the rod provides a light source for a position sensitive photodiode, thereby enabling position measurement (Pacific Silicon Sensors, www.pacific-sensors.com, PSS-DL100-7PCBA duolateral (2-axis) position sensing module, with PSS-DL-100 position sensing photodiode (PSD)). The applied force is under computer control via a data acquisition board (Allios 16-bit A/D, D/A, 50 kHz sampling <http://bioinstrumentation.mit.edu>) and a voltage to current amplifier. A graphical user interface designed in Visual Studio .NET (www.microsoft.com) includes a digital control algorithm for maintaining a desired force based on the force output measured by the load cell (Figure 4.16). Vertical sample positioning can be achieved via a stepper motor and linear stage (Parker linear stage with a Zeta57-51-MO stepper motor and a Compumotor Zeta

6104 Indexer Drive connected to the RS-232 port, www.compumotor.com), while horizontal alignment is achieved via a micrometer driven stage.

Form1 FILE EXIT

Isotonic Cyclic Testing

 March 07, 2004

Sample Properties

width (mm)
 thickness (mm)
 The length of the sample is given by clicking the read right button

C:\Documents and Settings\All Users\John\Alios\Calibration\Alios\CalibrationParameters\aliosgo.txt

Set Output Voltages V
 Get Voltage char V
 char V

Average compensation speed

Electrochemical Cell

Eout channel 0
 Iout channel 1
 Counter channel 2

Motor Controls

Increment (mm)

Displacement
 Velocity
 Acceleration

Force Channels:

Load Cell Scale Factor (N/V) Output Channel P
 Shaker Force Scale Factor (N/A) Input Channel I
 Current Scale Factor (A/V) D
 Force sensor acquisition frequency (Hz)

Displacement

PSD DC Offset

Y Out Offset Channel
 Y Sum Offset Channel
 Y intercept
 PSD factor

mm
 mm
 MPa

Run

Current Gain (A/V)
 Potential Gain (A/V)
 Sample Interval (s)
 Delay Before Stress Applied (s)

Stress series to be applied

MPa
 Isotonic Hold Duration (s)
 Voltage step in s

C:\Documents and Settings\Administrator\My Documents\Patrick\data\test.m Data File Name

PSD Filter Gain
 AMEL Current Offset

Figure 4.16 Custom-build control panel to operated the electrochemical DMA programmed in Visual Studio .NET (www.microsoft.com).

The custom-build E-DMA enables us to perform stress-strain measurements at various strain rates, up to a 100 Hz bandwidth. The minimal resolvable displacement and force are 1 μm and 1 mN respectively, while the maximum measurable displacement is 3 mm and the maximum applicable force is 1 N². For a typical conducting polymer film with a cross-

² This value can be increased by changing the load cell to one with a higher load capability.

section of 2 mm by 20 μm this corresponds to a resolvable stress range from 25 kPa to 25 MPa and a resolvable displacement range from 0.017 % to 50 %. The typical initial active length of films tested in the E-DMA was kept the same throughout testing at 6 mm. Finally, this apparatus enables electrochemical potential or current to be digitally controlled via a computer control high-current Amel potentiostat/galvanostat (model 2053, <http://www.amelsrl.com>), thereby allowing active stress and active strain to be monitored as a function of material oxidation state.

4.4.5 Temperature Characterization: Thermal / Infrared Camera

To study the temperature distribution within the conducting polymer as a function of electrical current, an FLIR ThermoVision A40M infrared camera connected to an IBM T42p laptop via IEEE 1394 FireWire was used (<http://www.flirthermography.com>). This camera allows us to record variations of temperature as a function of time with a sensitivity of 0.08 $^{\circ}\text{C}$ (at 30 $^{\circ}\text{C}$). Its spectral range spans 7.5 to 13 μm .

4.5 Conclusion

The study of conducting polymer actuators requires extensive knowledge of instrumentation and of experimental methods for materials characterization. First, the synthesis (polymerization) of these novel materials need to be precisely controlled and monitored, and the deposition parameters systematically varied. Then rigorous testing of the final polymer materials takes place. This includes characterization of physical properties, passive and active mechanical properties. In the next Chapters the utilization of the instruments presented herein for various characterization experiments is presented.

4.6 References

- Bard Allen J. and Faulkner L. R., "Electrochemical Methods, Fundamentals and Applications", 2nd Ed. Wiley: New York, (2000).
- Full R.J. and Meijer K., "Metrics of Natural Muscle Function", *Electroactive Polymers [EAP] Actuators as Artificial Muscles -Reality, Potential, and Challenges*, Bar Cohen Y. Editor, SPIE Press, pp. 67-83, (2001).
- Hunter I.W. and Korenberg M.J., "The Identification of Nonlinear Biological-Systems - Hammerstein and Wiener Cascade Models", *Biological Cybernetics*, Vol. 55, (2-3): pp. 135-144, (1986).
- Kittlesen G.P., White H.S. and Wrighton M.S., "Chemical Derivation of Microelectrode Arrays by Oxidation of Pyrrole and N-Methylpyrrole: Fabrication of Molecule-Based Electronic Devices", *Journal of the American Chemical Society*, Vol. 106, pp. 7389-7396, (1984).
- Korenberg M.J. and Hunter I.W., "The Identification of Nonlinear Biological Systems: Volterra Kernel Approaches", *Annals of Biomedical Engineering*, Vol. 24, (2): pp. 250-268, (1996).
- MacDiarmid A.G., "Synthetic Metals: A Novel Role for Organic Polymers", *Synthetic Metals*, Vol. 125, pp. 11-22, (2002).
- Madden J.D., Madden P.G. and Hunter I.W., "Polypyrrole Actuators: Modeling and Performance", *Smart Structures and Materials 2002: Electroactive Polymers Actuators and Devices*, Yoseph Bar-Cohen, Editor, Proceedings of the SPIE, (2001).
- Madden P.G., Madden J.M. and Hunter I.W., "Parallel Electrochemical Methods to Accelerate Electroactive Material Discovery and Optimization", *Material Research Society Symposium Proceedings*, Vol. 698, pp. EE1.7.1-EE1.7.6, (2001).
- Ofer D., Crooks R.M. and Wrighton M.S., "Potential Dependence of the Conductivity of Highly Oxidized Polythiophenes, Polypyrroles, and polyaniline: Finite Windows of High Conductivity", *Journal of the American Chemical Society*, Vol. 112, pp. 7869-7879, (1990).
- Rinderknecht D.G., "Design of a Dynamic Mechanical Analyzer for the Active Characterization of Conducting Polymer Actuators", *Bachelor of Science Thesis, MIT*, Supervised by Patrick A. Anquetil (2002).
- Van der Pauw L.J., "A Method of Measuring Specific Resistivity and Hall Effect of Discs of Arbitrary Shape", *Philips Research Reports*, Vol. 12, (1): pp. 1-9, (1958).
- Vandesteeg N., "MIT - private communication", (2003).

Chapter 5

Electrochemical Synthesis of Polypyrrole

Actuator Films

This Chapter describes the procedure used in this thesis to synthesize high quality polypyrrole films. High quality means that the polymer films are mechanically robust and highly conductive. The knowledge of what makes a good polypyrrole (PPy) film is important for synthesis and discovery of novel materials. The superior morphology of these PPy films is presented and used as a benchmark for the synthesis of novel actuator materials based on molecular designs throughout later Chapters. Schemes and methods used to move from a batch synthesis serial process to a semi-industrialized version are also discussed.

5.1 Electrodeposition synthesis process

As presented in Chapter 3 and 4, the synthesis route used to produce PPy films is the electrochemical deposition onto a conductive electrode. The electrochemical setup and a typical resulting film are presented in Figure 5.1. It consists of a working electrode onto which the polymer is deposited, a controlled source of current (or galvanostat) an electrolyte, a solvent and a counter electrode to close the electrical circuit. The advantages of using the electrochemical synthesis route are:

- Offering a growth process similar to Nature, rather than an assembling one
- Not making use of any catalysts
- Providing homogeneous and directed doping of the polymer, compared to chemical oxidation (in addition, chemical oxidation often leads to powders, not films)
- Accessibility to electrochemical synthesis parameters to estimate growth rate and use of reactants.

The disadvantages of using an electrochemical synthesis route to polymerize conducting polymers are:

- Low molecular weight. The molecular weight of electrochemically synthesized polymers hardly exceeds 5,000 [Swager T. 2004]. Chemical synthesis of conducting polymer such as PPy, however even yields lower molecular weight. [Gregory R.V. et al. 1989]

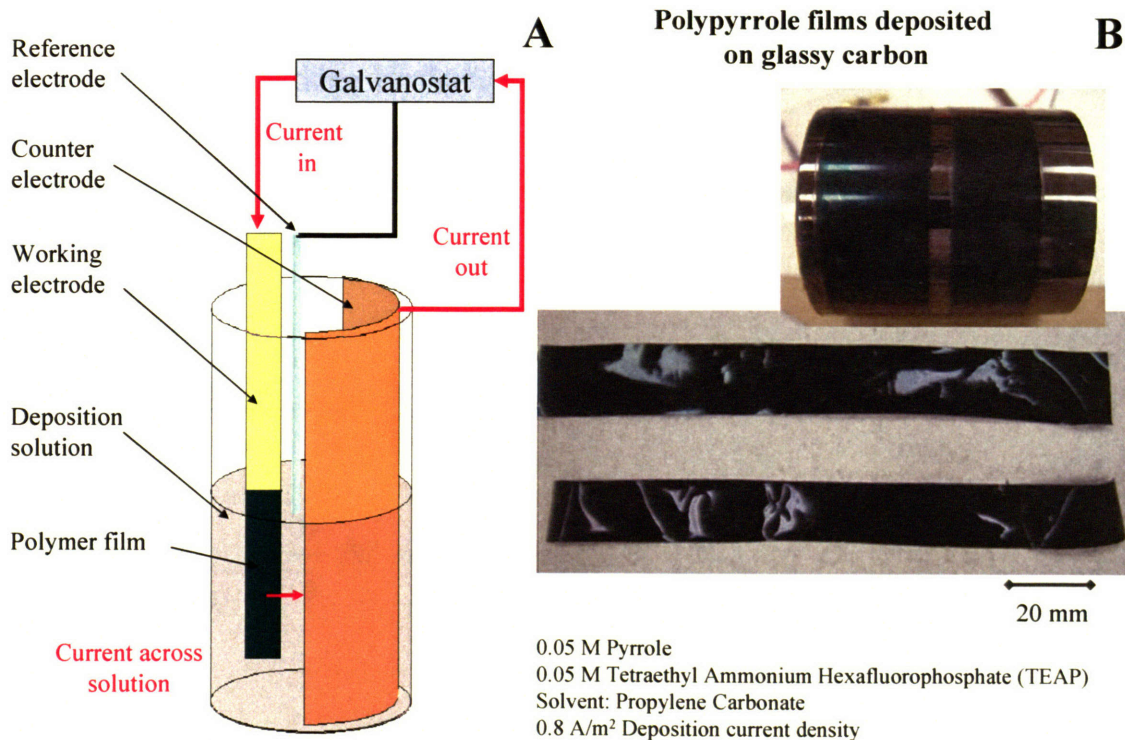
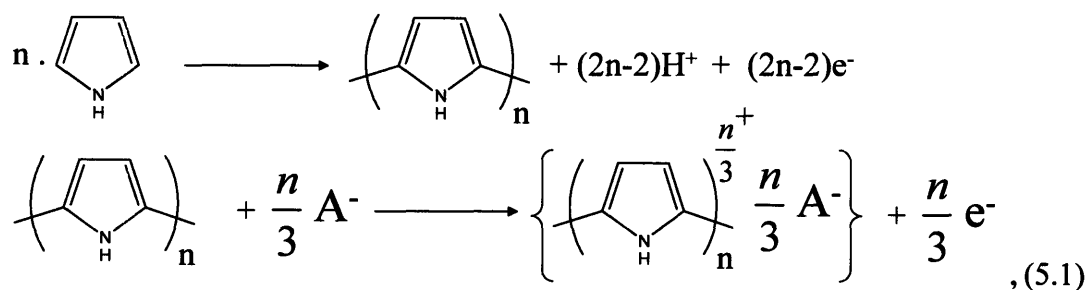


Figure 5.1: Schematic electrochemical synthesis setup cell (A) and resulting PPy film (B). The films were 27 μm thick, 20 mm wide and approximately 160 mm long. The film side shown here has a shiny look, which is characteristic for the crucible side of PPy films.

- The resulting conjugated polymers come as films and are difficult to post-process. Other methods involving colloidal dispersions of polypyrrole [Armes S.P. 1998] counter-ion [Lee J.Y. et al. 1995] or side chain-induced solubilization [Salmon M. et al. 1982] allow processing of polypyrrole at the cost of electrical conductivity.

Adapting the method of Yamaura and Colleagues [Yamaura 1992], 0.05 M of freshly distilled polypyrrole (PC) is mixed with propylene carbonate, an inert solvent containing 0.05 M of Tetraethylammonium Hexafluorophosphate (TEAP) and 1%/vol Millipore water (www.millipore.com). Synthesis is performed under galvanostatic condition (i.e. constant current using an Amel potentiostat/galvanostat (Model 2053, www.amelsrl.com) or an Agilent E3631A Power Supply) onto a cylindrical conducting glassy carbon substrate (Alfa Aesar, www.alfa.com). The electrochemical cell is closed via a copper sheet counter electrode (Aldrich, www.aldrich.com). Galvanostatic depositions are conducted at current densities of 0.8 A/m² for 8 to 16 hours resulting in film thickness between 10 and 28 μm. Deposition takes place at low temperature (- 35 °C). The resulting films of polypyrrole are then peeled off the working electrode substrate, rinsed and conserved in a PC solution containing 0.1 M TEAP and no monomer.

The electrochemical reaction taking place at the working electrode (onto which the polymer is deposited) is the following:



with $n > 2$ and where e^- are electrons and A^- the anion (or counterion) necessary to balance the charge on the polymer. The counterion is incorporated at the time of synthesis and is intercalated between PPy chains [Nogami Y. et al. 1994]. Elemental analysis shows that dry

films have an oxidation state of 0.3 charges per monomer, hence the $n/3$ factor in reaction (5.1). Polymerization is believed to occur via chain growth coupling of oxidized monomers in radical cation form. Polymerized PPy oligomers eventually precipitate on the working electrode out of solution once a solubility limit is reached.

Overall for n molecules of monomers, $(2n - 2) + \frac{n}{3} = \frac{7}{3}n - 2$ electrons are consumed:

$$N_{\text{molecules}} = \frac{3}{7}(N_{\text{electrons}} + 2) \quad (5.2)$$

This relationship shows the power of the electrochemical synthesis approach. The amount of charge passed through the electrochemical cell allows one to determine how much monomer and salt compounds as well as energy has been used at any given time during the production of polymer films. In addition, since deposition occurs in the direction of the electrode, the thickness t of the polymer film can also be estimated via the amount of charge passed:

$$t \propto Q = \int i dt \quad (5.3)$$

The linear electrochemical growth process is easily observable via an Electrochemical Quartz Crystal Microbalance (EQCM). PPy is grown onto a gold-coated quartz crystal whose frequency of vibration is monitored. Addition of mass onto the crystal leads to a decrease in the oscillation frequency. Figure 5.2 shows the growth of PPy as a function of time as monitored by an EQCM balance. The film growth shown in Figure 5.2 was achieved under the exact same conditions as larger films described above. In this case, the current density of 0.8 A/m^2 equals an effective current of 0.158 mA (i.e. 9.86×10^{14} electrons/s), leading to a deposition speed of 120 ng/s (or 0.55 nm/s in thickness growing from the working electrode). The 5.6 hours deposition leads to a $11 \text{ }\mu\text{m}$ thick polymer film.

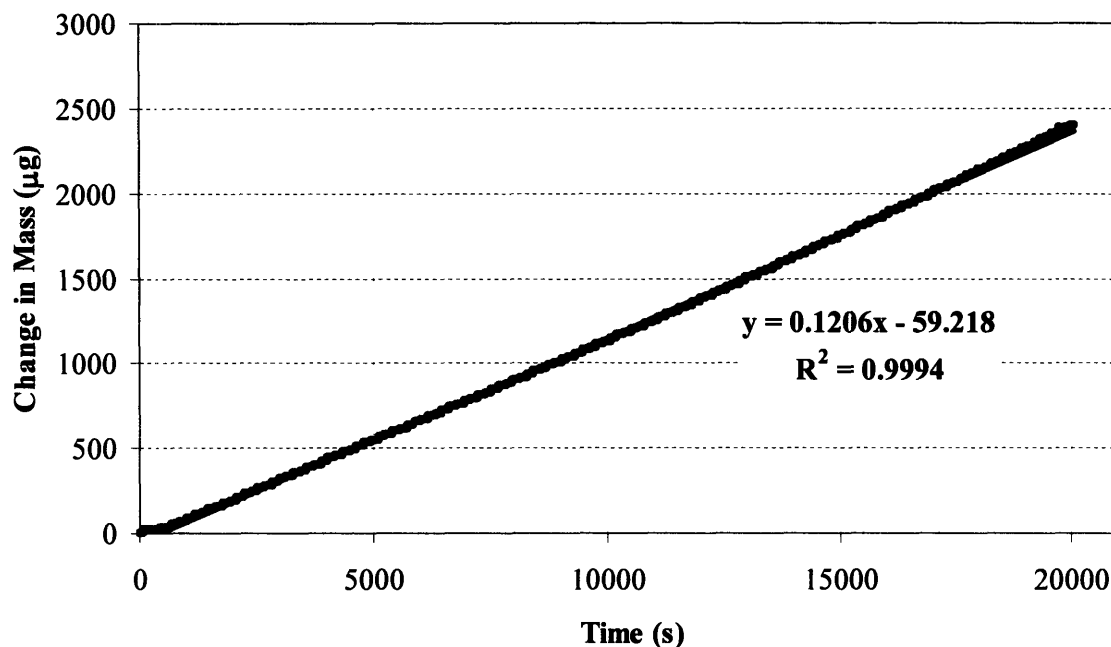


Figure 5.2: Linear growth of PPy as a function of time during deposition as monitored by the electrochemical quartz microbalance.

5.2 Synthesis of high quality conducting polymer films

5.2.1 Overview

The synthesis of conducting polymers is a complex, dynamic process covering a large parameter space. Throughout this work it was very important to be in a position where the properties of synthesized conducting polymers are easily reproducible. There are five main parameters affecting the polymerization of conducting polymers:

- Monomer
- Salt
- Solvent
- Electrode materials
- Electrochemical conditions (controlled current, or controlled potential)
- Synthesis conditions (temperature, concentrations of reactants)

The Monomer

The monomer used in this Chapter was freshly distilled pyrrole. Once distilled it has the form of a clear solution. Other monomers covered in this thesis (see Chapter 8 and 9) are powders that need to be dissolved in a solvent.

The Salt

Each sample of polypyrrole can be tremendously different depending on the ion and counter ion system that is used during synthesis. Note that the salt used has effects not only on film final conductivity and mechanical properties but also on the conductivity of the deposition solution (under controlled potential depositions). Ion systems typically used include sulfonated aromatics such as dodecylbenzene sulfonate or tetrafluoroborate or hexafluorophosphate, to cite a few [Smela E 2003]. All PPy films were synthesized with the tetraethylammonium hexafluorophosphate ion couple.

Electrode Materials

The material onto which the polymer is deposited plays a crucial role in the initial steps of the synthesis process. It governs both the oxidation process of the monomer as well as the morphology of the first layers of materials. Results in Figure 5.8 show also how sub-micron-sized motifs featured on the working electrode material appear on the polymer like a template. These initial layers determine the future morphology of the film. Yoon and al. showed that polishing the electrode material leads to smooth films [Yoon C.O. et al. 1999], while unpublished results from Davidson and colleagues suggest that the material of the electrode is responsible for polymer morphology and not the polishing process [Davidson S.N. et al. 2004]. Adhesion of the film onto the electrode is also important. In the initial steps of the deposition process, it is important that oligomers attach to the electrode surface and not diffuse back into solution. At the end of the synthesis it is desired that the film be easily peeled off the electrode. Glassy Carbon was used exclusively for the synthesis of polypyrrole, while gold coated PET and glassy carbon electrodes were used for the synthesis of novel thiophene-based conducting polymer actuators. The gold coated PET electrode has the advantage of being disposable.

The electrochemical and synthesis conditions

Careful attention to follow the synthesis protocol described in the previous section (5.1) and in particular rigor in using pure compounds and clean electrodes allows great repeatability. The use of a regulated low temperature bath is also crucial in generating high repeatability films. For example, the reaction of pyrrole monomers in radical cation with oxygen is less likely to occur at low temperatures. Similarly, although galvanostatic deposition leads to films with better morphology, care must be taken to prevent the potential to rise above overoxidation that would degrade the monomer (Figure 5.4).

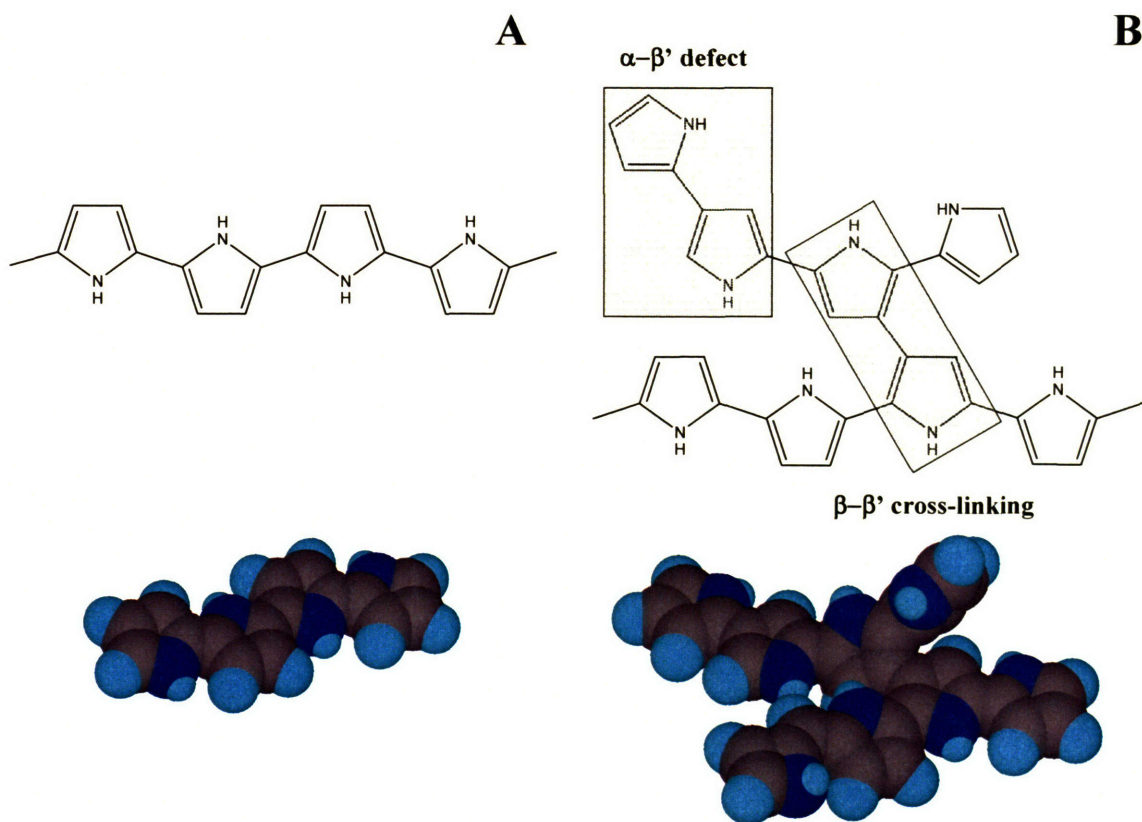


Figure 5.3: Idealized defect-free structure of polypyrrole and associated AM1 energy minimized solid model (A). Polypyrrole showing α - β' defects and β - β' crosslinking and associated AM1 energy minimized solid model. Notice how the planarity is lost by the β - β' linkage (B). The α - β' on the other hand, disrupts the conjugation and thus lead to poorer conductivity.

Typical Defects

A representation of polypyrrole such as the one shown in Figure 5.3A is an idealized image. Depending on the synthesis conditions, several defects such as α - β' couplings and β - β' cross-links appear (Figure 5.3B). Both defects lead to materials with poorer conductivity. The latter defects leads to perturbations of the molecule planarity, affecting intramolecular electrical conductivity, while the α - β' coupling disrupts the backbone conjugation¹. Note however that β - β' cross-links are beneficial for mechanical properties as they lock the polymer molecules together.

The highest quality films are prepared in an inert atmosphere such as N_2 and at low temperature as both factors prevent oxygen from reacting with oxidized pyrrole monomers. The combination of current-controlled conditions and low temperature allows slowing the deposition reaction and thus leads to films with higher conductivity and better mechanical properties.

Another defect that can plague conducting polymer films is a structural imperfection arising from overoxidation [Pud A.A. 1994]. Irreversible chemical changes arise at high potential (typically greater than +1.0 V versus Fc/Fc+). Overoxidation leads to the addition of carbonyl groups (C=O) to the conducting polymer backbone, reducing conjugation and ultimately reducing conductivity Figure 5.4. It is conceivable that film conductivity can be used to monitor the film's health during activation.

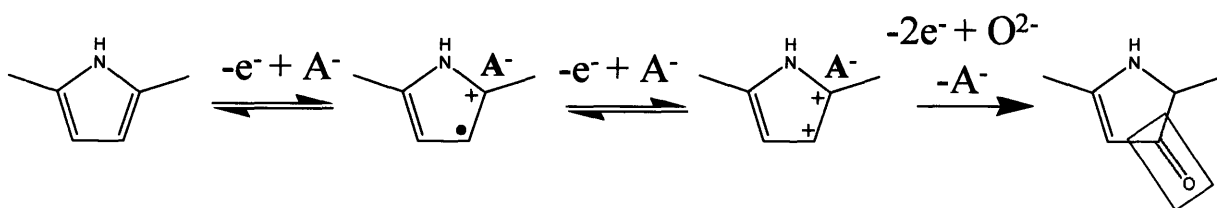


Figure 5.4: The four possible oxidation states of polypyrrole. The first three states are reversible, while the fourth one (far right) is irreversible. This later state is called overoxidation. A^- refers to the anion. Note that it is incorporated into the polymer film in step 2 and 3.

¹ Conjugation describes the alteration of single and double bonds along the conducting polymer backbone. As it ultimately allows electron delocalization it is at the heart of the conductivity mechanism in conducting polymers, (see Chapter 3).

In addition to be responsible for poor conductivity, overoxidation eventually leads to mechanical degradation. Addition of carbonyl groups ultimately changes the morphology of the polymer backbone leading to weak interchain interactions.

5.2.2 Synthesis Results

Figure 5.5 shows two typical 16 hour long deposition runs of PPy at - 35 °C. The potential, current and temperature are monitored via the Agilent-based acquisition system connected to a Tablet PC described in Chapter 4. Charge is derived from the current signal via Equation (5.3). Using Relationship (5.2) one can then determine that only 14.8 % of the monomer molecules and only 4.9 % of the anion molecules were used.

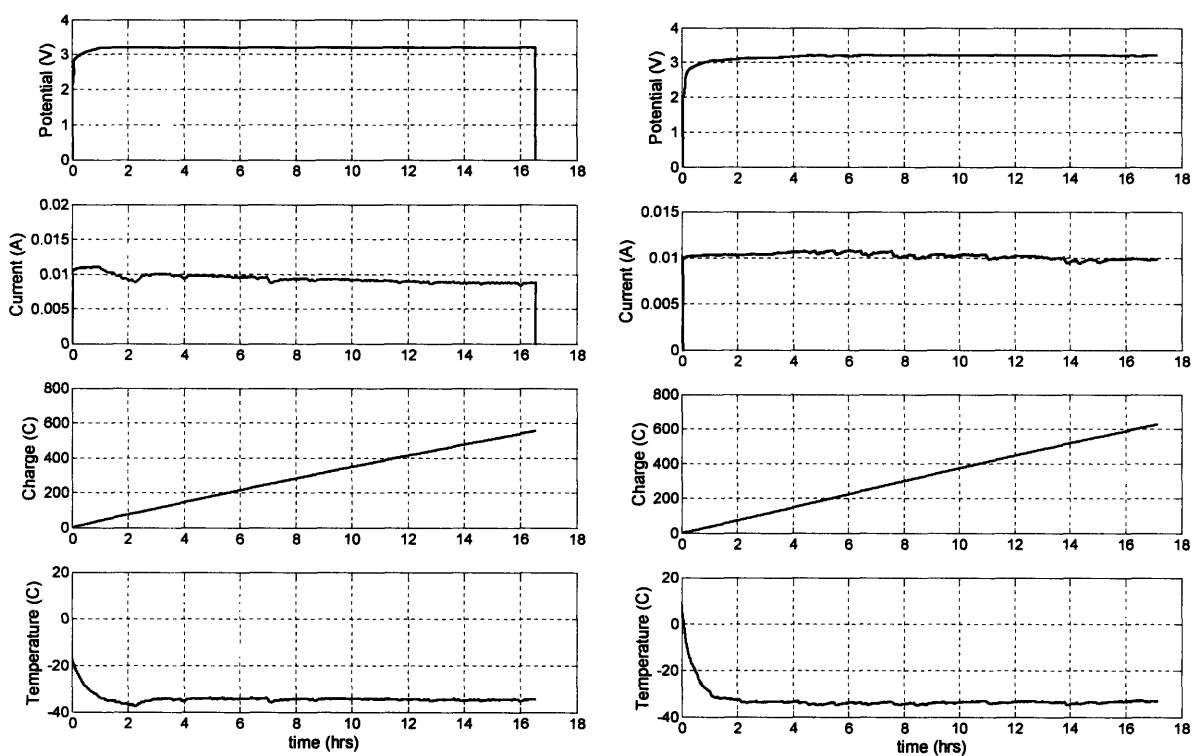


Figure 5.5: Typical deposition data during PPy deposition under galvanostatic conditions. Potential, current and resulting charge as well as temperature is plotted versus time. The left graphs refers to film PPy1 while the right one is PPy2

The current in both depositions is held constant at 10 mA (0.8 mA/cm^2), while the potential limited to 3.2 V (vs. counter) to prevent high potentials from degrading the polymerized material. Note that no reference electrode is used in the course of this synthesis. The copper counter electrode acts as pseudo reference electrode. The potential at the beginning of the synthesis process is 2.0 V (vs. counter) and rises to 3.2 V within 1 hour. Note that the potential limit imposed on the power supply (Agilent E3631A) leads to a slight decrease in the current response over time.

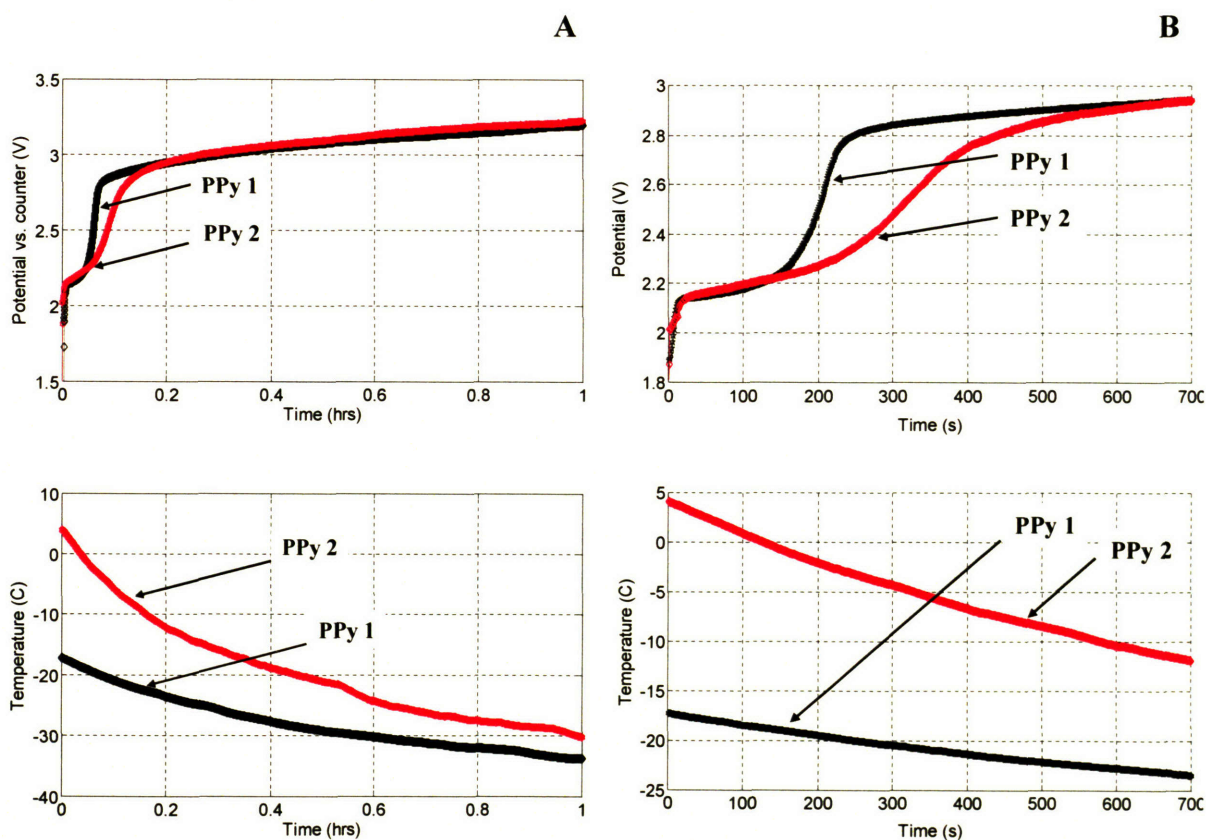


Figure 5.6: (A) First hour of the deposition of both PPy1 and PPy2 films. Around 180 s (0.05 hours) the potential evolves quickly from 2.1 V to 2.8 V, indicating that PPy oligomers form in solution first before precipitating onto the working electrode. By inspection, this process is delayed with increased temperature. This observation is supported by the EQCM data presented on Figure 5.7. (B) Close up.

Close observation of the first hour of the deposition process shows that two deposition regimes take place (see Figure 5.6). Initially the potential begins around 2.0 V (vs. counter). Within 180 to 400 s the deposition potential raises sharply to a second regime at higher

energy, around 2.8 V. This behavior is also observable with the EQCM microbalance, where the mass addition appears initially sluggish before it raises to a steady state. Dividing the resulting thickness of the film at the end of the deposition by the duration of the run would lead to an estimated thickness of ~ 70 nm at the time of deposition regime change.

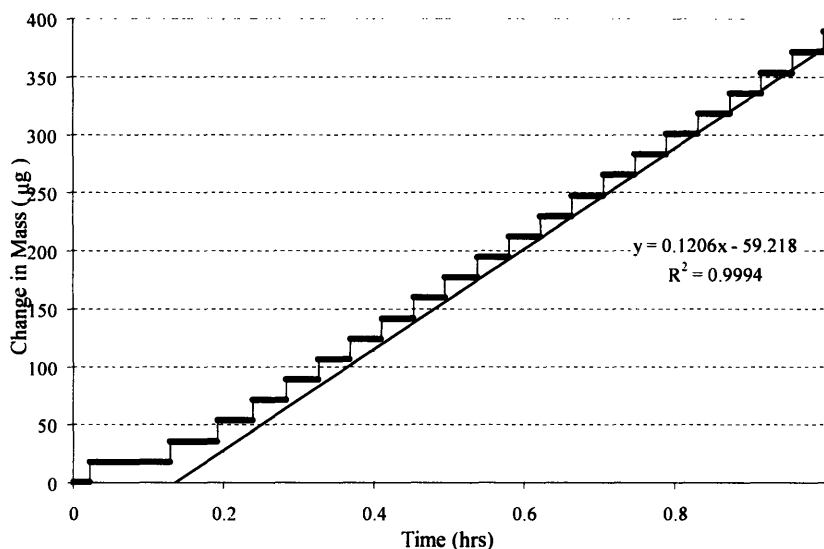


Figure 5.7: The EQCM data for a film under the same conditions shows as the one shown in Figure 5.6 shows that the rate of deposition is slower between 0 and 720 s (0.2 hrs). The line is the linear least square fit to the rest of the 5.5 hour deposition data (linear).

This observation is in accordance with previous findings suggesting that PPy polymerization first occurs in solution until a critical chain length is reached at which time nucleation on the working electrode begins [Scharifker B.R. et al. 1991; Tanaka K. et al. 1988]. The initial 2.0 V (vs. counter) corresponds to the energy of bringing the pyrrole monomers into their oxidized form (radical cation). PPy changes the surface property of the working electrode upon nucleation and thus raises the potential to 2.8 V (vs. counter) as it is less electrically conductive than glassy carbon. Figure 5.6 also suggests that this process might be temperature dependent. The synthesis process for PPy1 and PPy2 were exactly the same, except that the initial temperatures were different (by 18 °C). Both synthesis temperatures become the same (-35 °C) within 1 hour.

The properties of the resulting two films, PPy1 and PPy2 are presented in Table 5.1.

	PPy1	PPy2	Difference	Measurement Error
Conductivity (S/m)	3.81×10^4	4.0×10^4	0.19×10^4	$\pm 0.32 \times 10^4$
Density (wet) (kg/m^3)	1925	1851	74	± 110
Deposition time (hrs)	16.55	17	-	-
Thickness (μm)	25	26	1	± 1

Table 5.1: Comparison of two polypyrrole batches synthesized under the same galvanostatic conditions

Notice that these two films, synthesized from two different batches, but under the same conditions (except the initial temperature) exhibit similar properties. The slight difference in their characteristics is within the range of the experimental error.

Figure 5.8 shows Scanning Electron Microscope (SEM) micrographs of a sample of PPy1 film. Notice the quality of the morphology of the film. It is compact, solid and smooth. Both the solution side Figure 5.8(A&B) and the electrode side Figure 5.8(C&D) of the film are shown. The solution side of the film is characterized by a surface with some bumps, while the electrode side is smooth. Striations can be seen on Figure 5.8D. These arise from polishing marks on the glassy carbon crucible. In addition holes are also featured on the electrode side of the film. These likely arise from impurities such as adhesives from previous depositions remaining on the crucible. The passive and active mechanical properties of films from batch PPy1 and PPy2 are extensively studied in the following two Chapters (6 and 7).

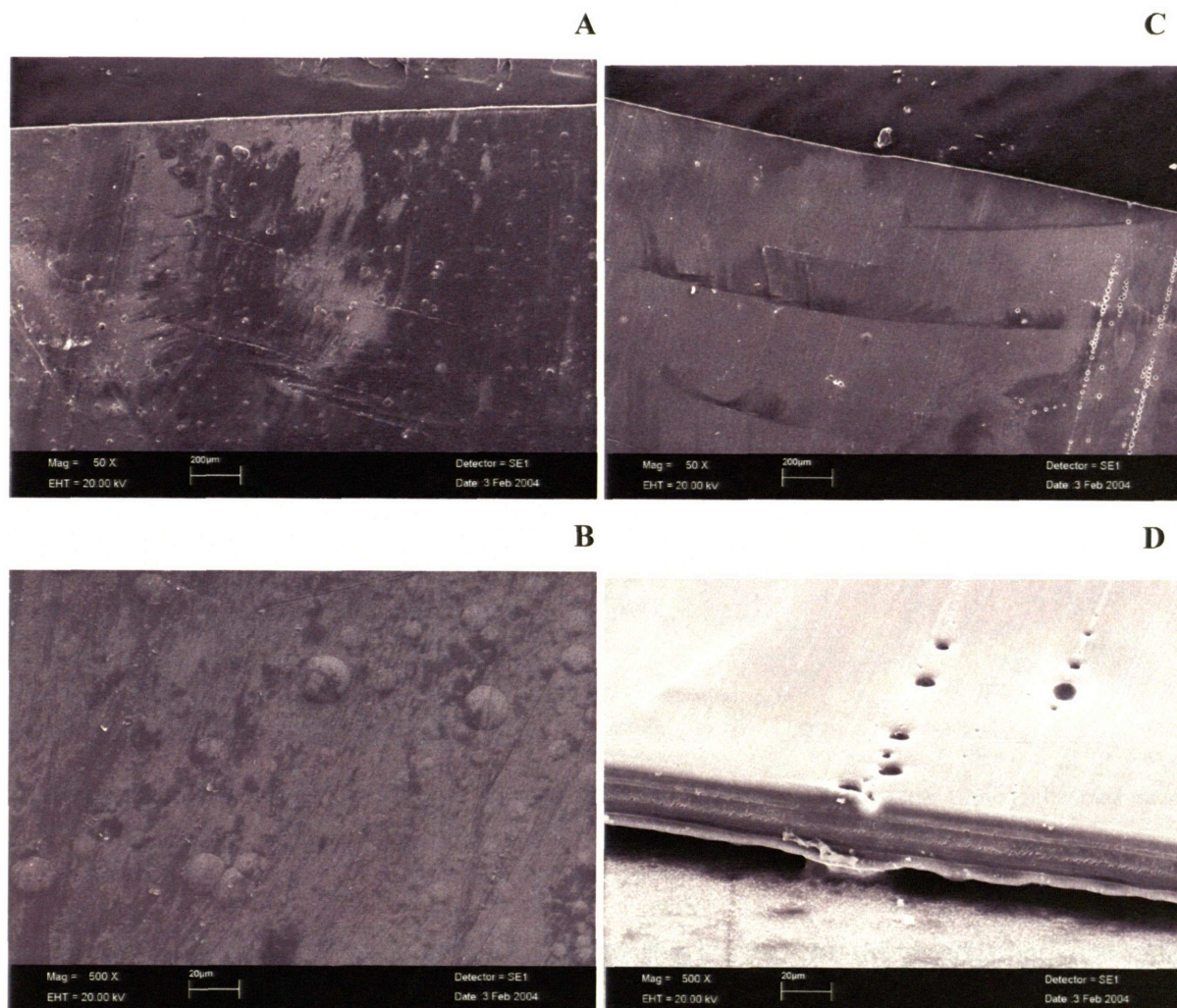


Figure 5.8: SEM micrographs of PPy1 films. The solution sides of the film are shown in subset A and B, while the electrode-side of the film in C and D. Note the holes in subset D are likely due to some remaining impurities on the deposition crucible preventing the polymer to nucleate properly.

The results of Figure 5.8 contrast with the general belief in the conducting polymer actuator community that PPy has a cauliflower-like structure [Ding J. et al. 2002; Hwang B.J. et al. 2000; Prissanaroon W. et al. 2002]. Recent findings in collaboration with Rachel Pytel show that a low current density may have a strong influence on the compactness and smoothness of PPy [Pytel R.Z. 2004]. For example, Figure 5.9 shows an SEM and AFM²

² AFM: Atomic Force Microscope

micrograph of the surface morphology of a polypyrrole film synthesized under a higher current density (1.25 A/m^2). The scale of Figure 5.9A is about the same as Figure 5.8D, while the one of the AFM micrograph is twice as large (Figure 5.9B). Although all reactants and were kept constant, and all the conditions but the current density were the same, the change in surface morphology is dramatic

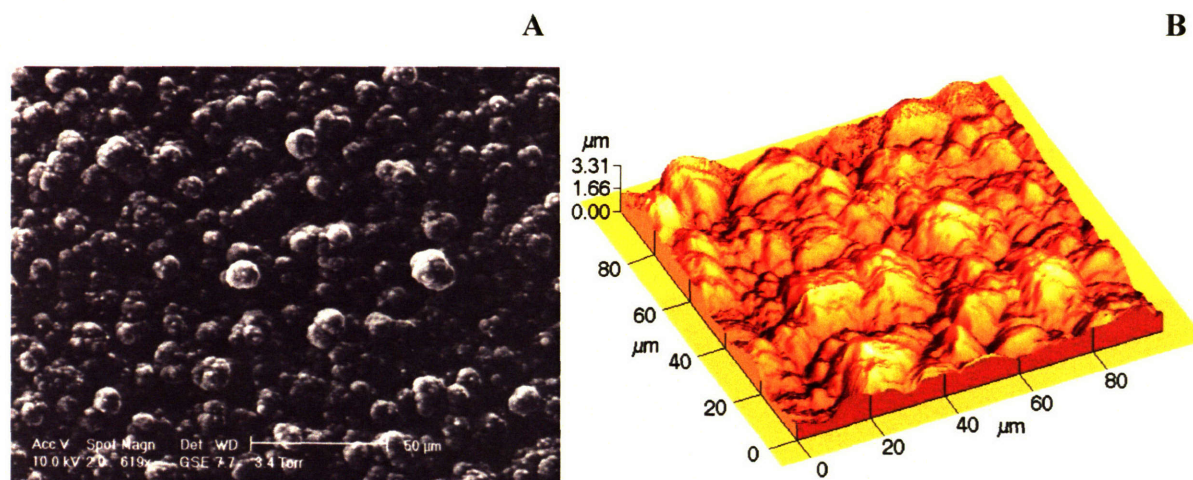


Figure 5.9: SEM and AFM micrograph of the surface morphology of a polypyrrole film synthesized under higher current density (1.25 A/m^2). The scale of (A) is about the same as Figure 5.8D.

Surface morphology has a great impact on the kinetics of the doping and undoping process during actuation. Maw and colleagues [Maw S. et al. 2001] realized that a lower current density leads to larger displacements, but did not correlate it to surface morphology.

5.3 Mass production: continuous deposition and fiber deposition

While the batch-like process of polymer synthesis optimized in this thesis leads to high quality films, continuous synthesis and processing is of importance for industrial applications. Two approaches were taken to explore industrial production of PPy. The first consists of producing PPy continuous films via a rotating drum electrode. The second involves creating polymer fibers from a circulating solution of monomer.

5.3.1 Continuous Deposition

Following the method proposed by Naarman [Naarman H. 1991], a continuous deposition apparatus was constructed [Gaige T.A. 2004]. The system allows synthesis of 45 mm wide conducting polymers of infinite length (provided the reactants are continuously supplied). It is composed of a double-bath liquid-to-liquid cooling system keeping the deposition solution at constant low temperature $-40\text{ }^{\circ}\text{C}$ Figure 5.10. The monomer is recirculated such that it can be kept homogeneous. This design also makes way for future closed loop control of the deposition reactants. Paratherm LR heat transfer fluid (<http://www.paratherm.com>) is used in the second bath as a heat transfer fluid.

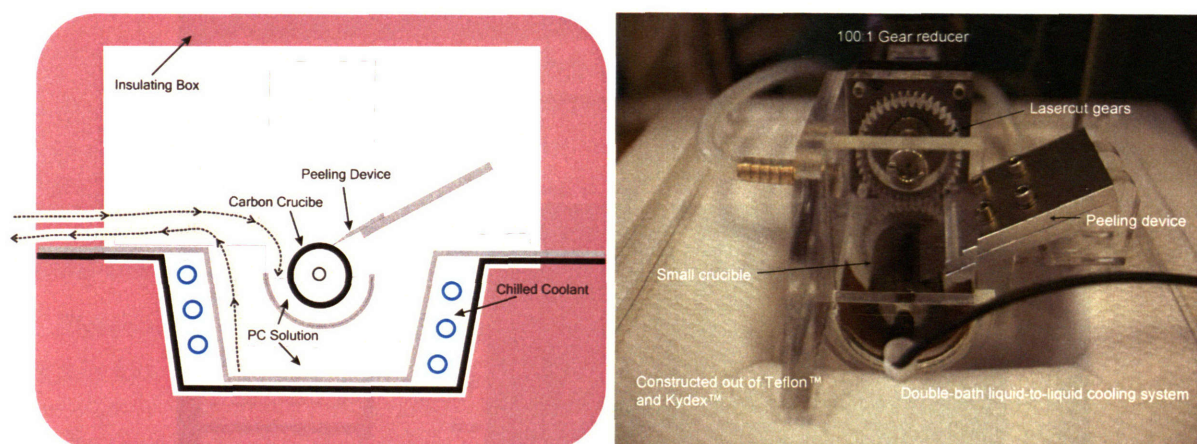


Figure 5.10: Continuous deposition apparatus developed at the MIT BioInstrumentation Laboratory. The whole system ensures continuous polymer deposition at $-40\text{ }^{\circ}\text{C}$. Monomer is recirculated to provide homogeneity and future control of reactants concentration. Courtesy of Terry Gaige [Gaige T.A. 2004].

A glassy carbon cylindrical crucible; 36 mm diameter, and 45 mm high, purchased from Alfa Aesar (www.alpha.com) is used as the rotating deposition surface. A Zeta 57-83M stepper motor driven by a Parker Compumotor 6104 (www.compumotor.com) indexer drive controlled through a standard RS-232 port on a PC drives the rotation of the crucible. The rotation of the stepper motor is amplified by a 100:1 PS23-100 AxisNE gear reducer (www.axisne.com). Laser cut Teflon gears transfer the torque down to the crucible. The counter electrode is a 0.4 mm thick sheet of copper. The sheet has a radius 10 mm larger than the crucible. A short wire is soldered to the end of the sheet to make an easy connection

to the power supply. The counter electrode is free to be removed so it can be cleaned and detarnished prior to a deposition. A cantilevered razor-blade allows continuous stripping of the PPy material off the rotating electrode as it is being synthesized.

The most important aspect of the continuous deposition experiment is the continuous recording of temperature, voltage, and current data. This is accomplished using a computer program designed in Visual Studio .NET (www.microsoft.com). The program, called the Deposition Control Center, records the measured data and plots it in real time in a graphic user interface shown in Figure 5.11. The Deposition Control Center also contains adjustable parameters for the control of the deposition current and the stepper motor.

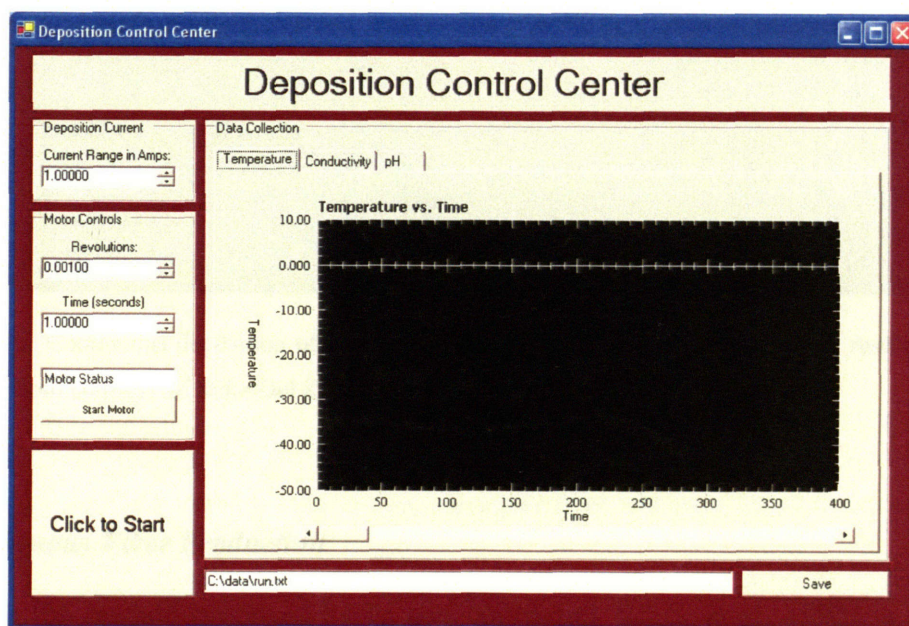


Figure 5.11: Screen shot of graphic user interface for the Visual Basic .NET program used to control and record parameters during a deposition.

Temperature measurements are made using Omega Type E precision fine wire (<http://www.omega.com>). Four thermocouples monitor the deposition temperature at various points of the system (primary and secondary bath, input and output of the recirculation system). The thermocouples are connected to an Agilent 20 Channel Multiplexer Card 34901A in an Agilent Data Acquisition/Switch Unit 34970A (www.agilent.com). Also connected to the 20 channel multiplexer are two inputs containing potential and current

signals from the AMEL Instruments Power Supply Model 2053 powering the synthesis (www.amelsrl.com). The measurements are then recorded digitally using a GPIB to USB adapter from the data acquisition unit to a standard PC running under Windows XP SP2 (www.microsoft.com).

Deposition occurs at slow rate of 0.5 A/m^2 . The crucible rotation speed is set at one revolution per 43,200s (12 hours per revolution) leading to a continuous film of conducting polymer. PPy films resulting from the continuous deposition system exhibit conductivities an order of magnitude lower than batch synthesized ones and weaker mechanical properties.

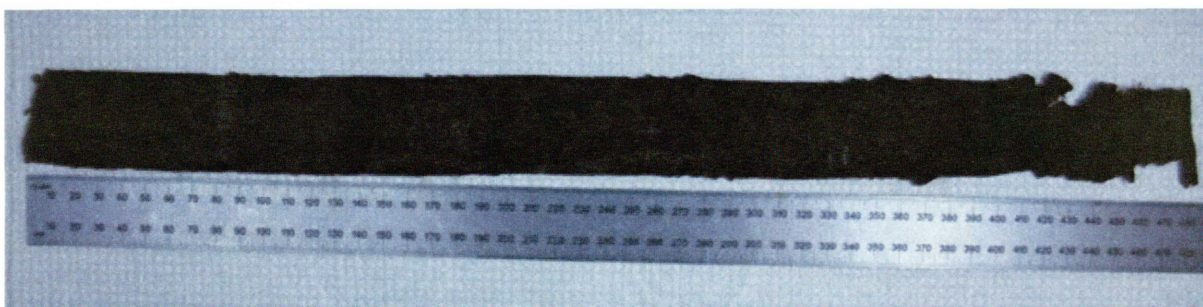


Figure 5.12: Continuous deposition of PPy for 36 hours. The crucible rotated 6times, resulting in a 480 mm long film. Photo courtesy of Mike Del Zio.

5.3.2 Continuous Fiber Production

Following the method proposed by Li and colleagues [Li S. et al. 1993], a conducting polymer fiber producing apparatus was constructed [Chen A.Y. 2004]. The deposition system is composed of an electrochemical flow cell composed, a 2 mL glass pipette (3.6 mm inner diameter) connected to Teflon tubing (6.35 mm inner diameter, www.masterflex.com) via two in-house designed bulbs (15 mm diameter). The monomer deposition mixture containing the monomer is kept in a reservoir (Figure 5.11). Flow initially occurs via gravity. A Masterflex L/S[®] Series Peristaltic Pump (www.masterflex.com) pumps the liquid back into the main reservoir kept at $-40 \text{ }^\circ\text{C}$. The whole system is thermally insulated. Deposition flow occurs at 2.8 mLs^{-1} , or a linear velocity of 275 mms^{-1} past the electrode. At

this speed the corresponding Reynolds number is on the order of 1500, which is within the laminar flow regime.

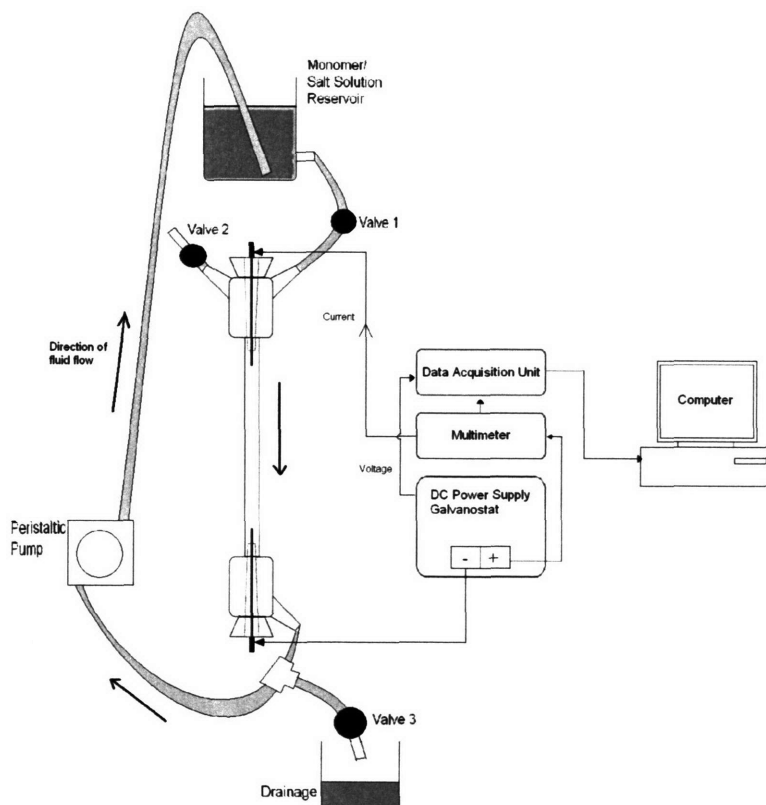


Figure 5.13: Fiber producing apparatus. Monomer + Electrolyte solution is circulated clockwise. Low flow speed at the cylindrical working electrode (top electrode) allows addition of polymer to the electrode. Diagram courtesy of Angela Chen [Chen A.Y. 2004].

Deposition occurred on the tip of a 0.3 mm platinum working electrode at a high current density of $4,240 \text{ A/m}^2$ powered by an Agilent E3632A DC power supply. Note that the velocity of the deposition solution behind the working electrode is near zero and allows oligomers to assemble. Figure 5.13 shows the fiber resulting from a 63 hour run. The fiber was 83 mm in length and between 0.8 to 1.05 mm in diameter. Note that the fiber's resulting diameter is larger than the working electrode diameter by a factor of 3. The fiber possessed some flexibility, but for the most part was very brittle. SEM micrographs show the rough texture of the fiber at various sections. The dendritic nature of the tip of the film suggests that the polymerization does not occur homogeneously. On the other hand, the smoothness

of the base of the fiber indicates that the fiber is smoothed as deposition progresses (zero velocity condition at the interface between the electrode and the liquid for a laminar flow). Several parameters of the system such as flow rate, cell diameter, current density, deposition voltage, and salt and monomer concentrations can be adjusted to affect the growth of the PPy fibers [Li S. and others 1993].

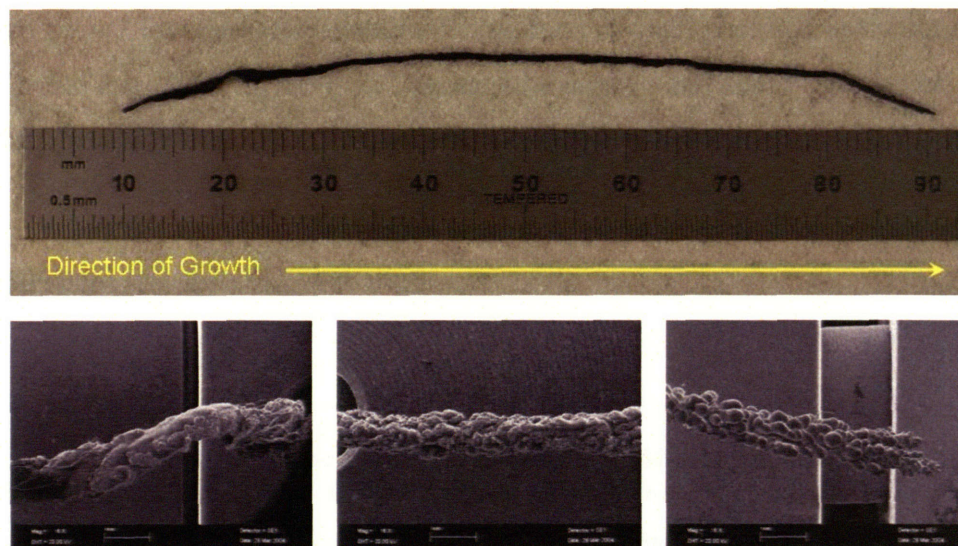


Figure 5.14: Fiber grown with the continuous fiber producing apparatus, including of three sections of the fiber (bottom). The resulting fiber was 83 mm long with a diameter ranging from 0.8 to 1.05 mm. Photo courtesy of Angela Chen [Chen A.Y. 2004].

The porous nature of the fiber is also characterized by a low density (843 kg/m^3 , compared to 1925 kg/m^3 for high quality PPy films). Conductivity and mechanical properties were much lower compared to the batch-synthesized high quality films. The fiber conductivity was 850 S/m , the Young's 0.155 GPa and the tensile stress 3.26 MPa (compare with Table 5.1).

Overall, while this method has the unique feature of producing polymer fibers, it is hampered by several limitations. The deposition is quite inefficient due to the circulation of the monomer: 63 hours of deposition only lead to about 55 mg of synthesized material. Second, the poor efficiency, coupled with poor mechanical and electrical properties, makes this approach unsuitable for industrial applications.

5.4 Discussion of results and conclusions

This Chapter presented the synthesis pathway to the formation of high quality conduction polymer films. The nucleation process of PPy was observed and the repeatability of the resulting films analyzed. Indications were found that the current density of the deposition may be largely influencing the deposition process. Two routes for industrial production of such high quality polymer films were pursued. While the synthesis of fibers proved impractical for large scale manufacturing, there is great potential in the rotating drum-electrode based approach. In the next Chapters the passive and active mechanical properties of PPy films from PPy1 and PPy2 batches are presented

5.5 References

- Armes S.P., In Handbook of Conducting Polymers, 2nd Edition, Stockheim T.A., Elsenbaumer R.L., Reynolds J.R. (Editors). Marcel Decker Inc., New York, pp. 423, (1998).
- Chen A.Y., "Electrodeposition of Conducting Polymer Fibers", MIT Bachelor Thesis, Supervised by Patrick A. Anquetil, (2004).
- Davidson S.N., Anquetil P.A. and Hunter I.W. , "Characterization of Polypyrrole Actuators Synthesized on Different Metal Electrodes", to be published, (2004).
- Ding J., Price W.E., Ralph S.F. and Wallace G.G., "Electrochemical Behavior of polypyrrole/sulfated poly(β -hydroxyether) composites", Synthetic Metals, Vol. 129, (67-71): (2002).
- Gaige T.A., "Continuous Conducting Polymer Deposition Device", MIT Bachelor Thesis, Supervised by Patrick A. Anquetil, (2004).
- Gregory R.V., Kimbrell W.C. and Kuhn H.H., "Conductive Textiles", Synthetic Metals, Vol. 28, pp. 823-835 , (1989).
- Hwang B.J., Santhanam R. and Lin Y.L., "Nucleation and growth mechanism of electropolymerization of polypyrrole on gold/highly oriented pyrolytic graphite electrode", Journal of the Electrochemical Society, Vol. 147, (6): pp. 2252-2257 , (2000).
- Lee J.Y., Kim D.Y. and Kim C.Y., "Synthesis of soluble polypyrrole of the doped state in organic solvents", Synthetic Metals, Vol. 74, (2): pp. 103-106, (1995).
- Li S., Macosko C.W. and Whilte H.S., "Electrochemical Processing of Conducting Polymer Fibers", Science, Vol. 259, pp. 957-960, (1993).
- Maw S., Smela E., Yoshida K., Sommer-Larsen P. and Stein R.B., "The effects of varying deposition current density on bending behavior in PPy(DBS)-actuated bending beams. ", Sensors and Actuators A, Vol. 89, pp. 175-184, (2001).

- Naarman H., "Strategies for Synthesizing Conducting Polymers", *Synthetic Metals*, Vol. 41, pp. 1-6, (1991).
- Nogami Y., Pouget J.-P. and Ishiguro T., "Structure of Highly Conducting PF6- -Doped Polypyrrole", *Synthetic Metals*, Vol. 62, pp. 257-263, (1994).
- Prissanaroon W., Brack N., Pigram P.J., Liesegang J. and Cardwell TJ, "Surface and electrochemical study of DBSA-doped polypyrrole films grown on stainless steel", *Surface and Interface Analysis*, Vol. 33, (8): pp. 653-662, (2002).
- Pud A.A., *Synthetic Metals*, Vol. 66, (1): pp. 1, (1994).
- Pytel R.Z., Private Communication, MIT BioInstrumentation Laboratory, (2004 Sep 30).
- Salmon M., Kanazawa K.K., Diaz A.F. and Krounbi M., *Journal of Polymer Science, Polymer Letters*, Vol. 20, pp. 187, (1982).
- Scharifker B.R., Garcia-Pastoriza W. and Marino W., "The Growth of Polypyrrole Films on Electrodes", *Journal of Electroanalytical Chemistry*, Vol. 300, pp. 85, (1991).
- Smela E, "Conjugated Polymer Actuators for Biomedical Applications", *Advanced Materials*, Vol. 15, (6): pp. 481-94, (2003).
- Swager T., Private Communication, (2004 Aug).
- Tanaka K., Shichiri T., Wang S. and Yamabe T., "Electronic Structure of Polyiminovinylene as a Tractable Model for Polyaniline", *Synthetic Metals*, Vol. 24, pp. 203-215, (1988).
- Yamaura M Sato K and Iwata K, "Memory Effect of Electrical Conductivity Upon the Counter-Anion Exchange of Polypyrrole Films", *Synthetic Metals*, Vol. 48, (337-354): (1992).
- Yoon C.O., Sung H.K., Kim J.H., Barsoukov E., Kim J.H. and Lee H., "The effect of low-temperature conditions on the electrochemical polymerization of polypyrrole films with high density, high electrical conductivity and high stability", *Synthetic Metals*, Vol. 99, pp. 201-212, (1999).

Chapter 6

Thermal Treatment of Polypyrrole

Actuator Films

The mechanical properties and the performance of conducting polymers are a function of the synthesis process (Chapter 5). The actuators presented in this thesis are intended to be incorporated into devices and achieve active functions. Understanding and characterizing the mechanical properties of these materials, both active and passive, is very important. Passive properties show how well the material can hold a given load, while active properties represent the contractile behavior of these materials. In this Chapter the passive mechanical properties of PPy-based actuators are studied. Chapter 7, on the other hand, will focus on the active properties of polypyrrole.

6.1 Overview of the Experimental procedure

The goal of this Chapter is to assess how passive mechanical properties of PPy films can be influenced by post-synthesis processing. Note that post-processing is an important step in the industrial manufacturing of today's polymers. There are thus three questions that this Chapter tries to answer:

1. Can the mechanical properties and performance of conducting polymers be influenced and controlled via processing?
2. How repeatable is this process?
3. Can these “enhanced” mechanical properties be irreversibly “frozen” into place, for instance when the actuator is re-immersed into its electrolyte environment, necessary for actuation?

6.2 Experimental Procedure

Films were synthesized following the procedure described in Chapters 4 and 5. The films presented in this Chapter are exclusively from the PPy1 and PPy2 batches presented in Chapter 5. Note that in this Chapter, the polymer film is subject to no potential and that only its mechanical properties are recorded. All passive mechanical measurements were done using a Perkin Elmer Dynamic Mechanical Analyzer 7e, which allows one to test films in air or in an electrolyte solution.

6.3 Thermal Relaxation in Electrolyte (0.05 M TEAP in PC).

This study began with an initial discovery that a film heated to 90 °C showed irreversible behavior in its strain response. Following this initial discovery, further experiments were undertaken to determine the cause of this response.

A fresh sample of PPy (10.68 mm long, 1.45 mm wide and 20 μm thick) was clamped into a Perkin Elmer DMA 7e, held at constant force (1.4 MPa) and inserted into a beaker containing 0.05 M TEAP solution in PC. The baker containing the clamped polymer was then placed into the instrument’s furnace, where it was subject to a ramp in temperature. Figure 6.1 shows the contraction resulting when the temperature is ramped at 5 °C/s from 25 °C to 90 °C and then reversed to 52 °C.

Initially, the film contracts and the rate of contraction increases with increasing temperature. At the end of the process, the film length contracted by 2 %. Note that the dimensional changes are not purely functions of temperature, as would be characteristic of

thermal expansion. Instead, there appears to be a relaxation of the polymer structure, which is accelerated with increasing temperature.

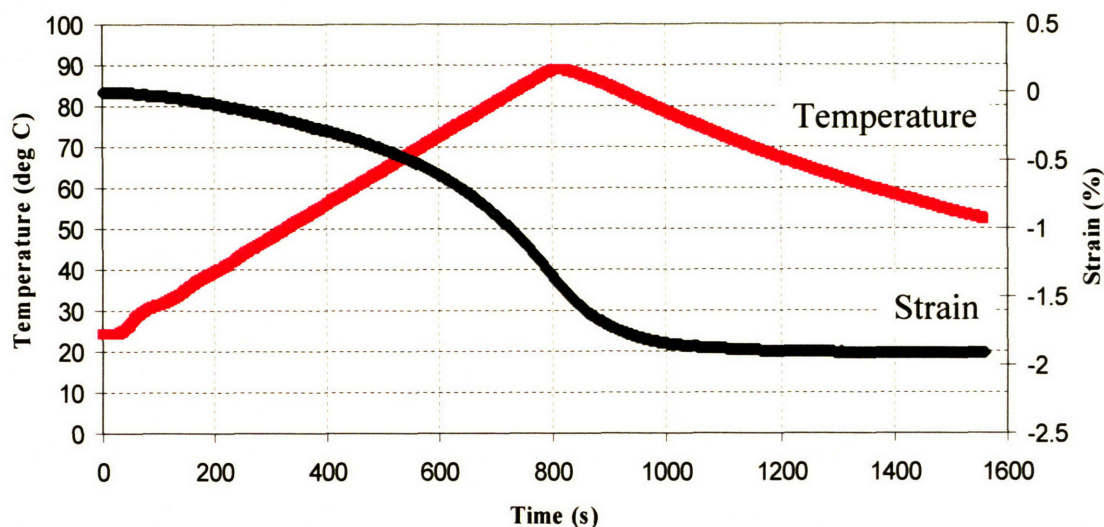


Figure 6.1: Strain response of a PPy film in electrolyte subject to a heating ramp up to 90 °C

One possible explanation for the observed dimensional changes is that heat enables the film to relax toward a thermodynamically favorable state. Second, unlike metals, for example, PPy shrinks with increasing temperature. Although surprising, this behavior is typical of polymer networks and called the Gulch-Joule Effect [Grosberg A.Yu and Kohkhlov A.R.]. At the heart of polymer elasticity is the entropy of the long polymer chains. As the polymer sample is stretched, the entropy of the different molecules being elongated decreases. Reversibly as temperature is increased, entropy increases thus causing the molecule to occupy more conformations. As a result, the polymer film shrinks. Note that the cause of the polymer shrinking is not evaporation of solvent contained in the material as the polymer film is held in its “native” electrolyte.

To study the effect of heating a film of PPy in electrolyte, we now subject two PPy films to repeated heat waveforms, one from room-temperature (20 °C) to 30 °C and the other one to 90 °C (Figure 6.2). Notice again that no potential is applied to the material during these tests.

The two films of PPy are held at constant stress (2.5 MPa) for 42 hours directly after synthesis. Both films come from the same synthesis batch and their dimensions were 6.76 mm long, 2mm wide, and 24 μm thick (Figure 6.2A) and 8.64 mm long, 2.2 mm wide and 30 μm thick (Figure 6.2B). The samples were tested in the same electrolyte as the one used for synthesis (0.05 M TEAP in PC) and were initially allowed to relax at 20 $^{\circ}\text{C}$ for 6 hours. The heating waveforms consisted of three cycles from 20 to 30 $^{\circ}\text{C}$ and back (Figure 6.2A) and from 20 to 90 $^{\circ}\text{C}$ and back (Figure 6.2B) respectively for six hours intervals.

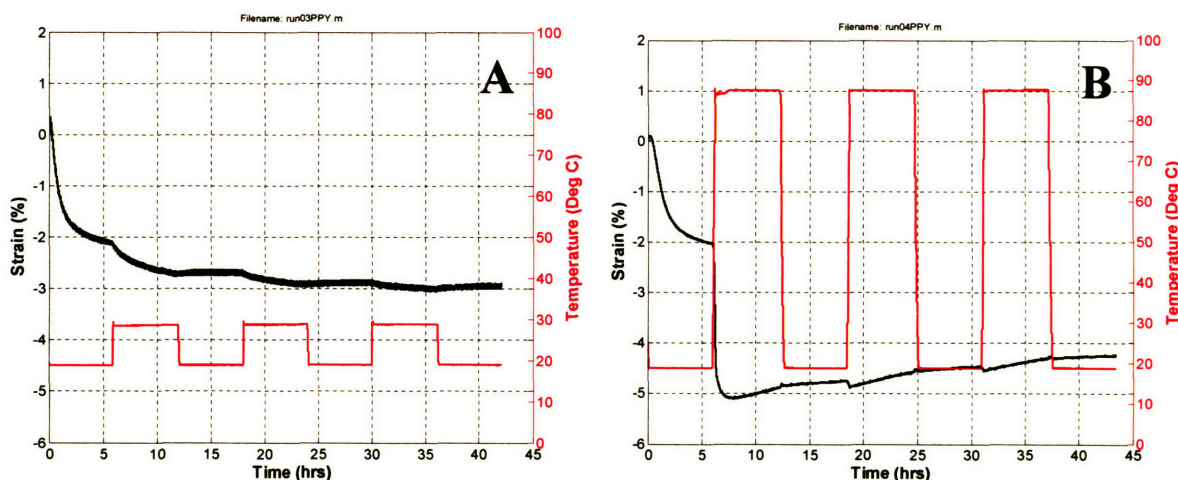


Figure 6.2: Effect of temperature on two PPy samples held in electrolyte at 2.5 MPa stress. The PPy films were from the same batch and held at the same stress: 2.5 MPa for 42 hours and cycled from 20 to 30 $^{\circ}\text{C}$ (A) and from 20 to 90 $^{\circ}\text{C}$ (B) respectively for 6 hours intervals in air.

During the first six hours of the experiment both films relax slowly by 2%. The rate of strain relaxation induced by holding a film at constant stress (2.5 MPa) during the first 6 hours at 20 $^{\circ}\text{C}$ is 3.32×10^{-4} %/s and is the same for both samples. As the temperature of the sample is increased, the rate of relaxation increases. At $t = 6$ hours Film A is heated to 30 $^{\circ}\text{C}$ and contracts at a rate of 1.15×10^{-4} %/s, while Film B contracts by 3.70×10^{-3} %/s (or a 32 \times increase). After 1.8 hours at 90 $^{\circ}\text{C}$, Film B has contracted by a total of 5.1 % and starts to slowly expand again. This expansion most likely corresponds to creep induced by the moderate stress (2.5 MPa) applied to the film.

Interestingly, only the first exposure to a high temperature leads to a large contraction. Subsequent temperature cycles have little effect on the strain behavior of the film. This may be an indication that irreversible structural changes of the film take place upon first exposure to a 90 °C temperature.

6.4 Dynamic Mechanical Analysis of Thermal Relaxation in Air

To test the hypothesis that irreversible structural changes occur in a polymer film upon exposure to a 90 °C temperature, the dynamic mechanical behavior of a film under similar conditions was probed. Dynamic mechanical analysis allows extracting both the real and the imaginary component of the complex modulus of the material tested (Chapter 4). The real part of the amplitude of the complex modulus is referred to as the dynamic modulus E' while its phase δ is characterized by the $\tan \delta$ value. Both the dynamic modulus E' and the $\tan \delta$ give an appreciation of a material's viscoelastic behavior. If the material is subject to a phase transition, then a peak in the $\tan \delta$ as well as an increase (or decrease) in the dynamic modulus appears.

A film of PPy (6.52 mm long, 2 mm wide and 24 μm thick) was held at a constant stress of 2.5 MPa for 7.5 hours. For this test, it is important that the movement of the probe holding the polymer film is not affected by the environment surrounding it. Therefore this test was performed in air. After one hour equilibrium at 20 °C, the film was heated at a rate of 5 °C/to 90 °C and held at this temperature for 6 hours (Figure 6.3A). Following the heating period at 90 °C, the PPy film was cooled down at 10 °C/s back to 20 °C. Next the film was subjected to another 10 hour period of heating at 90 °C and cooled back to 20 °C for an additional 10 hours (Figure 6.3B).

As shown in Figure 6.3, we notice that upon the first 90 °C exposure, the film contracts by almost 11 % at a strain rate of 8.47×10^{-3} %/s. As previously seen in Figure 6.1, the film does not expand back to its original length when cooled back to room temperature (20 °C). In addition, the subsequent heating run does not trigger a similar film contraction like in the first cycle. Inspection of the dynamic response also shows a peak in the $\tan \delta$ at the time the sample reaches 90 °C for the first time and a rise in the dynamic modulus E' from 1 GPa to

1.4 GPa. Similarly, this behavior does not take place once the film is subject to a second 90 °C wave following the first one.

The data shown in Figure 6.3 is evidence that an irreversible material relaxation occurs upon exposure to a temperature around 90 °C. In this particular case, the film is placed in air but still contains some solvent. Hence the contraction of 11 % of the film is due to both the material relaxation as well as solvent evaporation. In comparison a film placed in solvent and subject to a 90 °C wave contracted by 5 % (Figure 6.1), suggesting that 6 % of the contraction of the film placed in air was due to solvent evaporation. In the following section it will be shown that this is indeed the case.

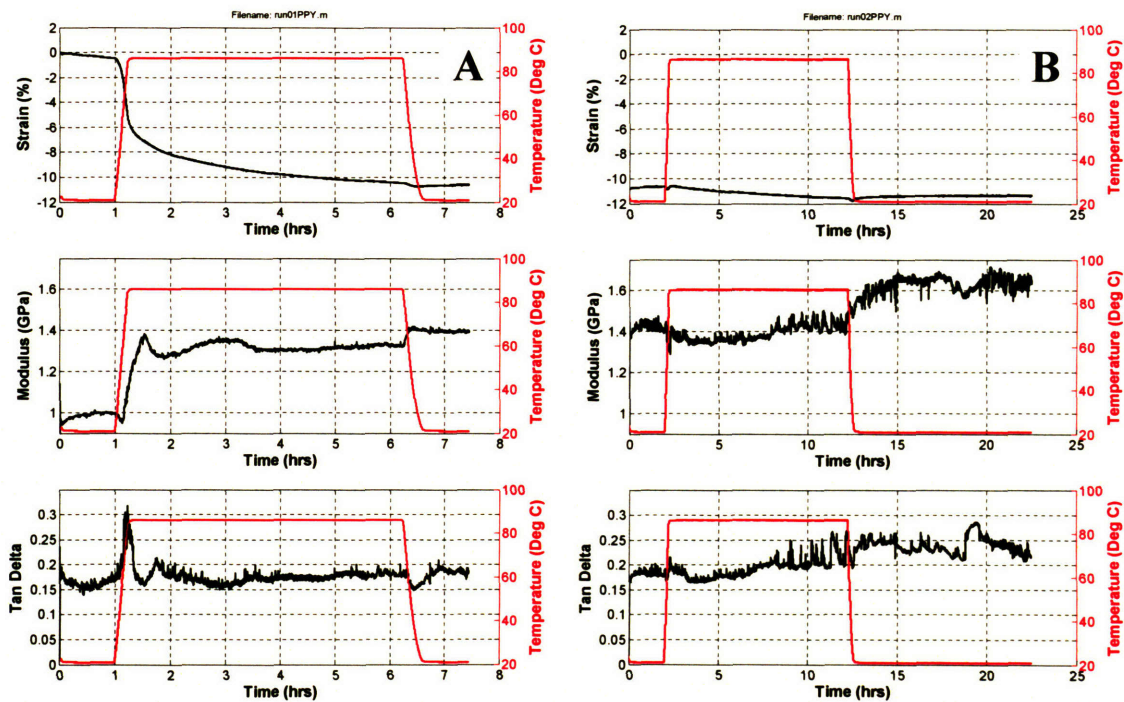


Figure 6.3: Analysis of irreversible mechanical deformation of PPY subject to temperatures as high as 90 °C. The film's dynamic modulus as well as its $\tan \delta$ change upon the first exposure to 90 °C and do not change in the following temperature rise. Part A depicts the first 7.5 hours of the run while Part B shows the following 23 hours.

6.5 Thermal Relaxation in Vacuum

6.5.1 Effect on Film Mass and Electrical Properties

To study the effect of subjecting PPy to a temperature around 90 °C, PPy films were placed into a VWR vacuum oven for 2 hours under a vacuum of 9.14×10^4 Pa (27 inch Hg). Subjecting a sample to vacuum and to a high temperature allows for all remaining solvent to escape the material. The dimension, mass, and conductivity of the PPy samples were measured and their density calculated prior and after the vacuum oven treatment. In addition, mechanical properties of the film such as tensile strength, and Young's modulus were recorded as well.

Table 6.1 shows side by side a sample each of PPy1 and PPy2 batches. With respect to Table 6.1, note that the conductivity of the films hardly changes, whereas their mass and dimensions on the other hand change by a large percentage. The vacuum treatment leads to a mass loss of 32 % and 29 % for PPy1 and PPy2 films respectively. This mass loss corresponds to solvent evaporating from the film upon exposure to vacuum at high temperature. Interestingly this evaporation is associated with a volumetric "contraction". The largest dimensional change associated with this mass loss appears to be in the thickness direction (28 and 32 % respectively). This agrees with observations made by Smela and colleagues that PPy has a layered structure parallel to the plane of the substrate it is deposited on [Smela E. and Gadegaard N. 1999]. A model of swelling suggests that solvent and salt molecules go in between these layers and displace them, thus creating expansion on the order of 30% in the direction of the thickness. Future work should focus on trying to harvest that large contraction in the off-plane direction. A stack of PPy/electrolyte gel/PPy/electrolyte gel... containing 1000 layers would lead to displacements on the order of 7 mm.

The fact that conductivity hardly changes upon vacuum treatment is important. It shows that heat (under vacuum) does not affect the integrity of polypyrrole. One concern of exposing polypyrrole to high temperatures would be for oxidative degradation to take place. This would lead surrounding oxygen molecules to attack the β position (see Chapter 5) on the pyrrole ring thus affecting its mechanical integrity. Hence the polymer can be treated without affecting its conductivity for future usage as an actuator. In the following section the

effect that thermal vacuum treatment has on the mechanical properties of the film will be presented.

	PPy1	PPy2
Conductivity before (S/m)	3.81×10^4	4.0×10^4
Conductivity after (S/m)	3.65×10^4	3.74×10^4
Conductivity difference	- 4.1 %	- 3.9 %
Density before (kg/m^3)	1925	1851
Density after (kg/m^3)	2017	1956
Density difference	- 4.7 %	- 3.7 %
Mass before (g)	2.286	2.262
Mass after (g)	1.552	1.673
Mass difference (g)	- 32 %	- 29 %
Dimensions before [l(mm) \times w(mm) \times t(μm)]	$23.75 \times 2 \times 25$	$23.5 \times 2 \times 26$
Dimension after [l(mm) \times w(mm) \times t(μm)]	$22.5 \times 1.9 \times 18$	$22.5 \times 1.9 \times 19.5$
Dimension difference [l \times w \times t]	5.3 % 5 % \times 28 %	4.3 % \times 5 % \times 25 %
Volume difference	35 %	32 %

Table 6.1: Comparison of two PPy films from batch PPy1 and PPy2 prior to and after being subjected to a vacuum treatment consisting of a 2 hour exposure to 90 °C under a vacuum of 9.14×10^4 Pa (27 inch Hg).

6.5.2 Effect on Mechanical Properties

In this section, films from the PPy1 batch were placed into a VWR vacuum oven for 2 hours at 90 °C under a vacuum of 9.14×10^4 Pa (27 inch Hg). The films were then clamped onto a Perkin Elmer DMA 7e for mechanical testing. The films lengths were all 10.5 mm (between clamps) while their width ranged between 2.25 and 3 mm. Destructive testing was performed on them by applying a stress ramp input of 5,000 kPa/min. The resulting strain is then plotted against the applied stress. From this curve Young's modulus, tensile strength and elongation to break can be extracted.

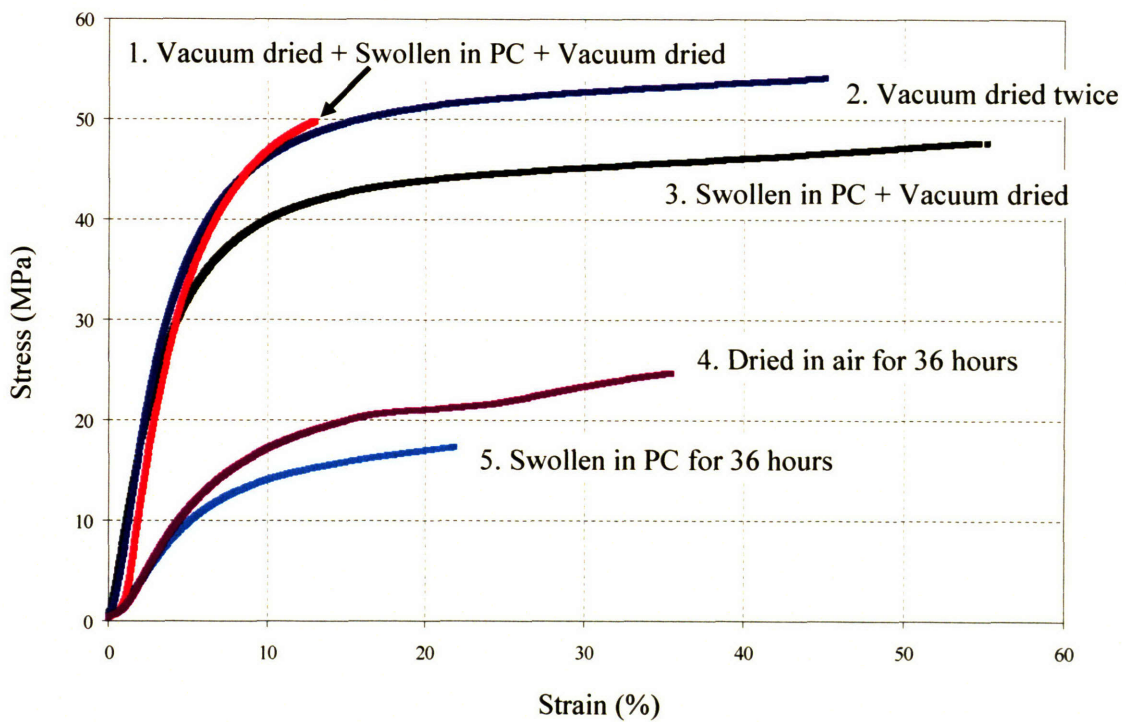


Figure 6.4: Comparison of various samples from PPy1 batch under different treatment conditions. Note the increased mechanical properties of vacuum dried films compared to films swollen in solvent and electrolyte.

Figure 6.4 shows results for five different polypyrrole films from PPy1 batch. From top to bottom, below are the conditions that were applied to each film:

- Film 1 was dried for 2 hours at 90 °C under a vacuum of 9.14×10^4 Pa (27 inch Hg), then swollen again in PC solution containing 0.05 M TEAP electrolyte for 24 hours. Following this, the samples were subjected to the same vacuum treatment as the one in the first step.

- Film 2 was dried twice for 2 hours at 90 °C under a vacuum of 9.14×10^4 Pa (27 inch Hg) within a period of 36 hours.

- Film 3 was first swollen in a PC+Electrolyte solution for 24 hours followed by a 2 hour treatment at 90 °C under a vacuum of 9.14×10^4 Pa (27 inch Hg).

- Film 4 was left in air for 36 hours.

- Film 5 was kept in a PC+Electrolyte solution for 36 hours.

Table 6.2 summarizes all the mechanical data for films 1 through 5.

Film #	Treatment	Young's Modulus [GPa]	Tensile Strength [MPa]	Elongation to Break (%)
Film 1	Dried + swollen + dried	1.02	49.6	13.6
Film 2	Dried twice	0.89	54	44.9
Film 3	Swollen in PC+Elec. + dried	1.04	47.6	32.5
Film 4	In air for 36 hours	0.245	24.7	36
Film 5	In PC+Elec. for 36 hours	0.21	17.3	22.5

Table 6.2: Summary of stress-strain mechanical tests performed on Films 1 through 5 (PPy1 batch).

Inspection of Figure 6.4 shows how much the mechanical properties of PPy change upon exposure to heat under vacuum. Heat treated samples under vacuum showed a higher stiffness and a larger tensile strength and elongation to break than non-treated films. Interestingly, Film 4 which was left in air for 36 hours shows a mechanical behavior in between the oven-treated and the non-treated samples. In this particular case, solvent is present in the film, but some of it may have evaporated during the 36 hour period. Note that the mechanical response of Film 4 is more similar to Film 5, the PC saturated film, than to the vacuum dried ones. This suggests that a significant amount of solvent is still present in the film after 36 hours as confirmed by weight measurement. This implies that one should be

careful before performing mechanical tests and either dry the film or saturate it in PC + electrolyte to make sure its initial conditions are known.

Finally Figure 6.4 shows how repeatable the drying process is. Film 1 and 2 were both dried twice but Film 1 was allowed to swell in PC in between the two drying processes. Film 3 which was only dried once shows also a similar mechanical response to stress.

To test the repeatability of the drying process across batches and at different time, two films from the PPy2 batch were dried together under the same conditions, but mechanically tested within a one week interval. Figure 6.5 shows how repeatable the drying process is. Both mechanical curves are nearly identical. The mechanical properties of these two films (Film 6 and 7) are presented below in Table 6.3. The films were both 5 mm long while their width was 2 mm and 1.8 mm for Film 6 and 7 respectively. Destructing testing was performed on the samples by applying a stress ramp input of 5,000 kPa/min.

Film #	Treatment	Young's Modulus [GPa]	Tensile Strength [MPa]	Elongation to Break (%)
Film 6	Dried once	0.84	53.6	42
Film 7	Dried once, test after 1 week	0.84	54	46.4
Film 8	Dried once, 2000 kPa/min	0.84	54	46.4

Table 6.3: Summary of stress-strain mechanical tests performed on Films 6 through 8 (PPy2 batch).

Note that the deformations shown in Figure 6.5 are very large compared to typical engineering materials such as steel or aluminum. This can be explained by using the rubber elasticity theory. Curled-up polymer chains stretch during deformation but are hindered in sliding past each other by bonds between them and other polymer molecules. The stretching of the coiled molecules shows a reversible elastic response. As stretching is prolonged, the entangled molecules are able to move more freely, leading to a plateau response as seen in Figure 6.5. Vacuum treatment removes the solvent and thus allows PPy molecules to interact

with each other. This enhances the stiffness and the overall elongation capability of the material in addition to relaxing internal stresses as shown in section 6.3.

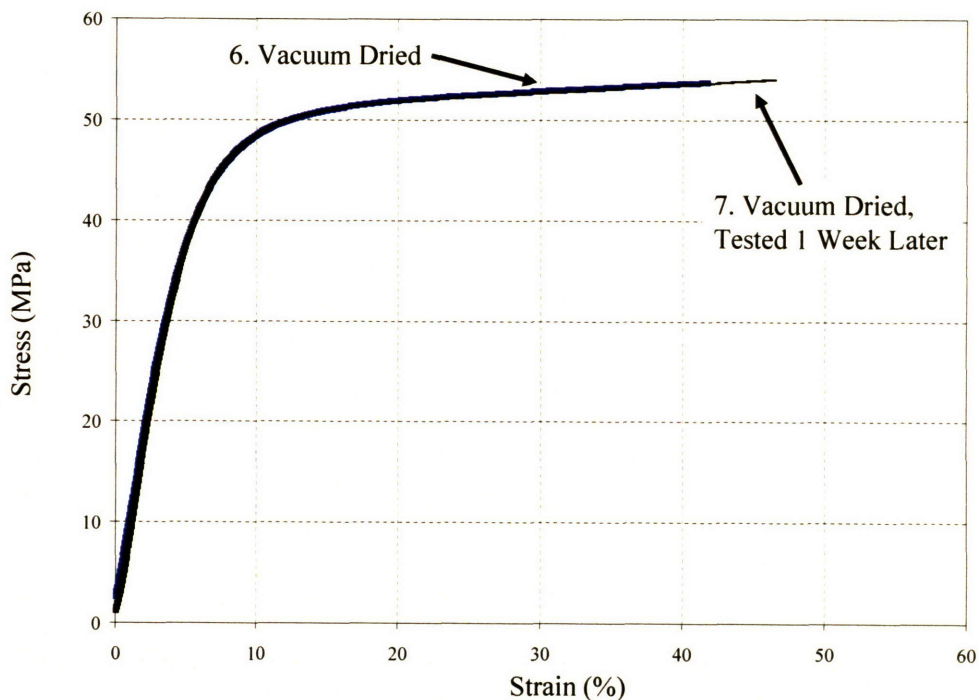


Figure 6.5: Films from PPY2 batch mechanically tested after the drying treatment. Although both films were dried at the same time, their mechanical testing was done a week apart.

This behavior is even more accentuated for tests occurring at a slower ramp input of 2,000 kPa/min. Figure 6.6 shows the result of stretching PPY at a 2,000 kPa/min. rate. The film was 4 mm wide and 12 mm long (between clamps). Note the long linear drawing regime between 15 % and 75 % elongation. Such a behavior is characteristic of a semi-crystalline material [Oswald T.A. and Menges G. 2003]. Elongation of Film 8 on Figure 6.6 was 116 %, Young's modulus 0.85 GPa and the film reached 75 MPa without breaking.

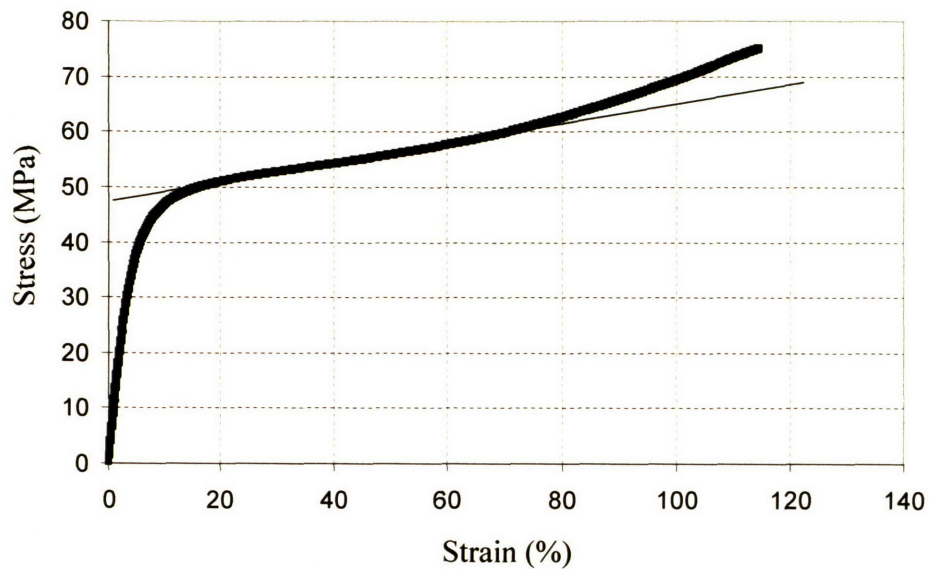


Figure 6.6: Large strain achieved in PPY. A straight line shows the drawing property of the film between 15 and 75 % elongation (Film 8).

6.5.3 Post Treatment Analysis: Exposure to 90 °C Cycles in a DMA in Air

To study the irreversible relaxation when heating PPY in vacuum to 90 °C, we subject a sample of PPY following heat treatment in vacuum to repeated 90 °C heat waveforms while it is mechanically probed in a Perkin Elmer DMA 7e. This experiment is similar to the one presented in Figure 6.2, where a PPY film held under constant 2.5 MPa stress is cycled in 6 hours intervals between 20 °C and 90 °C. For this experiment, however, mechanical testing is not done in electrolyte but in air.

Figure 6.7A shows the strain result of this experiment, while Figure 6.7B shows an untreated sample for comparison also held in air. Both films came from PPY2 batch and their dimensions were 7.42 mm long and 2 mm wide and 7.85 mm long and 2 mm wide respectively. The initial vacuum heat treatment was 2 hours at 90 °C under a vacuum of 9.14×10^4 Pa (27 inch Hg).

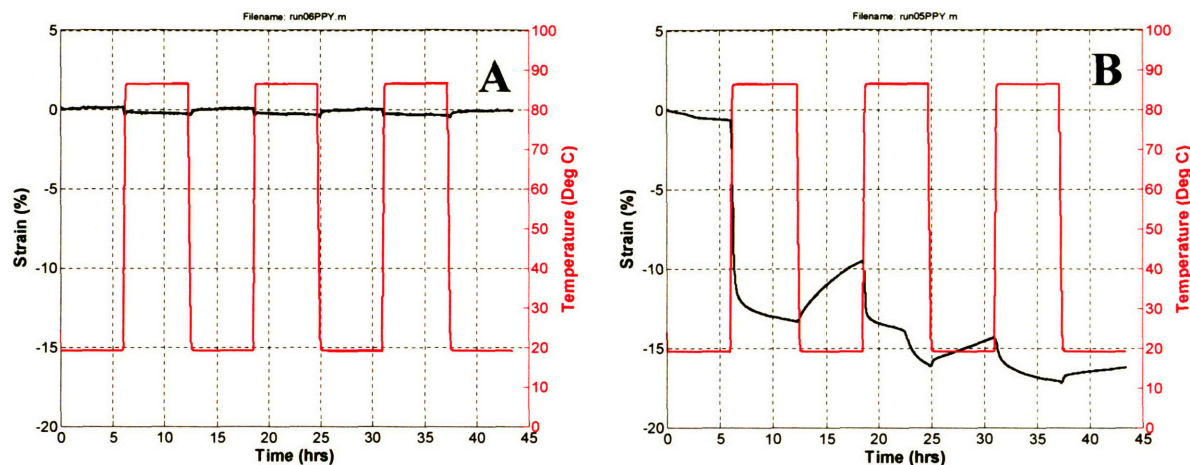


Figure 6.7: Response of a vacuum-treated PPY film subject to 6 hour long 20 °C and 90 °C temperature intervals in air (A). An untreated sample subject to the same heat waveform is presented for comparison (B). Note how little influence the temperature change has on the vacuum-treated film (A) compared to a non-treated film (B).

The difference between a vacuum-treated and an untreated sample is dramatic. The strain from the treated sample is barely affected by the 20-90 °C heat wave. In the following section this run will be used to estimate the coefficient of thermal expansion of PPy. On the other hand, the untreated PPy sample contracted by 16.5 % by the end of the same 42 hour trial. This is further evidence that an irreversible material relaxation takes place when PPy is initially subject to a temperature of at least 90 °C and agrees with findings of section 6.2.

6.5.4 Post Treatment Analysis: Expansion Due to Ion “Re-swelling”

In this section, the effect of immersing a vacuum-treated sample back into an electrolyte solution is studied. It allows understanding of the dynamics of expansion due to ion “re-swelling” into a film from which all the electrolyte and solvent have been removed via vacuum treatment at elevated temperature.

A PPy film held under constant 2.5 MPa stress is cycled in 6 hour intervals between 20 °C and 30 °C in a 0.05 M TEAP in PC solution. Figure 6.8A shows the strain result of this experiment for a vacuum-treated sample, while Figure 6.8B shows the strain for an

untreated one subject to the same heat waveform. The latter films were placed in the PC + 0.05M TEAP solution directly after synthesis while the first one was initially vacuum heat treated for 2 hours at 90 °C under a vacuum of 9.14×10^4 Pa (27 inch Hg). Note that the data of Figure 6.8B is the same as the one in Figure 6.2A. Both films came from PPy2 batch and their dimensions were 7.42 mm long and 2 mm wide and 7.85 mm long and 2 mm wide respectively.

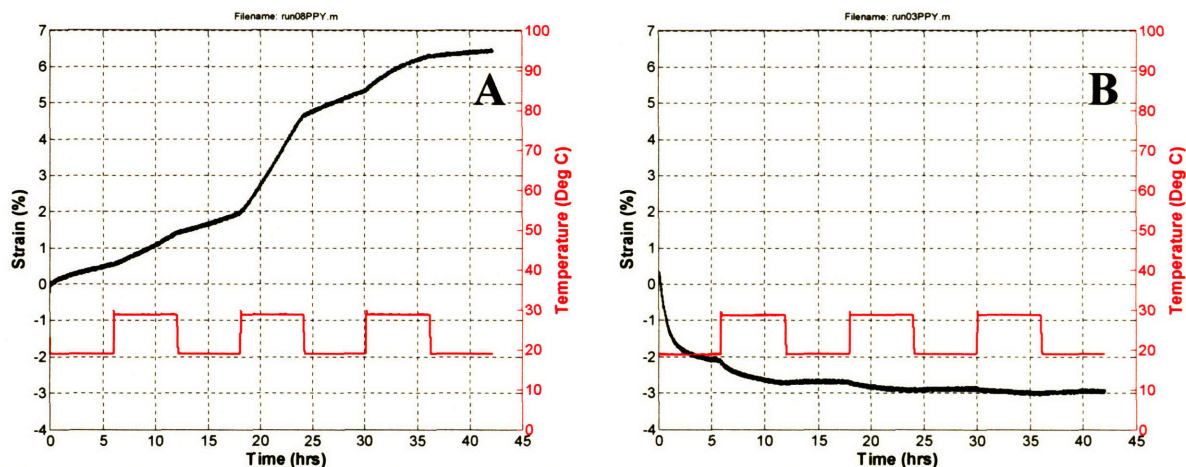


Figure 6.8: Response of a vacuum-treated PPy film subject to 6 hours long 20 °C and 30 °C temperature intervals in electrolyte (A). An untreated sample subject to the same heat waveform is presented for comparison (B). Note how little influence the temperature change has on the vacuum-treated film (A) compared to a non-treated film (B).

Analysis of Figure 6.8A shows that a vacuum-treated PPy film subsequently placed back into electrolyte swells again instead of contracting as would the non-treated one (Figure 6.8B). The elongation of PPy in Figure 6.8A appears to follow slight first order dynamics, characteristic of a diffusion process, and its rate of elongation increases when the temperature is cycled from 20 to 30 °C. At the end of the 42 hour run, the elongation appears to have stabilized at 6.5 % elongation. This elongation is comparable to the length change due to the contraction when solvent is removed from the film following the vacuum treatment at 90 °C (see Table 6.1).

Finally the mechanical stability of the vacuum treatment has to be tested when a sampled is placed back into its electrolyte solution. To do so, the mechanical properties of the PPy sample presented above, in Figure 6.8A (Film 9), were tested following the “re-swelling” process also described above (6 hours heating cycles between 20 and 30 at a stress of 2.5MPa for a total of 42 hours).

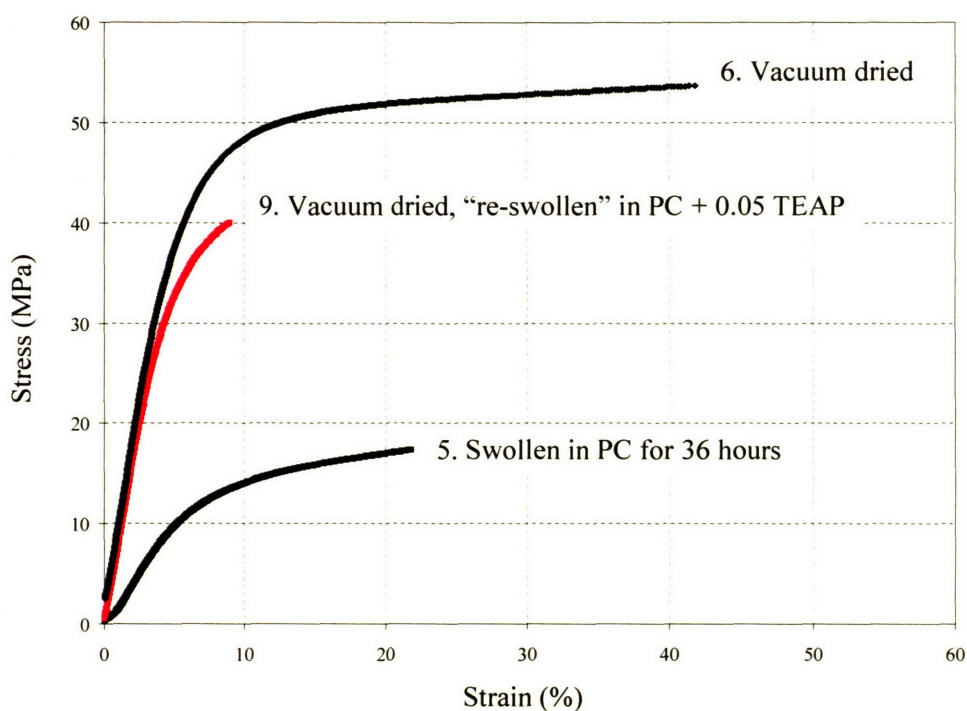


Figure 6.9: Films from PPy2 batch mechanically tested after the “re-swelling” process following the vacuum treatment. Both Film 5 and 6 from Figure 6.4 and Figure 6.5 are shown for comparison. The mechanical properties are very similar to Film 6 which was tested in air (and hence not “re-swelled”).

Figure 6.9 shows the mechanical response of Film 9 (re-swollen after vacuum treatment) when subject to a stress ramp input of 5,000 kPa/min. Both Film 5 and 6 from Figure 6.4 and Figure 6.5 are shown for comparison. The mechanical properties of Film 9 are very similar to Film 6 which was tested in air (and hence not “re-swelled”). In addition, the stiffness and tensile strength are much higher than a non-vacuum-treated PPy film that was conserved in its electrolyte. This result shows that the mechanical properties of a PPy film are permanently affected by subjecting it to a temperature as high as 90 °C for 2 hours under

vacuum. This further confirms the hypothesis that an irreversible material relaxation takes place when PPy is subject to a temperature of 90 °C.

Film #	Treatment	Young's Modulus [GPa]	Tensile Strength [MPa]	Elongation to Break (%)
Film 9	Dried once, placed in PC	0.8	40	8.9

Table 6.4: Summary of stress-strain mechanical tests performed on Film 9 (PPy2 batch).

6.6 Thermal Properties

6.6.1 Destructive Heating of PPy

While all the thermal treatment presented herein was performed at 90 °C, it is necessary to understand how the material behaves at a wide range of temperatures and at what temperature the material starts to mechanically fail. In this section two experiments intending to assess these properties are described.

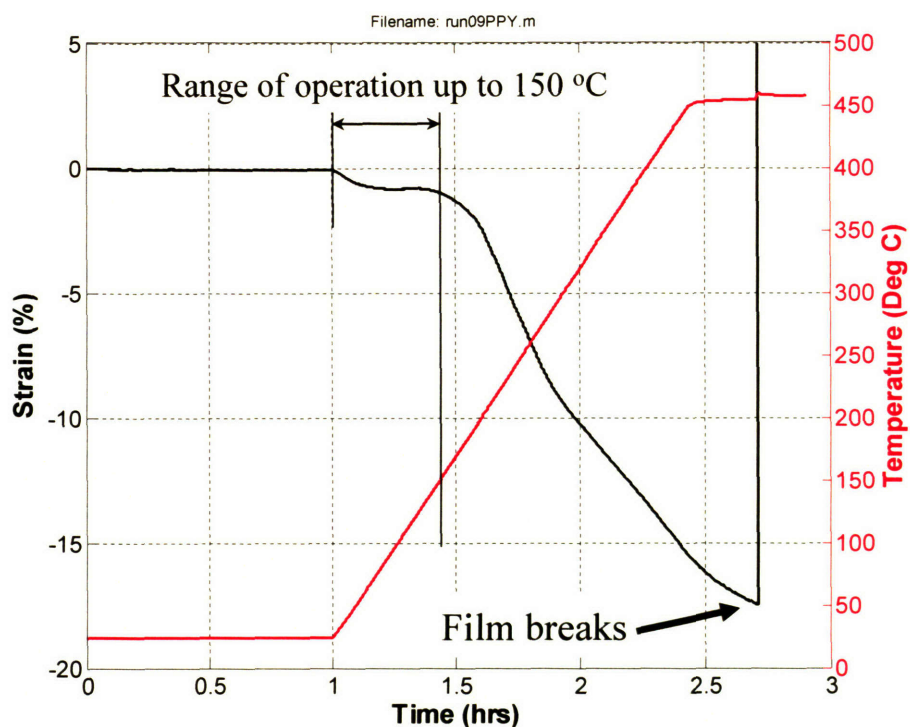


Figure 6.10: Mechanical degradation of PPy when subject to high temperatures (up to 460 °C).

The first experiment consists of heating a sample of PPy2 batch at a rate of 10 °C/min up to 460 °C. A 11.5 mm long, 2 mm wide and 25 µm thick PPy film was clamped into the Perkin Elmer DMA 7e and held at constant 2.5 MPa stress for a period of 3 hours. The whole experiment was done in air (as opposed to in electrolyte). Figure 6.10 shows that a large drop in strain occurs once a temperature beyond 150 °C is reached, indicating mechanical degradation of the film. The film eventually breaks shortly after reaching 460 °C. Inspection of the film following this experiment shows that it is very brittle (almost

powder-like), further indicating that mechanical degradation occurred. From Figure 6.10 an upper bound of 150 °C can be set as the operating range of PPy before thermal degradation occurs.

In the second experiment, heat is induced via Joule heating by passing a current through the sample. At the same time, the film was held at constant stress (2.5 MPa) in the custom-build electrochemical DMA, allowing recording film length as a function of time. An FLIR Systems (<http://www.flirthermography.com>) ThermoVision A40 M infrared video camera allows monitoring of the heat induced in the sample via Joule heating.

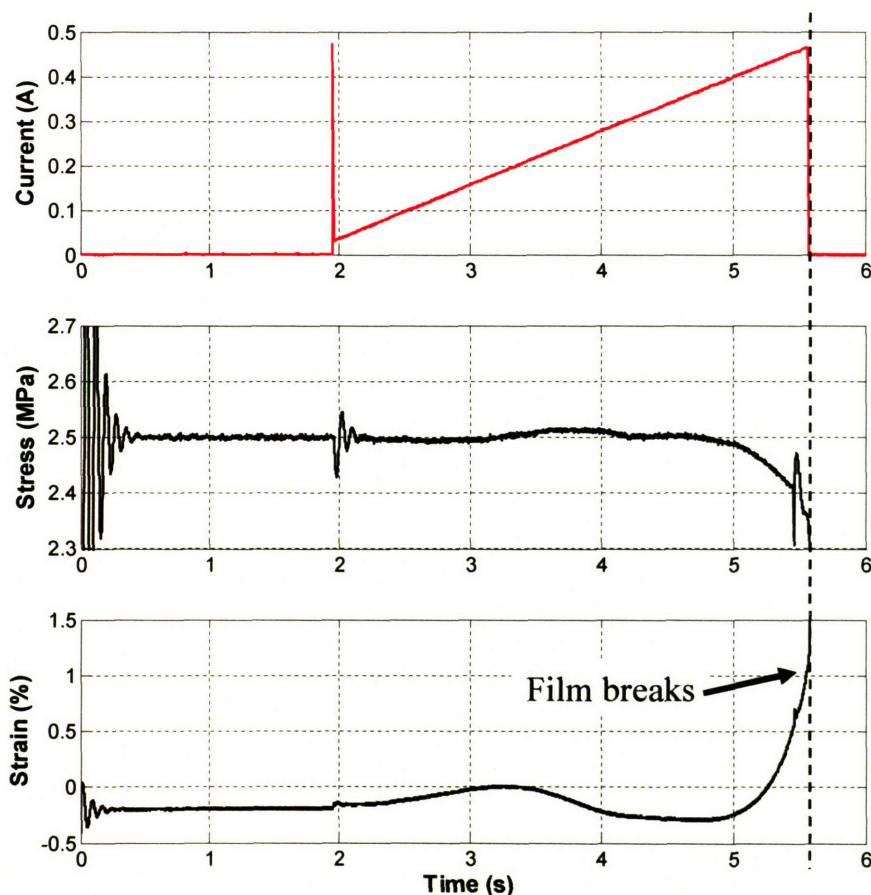


Figure 6.11: Corresponding current, stress and strain signal resulting from Joule heating a sample

A 28 mm long, 4.25 mm wide and 20 μm thick film was placed in the custom-build electrochemical DMA (E-DMA). The clamps of the E-DMA contain electrical contacts allowing one to subject the film to a current ramp of 125 mA/s starting at 25 mA. Current,

stress and strain are recorded (Figure 6.11) and the subsequent film heating monitored via the IR camera (Figure 6.12).

Figure 6.11 shows that the strain response is initially almost constant. Both the stress and strain signal show that the film starts to give way when a current of 400 mA is reached at $t = 5$ s. Inspection of the IR signature at the same time shows that a temperature higher than 160 °C is reached. Figure 6.12 shows clearly how the mechanical integrity of the PPy film gives way and subsequently brakes. Knowing the cross-section of the tested PPy film, the current carrying capacity of this PPy sample (in air) is estimated at 4.7×10^6 A/m². This value is similar to copper and shows the great potential of PPy wires as energy transmission materials. Note again that this measurement is done in air, not in an electrolyte.

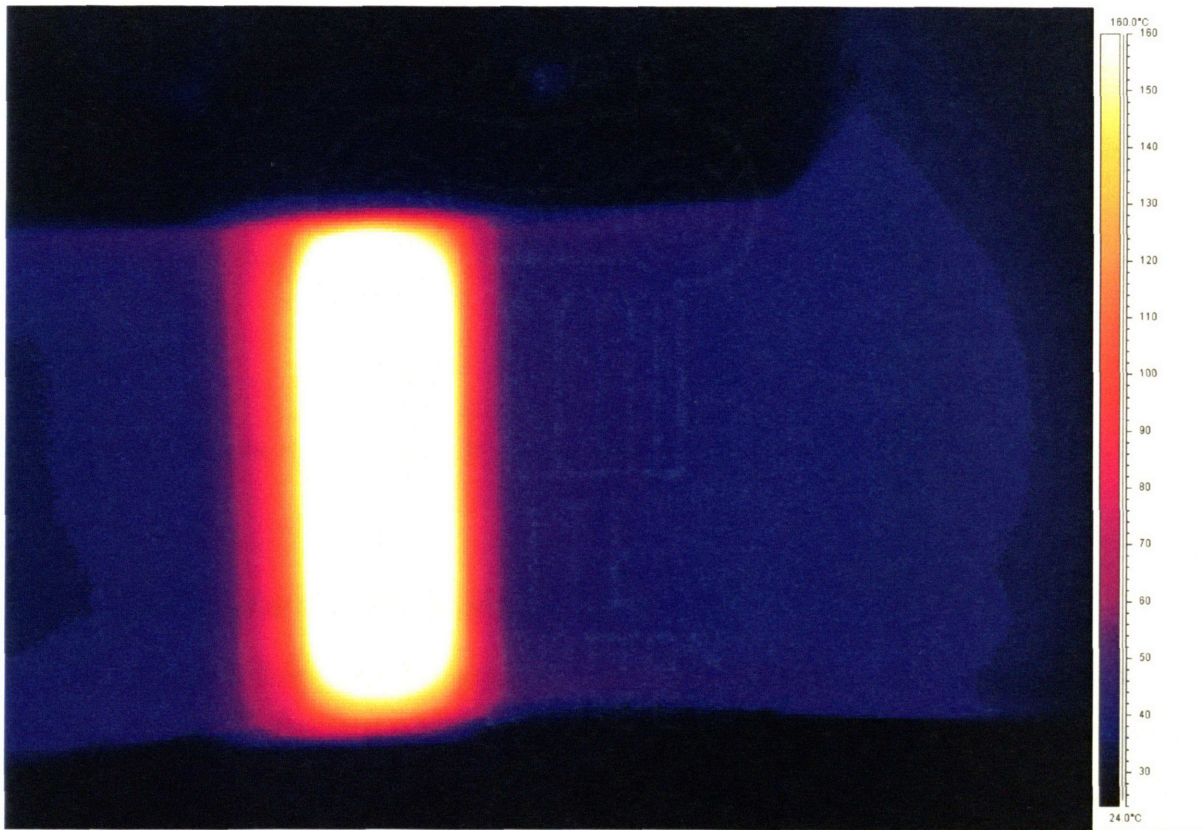


Figure 6.12: Infrared frame from the FLIR ThermoVision A40M camera showing the heat distribution in a PPy sample before break (160 °C). Note that the white color in this figure corresponds to a temperature of 160 °C and that the PPy is held at constant 2.5 MPa.

Concluding this Chapter, in the following two sections the basic material properties such as the specific heat capacity and the coefficient of thermal expansion are presented.

6.6.2 Specific Heat Capacity of PPy

The specific heat capacity is a material parameter describing how much heat is required to raise its temperature by 1 degree Kelvin per unit mass. The heat capacity of PPy was found to be 1.558 kJ/kg/K at 25 °C. As shown in Table 6.4, such a value is typical of a polymer.

Material	Specific Heat Capacity (kJ/kg/K)
Water	4
Polypropylene	1.925
PPy	1.558
Teflon	1.050
Copper	0.385

Table 6.5: Specific Heat Capacity of PPy compared to other materials. The PPy films is from PPy1 batch

6.6.3 Coefficient of Thermal Expansion

An obvious follow-up to the previous section is to determine the coefficient of thermal expansion of PPy after it has been subject to a 2 hour treatment at 90 °C under vacuum. Inspection of the data shown in Figure 6.7A (PPy subject to vacuum treatment + tested at 6 hours intervals at 20 and 90 °C) allows one to determine that the thermal expansion of vacuum-treated PPy is about 44×10^{-6} /K. This value is within the range of typical plastic materials such as polypropylene and polycarbonate as shown in Table 6.6.

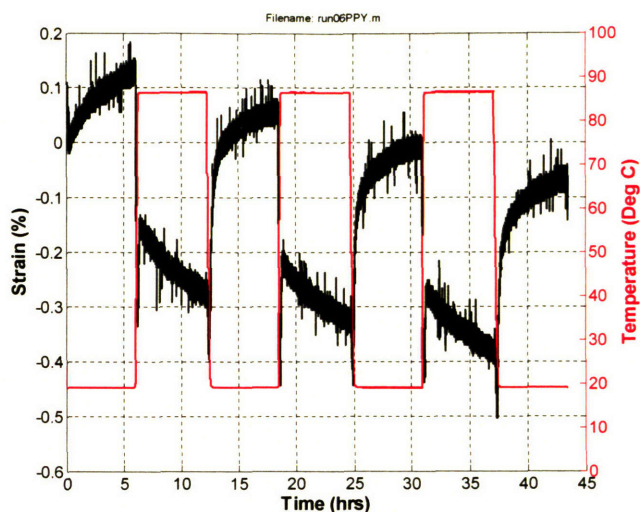


Figure 6.13: PPy film from PPy2 batch (and vacuum-treated), subject to 6 hours temperature scans between 20 and 90 °C. Inspection allows one to estimate the coefficient of thermal expansion of PPy films synthesized in this work.

Material	Coefficient of Thermal Expansion ($10^{-6} / \text{K}$)
Polypropylene	130
PPy	44
Polycarbonate	22
Copper	14 – 18
Steel	19 – 11

Table 6.6: Coefficient of thermal expansion of PPy compared to other materials

6.7 Conclusion

In this Chapter, the properties of polypyrrole when subject to heat were studied. It was found that an irreversible mechanical strain relaxation takes place when samples are subject to prolonged temperatures around 90 °C. Experiments allowed determining that the mechanical properties of PPy films following the vacuum treatment are repeatable across batches, and stable across time. Typical vacuum-treated PPy films exhibit the following mechanical properties: 0.81 GPa stiffness, 54 MPa tensile strength, and 46.4 % elongation to break. The effect of the vacuum treatment on the mechanical properties is also conserved when the film is placed back in a electrolyte solution, further confirming the hypothesis that an irreversible material relaxation takes place when PPy is subject to a temperature of 90 °C. In addition, as PPy needs a electrolyte solution to be electroactivated, this result shows that post-processing is a viable method to affect actuator properties. Finally thermal properties of PPy such as the heat capacity (1.558 kJ/kg/K), the coefficient of thermal expansion (44×10^{-6} /K) and the maximal operating temperature were determined (150 °C). The experiments presented in this Chapter further deepen our understanding of PPy as an engineering material, which is crucial for employing conducting polymer actuator in real applications.

6.8 References

- Grosberg A.Y. and Kohkhlov A.R., "Giant Molecules", *Academic Press, ISBN 0-12-304130-9, (1998)*.
- Oswald T.A. and Menges G., "Material Science of Polymers for Engineers", *2nd Edition, Hanser Publishers, Munich, (2003)*.
- Smela E. and Gadegaard N., "Surprising Volume Change in PPy(DBS): An Atomic Force Microscopy Study", *Advanced Materials, Vol. 11, (11): pp. 953-957, (1999)*.

Chapter 7

Experimental Characterization of Polypyrrole Actuators in Ionic Liquids

In this Chapter, the contractile properties of conducting polymer actuators activated in room-temperature ionic liquids are examined. These electrolytes dramatically enhance the active properties of conducting polymers compared to classical electrolytes such as propylene carbonate containing 0.1 M tetraethylammonium hexafluorophosphate ions (0.1 M TEAP in PC). Recoverable active strains as high as 16.3 % were recorded for polypyrrole activated in 1-butyl-3-methyl imidazolium tetrafluoroborate room-temperature ionic liquid. The property-enhancement features of room-temperature ionic liquids in terms of increased actuator active strains and cycle life are discussed herein¹.

7.1 Imidazolium-based Room Temperature Liquid Salts

Typical actuation limitations such as achievable strain, strain-rate, and ultimately cycle degradation result from electrochemical material degradation due to the application of an excessively large potential to the material. The measure of the degree of actuator

¹ Part of this Chapter appeared in [Anquetil P.A. et al. 2004]

electrochemical robustness is assessed by the so-called electrolyte and polymer potential window. For PPy in propylene carbonate, for example, the typical maximum potential applicable to the actuator film without degradation is about 0.4 V vs. Ag/Ag⁺ [Madden J.D. 2000]. Recent studies by Lu [Lu W. et al. 2002] show that the electrochemical potential of PPy can be extended to 4 V by using ionic liquids comprising 1-butyl-3-methyl imidazolium cations (BMIM) (Figure 7.1). In addition Lu et al. observed an increase in conducting polymer device cycle life by using ionic liquids over traditional electrolytes. In this Chapter it is shown that a large electrolyte potential window also translates into an increase in the actuator's active strain performance.

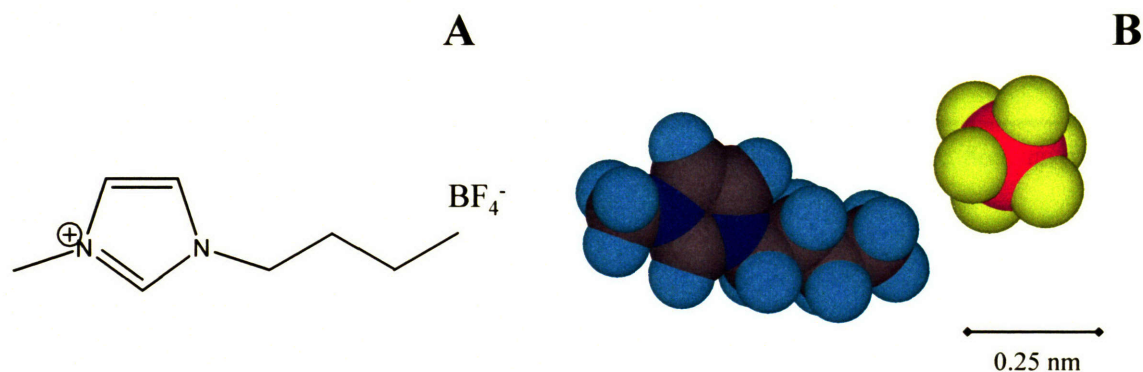


Figure 7.1: Structure of 1-butyl-3-methyl imidazolium hexafluorophosphate (BMIM-BF₄) room temperature liquid salt (A). The 3D space filling models of the salt molecules are shown in (B).

The ionic liquids considered in this study were 1-butyl-3-methyl imidazolium tetrafluoroborate (BMIM-BF₄) and 1-butyl-3-methyl imidazolium hexafluorophosphate (BMIM-PF₆). Both room temperature ionic liquids were purchased from Solvent Innovation, GMBH (www.solvent-innovation.com). BMIM-BF₄ was selected over BMIM-PF₆ as it has a higher ionic conductivity and a higher melting point in a comparable electrochemical window (Table 7.1). A high ionic conductivity is important to minimize the resistive loss when activating a conducting polymer in an electrochemical cell. A low melting point determines the range of applications in which an actuator in ionic liquid can be used.

<i>Property</i>	<i>BMIM-BF4</i>	<i>BMIM-PF6</i>
<i>Electrochemical Window (at 20 °C)</i>	<i>4.1 V</i>	<i>4.15 V</i>
<i>Melting Point</i>	<i>- 65 °C</i>	<i>16 °C</i>
<i>Density</i>	<i>1203.5 kg/m³</i>	<i>1305.9 kg/m³</i>
<i>Conductivity</i>	<i>0.35 S/m</i>	<i>0.16 S/m</i>
<i>pH</i>	<i>7.9</i>	<i>7.5</i>
<i>Purity</i>	<i>98 %</i>	<i>98 %</i>

Table 7.1: Physical properties of BMIM-BF4 room temperature ionic liquid. Source: www.solvent-innovation.com

7.2 Experimental Procedure

PPy films from PPy2 batch (see Chapter 5) were utilized and characterized throughout this Chapter. Neither silver perchlorate nor silver nitrate dissolves in BMIM-based liquid electrolyte thus preventing the construction of Ag/Ag⁺ reference electrodes using an ionic liquid as solvent (as described in Chapter 4). Instead, a silver wire from the BAS Bioanalytical Systems (www.bioanalytical.com) reference electrode kit was used as a pseudo reference electrode. Passive mechanical testing was performed using a Perkin Elmer DMA 7e and active mechanical analysis was performed using a custom-built electrochemical DMA (E-DMA, Chapter 4).

7.3 Passive Mechanical Properties of PPy in Ionic Liquids

As stated in Chapter 6, it is important to understand the passive properties of the actuators as they describe how a material behaves mechanically under static or dynamic loads. These

passive properties include Young's modulus, the tensile strength, and elongation to break. Furthermore, the actuator response needs to be characterized upon exposure to the electrochemical environment in which it will be eventually actuated.

To properly study how a PPy film behaves upon immersion in BMIM-BF₄ ionic liquid electrolyte, the remaining synthesis electrolyte (i.e. propylene carbonate + 0.05 M TEAP) needs to be removed first. Following the similar experimental procedure presented in Chapter 6, the PPy film is initially dried for 2 hours under vacuum at 90 °C, 9.14×10^4 Pa (27 inch Hg). Upon completion of this process, the vacuum treated PPy film can then be immersed in BMIM-BF₄ for further study. One of these studies probes the stress-strain relationship of a vacuum dried PPy film after it has been immersed for one hour in BMIM-BF₄.

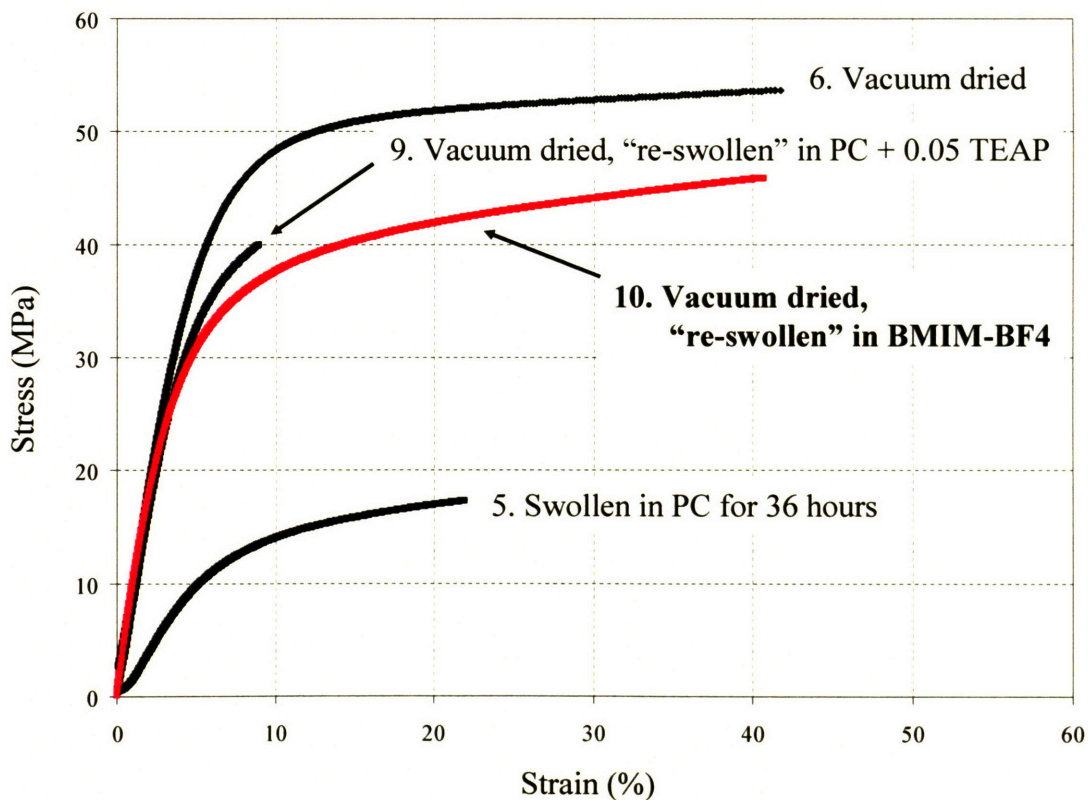


Figure 7.2: Films from PPy2 batch mechanically tested after the “re-swelling” process, taken from Chapter 6 (Figure 6.9). Film 10 in this Figure was immersed in BMIM-BF₄ ionic liquids after being vacuum treated. Similarly, all films presented here were initially vacuum dried for 2 hours.

Figure 7.2 compares the stress-strain behavior of various PPy films “re-immersed” in electrolyte, following a vacuum treatment. The curves of films 5,6 and 9 are reproduced from Chapter 6 for comparison. Inspection of Figure 7.2 shows that a PPy film immersed in BMIM-BF₄ following its vacuum treatment (Film 10) behaves similarly to a vacuum dried PPy film re-immersed in its “synthesis” PC+TEAP electrolyte. It is interesting to note that the modified PPy properties achieved via vacuum and heat treatment are also irreversible when the PPy film is subsequently immersed in an ionic liquid such as BMIM-BF₄.

To study the swelling mechanism occurring in regular PPy when immersed in BMIM-BF₄, a 20 mm long, 2 mm wide, and 10 μm thick non-dried PPy film was clamped in the E-DMA and held at constant stress of 2.5 MPa. Strain relaxation induced by the diffusion of ions in or out of the polymer was then observed for one hour.

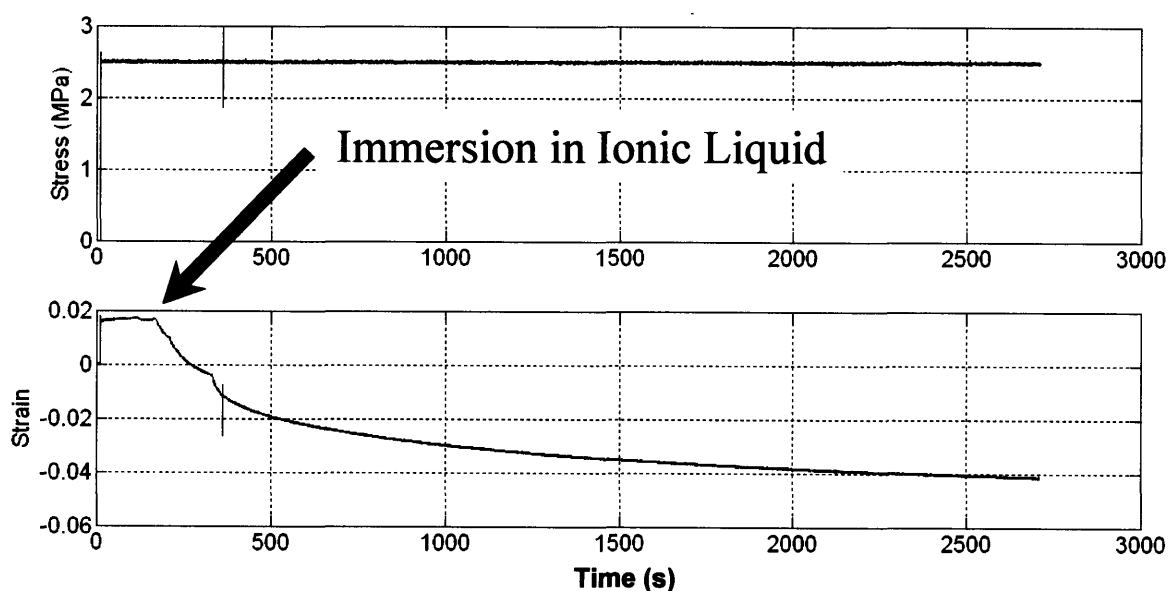


Figure 7.3: Immersion of PPy in ionic liquids 240 s into the experiment (arrow). The film is held at constant 2.5 MPa stress for almost 1 hour, while the change in strain resulting from immersion in BMIM-BF₄ is observed.

As shown in Figure 7.3, the non-dried PPy film is initially held in air at 2.5 MPa and immersed in BMIM-BF₄ at $t = 240$ s, while its strain response is recorded. Observation of this process reveals that the PPy film contracts by 4 % upon immersion in a BMIM-BF₄ solution. As this PPy film is not dried and no potential is applied to the polymer film during

testing, it is conceivable that BMIM-BF₄ behaves as a “bad solvent” for PPy, driving the remaining synthesis propylene carbonate out of the film. It is not conceivable that ion molecules passively diffuse out of the polymer film as no potential is applied and the oxidation state of the material is not changed. This hypothesis is confirmed by measuring that the conductivity before and after immersion into BMIM-BF₄ has not changed.

7.4 Active Low Frequency Isometric Actuator Testing

7.4.1 Overview

The goal of this section is to present the experimental characterization of PPy actuation in ionic liquids. Activation of polypyrrole actuators into a liquid salt leads to surprising active behavior. Initial results presented in Figure 7.4 show large recoverable strains of 16.3 % (24 % maximum achievable strain) for polypyrrole in 1-butyl-3-methyl imidazolium tetrafluoroborate (BMIM-BF₄) under isotonic conditions (2.5 MPa). Current and voltage were applied to the electroactive material and recorded under digital control using an Amel potentiostat (model 2053, <http://www.amelsrl.it>) controlled by the E-DMA (Chapter 4), thereby allowing contractile properties to be measured and related to charge transfer.

A sample of polypyrrole (6 mm long, 2 mm wide, and 10 μm thick) was attached between two nylon clamps containing stainless steel electrical contacts and held at constant 2.5 MPa initial stress load, and immersed in a bath containing BMIM-BF₄ electrolyte. The electrochemical cell circuit was composed of the polymer sample and a stainless steel counter electrode. A sawtooth potential was applied to the film and monitored via a silver wire pseudo-reference electrode. The sawtooth potential was varied between 1.7 V and -0.8 V versus the silver wire pseudo-reference electrode. Note that the Open Circuit Potential of the polypyrrole electrode (OCP) was 0.443 V versus the silver wire and that the actual potential input was therefore varied by ± 1.25 V versus OCP². In this particular test, the activation frequency was 0.005 Hz (200 s per cycle). The input potential, charge response and resulting active strain of the polypyrrole actuator in BMIM-BF₄ are presented in Figure 7.4.

² The OCP is an indication of the initial state of the film before it is activated. Note that it only represents a temporary electrochemical equilibrium that is a function of the history of the film.

In Figure 7.4 we notice several unusual features:

- An initial active strain of 24 %;
- An overall creep of 20 % after 5 cycles that is reduced to 3 % per cycle after the 3rd cycle;
- A recoverable strain of 16.3% (contraction) produced at each cycle;
- Charge flowing into the film is opposite sign from the measured active linear strain, suggesting that the imidazolium cation and not the small BF_4^- is diffusing into the polymer;
- A charge amplitude of 0.42 C;
- An absolute strain to charge ratio of $1.37 \times 10^{-10} \text{ m}^3/\text{C}$. Notice that this value of the strain to charge is comparable to the typical quoted values for PPy actuated in 0.1 M TEAP in propylene carbonate: $1.3 \pm 0.3 \times 10^{-10} \text{ m}^3/\text{C}$ [Madden J.D. 2000].

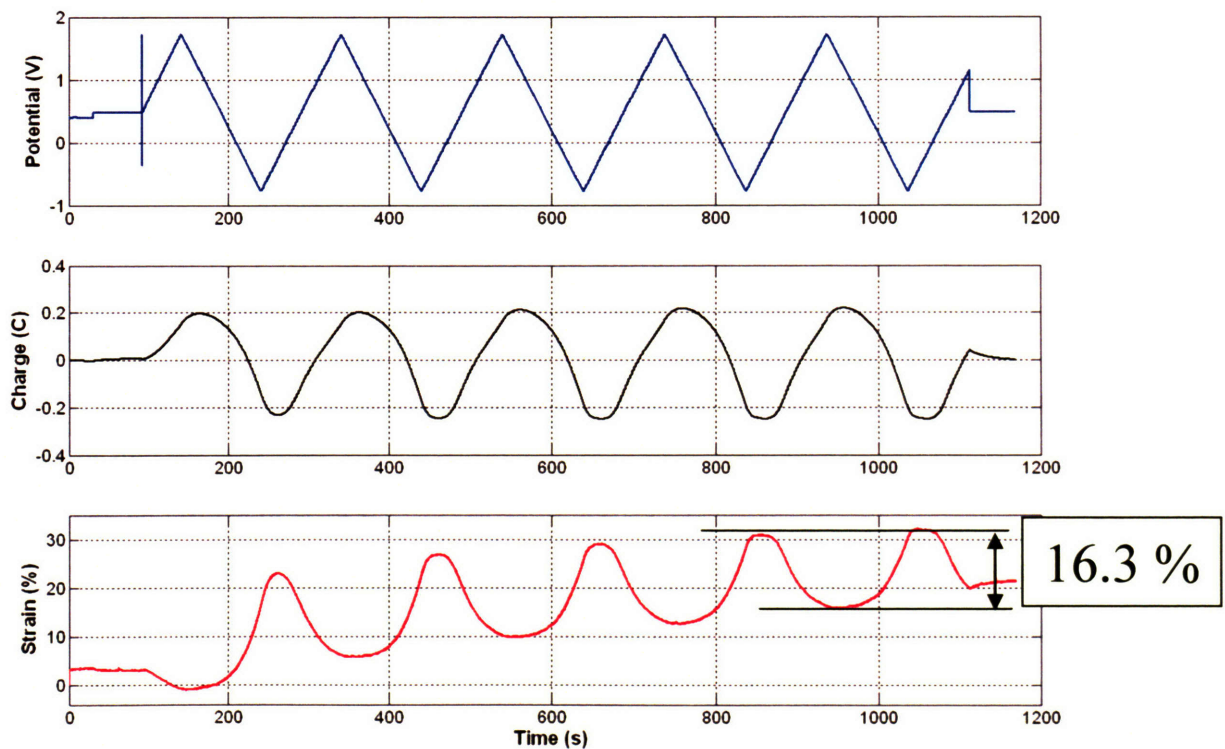


Figure 7.4: 16.3% recoverable strain (24% maximum) in polypyrrole actuators activated in BMIM-BF₄

This result is the first demonstration that linear strains in excess of 16.3% can be recovered by a polypyrrole conducting polymer actuator against a load of 2.5 MPa. However, these large strains are accompanied by a large creep, resulting in an average unrecoverable extension of the film of 3 % per cycle after the 3rd cycle of activation. It is hypothesized that the BMIM cation diffuses into the polymer and is responsible for actuator strain response. The speed of actuation for this 10 μm film is quite slow, though: 0.36 %/s (compared with 3 %/s for PPy activated in 0.1 M TEAP in PC at 5 MPa). The larger size of the BMIM cation compared to the PF6⁻ anions (2.5 times smaller) could explain why the speed of contraction is decreased from a typical value of 3%/s achieved for PPy activated in 0.1 M TEAP in PC.

7.4.2 Long vs. short activation cycles

Similar to the previous Section, a PPy film activated in BMIM-BF4 but at a faster rate of 100 s per cycle (0.01 Hz) shows the following features (Figure 7.5):

- An initial active strain of 20 %;
- An overall creep of 21 % after 5 cycles that is reduced to 2 % per cycle after the 3rd cycle;
- A recoverable strain of 14.5 % (contraction) produced at each cycle;
- An inverse charge to strain relationship suggesting that the BMIM moiety of the salt diffuses into the polymer;
- A charge amplitude of 0.38 C;
- An absolute strain to charge ratio of $1.45 \times 10^{-10} \text{ m}^3/\text{C}$, compared to $1.3 \pm 0.3 \times 10^{-10} \text{ m}^3/\text{C}$ for PPy actuated in 0.1 M TEAP in propylene carbonate [Madden J.D. 2000].

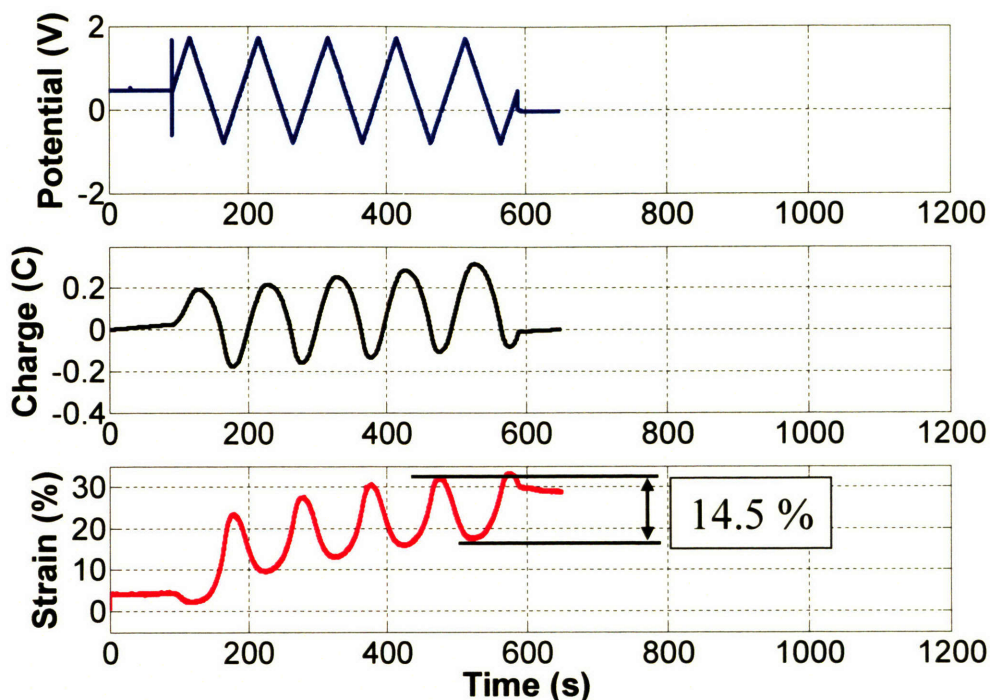


Figure 7.5: 14.5% recoverable strain (20% maximum) in polypyrrole actuators activated in BMIM-BF₄

In subsequent experiments on the same film, the activation rate was increased from 0.005 Hz to 0.01 Hz, 0.02 and 0.2 Hz, and the active strain response recorded. The amplitude of the activation input waveform was kept the same: ± 1.25 V versus OCP, where OCP is the open circuit potential; initially 0.443 V versus silver wire.

Figure 7.6 shows the result of this experiment presented such that the scale of each graph remains the same to allow easy comparison. Analysis of Figure 7.6 reveals that the strain amplitude increases as the activation cycle frequency is decreased. On the other hand the strain to charge ratio increases as the cycle frequency is increased, meaning that the electrical to mechanical energy conversion is more efficient at higher cycle frequencies. These results are summarized graphically in Figure 7.7.

From the data presented in Figure 7.6 and Figure 7.7, key properties of PPy actuator activated in ionic liquid emerge:

- The large potential window and (almost) zero water content of ionic liquids allow oxidation (or reduction) of a conducting polymer actuator at high potentials for a significant duration without inducing any polymer degradation.

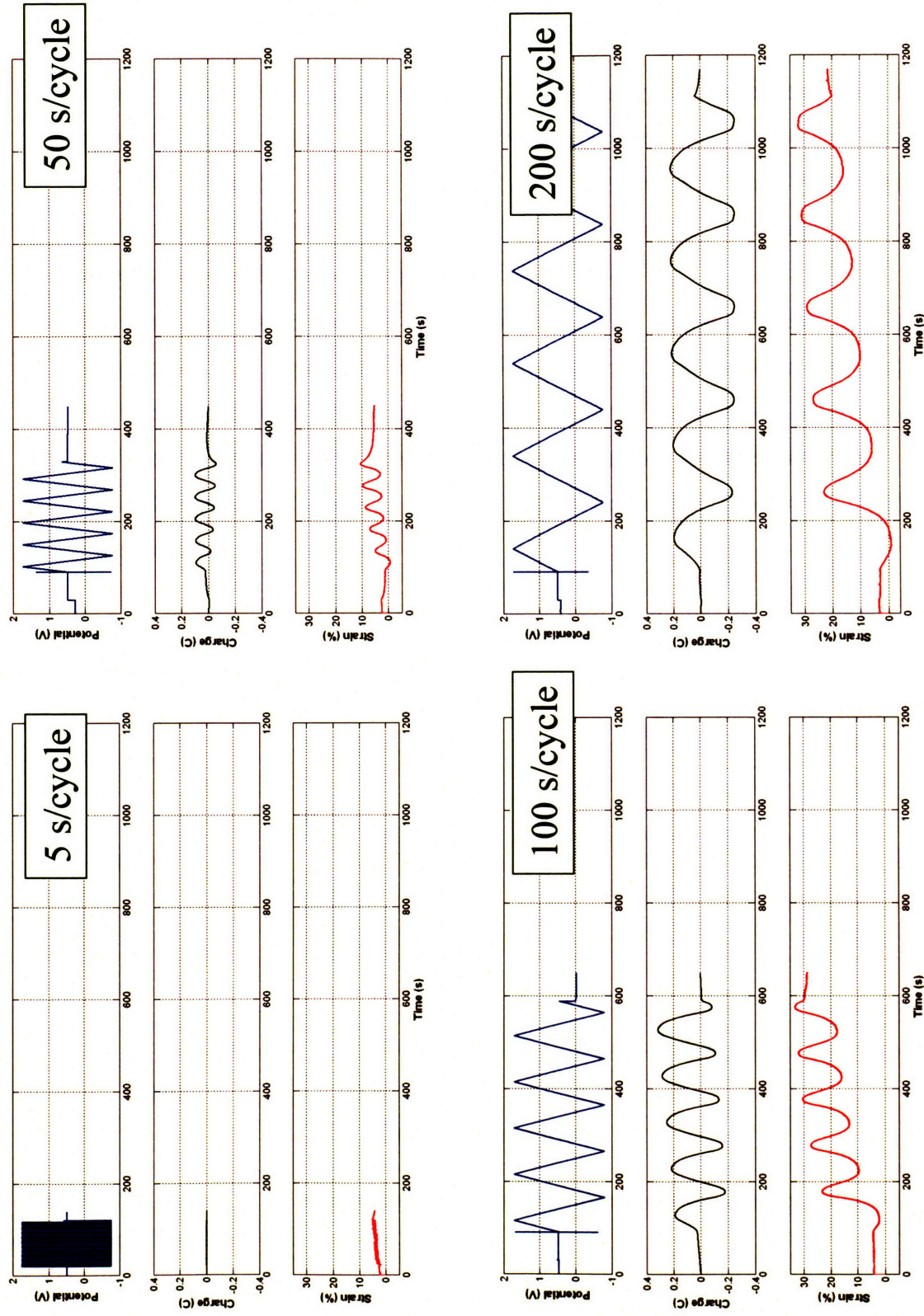


Figure 7.6: Activation at various cycle with a 2.5 V amplitude (± 1.25 V versus OCP) presented using the same scale for each graph.

- As a result, cycles of 200 s can be sustained at a high oxidation potential amplitude (such as 2.5 V) without causing polymer degradation.
- Strain amplitude is dependent on the activation cycle frequency. As the cycle frequency is decreased, the strain amplitude increases. This can be also attributed to the stability of PPy activated in ionic liquids. Exposure to long cycle times allows ample time for the polymer film to be fully charged and ions to subsequently diffuse in without typically undergoing material degradation.
- Interestingly, the charge to strain conversion is most efficient at high cycle frequencies. It is possible that parasitic reactions take place at low frequencies, leading to undesired charge consumption. Kinetic dependence of the BMIM ion diffusion constant could also offer an explanation for this behavior. Further characterization of the rate dependence of PPy activated in BMIM-BF₄ will need to take place.

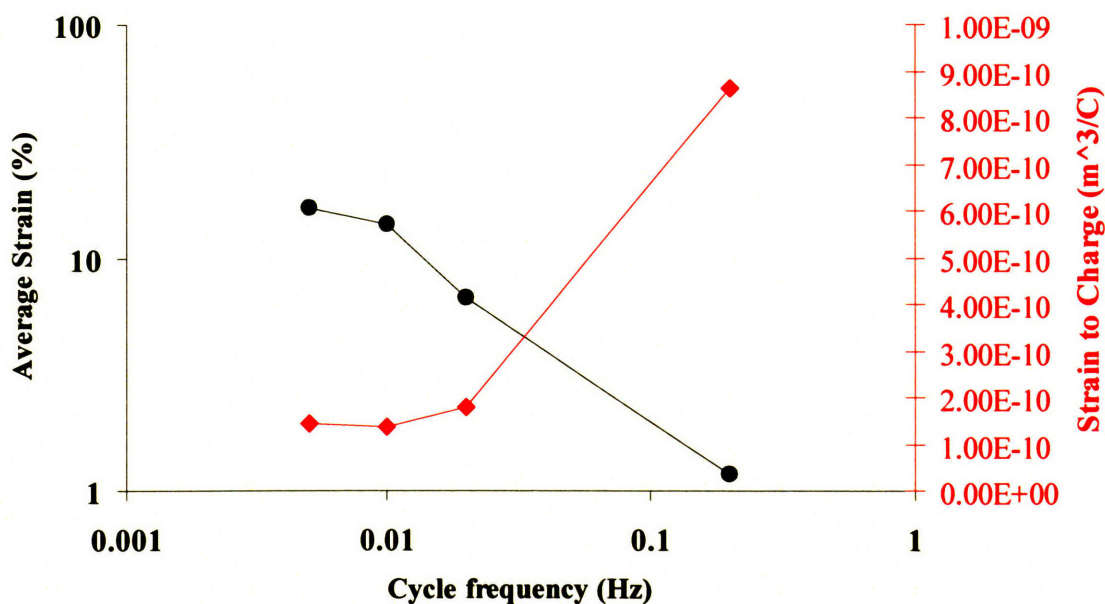


Figure 7.7: Analysis of the average strain and the average strain to charge ratio for activation at various activation cycle frequencies.

Finally in Figure 7.8, two identical PPy films are activated in different electrolyte environments. The first PPy sample is activated in BMIM-BF₄ and its response compared to a sample activated in a traditional 0.1 M TEAP in PC electrolyte. Both films were held at the same 2.5 MPa isotonic stress and activated using the same input activation waveform: 2.5 V amplitude at 50 s/cycle. PPy actuated in BMIM-BF₄ exhibits a strain amplitude of 6 % and a significant creep (5 % after 5 cycles). On the other hand, PPy powered in 0.1 M TEAP in PC shows a much smaller strain amplitude (1.75 %) but also no creep at all. Figure 7.8 clearly demonstrates that the response of PPy activated in ionic liquids is significantly different.

From this section, it is concluded that ionic liquids enable the generation of gigantic strains compared to traditional propylene carbonate based electrolytes, while also exhibiting significant creep. The analysis of the creep behavior of PPy in ionic liquids will be the focus of the next sections.

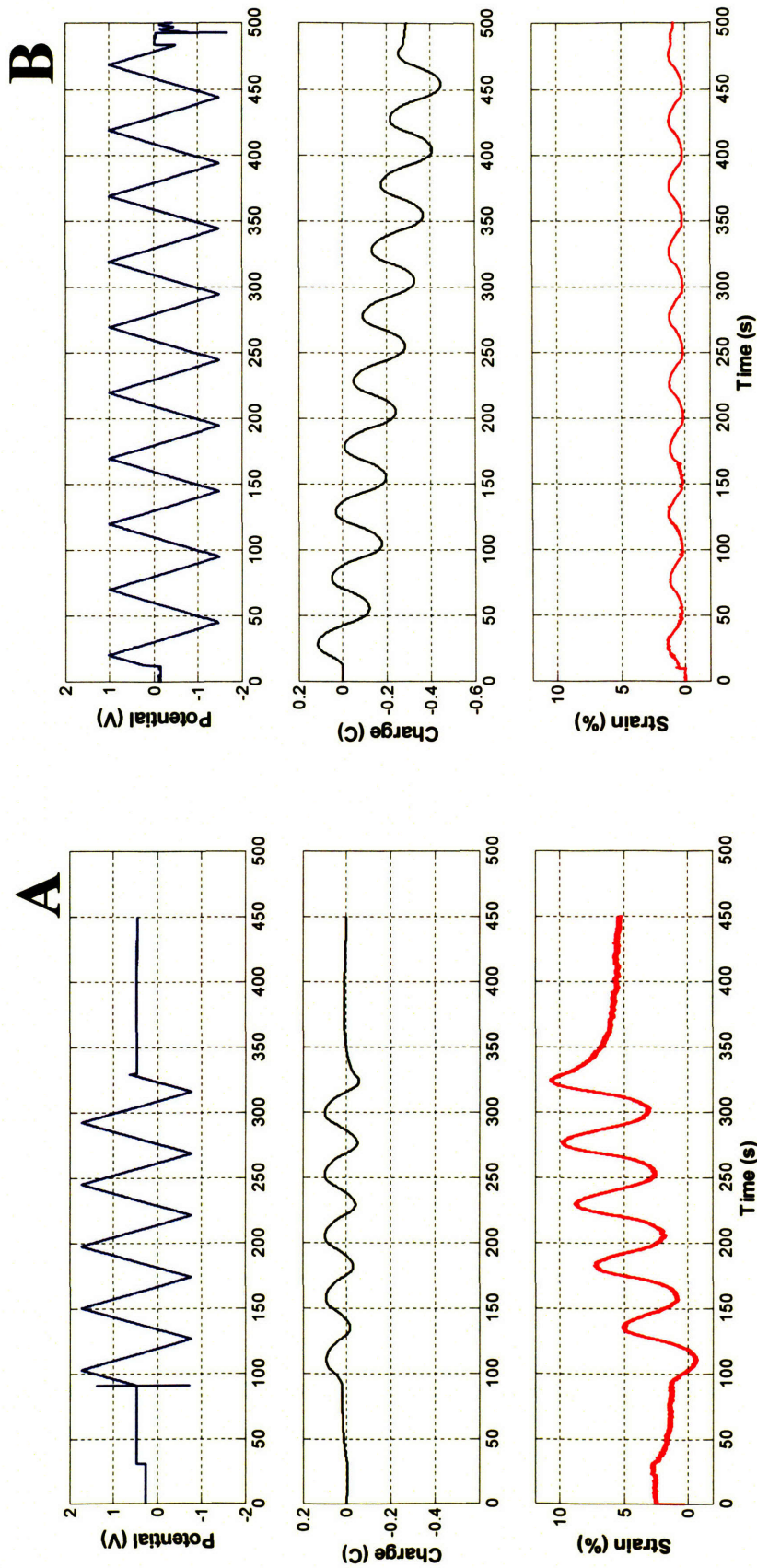


Figure 7.8: Comparison of actuation cycles in BMIM-BF4 and in 0.1 M TEAP in PC. Both PPy films were actuated with a 2.5 V amplitude voltage at 50 s/cycle. Clearly strain is increased by activation in ionic liquids. Note also that the charge amplitude is slightly larger for the film actuated in 0.1 TEAP in PC. Both graph A and B are plotted at the same scale.

7.4.3 Effects of Load on Active Strain

The next step of characterizing PPy conducting polymer actuators in BMIM-BF₄ consists of establishing if the strain measured upon electroactivation varies as a function of load. As an actuator will ultimately be employed at various loads, it is important to know if its active behavior is dependent on applied stress.

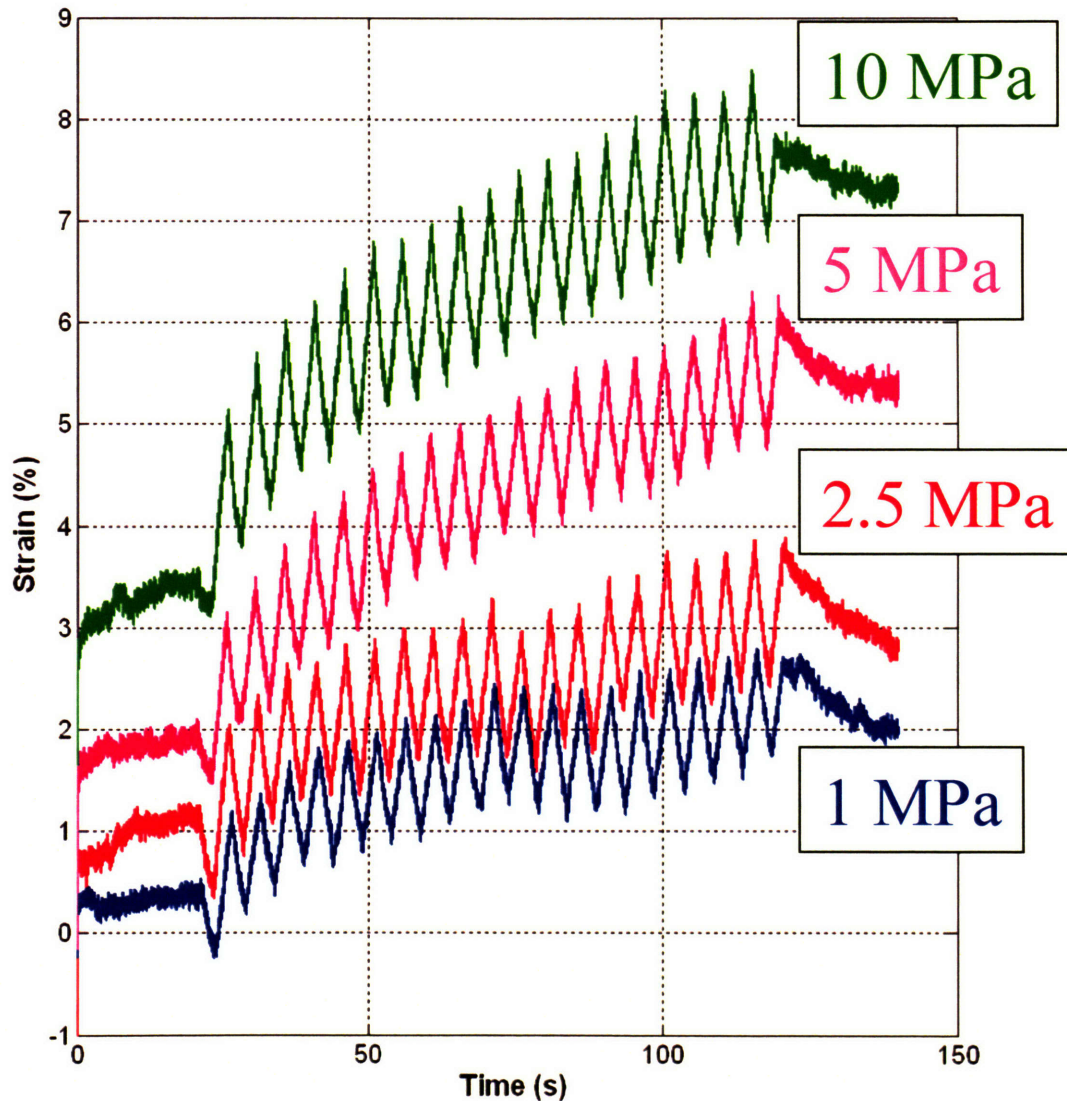


Figure 7.9: PPy film in BMIM-BF₄ activated and held at various stresses (from 1 to 10 MPa). The response amplitude is independent of applied stress.

To study the effects of load on the active strain generated by PPy actuators in BMIM-BF₄ electrolyte, a PPy film sample (6 mm long, 2 mm wide, and 10 μm thick) was clamped in the E-DMA and held at 1, 2.5, 5, and 10 MPa. For each load, the PPy film was subject to the same actuation input waveform (± 1.25 V versus OCP, at 5 s/cycle). The result of these experiments overlaid on the same graph is shown in Figure 7.9. Inspection of Figure 7.9 reveals that the strain amplitude is absolutely similar (in shape, amplitude, and frequency), independent of applied stress.

In Figure 7.10 the strain to charge ratio extracted from the curves of Figure 7.9 is plotted as a function of applied stress. Analysis of this data shows that the strain to charge ratio is independent of applied load and equal to $8.76 \cdot 10^{-10} \text{ m}^3/\text{C}$.

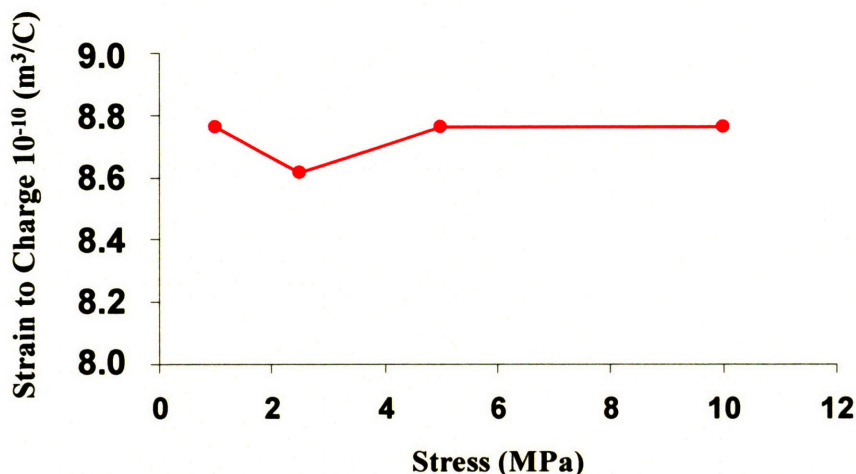


Figure 7.10: Comparison of strain to charge ratio for the PPy films presented in Figure 7.6. The strain to charge remains independent of stress for stresses ranging from 1 to 10 MPa.

7.4.4 Creep Effects during Activation in Ionic Liquids

In this Section the creep behavior of PPy films when electrochemically activated in ionic liquids is presented. First of all the steady state creep after the four activation sequences of Figure 7.9 are summarized in Figure 7.11. Note that for these four experiments the PPy film was held at different stresses (1, 2.5, 5, and 10 MPa) but activated under the same conditions (100 s PPy activation run at 2.5 V amplitude).

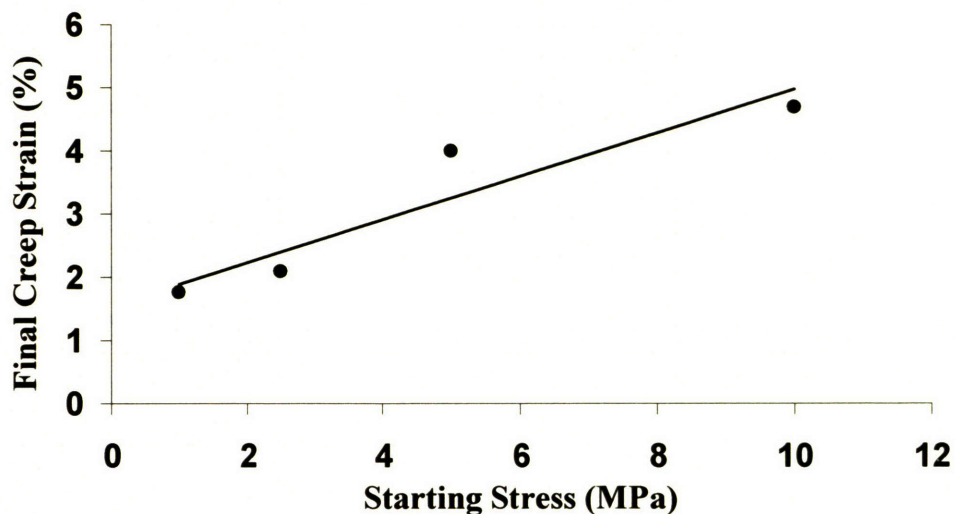


Figure 7.11: Steady state creep as a function of applied stress.

Inspection of Figure 7.11 shows that the value of the final creep increases linearly as a function of applied initial load onto the polymer film.

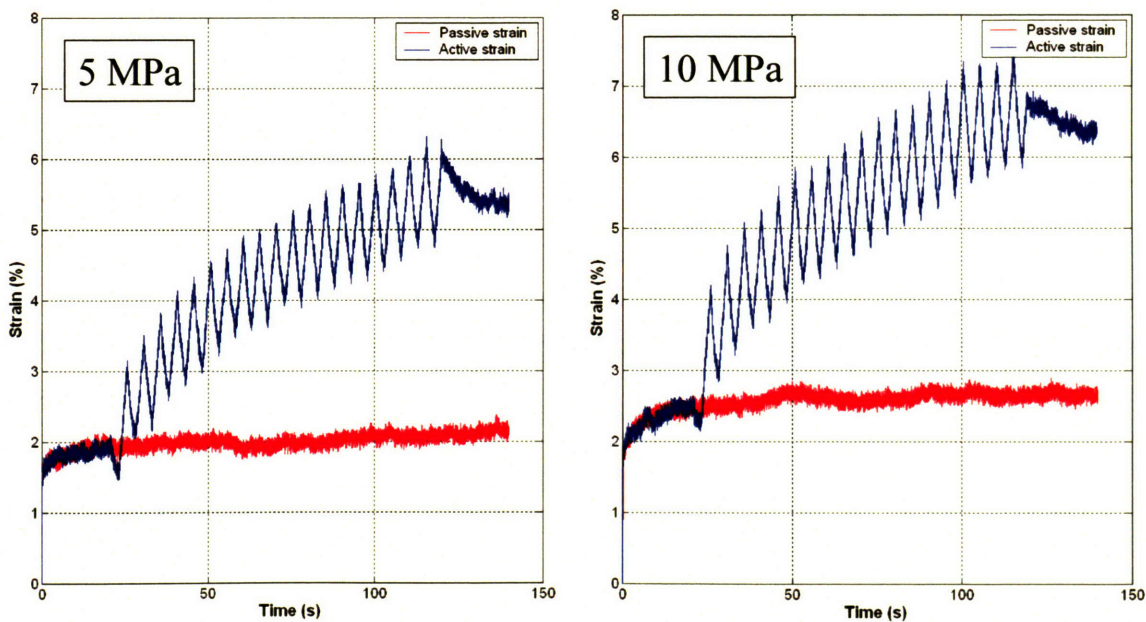


Figure 7.12: (A) Difference between two films held at 5 MPa where the one shown on the blue curve is activated with a 2.5 V amplitude, 5 s/cycle amplitude, while the one shown in the red curve is not electrochemically activated at all. (B) Same as (A), but at 10 MPa stress.

Figure 7.12 shows two experiments in which two films are held at 5 MPa (10 MPa for the second experiment) constant stress, while one is activated (blue curve, 2.5 V amplitude, 5 s/cycle) and the second one (red curve) is not. For both experiments, the difference between the creep of the activated versus the non activated one is striking. The passive responses of both films initially match. However, as soon as one actuator film is activated, its creep augments significantly. As a result this creep is called “initial active creep”. This behavior is probably induced by incorporation (i.e. swelling) of BMIM ions into the PPy bulk material as creep significantly occurs during the expansion phase. This indicates that the nanoscale morphology of the polymer material might become affected by such an incorporation. This topic is of high interest to ultimately understand actuation from the molecular level up in classical actuators such as PPy and should be studied in the future.

From Figure 7.13 and Figure 7.12, one can deduce that the PPy film initial active creep obeys a 1st order exponential creep model which is superposed to the active polymer response:

$$Creep(t) = a[1 - e^{b \cdot t}], \quad (7.1)$$

where a and b are two parameters which can be experimentally fitted to activation data. For example, for the data set shown in Figure 7.5:

$$Creep(t) = 0.06[1 - e^{-0.012 \cdot t}] \quad (7.2)$$

The overall model for electroactivation of conducting polymers activated in ionic liquids thus becomes:

$$\varepsilon = \frac{\sigma}{E} \left[1 - e^{-\frac{t}{\tau}} \right] + \alpha \cdot \rho, \quad (7.3)$$

where ε is the strain, σ the Stress, E is Young’s modulus, α the strain to charge ratio and ρ is the charge per unit volume (input). Figure 7.14 shows how well such a model, based on two

free parameters can predict the passive and active behavior of PPy polymers in ionic liquids. The dataset used in Figure 7.14 is the one originally presented in Figure 7.5:

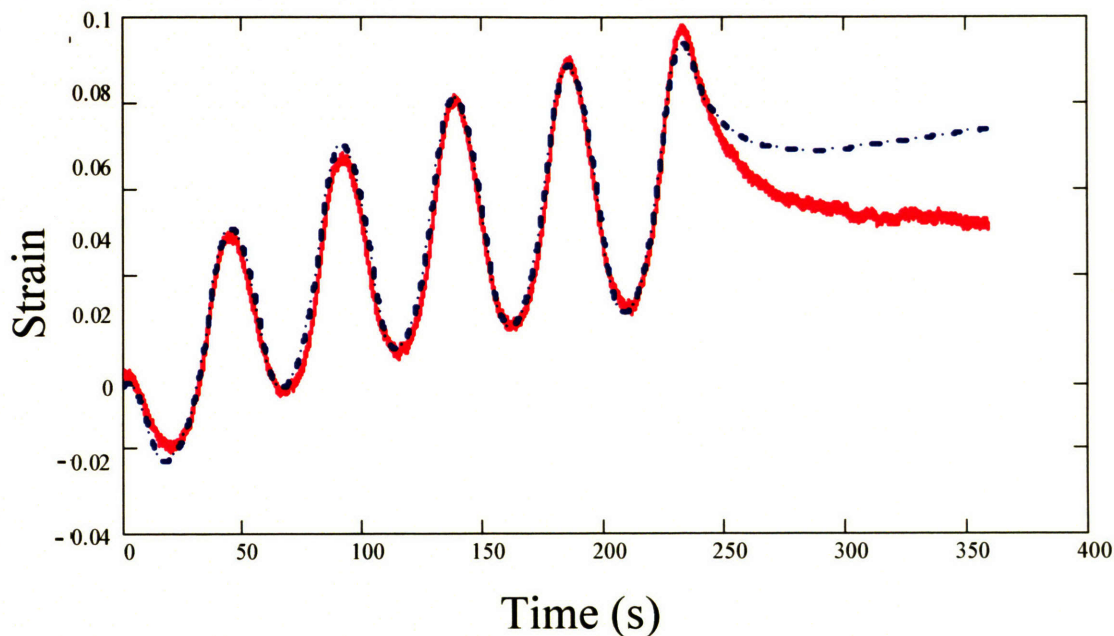


Figure 7.14: Data (red) and model (blue) simulating strain response from charge input. The data is the one originally presented in Figure 7.5.

7.4.5 Cycle Life

Cycle life is a measure of how many cycles a conducting polymer actuator can be activated before its performance characteristics start to degrade. In the following tests, the activation frequency was increased to about 3 Hz and the resulting strain and cycle life were measured at that frequency. A newly synthesized polypyrrole film (6 mm long, 2 mm wide, and 10 μm thick) was held at 2.5 MPa and activated between +4.5 V and -4.0 V versus silver pseudo-reference electrode.

7. Experimental Characterization of Polypyrrole Actuators in Ionic Liquids

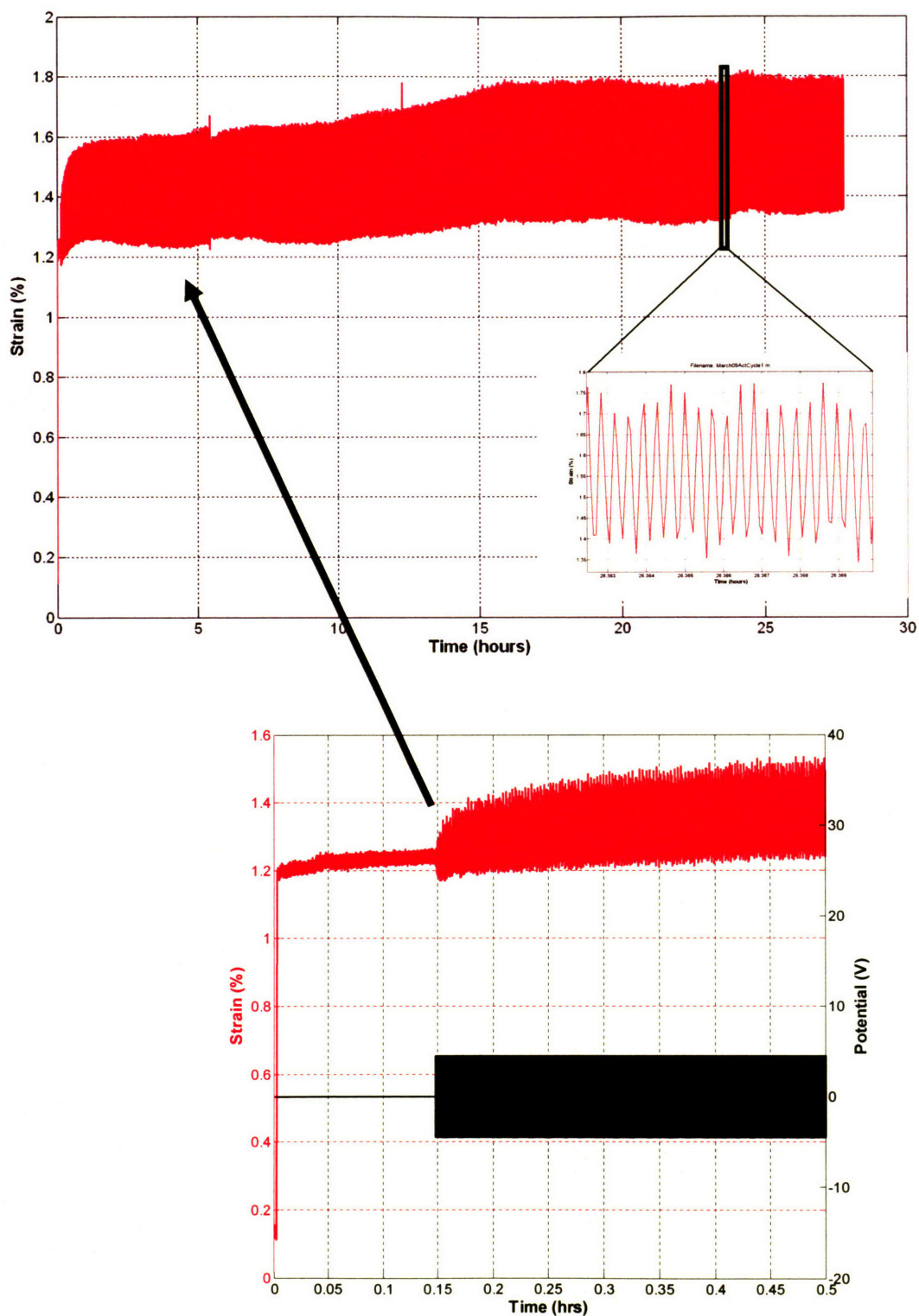


Figure 7.15: PPy film activated in BMIM-BF₄ for 100,000 cycles at 3 Hz. No degradation was observed after the process. The bottom sub-figure shows the initial ½ hour of the experiment. The activation waveform was started at t = 0.15 hrs.

Figure 7.15 shows PPy cycle life measurement in excess of 100,000 cycles at 0.5% linear strain, 2.5 MPa stress when activated at 3Hz cycle frequency in activated in BMIM-BF₄ ionic liquids. No degradation and no decrease of linear strain amplitude were observed after conducting the 100,000 cycle test. The mechanical strength of this cycled film was then compared to a non-activated and an activated PPy film placed in 0.1 M TEAP in PC electrolyte. As shown in Figure 7.16, the passive mechanical response of the PPy film cycled 100,000 times in BMIM-BF₄ show similarities to the one that has not been activated. In contrast, the PPy film activated for 1,000 cycles in propylene carbonate + 0.01 M TEAP shows weaker mechanical properties (almost a factor three decrease in stiffness)

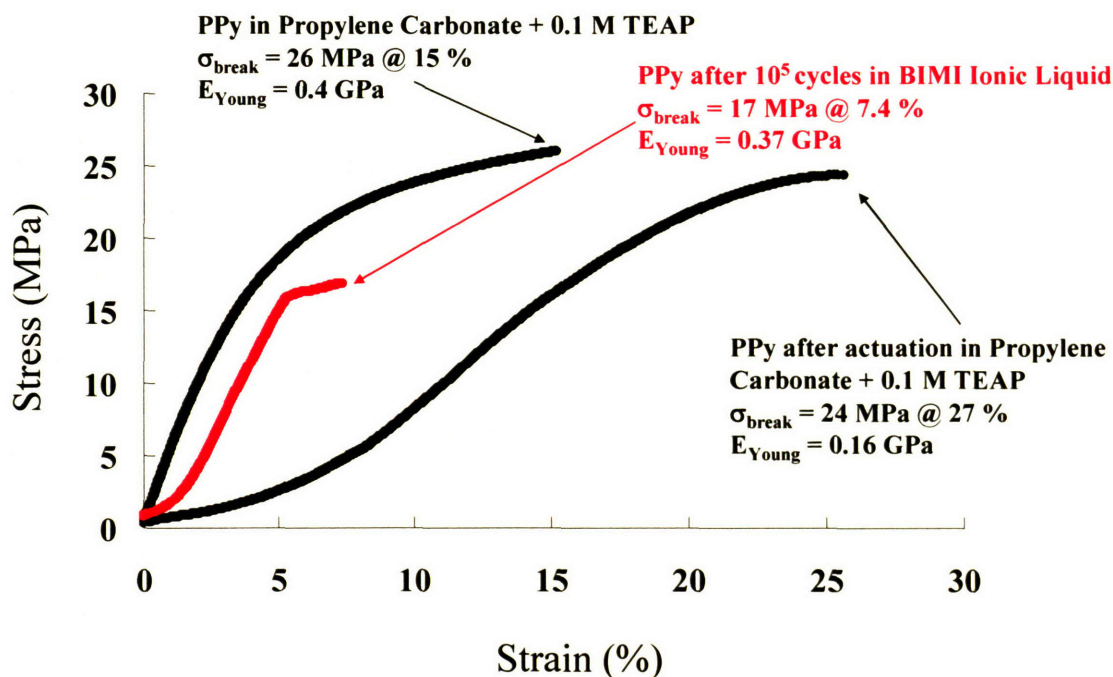


Figure 7.16: Passive mechanical properties of PPy activated for 100,000 cycles (in red) in BMIM-BF₄ compared to a film activated for 1,000 cycles in a 0.1 M TEAP + PC and an untouched PPy film stored in 0.1 M TEAP + PC. The stiffness of the film cycled in BMIM-BF₄ is similar to the untouched one.

7.5 Conclusion

The electrochemical and mechanical (passive and active) characterizations performed on polypyrrole synthesized in 0.05 M TEAP in propylene carbonate and activated in BMIM-BF₄ ionic liquid were presented in this Chapter. It was initially shown that the BMIM-BF₄ does not affect the passive mechanical properties of PPy. Activation of polypyrrole in ionic liquid resulted in unusual active behavior such as recoverable linear strains in excess of 16.3% against a load of 2.5 MPa at a speed of 0.36 %/s. However, these large strains are accompanied by large creep, resulting in an average unrecoverable extension of the film by 3 % per cycle. The active creep behavior of PPy in ionic liquids was identified as obeying first order dynamics. Further characterization and electrochemical modeling should lead to a better understanding of this system and the roots of the observed active creep behavior. Finally the stability of conducting polymer systems when activated in ionic liquids is shown by cycling a PPy film at 3 Hz for a 100,000 cycles without observing any significant polymer damage. The activation results for polypyrrole in ionic solvent are compared to the 0.1 M TEAP in PC actuator performance benchmark as well as to human skeletal muscle below (Table 7.1).

Properties	Polypyrrole activated in BMIM-BF ₄	Polypyrrole activated in 0.1M TRAP in PC	Mammalian skeletal muscle [Hunter I.W. and Lafontaine S. 1992]
Displacement (Strain)	16.3 % reversible (at 2.5 MPa) 24 % max. (at 2.5 MPa)	2 % (at 10 MPa)	20 %
Active Stress (Load)	> 10 MPa	40 MPa	0.35 MPa
Velocity (Strain Rate)	0.36 %/s (at 5 MPa)	3 %/s (at 5 MPa)	>100 %/s
Power to mass	20 W/kg	150 W/kg	50 –100 W/kg
Operating Voltage	1 – 5 V	1 – 5 V	-
Strain to Charge Ratio	1.7 to 8.8×10 ⁻¹⁰ S/m	1.3×10 ⁻¹⁰ S/m	-
Conductivity	4.5×10 ⁴ S/m	4.5×10 ⁴ S/m	-
Cycle Life	>10 ⁵ (at 3 Hz and 0.5 % strain)	10 ⁵ (at 3 Hz and 0.3 % strain)	>10 ⁷

Table 7.1: Comparison of polypyrrole actuators actuated in liquid salt with a similar polymer activated in PF₆⁻ based propylene carbonate solution.

7.6 References

- Anquetil P.A., Rinderknecht D., Vandesteeg N.A., Madden J.D. and Hunter I.W., "Large Strain Actuation in Polypyrrole Actuators", *Proceedings of the SPIE conference on Smart Structures and Materials 2004*,
- Hunter I.W. and Lafontaine S., "A Comparison of Muscle with Artificial Actuators", *Technical Digest IEEE Solid State Sensors and Actuators Workshop*, pp. 178-185, (1992).
- Lu W., Fadeev A.G., Qi B., Smela E., Mattes B.R., Ding J., Spinks G.M., Mazurkiewicz J., Zhou D., Wallace G.G., MacFarlane D.R., Forsyth S.A. and Forsyth M., "Use of Ionic Liquids for pi-Conjugated Polymer Electrochemical Devices", *Science*, Vol. 297, pp. 983-987, (2002).
- Madden J.D., "Conducting Polymer Actuators", *MIT PhD Thesis*, (2000).

Chapter 8

Synthesis and Characterization of poly(calix[4]arene *bis*-bithiophene) and poly(quarterthiophene)/S-PHE Actuators

This Chapter is devoted to the synthesis and characterization of poly(calix[4]arene *bis*-bithiophene) and poly(quarterthiophene) poly(QT), a novel muscle-like material based on rational molecular design. The mechanism of contraction of this molecule is based on π - π dimer formation between quarterthiophene units. To enhance the mechanical stability of poly(QT) a polymer composite is formed with a flexible sulfated poly- β -hydroxy ether (S-PHE) matrix polymer. The two conference papers¹ that follow describe for the first time the synthesis of poly(QT) and poly(QT)/S-PHE as actuators and the characterization of their passive and active properties.

¹ Part of the evaluation of a thesis involves determining the contributions of the thesis author. The two papers that follow have multiple authors, each of which made contributions to the work. The synthesis of the quarterthiophene (QT) and the calix[4]arene bis-bithiophene (calix(BBT)) were done by Hsiao-hua (Bruce) Yu. The in-situ EPR evaluation was also contributed by Hsiao-hua (Bruce) Yu. John Madden and Peter Madden contributed to important discussions. Professor Swager and Professor Hunter provided supervision and guidance. The synthesis of poly(QT) and poly(calix(BBT)) polymers is Patrick Anquetil's contribution. Patrick Anquetil performed all the passive and active mechanical tests and wrote the two articles.

Thiophene-based Conducting Polymer Molecular Actuators

Patrick A. Anquetil^{*a}, Hsiao-hua Yu^b, John D. Madden^a, Peter G. Madden^a,
Timothy M. Swager^b and Ian W. Hunter^a

^aBioInstrumentation Laboratory, Department of Mechanical Engineering;

^bDepartment of Chemistry; Massachusetts Institute of Technology, 77 Massachusetts Ave.,
Cambridge, MA, 02139, USA

ABSTRACT

Traditional conducting polymer actuators such as polypyrrole offer tremendous active stress at low actuation voltages but with moderate strain, strain-rate and efficiency. We report the synthesis of novel thiophene based conducting polymer molecular actuators, exhibiting electrically triggered molecular conformational transitions. In this new class of materials, actuation is the result of conformational rearrangement of the polymer backbone at the molecular level and is not simply due to ion intercalation in the bulk polymer chain upon electrochemical activation. Molecular actuation mechanisms results from π - π stacking of thiophene oligomers upon oxidation, producing a reversible molecular displacement which is expected to lead to surprising material properties such as electrically controllable porosity and large strains. The hypothesis of active molecular conformational changes is supported by *in situ* electrochemical data. Single molecule techniques are considered for molecular actuator characterization. Mechanical properties of these new materials are currently being assessed.

Keywords: Molecular actuator, conducting polymer, thiophene, large strain, molecular design, single molecule, high-throughput synthesis, optical tweezers, AFM.

1. INTRODUCTION

Human skeletal muscle exhibits properties in combined terms of active strain, active stress, active strain rate, variable stiffness, power to mass ratio and bandwidth which classical actuator technologies do not match [1]. On the other hand, conducting polymer materials offer properties enabling the creation of biomimetic artificial muscles. Polypyrrole-based actuators, for example, generate forces per cross-sectional area that are up to two orders of magnitude greater than human muscle (40 MPa) with equal power to mass ratios (39 W/kg). In addition, these actuators require low drive voltages and offer typically limited active strain (2%) and limited active strain rate (1%/s) [2].

Actuation in conducting polymers such as polypyrrole or polyanilines is based on electrochemical oxidation and a resulting diffusion and intercalation of ionic species into the polymer bulk film [3]. This ionic intercalation process arises to maintain electro-neutrality during the oxidation process, leading to significant volume changes. In addition, accommodation of these ions and their associated solvated species is favored by the weak polymer interchain interactions compared to the modulus along the polymer molecular backbone [4]. As a result strains on the order of 2% are produced upon electroactivation. It is conceivable that ultimately the maximum strain achievable in these "classical" conducting polymer actuators is going to be limited by the inability of the polymer molecular backbone to significantly change length to accommodate further ions.

Nature being our source of inspiration [5] [6] [7], a more powerful approach is to design conducting polymer backbones with chemically driven shape changes that translate into large alterations of their length in response to electrically induced changes in oxidation state. Advances in synthetic organic chemistry enable the creation and manipulation of such molecules that mimic natural mechanisms. They are built upon novel molecular design elements for creating volume changes. Diversity in material properties and characteristics is introduced through a combination of design

* Correspondance: patanq@mit.edu, <http://bioinstrumentation.mit.edu>

elements. These include molecules that distort from bent to planar structures upon electrochemical activation, materials that undergo volume changes due to stacking of redox units and molecular scaffolds that behave as “accordion-like” structures capable of being switched between an extended and a tightly folded molecular structure.

Molecular actuators, i.e. biological or synthetic molecular systems performing work upon consumption of energy have triggered great interest in various fields such as biology, chemistry, chemical engineering and mechanical engineering [8], [9], [10], [11]. Various biological machines such as the ATP synthase, or kinesins have been studied extensively; Synthetic non-conducting polymer molecules embedding metal complexes that exhibit electron-induced (redox) chirality have been created [12]; Molecular (robotic) grippers made from resorcin[4]arene have been demonstrated [13], to cite just a few. A possible mechanism of molecular actuation using cyclooctatetrathiophene conducting polymers has also been recently investigated by Marsella and colleagues [14].

Within the framework of molecular actuation, we present herein two thiophene-based candidate conducting polymer molecules which have been synthesized in our laboratory from monomers designed for particular actuation purposes. One compound under study features an accordion like polymer formed by calix[4]arene hinges separated by conducting quarterthiophene rods. The second compound considered is quarterthiophene alone. In both compounds, actuation is believed to result from π -stacking of thiophene oligomers upon oxidation, producing a reversible molecular displacement. Polymer synthesis, mechanical and electrical properties as well as principle of molecular actuation of these novel compounds are discussed.

2. MOLECULAR MUSCLE CANDIDATES

The first thiophene-based molecular actuator candidate, polymer **1**, shown in Figure 1, employs hinge molecules (calix[4]arene) interconnected by rigid rods (quarterthiophene). The rods attract one another in the oxidized state, contracting the material. This actuation characteristic results from π - π stacking of thiophene oligomers upon oxidation, producing a reversible molecular displacement [15]. The second candidate, polymer **2** is poly(quarterthiophene) (poly(QT)), a system used to study the π -stacking effect of the oxidized thiophene oligomers upon oxidation. In other words, this latter candidate is a non-hinged version of the poly(calix[4]arene-bithiophene) molecule.

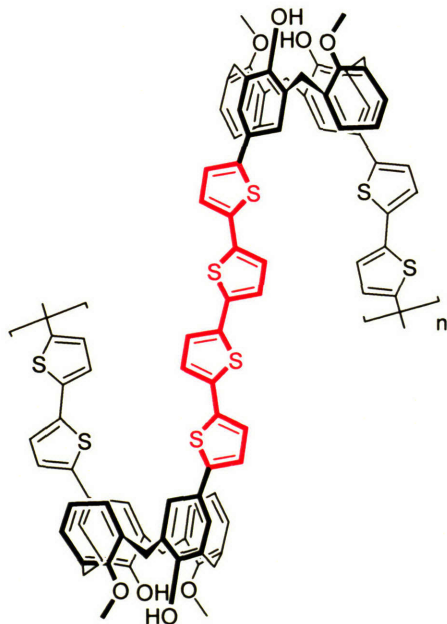


Figure 1: Structure of calix[4]arene-bithiophene.

Rigid 3-dimensional structures with significant amounts of free internal volume are ideal prospects for the formation of novel materials capable of unprecedented volume changes. Calix[4]arene is a particularly attractive building block to incorporate into an actuator polymer. It is well known that calixarenes have the property of producing well-defined binding sites and have a large versatility for functionalization [16]. Furthermore, the calix[4]arene scaffold has the ability to exist in a number of different conformations which are often in thermal equilibrium labeled as the cone, 1,2-alternate, 1,3-alternate, and partial cone (Figure 2). The calix[4]arene scaffold is a hinge structure introducing many possibilities for the formation of materials with novel architectures and shape changing ability.

Various conformations of the calix[4]arene scaffold can be synthesized by alkylation of the phenolic groups. In particular the addition of n-propyl groups is effective at restricting the calix[4]arene core from equilibrating between different conformations, producing primarily the cone conformation [17]. This scaffold is then chemically combined with bithiophene groups to form a C-shaped molecule. Synthesis of polymer **1** has been reported elsewhere [18].

Oxidation under either electrochemical or chemical conditions leads to polymer **1** which has a pinched cone conformation based upon the conformational preferences of the monomer (as determined by NMR spectroscopy). The cone conformation of the calix[4]arene scaffold allows generation of an accordion-like molecule upon polymerization.

Polymer **1** is a promising actuating material. Key features of this material include the deformable calix[4]arene scaffold and the redox active quarterthiophene units. The proposed actuation mechanism and a 3-dimensional space-filling model showing the collapse of a monomer are represented conceptually in Figure 3. The initial polymer displays an equilibrium conformation that has the quarterthiophene groups in a non-aggregated state. Upon oxidation the quarterthiophene groups have a strong tendency to aggregate into a π -stacked structure [15]. Inspection of the space-filling model in Figure 3 suggests that one dimensional changes of as large as a factor of 5 are possible for Polymer **1**.

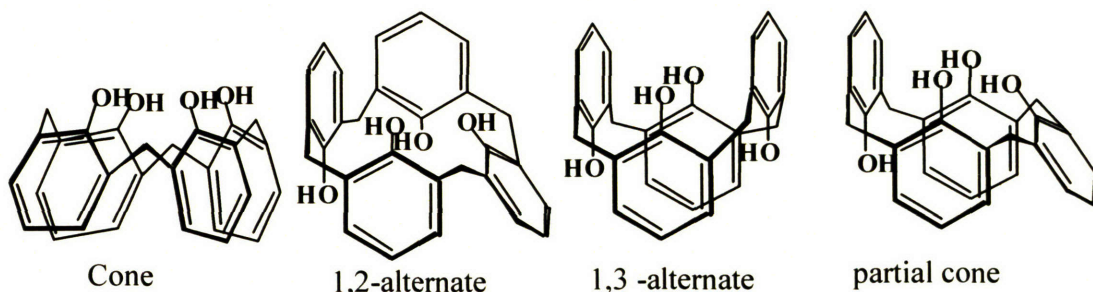


Figure 2: Calix[4]arene and its molecular conformations.

Polymer **2** is a non-hinged version of polymer **1**, where molecular contracting elements are freely dispersed in the polymer film. The structure of polymer **2** is shown in Figure 4. Similarly as for polymer **1** the quarterthiophene groups have a strong tendency to attract each other and form a π -stacked structure upon oxidation.

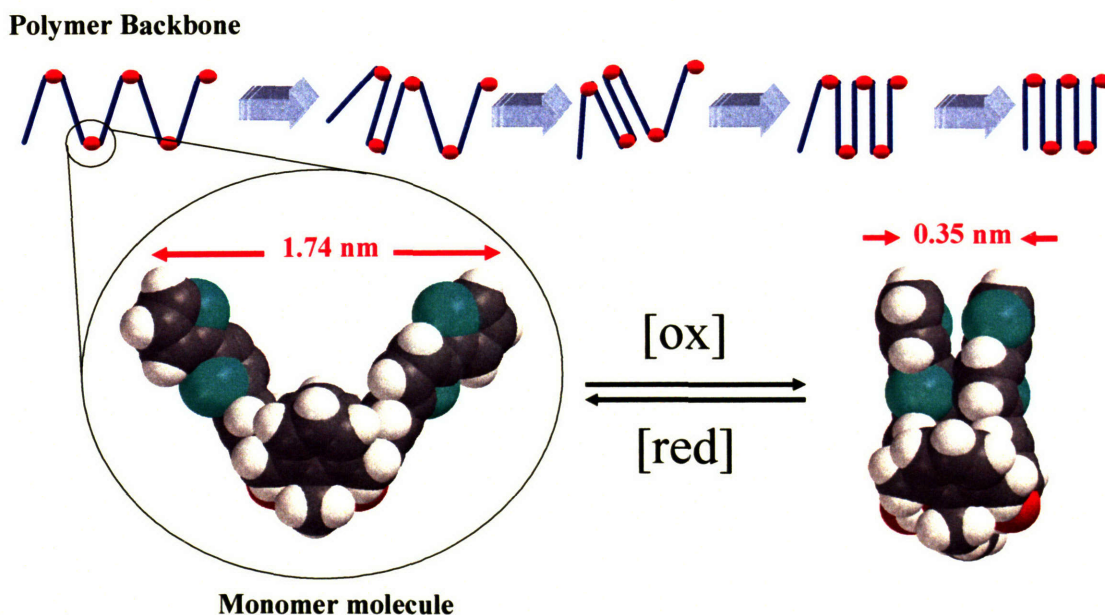


Figure 3: Schematic actuation mechanism of polymer **1**.

To develop artificial muscle technology for applications in life-like robotics, active prostheses or medical devices it is necessary to obtain the contractile material in bulk form. However, early films of the novel thiophene based monomers

that were grown have been brittle and difficult to handle. Polymer composites of the active polymer with a sulfated polymeric anion were therefore created to increase the mechanical robustness of the films, following the example of Wallace et al. in polypyrrole [19]. This additional polyelectrolyte is Sulfated Poly- β -Hydroxy Ether (S-PHE). It is designed to form a supporting elastic matrix for the new contractile compounds. Notice that the S-PHE polymer is a large molecule, its molecular weight exceeding 30,000 g/mol. The polyelectrolyte is added to the deposition solution during electrochemical polymerization and hence replaces typical salts used, such as tetraethylammonium hexafluorophosphate for example. The structure of the S-PHE is shown in Figure 5. The Molar Ratio (MR) of sulfate groups (n) to hydroxyl groups (m) is also referred as the sulfation ratio and is computed as follows: $MR = n/(n + m)$.

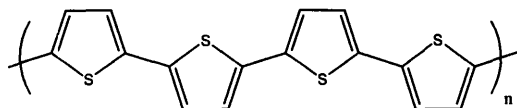


Figure 4: Structure of poly(quarterthiophene), (poly(OT)).

Two different polymers incorporated within the same material will typically phase separate. The sulfate group in the S-PHE, however, enhances the coulombic interaction between each phase of the composite resulting in the minimization of the phase separation between conducting and insulating polymer. Incorporation of the polyanion into the polymer film has the following consequences: first, it provides an elastic mechanical support to the polymer

molecules, reducing film brittleness. Second, the lack of polyanion mobility has the effect that charge compensation during oxidation or reduction is mainly achieved by diffusion of cationic species into the polymer composite. In traditional single phase conducting polymer actuators such as polypyrrole, both ionic species diffuse into and out of the polymer during oxidation and reduction with rates that are size and geometry dependent. The larger the ion, the more likely it is to be immobilized via entanglement. Polyanions such as S-PHE are large enough that they are effectively locked in place.

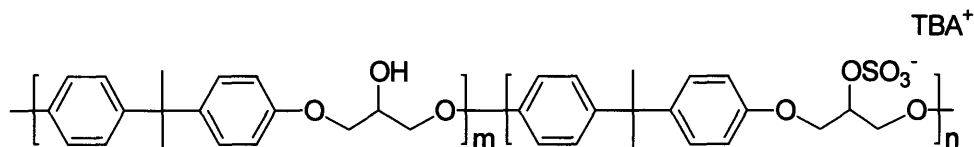


Figure 5: Structure of the S-PHE polyelectrolyte.

3. EXPERIMENTAL

3.1. Reagents

Calix[4]arene-bithiophene and quarterthiophene (QT) monomers were designed and synthesized in our laboratory according to synthesis techniques presented elsewhere [18] and their structure verified by NMR. Tetraethylammonium hexafluorophosphate (TEAP), Tetrabutylammonium hexafluorophosphate (TBAP), dichloromethane and acetonitrile were obtained from Aldrich¹. Several Sulfated Poly(β -HydroxyEther) (S-PHE) polyanions candidates with different MR sulfation ratio were synthesized according to the method of Wernet [20]. Ag/Ag⁺ reference electrodes (BAS Bioanalytical Systems²) were constructed from 0.1 M TEAP and 0.01 M AgNO₃ in acetonitrile and referenced versus the Fc/Fc⁺ redox couple (Aldrich¹).

3.2. Preparation of polymers

Synthesis was performed by electrodeposition under galvanostatic or swept potential conditions onto a conducting substrate. The working electrode materials were glassy carbon or 200 nm gold coated PET films (Alfa Aesar³) and the

¹ www.aldrich.com

² www.bioanalytical.com

³ www.alfa.com

counter electrode was a copper sheet (Aldrich¹). Conducting polymer films were grown from a solution of 5 mM calix[4]arene-bithiophene or quarterthiophene (QT) monomer, 0.1 M tetraethylammonium hexafluorophosphate and diverse S-PHE concentrations (0.02; 0.2; 0.5; 1; 2 %weight) as well as MR values (1; 0.09; 0.06) in acetonitrile. Galvanostatic depositions were conducted at current densities of 1.25 A/m² for 5 hours resulting in film thickness between 120 and 150 μm. Deposition took place at room temperature (25 °C). The resulting films of poly(QT)/S-PHE were then peeled off the working electrode substrate, rinsed in acetonitrile and allowed to dry for 24 hours. Poly(QT)/S-PHE films had conductivities of 10⁻¹ S·m⁻¹, densities of between 550 and 750 kg·m⁻³ dry, tensile strengths of 20 MPa in their dry form and of 1.3 MPa when soaked in acetonitrile. Polymerization was also performed using swept potential methods (-0.2 V to +1.0 V vs. Fc/Fc⁺ at a rate of 100 mV/s).

3.3. Techniques and instrumentation

Electrodepositions and electroactivations were carried out with a potentiostat (Amel⁴, Model 2049). Bulk conductivity measurements were conducted on a custom built four point measurement apparatus connected to a multimeter (Keithley⁵, model 2001). *In situ* conductivity measurements were acquired using interdigitated microelectrodes [21].

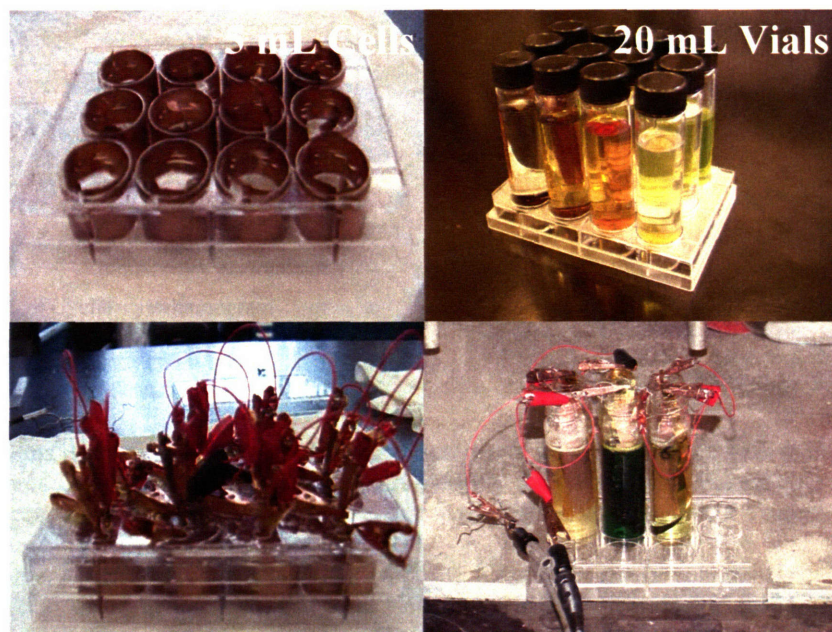


Figure 6: 12 cell high throughput deposition system, allowing synthesis of as many as 12 films in parallel.

To enhance productivity of synthesizing films, parallel high throughput electrochemical synthesis methods were developed. The purpose was to reduce the time necessary to scan through a large synthesis parameter space. In addition, such a small volume parallel system allowed us to utilize minimal quantities of monomer compound as possible. In a typical parallel synthesis setup as shown in Figure 6, up to 12 polymers can be synthesized at the same time. Considering that single polymer film synthesis may take as much as 5 hours of deposition time, the high throughput synthesis technique enabled acceleration of material discovery time. The parallel deposition system is based around a 12 well tissue culture plate (Falcon⁶, 35,3225) typically used for biological studies. Each well can contain up to 5 mL of solution. This volume can be increased to 20 mL by using tall vials (VWR⁶). Details of this system have been previously described [22].

⁴ www.amelsrl.com

⁵ www.keithley.com

⁶ www.vwr.com

4. POLYMER SYNTHESIS RESULTS

Poly(calix[4]arene-bithiophene) films were synthesized with 0.1M TEAP in dichloromethane under galvanostatic conditions (1.25 A/m^2 , 0.125 mA/cm^2). A typical cyclic voltamogram (100 mV/s) of the deposition process is shown in Figure 7. Note that the oxidation voltage is +0.8 V versus Fc/Fc⁺. Additionally the increase in current after each potential scan shows that material is being added to the working electrode.

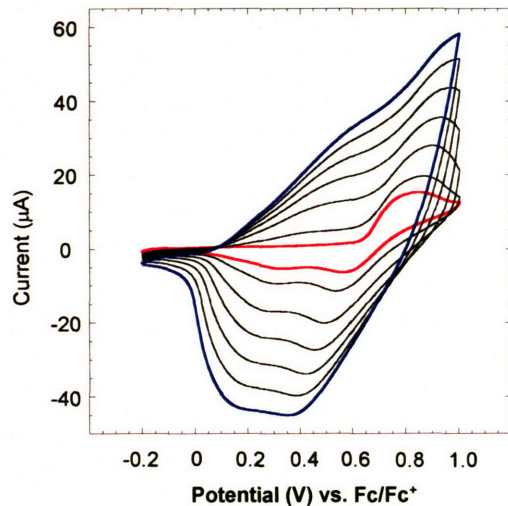


Figure 7: Cyclic voltamogram of a dichloromethane solution containing 5 mM calix[4]arene-bithiophene and 0.1 TEAP at a gold coated PET electrode. Scan rate is 100 mV/s.

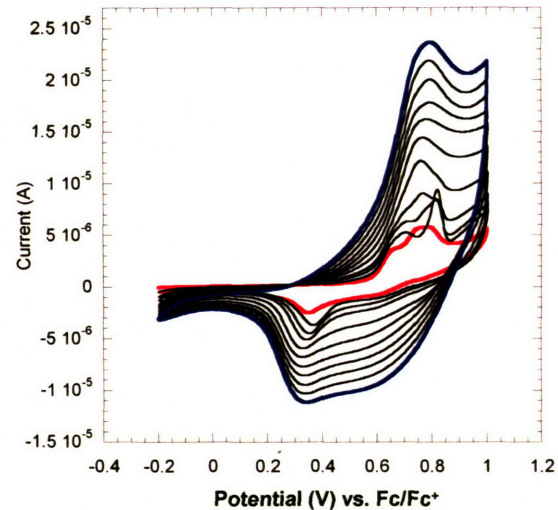


Figure 8: Cyclic voltamogram of an acetonitrile solution containing 5 mM quarterthiophene and 0.1 M TEAP at a gold coated PET electrode. Scan rate is 100 mV/s.

Similarly, poly(QT) films used for in-situ conductivity measurements were synthesized with 0.1M TEAP in acetonitrile (not dichloromethane) under galvanostatic conditions (1.25 A/cm^2). A typical cyclic voltamogram (100 mV/s) obtained during the deposition process is shown in Figure 8. Note that the oxidation voltage is +0.8 V versus Fc/Fc⁺.

Poly(calix[4]arene-bithiophene)/S-PHE free standing composite films were grown galvanostatically (1.25 A/m^2) from a solution containing 5 mM calix[4]arene-bithiophene, 2 %weight S-PHE (MR = 1) and 0.1M of TEAP in acetonitrile. Similarly, poly(QT)/S-PHE free standing composite films were grown galvanostatically (1.25 A/m^2) from a solution containing 5 mM QT, 2 %weight S-PHE (MR = 1) and 0.1M of TEAP in acetonitrile. Figure 9 compares the morphologically superior characteristics of a poly(QT)/S-PHE polymer composite film with a simple QT film. Notice that the simple QT film has the form of a brittle (powder like) material with absolutely no mechanical strength. On the other hand the QT/S-PHE composite exhibits a tensile strength of 20 MPa (dry).

5. BULK ACTUATOR PROPERTIES

Films of poly(QT) were prepared as described in the previous Section. The parallel synthesis system allowed us to vary the deposition concentration of S-PHE or salt within a batch of films and to quickly find optimal deposition parameters towards mechanically strong films. Initial observations indicate that films made from a deposition solution containing at least 2 % by weight S-PHE (MR = 1) and 0.1M TEAP show better mechanical integrity than films made at lower S-PHE or salt concentrations. No mechanically stable films were achieved at very low concentration of S-PHE (0.02%weight, MR = 1).

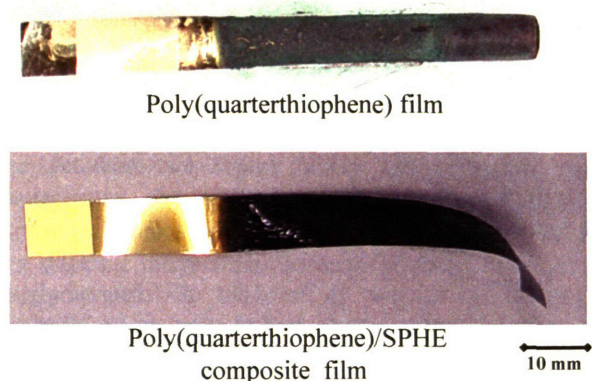


Figure 9: Effect on poly(QT) polymer film strength of blending with the S-PHE polyanion.

Such films of Poly(QT) demonstrated a tensile strength of 20 MPa when dry. The value of the tensile strength is decreased by more than an order of magnitude to 1.2 MPa when the films are immersed in 0.1M TEAP in acetonitrile. Such behavior can be attributed to partial softening of the S-PHE polyanion matrix when placed in acetonitrile. Observations indicate that the S-PHE polyelectrolyte is acting as a matrix, holding the polymerized monomers together. In fact, at too low S-PHE concentrations (0.02 %weight, MR = 1) the QT monomers initially polymerize on the substrate surface (in inhomogeneous domains) but do not adhere to the surface (see Figure 9) forming a thin powder of polymer at the bottom of the deposition cell. A soft polyanion matrix is desirable to allow molecular conformational rearrangement of the polymer backbone upon electrochemical activation in bulk polymer films. Greater conformational freedom allows the conducting polymer

molecule to expand in contract at the molecular level, allowing for larger active strains.

On the other hand, Poly(QT)/S-PHE composite film conductivity is low (10^{-1} S/m), compared for example to polypyrrole ($3 \cdot 10^4$ S/m) [23]. A possible explanation for such a low conductivity might be due to the size of the S-PHE molecule preventing high doping levels in poly(QT)/S-PHE films. In fact, we observe an increase of conductivity by an order of magnitude between films that have been synthesized with addition of a smaller salt ion such as TEAP vs. films that contained only the S-PHE polyanions.

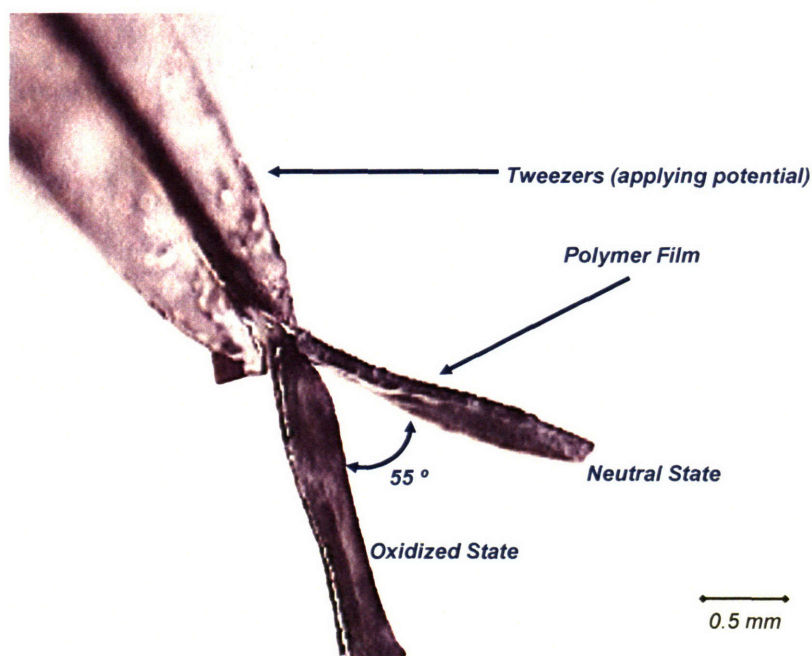


Figure 10: Poly(QT) film in actuation electrochemical cell test setup as seen under the microscope. The film is held by a pair of stainless steel tweezers which also act as a working electrode. The micrograph shows the oxidized state (contracted) and expanded state (expanded) overlaid on the same frame.

Initial activation studies using the beam-bending method [24] were conducted under a stereo microscope (Zeiss). A strip of poly(QT) (2.25 mm long, 0.375 mm wide and 80 μ m thick) was held in between a pair of stainless steel tweezers. Potentials of $\pm 5V$ vs. Fc/Fc^+ were applied to the working electrode for 4 seconds in an electrochemical cell containing 0.1M TEAP and a stainless steel counter electrode. The resulting actuation was monitored with a digital video camera (Sony DFW-V300).

Our initial actuation experiments (Figure 10) show that the poly(QT) system exhibits reversible strains in levels of $20 \pm 3\%$. These high strains are observable close to the pair of tweezers where the bilayer bends to a large radius of curvature. It is speculated that low film conductivity prohibits contractions far away of the point of electrical

contact. Note that this result is not a direct confirmation of molecular actuation, but serves to demonstrate that poly(QT) is electroactivable.

6. NOVEL ACTUATION PRINCIPLE

The actuators we report herein use reversible molecular conformational transitions to generate controllable displacements and work. One possible physical effect leading to such molecular rearrangements is the formation of π -dimers (e.g. the tendency of π orbitals to align due to Pauli's exclusion principle) upon oxidation of the material. π - π stacking interactions between aromatic units in supramolecular structures help to create robust macroscopic conglomerates. In the case of polymer 1 and polymer 2 it is energetically more favorable for two adjacent quarterthiophene units to have their π -orbitals overlap and rearrange in π -dimers, potentially leading to large molecular conformational changes [15].

In situ conductivity measurements allow probing polymer film conductivity as function of oxidation state hence giving an insight into electrochemical processes taking place at the molecular level. Films of poly(QT) prepared as described in Section 4, were cycled at 25 mV/s at potentials between -0.2 V and 1 V vs. Fc/Fc⁺ and their conductivity measured against a bias of 40mV using interdigitated microelectrodes. Figure 11 shows the relative conductivity of a poly(QT) film vs. oxidation potential, overlaid with a cyclic voltammogram. Notice the large relative conductivity hysteresis in Figure 11, where a potential difference of 0.5 V is required to reverse the relative conductivity of poly(QT) from conducting to insulating during the reverse sweep.

Such a large hysteresis indicates that more energy is required to switch poly(QT) from its oxidized state to its reduced state and vice versa, giving strong evidence that a more stable structure (possibly the π -dimer) has been formed as a result to the initial anodic potential sweep in which the quarterthiophene groups were oxidized. In other words, the higher stability of the π -dimer in poly(QT) makes the aggregated state harder to reduce, causing the large hysteresis in the current voltammogram. On the other hand, such a behavior could be also attributed to electrochemical kinetic limitations such as electron transport or ion diffusion. However film relative conductivity is high over the entire potential range of the reduction sweep, indicating that such kinetic limitations do not take place.

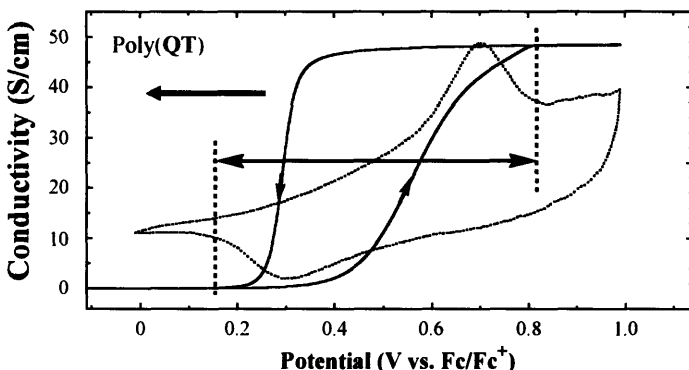


Figure 11: Cyclic voltammetry (25 mV/s) / *in situ* conductivity combined experiments of a poly(QT) at an interdigitated microelectrode in acetonitrile.

Now that we assume that π - π stacking of quarterthiophenes redox units is the driving force for actuation, let's consider how much energy can be produced during such a contraction. From theoretical and experimental studies on quarterthiophene dimers in solution, the barrier of dissociation of π -stacks is found to be $2.5 \cdot 10^{-20}$ J (0.16 eV or 3.6 kcal/mol) [25], [26]. Notice that this energy value is an order of magnitude larger than the Van der Waals bonding energy. It is also equivalent to $6.1 k_B T$ (where k_B is Boltzmann's constant and T is the absolute temperature; at room temperature $1 k_B T$ is $4.1 \cdot 10^{-21}$ J). Hence the π -dimer is considered to be an electro-reversible chemical bond. It is interesting to notice

that molecular actuators found in nature operate within the same energy range. The ATP synthase, for example - which is a 10 nm rotational ATP synthesizing molecular motor found in mitochondria, bacteria and chloroplasts - produces $20 k_B T$ of work per ATP synthesized (1/3 of rotation) [27]. Similarly, single actin-filament /myosin-head interaction in human skeletal muscle produces between 3 and $15 k_B T$ of work.

Previous AM1 (Austin Model 1) molecular simulations [18] show that two arms of the poly(calix[4]arene-bithiophene) molecular actuator can theoretically contract by 2.81 nm upon oxidation [32]. Dividing the amount of work generated per monomer unit of $2.5 \cdot 10^{-20}$ J by the active molecular displacement, it is estimated that a single molecule of calix[4]arene-quarterthiophene will produce at most 8.9 pN of average active force.

Let's now analyze the theoretical maximal efficiency of such a molecular actuator. As each QT arm needs to be oxidized to form a π -stack we can assume that the removal of one electron per calix[4]arene-quarterthiophene unit is required to achieve π -stacking. From the poly(QT) film electroactivation cyclic voltamogram (Figure 11) we observe that there is a potential difference of 0.5 V between the oxidation and reduction wave. Therefore the electrical energy that is brought into the system during oxidation of a single polymer **1** molecule is $8 \cdot 10^{-20}$ J. Thus the proportion of energy converted to work (the electromechanical coupling efficiency) of polymer **1** as molecular actuator is potentially as high as 31 %.

Finally, let's consider the poly(calix[4]arene-bithiophene) as a bulk material, and try to estimate the upper bound on the average stress produced by molecular contraction. This is computed, given that stress times strain is the work per unit volume. The novel molecular muscle materials are designed with the goal of achieving 20 % strain contraction on average. We assume a bulk density of 1300 kg/m^3 , a molecular weight of 781 g/mole and an energy for π - π stacking of 3.6 kcal/mol . Considering that the two calix[4]arene-bithiophene monomer molecules are needed to achieve contraction, the maximal average stress is found to be 95 MPa.

7. DISCUSSION

While *in situ* conductivity measurements combined with electrochemical potential sweep technique provide indirect evidence for electrically triggered molecular conformational of the backbone of polymer **1** and **2**, direct evidence of molecular actuation is difficult to obtain from bulk film actuation experiments. Ultimately, knowing the force and stress generated by a single conducting polymer molecular chain or by a thin polymer fiber will give tremendous insights into the nano and the macro scale mechanical behavior of polymer molecular actuators

Such direct measurements of the mechanical properties of a single molecular chain or a thin polymer fiber could be achieved by using optical tweezers [28] or single molecule AFM techniques [29].

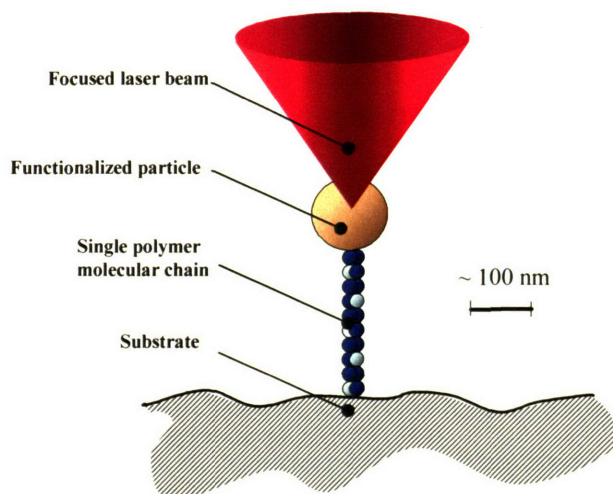


Figure 14: Single molecular muscle actuator testing apparatus using optical tweezers

In the case of optical tweezers, a single polymer chain is attached to a functionalized sub-micrometer sized dielectric particle trapped in a 3 dimensional force field produced by a laser beam (Figure 14). By modulating the intensity of the laser beam and using system identification, the stiffness of the optical trap is easily and accurately determined, thus making this instrument a sensitive force sensor ($0.2 \text{ pN/Hz}^{1/2}$ [30]). In addition, mechanical forces over a large dynamic range ($1-10^4 \text{ pN}$) and a microsecond time scale can be generated and monitored by using this instrument, [31]. We estimated that a single molecule of calix[4]arene-quarterthiophene will produce at most 8.9 pN of average active force, making optical tweezers ideal to monitor contractions of polymer **1**.

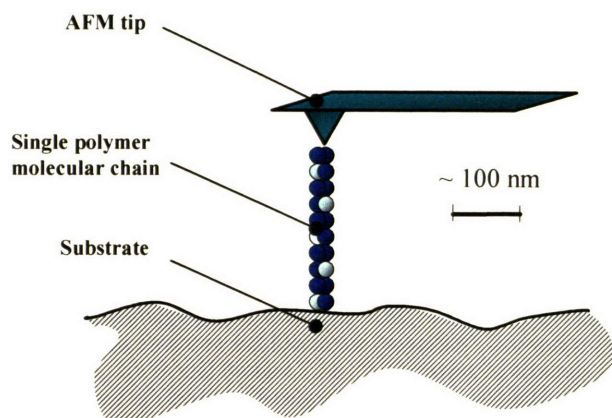


Figure 15: Single molecular muscle actuator testing apparatus using an AFM.

Similarly, an Atomic Force Microscope (AFM) can be used to carry single molecule actuator characterization (Figure 15). A single conducting polymer molecule is attached both to a substrate and an AFM cantilever tip by means of functionalized receptor/ligand interactions such as biotin/streptavidin or covalent bonding resulting from thiol/gold interactions. Soft AFM cantilevers typically have a spring constant of 0.01 N/m. Considering that a single hinged dimer unit of polymer **1** is expected to contract by 2.81 nm, the minimum force that is required to bend the cantilever to monitor a full contraction is 28.1 pN, which is above the average maximal force produced by a hinged dimer of polymer **1**. Softer cantilever will have to be manufactured to make mechanical measurements with an AFM. The key advantage of AFM techniques, however, lies in the fact that rigid molecule/cantilever coupling (compared to soft coupling in optical tweezers) allows high frequency probing of the single polymer molecule. In other words the AFM can be considered a single molecule dynamic mechanical analyzer (M-DMA). Optical tweezers on

the other hand are better suited to probe low force, low frequency regimes.

8. SUMMARY

Synthesis of novel thiophene based conducting polymer molecular actuators has been reported. These novel compounds are designed to utilize the effect of π - π stacking as a driving force for actuation. The hypothesis of active molecular conformational changes is supported by *in-situ* electrochemical data. Initial actuation studies of poly(QT)/S-PHE bulk films seem to indicate that large strains are observable in these novel materials. Single molecule techniques are considered for molecular actuator characterization. The creation of such muscle-like actuators will enable advances in autonomous and life-like robotics, artificial organs and prostheses, and micro/nanosystem fabrication.

9. ACKNOWLEDGEMENT

This work was supported in part by the Office of Naval Research under grant N00014-99-1-1022.

10. REFERENCES

- [1] Hunter I.W. and Lafontaine S., "A Comparison of Muscle with Artificial Actuators", *Technical Digest IEEE Solid State Sensors and Actuators Workshop*, pp. 178-185, 1992.
- [2] Madden J.D., Madden P.G. and Hunter I.W., "Polypyrrole Actuators: Modeling and Performance", *Electroactive Polymer Actuator and Devices Conference, SPIE 8th Annual International Symposium on Smart Structures and Materials, Newport Beach, CA*, 2001.
- [3] Baughman R.H., Shacklette S.W., Plichta E.J. and Becht C., "Electromechanical Actuators Based on Conducting Polymers", *Molecular Electronics*, pp. 267-289, 1991.
- [4] Baughman R. H., "Conducting Polymer Artificial Muscles", *Synthetic Metals*, Vol. **78**, pp. 339-353, 1996.
- [5] Vale R.D. and Milligan R.A., "The Way Things Move: Looking Under the Hood of Molecular Motor Proteins", *Science*, Vol. **288**, pp. 88-95, 2000.
- [6] Mahadevan L. and Matsudaira P., "Mobility Powered by Supramolecular Springs and Ratchets", *Science*, Vol. **288**, pp. 95-99, 2000.
- [7] Mao C., Sun W., Shen Z. and Seeman N., "A Nanomechanical Device Based on B-Z Transition of DNA", *Nature*, Vol. **397**,

8. Synthesis and Characterization of poly(calix[4]arene bis-bithiophene) and poly(quarterthiophene)/S-PHE Actuators

pp. 144-146, 1999.

- [8] Soong R.K., Bachand G.D., Neves H.P., Olkhovets A.G., Craighead H.G. and Montemagno C.D., "Powering an Inorganic Nanodevice with a Biomolecular Motor", *Science*, Vol. **290**, pp. 1555-1558, 2000.
- [9] Astumian R.D., "Making Molecules into Motors", *Scientific American*, pp. 57-64, July 2001.
- [10] Ballardini R., Balzani V., Credi A., Gandolfi M.T. and Venturi M., "Artificial Molecular-Level Machines: Which Energy to Make them Work?", *Accounts of Chemical Research*, Vol. **34**, pp. 445-455, 2001.
- [11] Collin J.P., Dietrich-Buchecker C., Jimenez-Molero M.C. and Sauvage J.P., "Shuttles and Muscles: Linear Molecular Machines Based on Transition Metals", *Accounts of Chemical Research*, Vol. **34**, pp. 477-487, 2001.
- [12] Zahn S. and Canary J.W., "Electron-Induced Inversion of Helical Chirality in Copper Complexes of N,N-Dialkylmethionines", *Science*, Vol. **288**, pp. 1404-1407, 2000.
- [13] Yamakoshi Y., Schlitter R.R., Gimzewski J.K. and Diederich F., "Synthesis of Molecular-Gripper Type Dynamic Receptors and STM-imaging of Self-Assembled Monolayers on Gold", *Journal of Materials Chemistry*, Vol. **11**, pp. 2895-2897, 2001.
- [14] Marsella M.J. and Reid R.J., "Toward Molecular Muscles: Design and Synthesis of an Electrically Conducting Poly[cyclooctatetrathiophene]", *Macromolecules*, Vol. **32**, pp. 5982-5984, 1999.
- [15] Kingsborough R.P. and Swager T.M., "Polythiophene Hybrids of Transition-Metal Bis(salicylideneimine)s: Correlation between Structure and Electronic Properties", *Journal of the American Chemical Society*, Vol. **121**, (38): pp. 8825-8834, 1999.
- [16] Fu D., Xu B. and Swager T.M., "3-Methylcalix[4]arene: A New Versatile Precursor to Inherently Chiral Calix[4]arenes", *Journal of Organic Chemistry*, Vol. **61**, pp. 802-804, 1996.
- [17] Xu B., Miao Y.J. and Swager T.M., "Palladium Couplings on a Metalocalix[4]arene: An Efficient Synthesis of New Functionalized Cavities", *Journal of Organic Chemistry*, Vol. **63**, pp. 8561-8564, 1998.
- [18] Yu H.-h., Pullen A.E. and Swager T.M., "Toward New Actuating Devices: Synthesis and Electrochemical Studies of Poly(11,23-bis[2,2'-bithiophene]-5-yl)-26,28-dimethoxycalix[4]arene-25,27-diol)", *Polymer Science Material Engineering*, Vol. **83**, (523): 2000.
- [19] Ding J., Price W.E., Ralph S.F. and Wallace G.G., "Synthesis and properties of a mechanically strong poly(bithiophene) composite polymer containing a polyelectrolyte dopant", *Synthetic Metals*, Vol. **110**, pp. 123-132, 2000.
- [20] Wernet W. and Stoffer J., *US Patent 5,061,401*, 1991.
- [21] Kittelsen G.P., White H.S. and Wrighton M.S., "Chemical Derivation of Microelectrode Arrays by Oxidation of Pyrrole and N-Methylpyrrole - Fabrication of Molecule-Based Electronic Devices", *Journal of the American Chemical Society*, Vol. **106**, (24): pp. 7389-7396, 1984.
- [22] Madden P.G., Madden J.M. and Hunter I.W., "Parallel Electrochemical Methods to Accelerate Electroactive Material Discovery and Optimization", *Material Research Society Symposium Proceedings*, Vol. **698**, pp. EE1.7.1-EE1.7.6, 2002.
- [23] Madden J.D., Cush R.A., Kanigan T.S. and Hunter I.W., "Fast Contracting Polypyrrole Actuators", *Synthetic Metals*, Vol. **113**, pp. 185-192, 2000.
- [24] Pei Q. and Inngan O., "Electrochemical Application of the Bending Beam Method. I. Mass Transport and Volume Changes in Polypyrrole during Redox", *The Journal of Physical Chemistry*, Vol. **96**, (25): pp. 10507-10514, 1992.
- [25] Brocks G. "Charged Oligothiophene Dimers and π -stacks: the Bipolaron Revisited", *Synthetic Metals*, Vol. **119**, pp. 253-254, 2001.
- [26] Yamamoto T., Kamarudin D., Arai M., Lee B.-L., Suganuma H., Asakawa N., Inoue Y., Kubota K., Sasaki S., Fukuda T. and Matsuda H., "Extensive Studies of π Stacking of Poly(3-alkylthiophene-2,5-diyl)s and Poly(4-alkylthiazole-2,5-diyl)s by Optical Spectroscopy, NMR Analysis, Light Scattering Analysis, and X-ray Crystallography", *Journal of the American Chemical Society*, Vol. **120**, pp. 2047-2058, 1998.
- [27] Elston T., Wang H. and Oster G., "Energy Transduction in ATP Synthase", *Nature*, Vol. **391**, pp. 510-513, 1998.
- [28] Omori R., Kobayashi T. and Suzuki A., "Observation of a Single Beam Gradient-Force Optical Trap for Dielectric Particles in Air", *Optical Letters*, Vol. **22**, pp. 816-818, 1997
- [29] Zlatanova J., Lindsay S.M. and Leuba S.H., "Single Molecule Force Spectroscopy in Biology using the Atomic Force Microscope", *Progress in Biophysics and Molecular Biology*, Vol. **74**, pp. 37-61, 2000.
- [30] Meiners J.C. and Quake S.R., "Direct Measurement of Hydrodynamic Cross Correlations between Two Particles in an External Potential", *Physical Review Letters*, Vol. **82**, (10): pp. 2211-2213, 1999.
- [31] D'Helon C., Dearden E.W. and Rubinsztein-dunlop H., "Measurement of the Optical Force and Trapping Range of a Single-Beam Gradient Optical Trap for Micron Sized Latex Spheres", *Journal of Modern Optics*, Vol. **41**, (3): pp. 595-601, 1994.
- [32] AM1 molecular simulations of Polymer 1's contraction mechanism, show that this molecule theoretically contracts from an open state (1.74 nm) to a collapsed state (0.34 nm). Centroid-centroid distance between quarterthiophene organic rings is ~ 0.34nm, indicative of strong π - π interactions between aromatic units. This theoretical distance between π -stacked thiophenes is higher compared to results found in the literature for quarterthiophene alone (between 0.313 and 0.315 nm) [33].
- [33] Brocks G. "Charged Oligothiophene Dimers and π -stacks: the Bipolaron Revisited". *Synthetic Metals*, Vol. **119**, pp. 253-254, 2001.

Recent Advances in Thiophene Based Molecular Actuators

Patrick A. Anquetil^a, Hsiao-hua Yu^b, John D. Madden^c, Timothy M. Swager^b and Ian W. Hunter^a

^aBioInstrumentation Laboratory, Dept. of Mechanical Engineering; Massachusetts Institute of Technology, 77 Massachusetts Ave., Cambridge, MA, 02139, USA

^bDept. of Chemistry; Massachusetts Institute of Technology, 77 Massachusetts Ave., Cambridge, MA, 02139, USA

^c Dept. of Electrical and Computer Engineering, The University of British Columbia, 2356 Main Mall, Vancouver, BC Canada V6T 1Z4

ABSTRACT

A new class of molecular actuators where bulk actuation mechanisms such as ion intercalation are enhanced by controllable single molecule conformational rearrangements offers great promise to exhibit large active strains at moderate stresses. Initial activation of poly(quarterthiophene) based molecular muscles, for example, show active strains in the order of 20%. Molecular rearrangements in these conjugated polymers are believed to be driven by the formation of π -dimers (e.g. the tendency of π orbitals to align due to Pauli's exclusion principle) upon oxidation of the material creating thermodynamically stable molecular aggregates. Such thiophene based polymers, however, suffer from being brittle and difficult to handle. Polymer composites of the active polymer with a sulfated polymeric anion were therefore created and studied to increase the mechanical robustness of the films. This additional polyelectrolyte is a Sulfated Poly- β -Hydroxy Ether (S-PHE) designed to form a supporting elastic matrix for the new contractile compounds. Co-deposition of the polyanion with the conducting polymer material provides an elastic mechanical support to the relatively stiff conjugated polymer molecules, thus reducing film brittleness. The active properties of such poly(quarterthiophene)/S-PHE polymer actuator composites based on intrinsic molecular contractile units are presented and discussed.

Keywords: Molecular actuator, conducting polymer, quarterthiophene, π - π stacking, large strain, molecular design, single molecule, sulfated polyanion, molecular design.

1. INTRODUCTION

Recent progress in developing conducting polymer actuators has shown tremendous progress towards incorporation of these contractile materials into products^{1,2,3,4}. These studies have revealed that polymer actuators exhibit very high active stresses (40 MPa peak) at moderate contractile strains (~2 to 5 %) and speeds (3 to 10 %/s), with high power to mass ratios (150 W/kg), cycle life exceeding the million cycles while being activated at low electrical voltages (~1 to 5 V)⁵. Such polymeric contractile materials have been developed to a point where they could be used in medical devices, small robots as well as innovative consumables and toys. However despite all these successes no material exists to date that matches or exceeds mammalian skeletal muscle in all its figures of merit⁶. Such figures of merit include active strain, active stress, active strain rate, power to mass and efficiency.

Actuation in traditional conducting polymer actuators such as polypyrroles or polyanilines is driven by a mechanism of ion intercalation, leading to moderate strains^{7,8}. Our group (like Marsella et al.⁹) has taken a new approach that moves away from a materials survey approach and towards a materials designer strategy where novel materials are created by incorporating property-designed molecular building blocks. Such molecular building blocks may include shape changing, load bearing, passively deformable or hinge-like molecular elements combined with precise control of the

* Correspondance: patanq@mit.edu, <http://bioinstrumentation.mit.edu>

material morphology at the nanometer scale. Our vision is that unprecedented actuating materials will be created by a bottom-up approach where specific molecular designs are incorporated into a material to achieve specific properties.

Within the framework of molecular actuation, we present herein chemically engineered units that are believed to change their molecular shape and produce force and displacement upon the application of an electrical stimulus. These materials utilize a molecular dimerization mechanism known as π - π stacking as the molecular actuation driving force. We will start by briefly presenting this molecular actuating mechanism and show how it can be incorporated into molecular materials designs. We will then show initial activation results of polymer films that were synthesized in our laboratory, including beam-bending and isometric actuation characterization.

2. ACTUATING MECHANISMS AT THE MOLECULAR LEVEL AND CANDIDATE MOLECULES

2.1 π - π stacking

Typical conducting polymers make use of ion intercalation as the actuation driving force⁷. We propose to use molecular driving forces to change the shape of the polymer backbone. Such forces can include the formation of hydrogen bonds, the twisting or planarization of a molecule as a function of backbone electron density and finally the formation of reversible chemical bonds. Units incorporating these reversible molecular conformational transitions are then built into polymer systems that are expected to lead to controllable displacement and work at the macroscopic level. In this paper we present the use of the formation of π -dimers with aromatic units upon oxidation as molecular actuation driving force. This molecular mechanism referred as π -dimerization or π - π stacking makes use of wavefunction overlap in π -conjugated polymers which is attractive in the oxidized state (electron deficient) and repulsive in the reduced state (filled electronic levels).

The π -stacked structure is typical of oxidized thiophene oligomers and has been studied experimentally by means of X-ray diffraction, Scanning Tunneling Microscopy (STM), Electron Paramagnetic Resonance Spectroscopy (EPR), as well as theoretical calculation^{10,11,12,13,14}. As shown in Figure 1, oxidation of two adjacent quarterthiophene molecules creates two radical cations with partially occupied Highest Occupied Molecular Orbitals (HOMO). This state is observable by means of EPR spectroscopy as it exhibits an unpaired electron in the π -system of the oxidized thiophenes (EPR active). With further oxidation, both HOMO orbitals mix to produce a new doubly occupied molecular orbital at lower energy. The formation of this new molecular orbital provides stabilization of the π -dimer as the electronic energy of the charged quarterthiophene groups has been lowered. Unlike the singly occupied molecular orbitals, the π -stacked structure is EPR silent due to the electron spin pairing. This process is reversible and described by,



where QT describes a quarterthiophene molecule. As stated above, evidence of a reversible transformation between π -stacked and un-stacked conformations as oxidation state is obtained using EPR spectroscopy. Figure 2A shows an EPR signal recorded during a 100 mV/s swept cyclic potential (-0.2 V to 1.3 V vs. Fc/Fc⁺) for the poly(quarterthiophene) polymer (poly(QT)). Notice the hysteresis obtained during the cathodic sweep (from 1.3 V back to -0.2 V) to revert the signal from EPR *silent* to EPR *active*. Such a large hysteresis indicates that more energy is required to switch poly(QT) from its oxidized state to its reduced state and vice versa, giving strong evidence that a more stable structure (possibly the π -dimer) has been formed as a result of the initial anodic potential sweep in which the quarterthiophene groups were oxidized.

In addition, similar hysteresis effects resulting from π -dimerization are observed from *in-situ* conductivity measurement. Interdigitated microelectrodes (Abtech Scientific^a) allow measuring film conductivity *in-situ* as a function of oxidation state. Films of poly(QT) were cycled at 10 mV/s at potentials between -0.2 V and 1.3 V vs. Fc/Fc⁺ and their

^a www.abtechsci.com

conductivity measured against a bias of 40mV (Figure 2B). Notice in Figure 2B that switching the relative conductivity of poly(QT) from conducting to insulating requires ~ 0.5 V of reverse potential, indicating that the π -dimer aggregated state is harder to reduce and thus confirming its higher stability. Note that such a behavior is unlikely to be attributed to electrochemical kinetic limitations such as electron transport or ion diffusion as the films relative conductivity is high over the entire potential range of the reduction sweep.

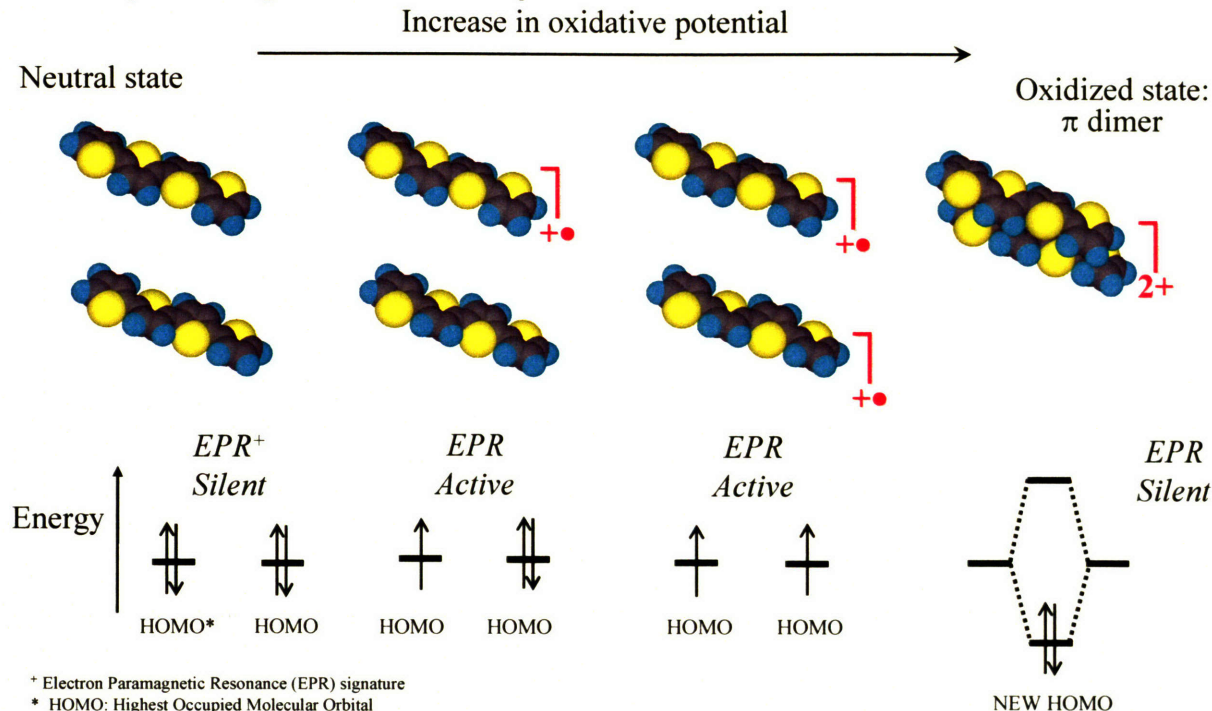


Figure 1: Mechanism of π - π dimer formation in quarterthiophene. The corresponding EPR spectroscopic signature is schematically represented below the 3D space filling molecular model. Each arrow represents the spin of an electron. A double arrow indicates that the Highest Occupied Molecular Orbital (HOMO) is fully occupied (EPR silent). A single arrow represents an unpaired spin or radical cation that is observable by EPR spectroscopy (EPR active).

Additionally, theoretical and experimental studies on quarterthiophene dimers in solution show that the barrier of dislocation of π -stacks is quite high: 2.5-10-20 J (0.16 eV or 3.6 kcal/mol), classifying the π -dimer as an electroreversible chemical bond^{15,16}. Notice that this energy value is on the same order of magnitude of the Van der Waals bonding energy and six times bigger than $k_B T$ (where k_B is Boltzmann's constant and T is the absolute temperature; at room temperature $1 k_B T$ is $4.1 \cdot 10^{-21}$ J)¹⁷.

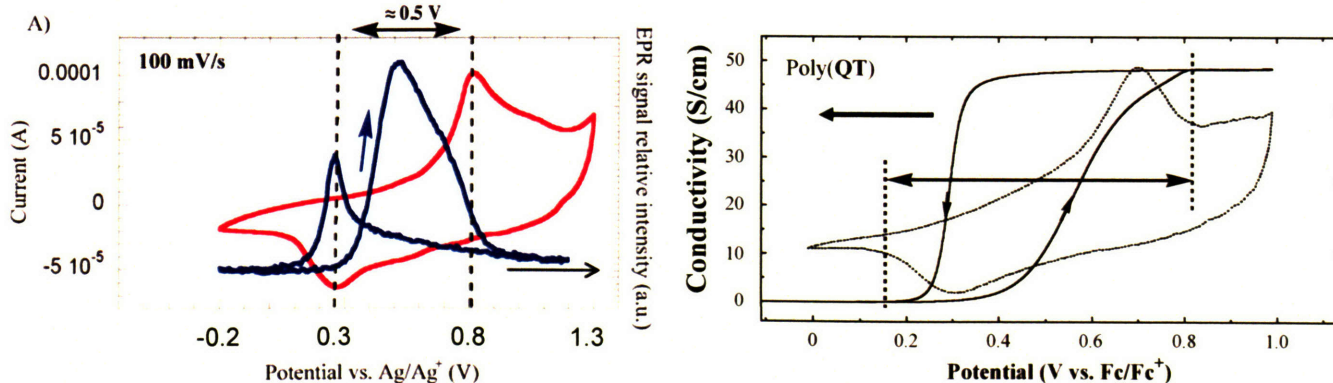


Figure 2: A) EPR signal relative intensity as a function of oxidation potential (100 mV/s scan rate). B) Film relative conductivity as a function of oxidation potential (10 mV/s scan rate).

2.2 Poly(quarterthiophene)

Our first molecular actuator candidate is poly(quarterthiophene): (poly(QT)). This system incorporates directly the π - π stacking molecular actuation mechanism presented in the previous Section. Polymerization of QT into poly(QT) occurs via oxidative electrochemical deposition. This system is easily synthesized and is appropriate for studying the mechanism of π - π dimerization. Figure 3 shows a simplified mechanism of polymerization of poly(QT).

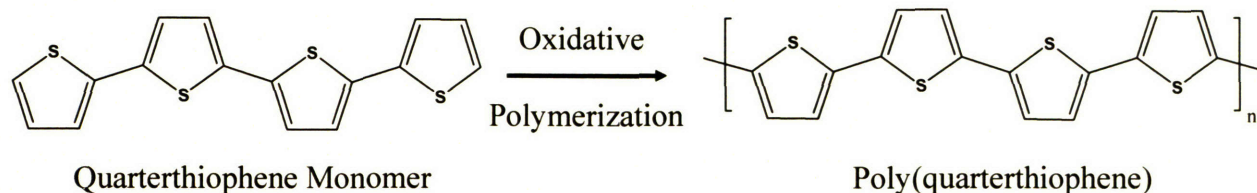


Figure 3: Oxidative polymerization of quarterthiophene monomer leading to poly(quarterthiophene), (poly(QT)).

2.3 Poly(calix[4]arene bis-bithiophene)

Our second candidate system for molecular actuation is poly(calix[4]arene bis-bithiophene): poly(calixBBT). It features an accordion-like molecule that can be switched from a zigzag open structure to a collapsed structure upon change of its oxidation state. It employs mechanically passive cone-shaped hinge molecules (calix[4]arene) interconnected by rigid rods (quarterthiophene) which are the active elements in this system. As mentioned above, the quarterthiophene active rods are designed to attract one another in the oxidized state, while the calix[4]arene units act as passive hinges, directing the contraction of the material into a folded molecular structure¹⁰. The cone conformation of the calix[4]arene scaffold allows generation of an accordion-like molecule upon monomer polymerization under either electrochemical or chemical conditions. This molecular contraction is driven by the π - π dimerization of thiophene oligomers rods upon oxidation, producing a reversible molecular displacement and has been described in great detail in previous publications^{18,19,20}. A 3-dimensional space-filling model showing the collapse and extension of a five-mer molecule is presented in Figure 4.

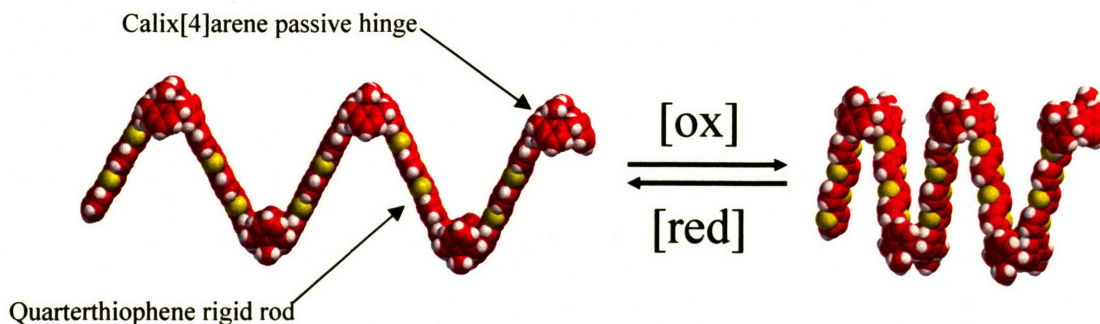


Figure 4: Proposed actuation mechanism for poly(Calix[4]arene bis-bithiophene) showing the expanded (left) and contracted (right) states.

2.4 Polymerization with an elastomeric sulfonate

Despite the promising molecular design presented above, these thiophene-based polymers suffer from being brittle and difficult to handle if polymerized electrochemically. In the case of QT it is our belief that the electropolymerization of the oligomeric quarterthiophene leads to low molecular weight polymers as the large size of the monomer may impair polymer growth. On the other hand, associating the active actuator polymer with a polyelectrolyte^b thereby creating a polymer composite can significantly improve mechanical properties. Following the example of Wallace et al. in polypyrrole² we used a Sulfated Poly- β -Hydroxy Ether (S-PHE) polymer as matrix-enhancing polyelectrolyte¹⁸. The polyelectrolyte is added to the deposition solution during electrochemical polymerization. Figure 5 shows the structure of the S-PHE molecule. The Molar Ratio (MR) of sulfate groups (n) to hydroxyl groups (m) is also referred as the sulfonation ratio and is computed as follows: $MR = n/(n + m)$.

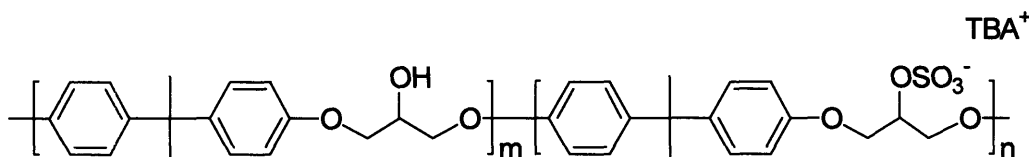


Figure 5: Structure of the S-PHE polyelectrolyte.

3. EXPERIMENTAL

3.1 Reagents

Quarterthiophene (QT) and Calix[4]arene-bis-bithiophene monomers were designed and synthesized in our laboratory according to synthesis techniques presented elsewhere^{19,20} and their structure verified by NMR. Tetraethylammonium hexafluorophosphate (TEAP), dichloromethane and acetonitrile were obtained from Aldrich^c. Several Sulfated Poly(β -HydroxyEther) (S-PHE) polyanions candidates with different MR sulfation ratio (0.06, 0.09, 1) were synthesized according to the method of Wernet²¹. S-PHE samples with another MR ratio (0.33 and 0.5) were graciously provided by Gordon Wallace and Jie Ding^d. Ag/Ag⁺ reference electrodes (BAS Bioanalytical Systems^e) were constructed from 0.1 M TEAP and 0.01 M AgNO₃ in acetonitrile and referenced versus the Fc/Fc⁺ (Ferrocene) redox couple (Aldrich¹). Miniature calomel reference electrodes (Acumet) were obtained from Fischer Scientific^f.

3.2 Preparation of polymers

Synthesis was performed by electrodeposition under galvanostatic or swept potential conditions onto a conducting substrate. The working electrode materials were glassy carbon (Alfa Aesar^g) or 200 nm gold coated PET films (Alfa Aesar) and the counter electrode was a copper sheet (Aldrich^c). Conducting polymer films were grown from a solution of 5 mM quarterthiophene (QT) monomer or calix[4]arene-bis-bithiophene (Calix), 0.1 M TEAP and diverse S-PHE concentrations (0.02; 0.2; 0.5; 1; 2 %weight) as well as MR values (1; 0.5 and 0.33) in acetonitrile, dichloromethane or a 30% acetonitrile – 70% dichloromethane solution. Galvanostatic depositions were conducted at current densities of 1.25 A/m² for 2.5 hours resulting in film thickness between 30 and 120 μ m. Deposition took place at room temperature (25 °C). The resulting films of poly(QT)/S-PHE and poly(calixBBT)/S-PHE were then peeled off the working electrode substrate, rinsed in acetonitrile and conserved in a 0.1 M TEAP in acetonitrile solution. Poly(QT)/S-PHE films had average conductivities about 10⁻¹ S·m⁻¹, densities (in dry state) between 550 and 750 kg·m⁻³, tensile strengths of 19.6 MPa in their dry form and of 1.3 MPa when soaked in acetonitrile. Films of poly(calixBBT) were conserved on their

^b A polyelectrolyte is an ionic polymer. In the case of the S-PHE, the polymer is negatively charged (anion) by sulfonate groups.

^c www.aldrich.com

^d Intelligent Polymer Research Institute, University of Wollongong, Australia

^e www.bioanalytical.com

^f www.fishersci.com

^g www.alfa.com

electrode substrate but have not been characterized at the time of this publication. Polymerization was also performed using swept potential methods (-0.2 V to +1.3 V vs. Fc/Fc^+ at a rate between 10 and 100 mV/s). Deposition of the polymers onto the electrode led to an increase in the current indicating polymer deposition after each cycle (potential sweep). Electrochemical strength^h of both poly(QT) and poly(calixBBT) films were later confirmed by performing cyclic voltammetry on the polymer covered substrate electrodes in 0.1 M TEAP in acetonitrile.

3.3 Techniques and instrumentation

Electrodepositions and electroactivations were carried out with a potentiostat (Amelⁱ, Model 2049). Bulk conductivity measurements were conducted on a custom built four point measurement apparatus connected to a multimeter (Keithley^j, model 2001). *In-situ* conductivity measurements were acquired using interdigitated microelectrodes (Abtech Scientific)²². *In-situ* EPR spectroscopic data was acquired using a platinum working electrode onto which poly(QT) was polymerized. Notice that poly(QT)/S-PHE composites have not been studied by EPR spectroscopy at this time. Passive and active mechanical testing methods and instrumentation are described in detail in Section 4 of this paper.

4. CHARACTERIZATION OF ACTUATOR PROPERTIES

4.1 Synthesis of poly(QT)/S-PHE free standing films

The novel monomers presented herein are designed and synthesized from scratch. Synthesis conditions have to be optimized towards highly conductive and mechanically strong materials. The freestanding mechanical properties of the active films are very important for building actuators as they determine both the active (contractile) and the passive (load bearing) performance. Material conductivity is important because it affects the speed at which the material can be activated (i.e. expanded or contracted).

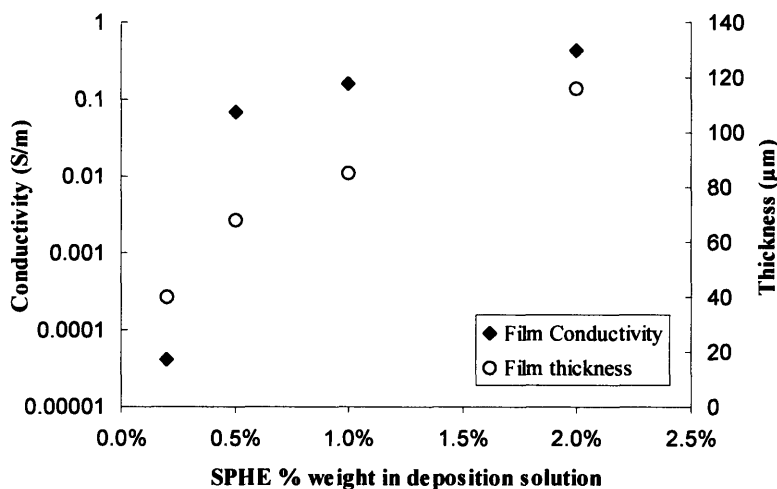


Figure 6: Poly(QT)/S-PHE sample conductivity (diamonds) and sample thickness (circles) as a function S-PHE % weight in the electropolymerization solution for 2.5 hours deposition at 1.25 A/m^2 .

The use of an elastomeric polyelectrolyte such as the S-PHE presented in Section 2.4 enables the creation of mechanically robust materials. This method, however significantly reduces polymer film conductivity as the S-PHE is an insulating polymer ($\sim 10^{-7} \text{ S/m}$). Studies to be published by Anquetil and Zimet as well as studies by Ding et al.²³ of polypyrrole/S-PHE show how the addition of S-PHE to a highly conductive polymer such as polypyrrole significantly

^h By electrochemical strength we meant that the current of the cyclic voltammogram did not decrease after each subsequent cycle, indicating that the polymer film remained attached to the substrate electrode

ⁱ www.amelsrl.com

^j www.keithley.com

reduces its conductivity. Similarly, the conductivity of poly(QT)/S-PHE films is affected by the addition of the S-PHE polyanion.

The films presented in Figure 6 were synthesized from an acetonitrile solution containing 5 mM QT, 0.1 TEAP and where the concentration of the S-PHE polyanion ($MR = 1$) was varied from 0.5 % weight to 2% weight. All films were deposited for the same amount of time (2.5 hours) under constant current conditions (1.25 A/m^2). Conductivity of the films ranged from $4.2 \cdot 10^{-5} \text{ S/m}$ to 0.16 S/m . It was found that conductivity increased as a function of S-PHE present in the deposition solution. We believe that a larger concentration of S-PHE enhances polymer growth. The S-PHE is a negatively charged polymer and co-deposits with QT at the positive working electrode. A larger S-PHE concentration in the deposition solution thus translates into more molecules that will assemble on the substrate, forming an elastomeric matrix onto which the deposited polymer can graft. This hypothesis is supported by the increase of material thickness as a function of S-PHE concentration while deposition time (2.5 hrs) and deposition current density (1.25 A/m^2) remained constant (circles in Figure 6). In addition the charge on the S-PHE is partially responsible for polymer doping along with PF_6^- ions. On the other hand thiophenes have been reported in the literature to reach conductivities of $2 \cdot 10^4 \text{ S/m}$ ²⁴. This significant decrease in conductivity could be explained by a combination of low QT polymer molecular weights and impaired interchain charge hopping due to the large size of the S-PHE backbone ($\sim 40,000$ molecular weight)²⁵.

4.2 Passive Mechanical properties

Passive mechanical testing of the poly(QT)/S-PHE was conducted using a Perkin Elmer Dynamic Mechanical Analyzer (DMA 7e)^k. It allows tensile tests to be performed on polymer films in or out of solution and at a controlled temperature. This apparatus was used to study the response of poly(QT)/S-PHE samples as a function stress. It was also used to study the mechanical properties of S-PHE films alone.

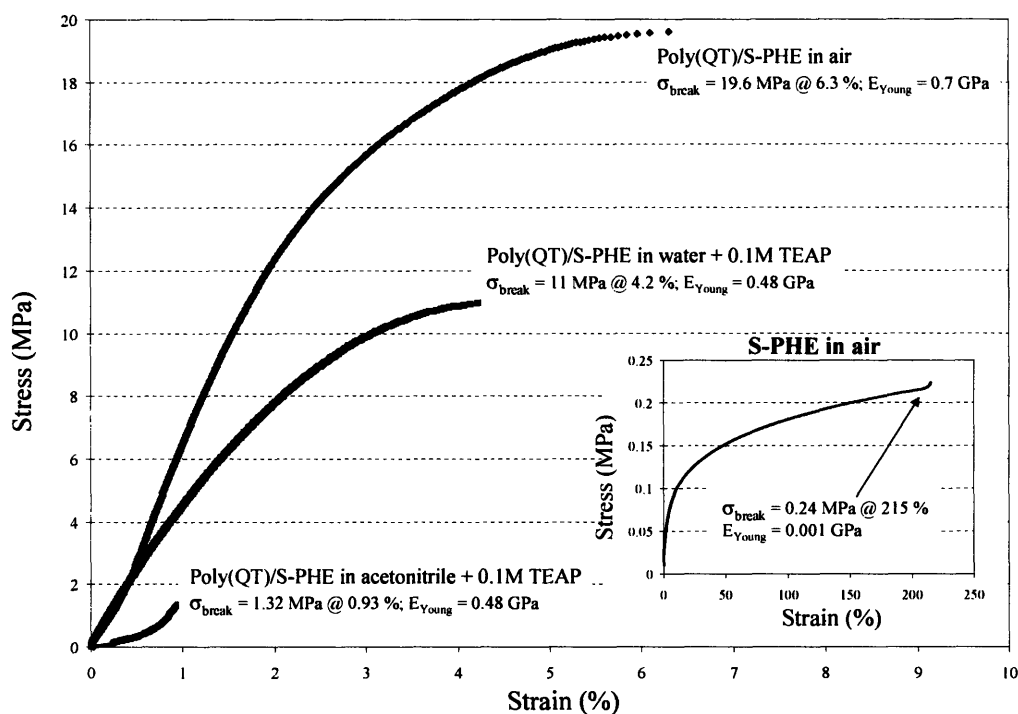


Figure 7: Mechanical response of the poly(QT)/S-PHE composite (dry, in 0.05 M TEAP in distilled water, in 0.1 M TEAP in acetonitrile and of standalone dry S-PHE).

^k instruments.perkinelmer.com

Based on the conductivity study presented above (Section 4.1), films of poly(QT)/S-PHE were synthesized such that selected synthesis parameters would lead to films with the highest conductivity. Films were synthesized from a solution of acetonitrile containing 5 mM QT, 0.1 M TEAP and 2 % weight S-PHE (MR = 1) at room temperature. Polymerization at 1.25 A/m² for 4.5 hours led to a 100 μm thick film. The polymers were then peeled off the electrode material and their passive as well as active mechanical properties studied. The active mechanical properties are presented in Section 4.3.

Figure 7 shows the mechanical response of a poly(QT)/S-PHE sample as a function of applied stress. Note that the mechanical passive response varies depending on the sample environment (dry, in 0.05 M TEAP in distilled water, in 0.1 M TEAP in acetonitrile). The tensile strength of dry poly(QT)/S-PHE composites peaks at 19.6 MPa, while it decreased to 11 MPa when the samples were placed in 0.05 M TEAP in water and further decreased to only 1.32 MPa when placed in 0.1 M TEAP in acetonitrile. Note on the other-hand that the tensile strength of the S-PHE alone is 0.22 MPa and it is very elastic (elongation to break ~ 215 %). It is speculated that the poor mechanical properties of poly(QT)/S-PHE composites are due in part to the re-dissolution of the elastomeric S-PHE once placed back into acetonitrile.

The passive mechanical properties of poly(QT)/S-PHE range from tensile strength between 19.6 and 1.32 MPa with elastic moduli between 0.7 and 0.48 GPa depending on the environment, which corresponds to strong mechanical properties for a conducting polymer. Such properties are useful for building actuators.

4.3 Bilayer beam bending testing

Following the method of Pei et al.²⁶, initial electromechanical testing was conducted using the bilayer beam-bending method. The displacement of a 80 μm thick poly(QT)/S-PHE bilayer was observed under a Zeiss Stemi SV-8 binocular microscope^l and recorded using a DFW-S300 digital Sony video camera^m under IEEE 1394 transfer protocol. Inspection of the video micrographs reveals that the part of the bilayer that bends has a length of $l_o = 0.15$ mm (total length of the bilayer is 2.25 mm). The bilayer bending angle θ is related to strain ($\Delta l/l_o$) via,

$$\frac{\Delta l}{l_o} = \frac{d}{2l_o} \cdot \theta, \quad (2)$$

where d is the thickness of the bilayer²⁷. Potentials of $\pm 5V$ vs. Fc/Fc^+ were applied manually to the polymer bilayer for less than 4 seconds in an electrochemical cell containing 0.1M TEAP in acetonitrile and a stainless steel counter electrode and the bilayer angle recorded via video microscopy. Figure 8 shows the calculated active strain performed by the poly(QT)/S-PHE bilayer. Notice that the poly(QT)/S-PHE samples used for this study were from the same batch as the ones characterized for passive mechanical properties (Section 4.2). Total strains as high as 21.4 % strains were recorded during these experiments and the best result is presented in Figure 8. Recoverable strain was 17.7 % and maximum strain rate 15.4 %/s.

Note, however, that while 94.1 % of the high strain exhibited by the poly(QT)/S-PHE system is recoverable and repeatable for several samples, we were not able to observe such high strains for more than one cycle. It is speculated that the high potentials applied to the system caused electrochemical destruction of the polymer. Notice also these high strains are observed close to the charge injection point into the bilayer, bending the polymer at a small bending radius. We believe that low film conductivity prohibits contractions far away for the point of electrical contact.

^l www.zeiss.com

^m www.sony.com

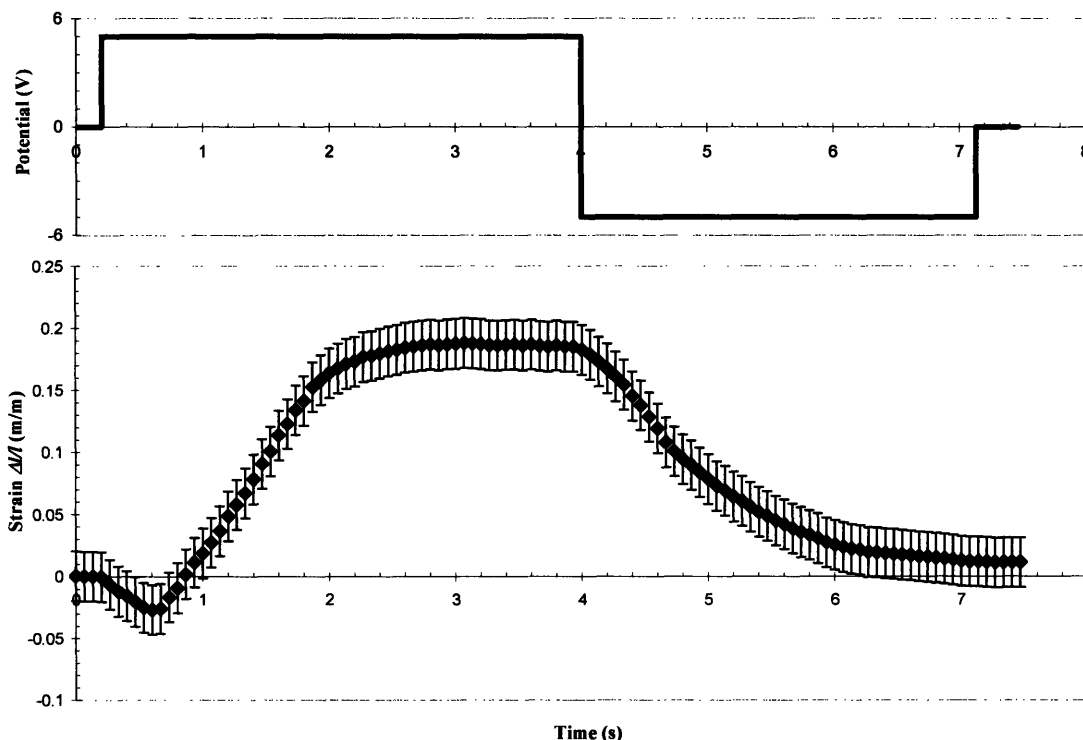


Figure 8: Active strain generated by the poly(QT)/S-PHE system in the bilayer beam-bending configuration

While this result does not describe the ability of the system to perform work it serves the purpose of demonstrating that poly(QT)/S-PHE can be successfully electro-chemo-mechanically activated. In the next Section we will describe isometric experiments showing that the system can produce a force against a load.

4.4 Low frequency isometric actuator testing

To demonstrate that poly(QT)/S-PHE can produce a force against a load, isometric (constant length) electroactive mechanical testing at low frequencies was conducted using a custom built isometric electromechanical testing apparatus. Notice that no commercial tensile testing device exists that adequately combines mechanical testing with electrochemical excitation and monitoring.

In this apparatus²⁸ a sample is held at constant length by a copper alligator clip clamped at each end of the polymer film and immersed horizontally into a 138 mm, 56 mm and 30 mm deep Nylon 6 / 6 bath filled with an electrochemical solution. These copper clips also serve as electrical contacts/charge injection points to the polymer. Note that while these clips are inserted into the electrochemical solution, their outside is electrically insulated by a Mylar tape. An aluminum rod connects the sample clamp to a linear translation stage powered by a stepper motor (Parker Automation CompuMotorⁿ). In series with the clamp is a load cell (Entran ELFS-T3E-10N load cell^o, with Vishay 2311 Signal Conditioning Amplifier^p), allowing one to record the applied force. The whole testing setup is under computer control via a PCI data acquisition board (Allios 16-bit A/D, D/A, 50 kHz sampling^q). A graphical user interface designed in

ⁿ www.compumotor.com

^o www.entran.com

^p www.vishay.com

^q bioinstrumentation.mit.edu

Microsoft Visual Basic 6.0^f allows the application of a certain displacement to the polymer sample, while acquiring passive and active stress generated by the material as well as electrochemical activity.

A sample of poly(QT)/S-PHE (length = 12 mm, width = 3.5 mm, thickness = 100 μm) was attached between the two copper alligator clips and held at constant length under a 1 MPa initial load. The electrochemical solution for this study was a 0.05 M TBAP in distilled water. The electrochemical cell circuit was composed of the polymer sample and a stainless steel counter electrode. Potentials of the cell were controlled by an Amel potentiostat via a Calomel reference electrode (sec. 3.2). In order to assure rapid double-layer charging at the polymer working electrode while not reaching overoxidation a shaped potential following the methods of Madden et al. was programmed in the testing algorithm²⁸. Starting with a polymer equilibrium voltage of -0.5 V vs. Calomel, the samples were cycled at 0.27 mHz (1 hour period) during 8 hours between -1.5 V and $+0.5$ V vs. Calomel with allowable potential peaks of ± 1 V vs. polymer equilibrium potential for the fast double-layer charging.

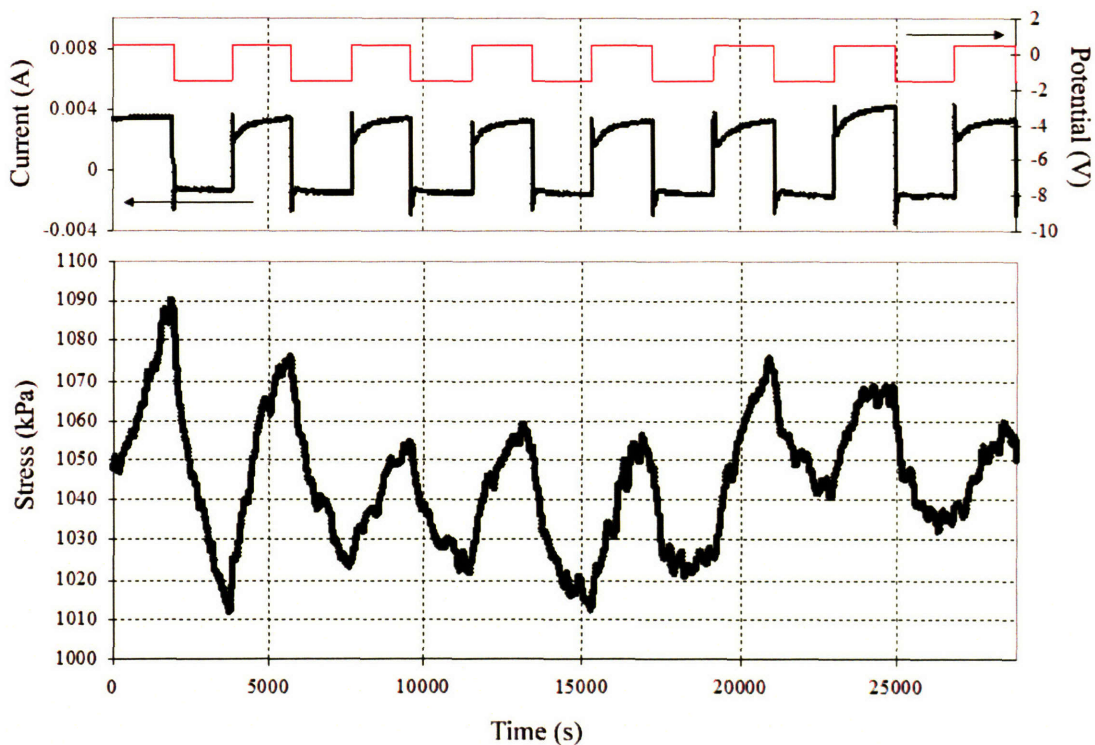


Figure 9: Isometric active mechanical testing of poly(QT)/S-PHE composites

Figure 9 shows a characteristic run under the conditions described above. Notice that peak stress generated attained 80 kPa and went as low as 35 kPa, showing that poly(QT)/S-PHE composites can produce a force against a load. It is speculated that low film conductivity prohibits stress generation far away from the points of electrical contact, thus only contracting the material close to its clamping edges. Further active mechanical characterization will involve isotonic (constant force) testing.

^f www.microsoft.com

4.6 Summary of key relevant properties and discussion

Electrical, electrochemical and mechanical (passive and active) characterizations were performed on the novel poly(QT)/S-PHE electroactive polymer. Table 1 below summarizes the properties of the poly(QT)/S-PHE actuator and compares it with mammalian skeletal muscle. While initial studies based on the beam-bending method showed strain in levels of 20%, these active material properties need to be measured in a linear configuration. To this effect a custom-made Electrochemical Dynamic Mechanical Analyzer (E-DMA) has been built in our laboratory that allows testing of samples under isotonic conditions²⁹. Key parameters to be measured as a function of applied load with this instrument include maximum active strain, power to mass, stored energy density, efficiency and cycle life. In addition methods typically used in muscle physiology such as the work-loop method or force velocity curves can also be employed to allow comparison of our artificial actuator technology with nature's muscle under common conditions³⁰.

Property	Mammalian Skeletal Muscle ⁶	Achieved in Poly(quarterthiophene)
Displacement (Strain)	20 %	21.4 % max. (bilayer) 17.7 % recoverable (bilayer)
Active Stress (Load)	350 kPa	80 kPa @ 1 MPa (isometric)
Velocity (Strain Rate)	100 %/s	15.4 %/s (bilayer)
Power to mass	50-100 W/kg	-
Efficiency	30 - 35 %	-
Stiffness (wet)	0.3 to 80 MPa (contracted)	0.48 GPa
Tensile Strength (wet)	0.3 MPa	1.4 to 11 MPa
Conductivity	-	0.16 S/m

Table 1: Comparison of poly(QT)/S-PHE actuator with mammalian skeletal muscle

5. CONCLUSION

We presented herein novel materials designed with a molecular mechanistic approach. Incorporation of an elastomeric sulfated polyanion leads to the creation of mechanically strong films of poly(QT)/S-PHE films. Initial activation studies of poly(QT)/S-PHE composites using the beam-bending method showed strain at levels of 20% while isometric testing demonstrated that these novel materials are able to produce a significant force against a load. However both active and passive mechanical properties need optimization before these new materials can be incorporated into products. The optimization process requires innovations in molecular architectures as well as nanoscopic organizations. Our goal is to find a single optimized material that compares with or exceeds mammalian skeletal muscle properties in more than one characteristic figure of merit.

6. ACKNOWLEDGEMENTS

This work was supported in part by the Office of Naval Research under grant N00014-99-1-1022.

We are grateful to Gordon Wallace and Jie Ding (University of Wollongong, Australia) for generous supply of some of the polyanions used in this work (S-PHE with MR = 0.33 and 0.5).

7. REFERENCES

1. Lu W., Fadeev A.G., Qi B., Smela E., Mattes B.R., Ding J., Spinks G.M., Mazurkiewicz J., Zhou D., Wallace G.G., MacFarlane D.R., Forsyth S.A. and Forsyth M., "Use of Ionic Liquids for pi-Conjugated Polymer Electrochemical Devices", *Science*, Vol. 297, pp. 983-987, (2002).
2. Ding J., Price W.E., Ralph S.F. and Wallace G.G., "Synthesis and properties of a mechanically strong poly(bithiophene) composite polymer containing a polyelectrolyte dopant", *Synthetic Metals*, Vol. 110, pp. 123-132, (2000).
3. Spinks G.M., Liu L., Wallace G.G. and Zhou D., "Strain Response from Polypyrrole Actuators under Load", *Advanced Functional Materials*, Vol. 12, (6+7): pp. 437-440, (2002).

4. Madden J.D., Madden P.G. and Hunter I.W., "Conducting Polymer Actuators As Engineering Materials", *Smart Structures and Materials 2002: Electroactive Polymers Actuators and Devices*, Yoseph Bar-Cohen, Editor, *Proceedings of the SPIE*, Vol. 4695, pp. 176-190, (2002).
5. Madden J.D., Madden P.G. and Hunter I.W., "Polypyrrole Actuators: Modeling and Performance", *Electroactive Polymer Actuator and Devices Conference, SPIE 8th Annual International Symposium on Smart Structures and Materials*, Newport Beach, CA, (2001).
6. Hunter I.W. and Lafontaine S., "A Comparison of Muscle with Artificial Actuators", *Technical Digest IEEE Solid State Sensors and Actuators Workshop*, pp. 178-185, (1992).
7. Baughman R.H., Shacklette S.W., Plichta E.J. and Becht C., "Electromechanical Actuators Based on Conducting Polymers", *Molecular Electronics*, pp. 267-289, (1991).
8. Baughman R. H. "Conducting Polymer Artificial Muscles", *Synthetic Metals*, Vol. 78, pp. 339-353, (1996).
9. Marsella M.J. and Reid R.J., "Toward Molecular Muscles: Design and Synthesis of an Electrically Conducting Poly[cyclooctatetrathiophene]", *Macromolecules*, Vol. 32, pp. 5982-5984, (1999).
10. Kingsborough R.P. and Swager T.M., "Polythiophene Hybrids of Transition-Metal Bis(salicylideneimine): Correlation between Structure and Electronic Properties", *Journal of the American Chemical Society*, Vol. 121, (38): pp. 8825-8834, (1999).
11. Graf D.D., Campbell J.P., Miller L.L. and Mann K.R., "Single-Crystal X-ray Structure of the Cation Radical of 3',4'-Dibutyl-2,5"-diphenyl-2,2'-terthiophene: Definitive Evidence for π -Stacked Oxidized Oligothiophenes", *Journal of the American Chemical Society*, Vol. 118, pp. 5480-5481, (1996).
12. Azumi R., Goetz G. and Baeuerle P., "Self-Assembly of Alkylsubstituted Oligothiophenes", *Synthetic Metals*, Vol. 101, pp. 569-572, (1999).
13. Sirringhaus H., Brown P.J., Friend R.H., Nielsen M.M., Bechgaard K., Langeveld-Voss B.M.W., Spierling A.J.H., Janssen R.A.J., Meijer E.W., Herwing P. and de Leeuw D.M., "Two-Dimensional Charge Transport in Self-Organized, High-Mobility Conjugated Polymers", *Nature*, Vol. 401, pp. 685-689, (1999).
14. Brocks G., " π -dimers of oligothiophene cations", *Journal of Chemical Physics*, Vol. 112, (12): pp. 5353-5363, (2000).
15. Brocks G., "Charged Oligothiophene Dimers and π -stacks: the Bipolaron Revisited", *Synthetic Metals*, Vol. 119, pp. 253-254, (2001).
16. Yamamoto T., Kamarudin D., Arai M., Lee B.-L., Suganuma H., Asakawa N., Inoue Y., Kubota K., Sasaki S., Fukuda T. and Matsuda H., "Extensive Studies of π Stacking of Poly(3-alkylthiophene-2,5-diyl)s and Poly(4-alkylthiazole-2,5-diyl)s by Optical Spectroscopy, NMR Analysis, Light Scattering Analysis, and X-ray Crystallography", *Journal of the American Chemical Society*, Vol. 120, pp. 2047-2058, (1998).
17. Israelachvili J. *Intermolecular and surface forces*. 2nd ed, p. 88 ed. London, San Diego: Academic Press; 1991. xxi, 450 p.
18. Anquetil P.A., Yu H.-h., Madden J.D., Madden P.G., Swager T.M. and Hunter I.W., "Thiophene-Based Conducting Polymer Molecular Actuators", *Smart Structures and Materials 2002: Electroactive Polymers Actuators and Devices*, Yoseph Bar-Cohen, Editor, *Proceedings of the SPIE*, Vol. 4695, pp. 424-434, (2002).
19. Yu H.-h., Pullen A.E. and Swager T.M., "Toward New Actuating Devices: Synthesis and Electrochemical Studies of Poly(11,23-bis[2,2'-bithiophene]-5-yl)-26,28-dimethoxycalix[4]arene-25,27-diol)", *Polymer Science Material Engineering*, Vol. 83, (523): (2000).
20. Yu H.-h., Xu B. and Swager T., "A Proton-Doped Calix[4]arene-Based Conducting Polymer", *Journal of American Chemical Society*, Vol. 125, pp. 1142-1143, (2002).
21. Wernet W. and Stoffer J., *US Patent 5,061,401*, (1991).
22. Kittelsen G.P., White H.S. and Wrighton M.S., "Chemical Derivation of Microelectrode Arrays by Oxidation of Pyrrole and N-Methylpyrrole - Fabrication of Molecule-Based Electronic Devices", *Journal of the American Chemical Society*, Vol. 106, (24): pp. 7389-7396, (1984).
23. Ding J., Price W.E., Ralph S.F. and Wallace G.G., "Electrochemical Behavior of polypyrrole/sulfated poly(β -hydroxyether) composites", *Synthetic Metals*, Vol. 129, (67-71): (2002).
24. Roncali J., "Synthetic Principles for Bandgap Control in π -Conjugated Systems", *Chemical Reviews*, Vol. 97, (1): (1997).
25. Roth S., "One-Dimensional Metals: Physics and Material Science", *VCH, Weinheim; New York; Basel; Cambridge; Tokyo*, pp. 111-148, (1995).
26. Pei Q. and Inganas O., "Electrochemical Application of the Bending Beam Method. 1. Mass Transport and Volume Changes in Polypyrrole during Redox", *The Journal of Physical Chemistry*, Vol. 96, (25): pp. 10507-10514, (1992).
27. Takashina W., Kaneko M., Kaneto K. and MacDiarmid A.G., "The Electrochemical Actuator Using Electrochemically-Deposited Poly-aniline", *Synthetic Metals*, Vol. 71, pp. 2265-2266, (1995).
28. Madden J.D., Cush R.A., Kanigan T.S. and Hunter I.W., "Fast Contracting Polypyrrole Actuators". *Synthetic Metals*, Vol. 113, pp. 185-192, (2000).
29. Anquetil P., Yu H.-h., Madden J.D., Madden P.G., Rinderknecht D., Swager T. and Hunter I., "Characterization of Novel Thiophene-Based Molecular Actuators", *Proceedings of the first biomimetics world congress*; Dec. 9-11, 2002, Albuquerque, NM, USA; in press.
30. Full R.J. and Meijer K., "Metrics of Natural Muscle Function", *Electroactive Polymers [EAP] Actuators as Artificial Muscles - Reality, Potential, and Challenges*, Bar Cohen Y. Editor, *SPIE Press*, pp. 67-83, (2001).

Chapter 9

Novel Polymer Actuator Systems Based on Molecular Actuating Building Blocks

In this Chapter, initial work towards creating novel polymers based on molecules capable of changing their conformational state is presented. The monomers are designed to provide large volume changes and forces via molecular conformational changes. While Chapter 8 focused on molecules that undergo volume changes due to stacking of redox units, this Chapter discusses molecules that distort from bent to planar structures upon electrochemical cycling. Efforts were directed towards the development of supramolecular organized structures to produce optimal forces and volume changes

9.1 poly(thianthrene *bis*-bithiophene)

Unlike the calix[4]arene scaffold, the thianthrene scaffold exhibits an active hinge-like reversible molecular expansion. Upon oxidation, the thianthrene unit actively transforms from a bent structure with a dihedral angle of 120° to a planar structure (180° dihedral angle) (Figure 9.1). Coupling of the thianthrene scaffold to stiff bithiophene arms amplifies the achievable strain. The thianthrene unit is expected to produce a 7 % strain along the backbone, according to initial AM1 quantum mechanical modeling. While the strain is less

than the desired 20 %, the molecular backbone is extremely stiff, allowing very large loads to be sustained during actuation. Notice that increasing the number of thiophene links increases the strain amplification, and will likely reduce material stiffness. Actuator material properties are thus tuned by molecular design.

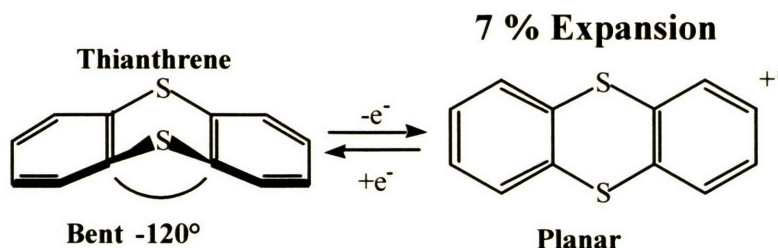


Figure 9.1: Conformational change of the thianthrene element upon oxidation.

Two configurations of a thianthrene-based polymer were studied. In the first configuration, bithiophene rods are attached on the 1,9 positions of the thianthrene, poly(thianthrene 1,9-*bis*-bithiophene), (Figure 9.2A) , while in the second one they are connected on the 2,3 positions, poly(thianthrene 2,3-*bis*-bithiophene), (Figure 9.2B). Polymerization of the thianthrene monomer leads to a polymer with an extremely stiff backbone which is expected to self-assemble into crystalline domains.

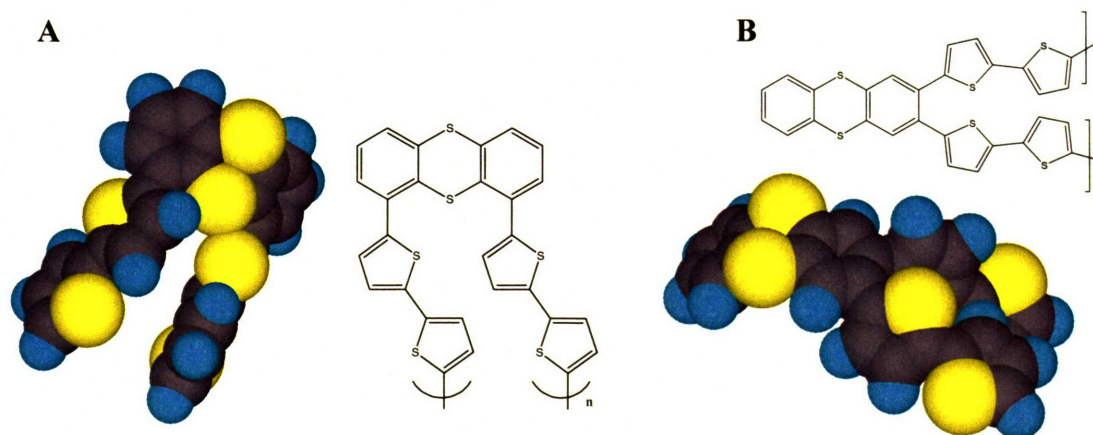


Figure 9.2: The thianthrene building block decorated with bithiophene rods at the 1,9 positions (A) and the 2,3 positions (B).

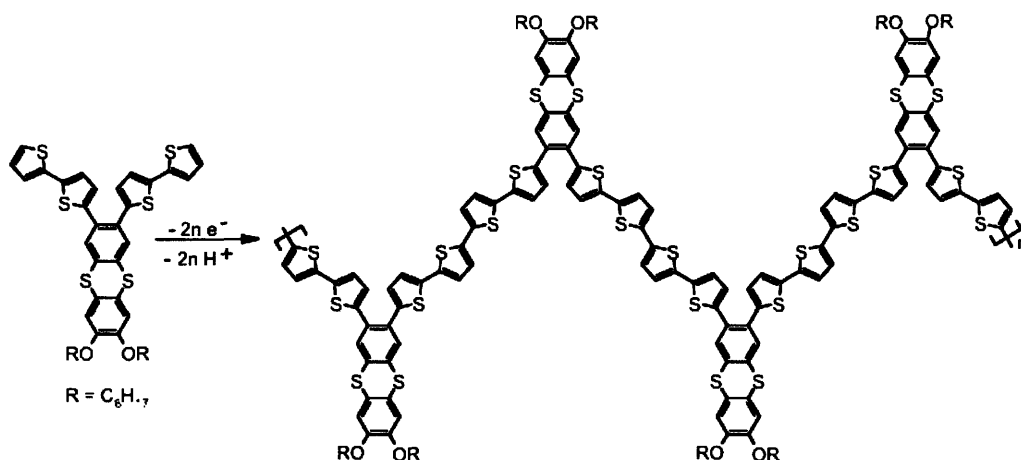


Figure 9.3: Polymerization of poly(thianthrene 2,3-*bis*-bithiophene) with thiophene units attached to the 2,3 positions.

While studies carried at a small scale (2 mm diameter button platinum electrode) show good electrochemical response, all attempts to polymerize poly(thianthrene *bis*-bithiophene) into a thin polymer film failed to produce a material stable enough to pursue mechanical characterization. Electrochemical polymerization led to brittle, powder-like materials. Alternative polymerization processes need to be developed to further study this molecule.

Other unsuccessful attempts include the synthesis of composites of poly(thianthrene *bis*-bithiophene) with an S-PHE matrix polymer (Chapter 8) and the synthesis of ten alternating layers of poly(thianthrene *bis*-bithiophene) with polypyrrole. The later experiments led to films only containing 5 % of poly(thianthrene *bis*-bithiophene) (as described by elemental analysis).

9.2 poly(phenylene-EDOT)

The mechanism of contraction of poly(phenylene-EDOT) is also based on the unfolding of the polymer backbone from a twisted to a planar structure upon oxidation. Such active backbone molecular transitions would potentially lead to a highly anisotropic contractile polymer material. This polymer is formed by a combination of phenylene and ethylene-dioxy-thiophene (EDOT) units. What makes this polymer an unusual candidate is how material properties can be changed and optimized for actuation by changing the monomer side chains (R-groups in Figure 9.4). The interaction between the sulfur and the nearby oxygen atoms is responsible for the molecular actuation driving force. In the neutral form, electrostatic interactions between these 2 groups of atoms lead to steric interactions, creating a twisted molecular backbone. Upon oxidation these groups have fewer electrons to share, leading to a molecular reorganization that translates into a flat structure.

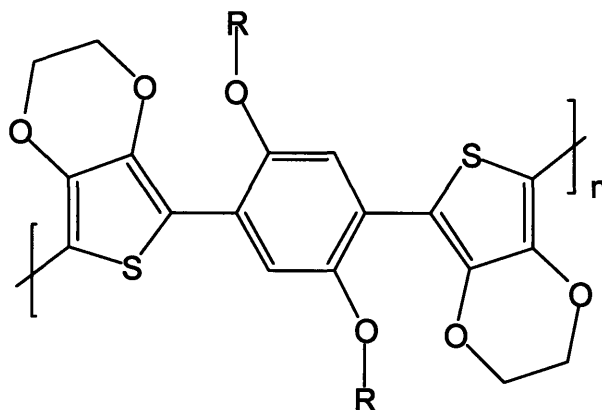


Figure 9.4: Structure of poly(phenylene-EDOT). The R-group was chosen to be $C_{16}H_{33}$.

Figure 9.5 shows initial AM1 simulations of a quatramer of phenylene-EDOT monomer subjected to charge removal (oxidation) and charge injection (reduction). The polymer is calculated to have a non-planar conformation in its neutral state and a twisted structure in its oxidized form, exhibiting 2.1 % strain along its backbone, but more than 85% change in its cross-sectional area

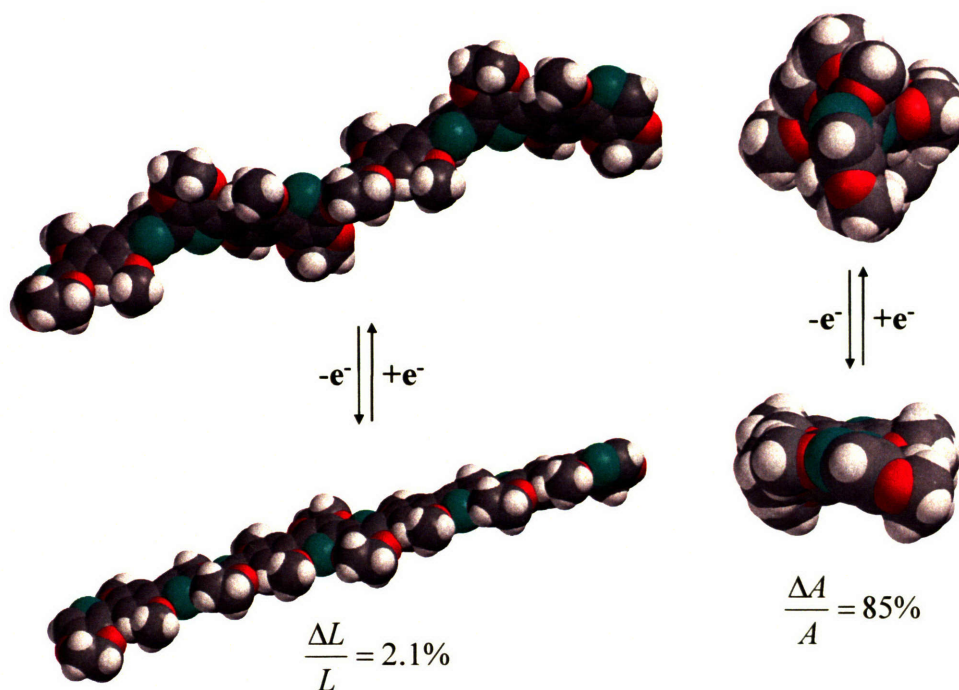


Figure 9.5; Actuation mechanism of poly(phenylene-EDOT).

While studies carried at a small scale (2 mm diameter button platinum electrode) show good electrochemical response, all attempts to polymerize poly(thianthrene *bis*-bithiophene) into a thin polymer film failed to produce a material stable enough to pursue mechanical characterization. Electrochemical polymerization led to brittle, powder-like materials. Alternative polymerization processes need to be developed to further study this molecule.

9.3 poly(vanadyl-EDOT)

The conducting polymer actuator materials based on molecular actuating elements presented above only contain organic molecules. Adding a metal transition complex such as vanadyl to the conducting polymer backbone can lead to surprising properties. The vanadyl-EDOT monomer for example incorporates a vanadyl transition metal compound with the well studied poly(EDOT) polymerizable group. The vanadyl moiety of this molecule is responsible for creating supramolecular ordering of the molecule into stacks (Figure 9.6). In addition it is designed to undergo a conformational change based on its redox switchable state. While the poly(EDOT) moiety assures good conductivity throughout the molecule, the vanadyl part assures the robustness and supramolecular conformation of the molecule.

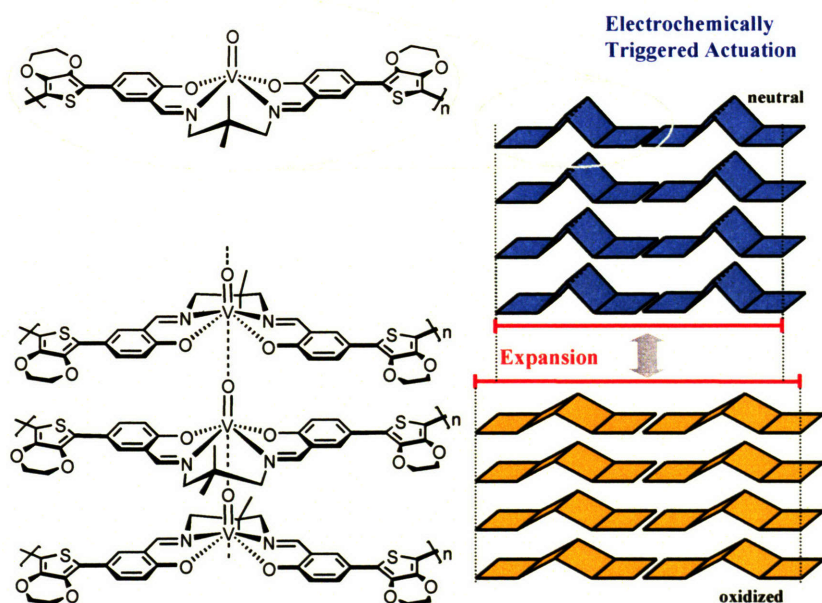


Figure 9.6: The metallo-organic hybrid conducting polymer poly(vanadylEDOT). The right hand side of the figure schematically describes the stacking capability of the Vanadyl units, leading to a nanostructured material. Diagram courtesy of Professor Swager.

The vanadyl-EDOT monomer has been investigated under standard in situ electrochemical conditions. This molecule has shown clean electrochemistry and upon oxidation electropolymerizes to give a poly(EDOT) backbone with vanadyl units

incorporated at distinct repeat units. The electrochemical characterization of this monomer is shown in Figure 9.7.

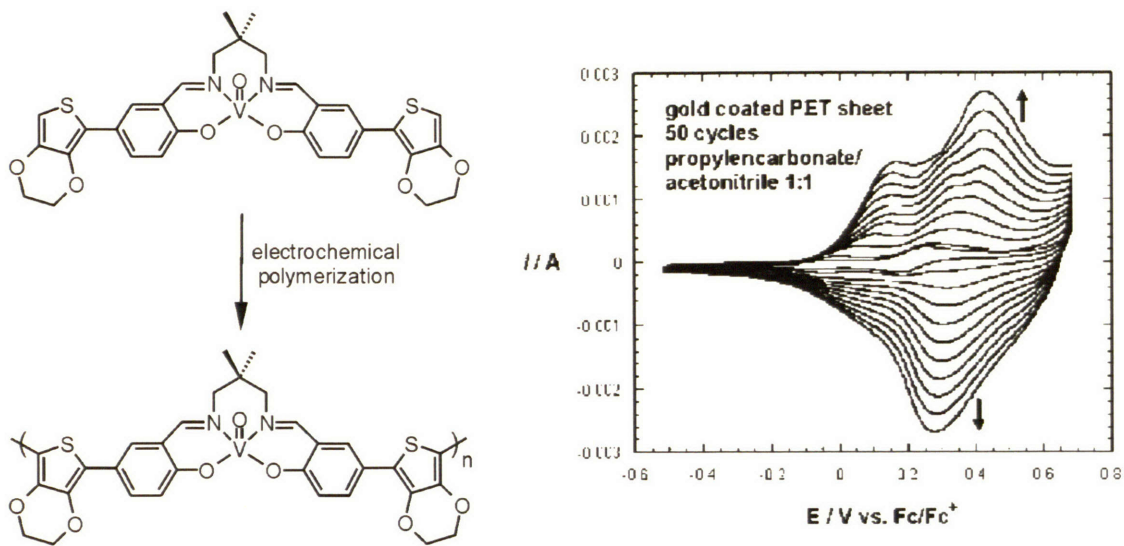


Figure 9.7: Electrochemical characterization of the poly(vanadyLEDOT) polymer.

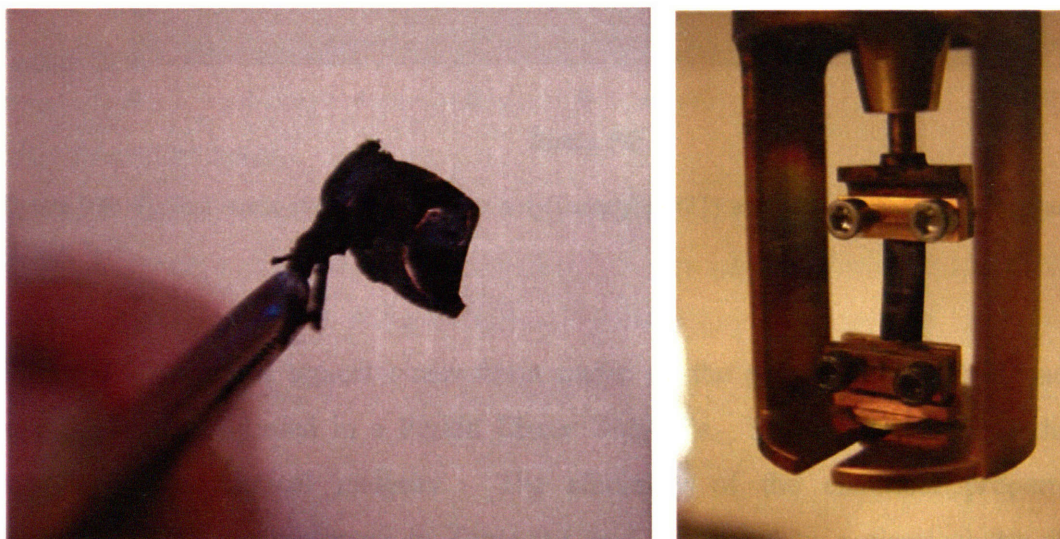


Figure 9.8: Free standing film of poly(vanadyLEDOT) held in tweezers (left). A sample of poly(VanadyLEDOT) clamped into the Perkin Elmer DMA 7e for measurement of its mechanical properties (right).

Poly(vanadyl-EDOT) was successfully synthesized into free standing polymer films via electrochemical deposition as shown in Figure 9.8. This is an important achievement in the search for novel contractile materials. Once a monomer can be polymerized into a free-standing polymer film, the thorough actuator characterization process can begin. This typically begins with the testing of conductivity and passive mechanical properties, followed by active mechanical testing, once the stability of the material is confirmed.

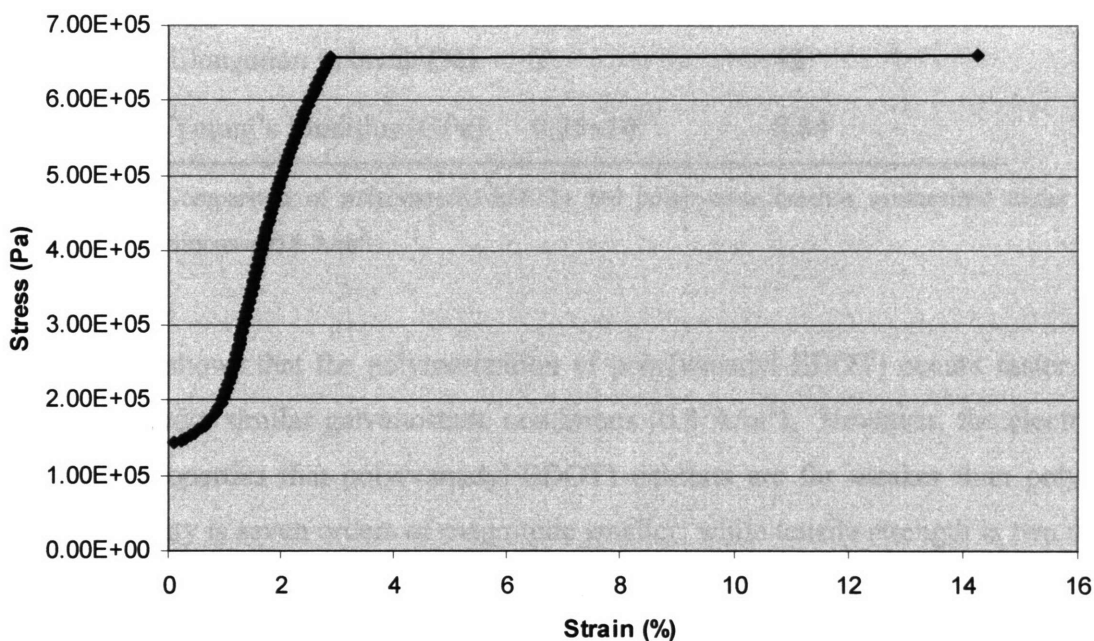


Figure 9.9: Typical stress-strain curve of the poly(vanadyl-EDOT) actuator polymer tested in the Perkin Elmer DMA 7e.

Figure 9.9 depicts a typical stress-strain curve of the poly(Vanadyl-EDOT) actuator polymer mechanically tested in a Perkin Elmer DMA 7e. This curve confirms that this polymer has a mechanical integrity. The summary of the electrical properties of poly(vanadyl-EDOT) are presented in Table 9.1 and compared to a classical dry film of polypyrrole as studied in Chapter 6.

	Poly(vanadyl-EDOT)	Dried PPy film for comparison (cf. Ch. 6)
Thickness (μm)	61	25
Deposition time (hrs)	12	16.55
Conductivity (S/m)	4.75×10^{-3}	3.81×10^4
Tensile Strength (MPa)	0.68	53.6
Elongation to break (%)	3	42
Young's Modulus (GPa)	0.25×10^{-3}	0.84

Table 9.1: Comparison of poly(vanadyl-EDOT) and polypyrrole batches synthesized under the same galvanostatic conditions at 0.8 A/m^2 .

Table 9.1 shows that the polymerization of poly(vanadyl-EDOT) occurs faster than for polypyrrole under similar galvanostatic conditions (0.8 A/m^2). However, the electrical and mechanical properties that poly(vanadyl-EDOT) exhibits are far weaker than polypyrrole. The conductivity is seven orders of magnitude smaller, while tensile strength is two orders of magnitude smaller than polypyrrole. Furthermore activation of poly(vanadyl-EDOT) led to no noticeable active strain.

Although the poly(vanadyl-EDOT) has weak electrical, mechanical and active properties, it is a promising material as it can be synthesized into free standing films without addition of supporting ionic polymer such as the S-PHE used for creating poly(quarterthiophene)/S-PHE composites described in Chapter 8. This characteristic should allow further investigations of this material to take place.

9.4 Conclusion

The difficulty to synthesize polymers based on molecular designs and strategies for higher performance contractile films outlined in this Chapter show the infancy of the field of synthetic molecular actuators. Novel artificial muscle materials are created via custom-

designed, electronically conductive polymers, whose molecular structure is optimized for electrical to mechanical energy conversion. The combination of sophisticated molecular design, mechanical testing, and materials systems integration for the optimization of actuating materials is absolutely unique. Although this approach has not lead yet to materials with higher active mechanical properties, it is our strong belief that this radical approach will be far superior in the long run, compared to classical materials surveys undertaken by other groups around the world.

Chapter 10

Conclusions and Outlook

10.1 Thesis Conclusions

The design and synthesis of novel functional materials is a major goal in both academic and industrial research programs around the world today. One of the goals this thesis addresses has been to develop materials that can efficiently convert an applied external stimulus such as electrical current, light, or heat into mechanical motion. The creation of lightweight, powerful and efficient actuators will impact fields such as biomechanical engineering, autonomous and life-like robotics, artificial organ and prosthesis design as well as micro/nanosystems fabrication, where a high power to mass muscle-like actuator is desirable. In such devices the physiological role our muscles play is mimicked in a purely synthetic and mechanical manner.

Conducting polymers were chosen for research as actuators based on a review of the relevant properties of all known actuators and active materials [Hunter I.W. and Lafontaine S. 1992], [Madden J.D. et al. 2004]. Key features of conducting polymer actuators include low drive voltages and high strength. They undergo moderate dimensional changes and have high energy storage capacity. In addition to actuators, electronic components (transistors, capacitors, diodes, etc.) and sensors (force, displacement, chemical, optical) can also be made

from conducting polymer materials, thus offering for the first time the possibility to construct systems from the same material via a co-fabrication process.

This thesis features the synthesis and characterization of novel conducting polymer muscle-like actuators. These actuators aim to match or exceed the properties of human skeletal muscle in key figures of merit including active strain, active stress, active strain rate, power to mass and efficiency. One strategy employed herein was to synthesize novel materials designed at the molecular level, utilizing effects such as π - π stacking or “backbone twisting” as a driving force for actuation. A framework for conducting polymer molecular actuator discovery was developed in which high-throughput synthesis and mechanical characterization techniques, in combination with modeling and molecular design, are being used to advance the field of synthetic contractile materials.

Nature being our source of inspiration, various naturally occurring molecular actuators were first presented and compared to man-made synthetic systems. These molecular motors exhibit complex mechanisms for converting chemical or electrical energy into mechanical work. The five synthetic contractile polymers proposed are: poly(quarterthiophene) - (poly(QT)), poly(calix[4]arene *bis*-bithiophene) – poly(calixBBT), poly(thianthrene *bis*-bithiophene) – poly(TBB), poly(VanadylEDOT) and poly(phenyleneEDOT). Note, however, that the retention of the molecular properties when the molecular motors are incorporated into a supramolecular or macroscopic assembly remains a challenge to be overcome (Chapter 2).

The theoretical limitations of polypyrrole as an actuator were presented. Metrics for evaluation included strain rate, maximal strain, stress and efficiency. These values were compared to theoretical estimates of rationally designed molecules such as the poly(calixBBT). This molecule can be tailored at the molecular level and theoretically leads to superior material performances. Upper theoretical bounds of the average performance properties of poly(calixBBT) were discussed and the theoretical limitations of classical conducting polymers such as polypyrrole presented (Chapter 3).

The study of conducting polymer actuators requires extensive knowledge of instrumentation and of experimental methods for materials characterization. First, the synthesis (polymerization) of these novel materials needs to be precisely controlled and monitored, and the deposition parameters systematically varied. Then rigorous testing of the

final polymer materials takes place. This includes characterization of physical properties, passive and active mechanical properties. To this effect, the commercial and in-house designed scientific instruments were presented and their characteristics discussed (Chapter 4).

Polypyrrole (PPy) has limited active properties, but represents a successful conducting polymer material in terms of its chemical stability, mechanical robustness and conductivity. For the development of novel actuators it is important to understand what makes a good conducting polymer material. To this effect, polypyrrole was used as a model actuator material. In addition, an optimization of its active properties was presented (Chapter 7).

A synthesis method for the formation of high quality PPy polymer films was presented. The nucleation process of PPy was observed and the repeatability of the resulting films analyzed. Indications were found that the current density of the deposition may be largely influencing the deposition process. Two routes for industrial production of such high quality polymer films were pursued. While the synthesis of fibers proved impractical for large scale manufacturing, there is great potential in the rotating drum-electrode based approach (Chapter 5).

The properties of polypyrrole subjected to heat were also studied. It was found that an irreversible mechanical strain relaxation takes place when samples are subject to prolonged temperatures around 90 °C. It was determined that the mechanical properties of PPy films following the vacuum treatment are repeatable across batches, and stable across time. Typical vacuum-treated PPy films exhibit the following mechanical properties: 0.81 GPa stiffness, 54 MPa tensile strength, and 46.4 % elongation to break. The effect of the vacuum treatment on the mechanical properties is also conserved when the film is placed back in a electrolyte solution, further confirming the hypothesis that an irreversible material relaxation takes place when PPy is subject to a temperature of 90 °C. In addition, as PPy needs an electrolyte solution to be electroactivated, this result shows that post-processing is a viable method to influence actuator properties. Finally thermal properties of PPy such as the heat capacity (1.558 kJ/kg/K), the coefficient of thermal expansion (44×10^{-6} /K) and the maximal operating temperature (150 °C) were determined. These experiments further deepened our understanding of PPy as an engineering material, which is crucial for employing conducting polymer actuators in real applications (Chapter 6).

The electrochemical and mechanical (passive and active) characterizations performed on polypyrrole synthesized in 0.05 M TEAP in propylene carbonate and activated in BMIM-BF₄ ionic liquid were then presented. It was initially shown that the BMIM-BF₄ does not affect the passive mechanical properties of PPy. Activation of polypyrrole in ionic liquid resulted in unusual active behavior such as recoverable linear strains in excess of 16.3% against a load of 2.5 MPa at a speed of 0.36 %/s. However, these large strains are accompanied by large creep, resulting in an average unrecoverable extension of the film by 3 % per cycle. The active creep behavior of PPy in ionic liquids was identified as obeying first order dynamics. Further characterization and electrochemical modeling should lead to a better understanding of this system and the reasons for the observed active creep behavior. Finally the stability of conducting polymer systems when activated in ionic liquids is shown by cycling a PPy film at 3 Hz for a 100,000 cycles without observing any significant polymer damage (Chapter 7).

Synthesis of novel thiophene based conducting polymer molecular actuators was reported. These novel compounds are designed to utilize the effect of π - π stacking as a driving force for actuation. The hypothesis of active molecular conformational changes is supported by *in-situ* electrochemical data. Incorporation of an elastomeric sulfated polyanion leads to the creation of mechanically strong films of poly(QT)/S-PHE films. Initial activation studies of poly(QT)/S-PHE composites using the beam-bending method showed strain at levels of 20% while isometric testing demonstrated that these novel materials are able to produce a significant force against a load. However both active and passive mechanical properties need optimization before these new materials can be incorporated into products. The optimization process requires innovations in molecular architecture as well as nanoscopic organization. (Chapter 8).

A total of five novel macromolecular platforms for molecular actuation were synthesized and characterized. These are all unique macromolecular structures specifically designed for particular active or passive properties (load bearing, large strain, stability, etc.). The difficulty to obtain mechanically strong films from these novel molecules shows that the field of synthetic molecular actuators is still in its infancy. A remaining challenge is to find the optimal conditions such that these novel materials to be produced as free standing films.

There is currently no set recipe for making the best actuators. Lessons and principles are learned in each design cycle (Chapter 9).

The development of artificial muscle technology is progressing rapidly. Strain rates, peak tension, and % length change for our polymer muscles are now approaching or exceeding values for biological tissue. For example, over the past 5 years, the strain performance of our conducting polymer actuators has increased more than 20 times. Figure 10.1 depicts on a linear scale the exponential growth of the maximum strain achieved in PPy actuators since 1996, while Figure 10.2 presents the improvement of strain rate over the same time frame. Projected maximum strain performance for 2006 is 30 %, whereas the strain rate is predicted to improve to 40 %/s.

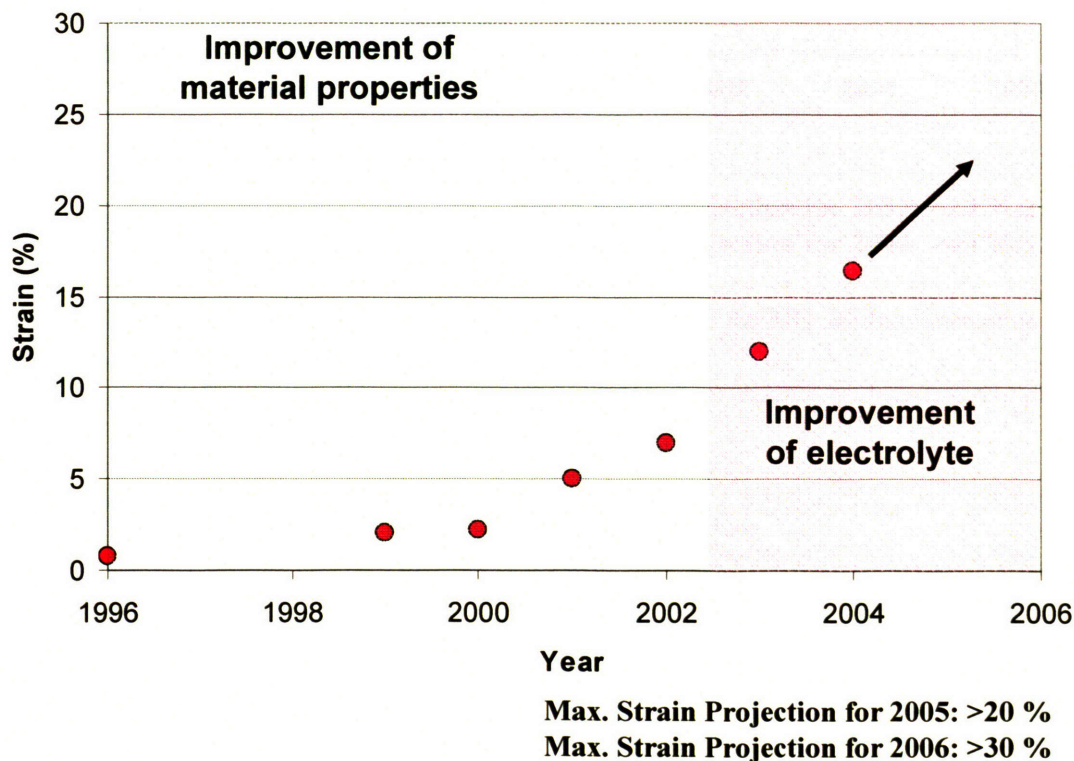
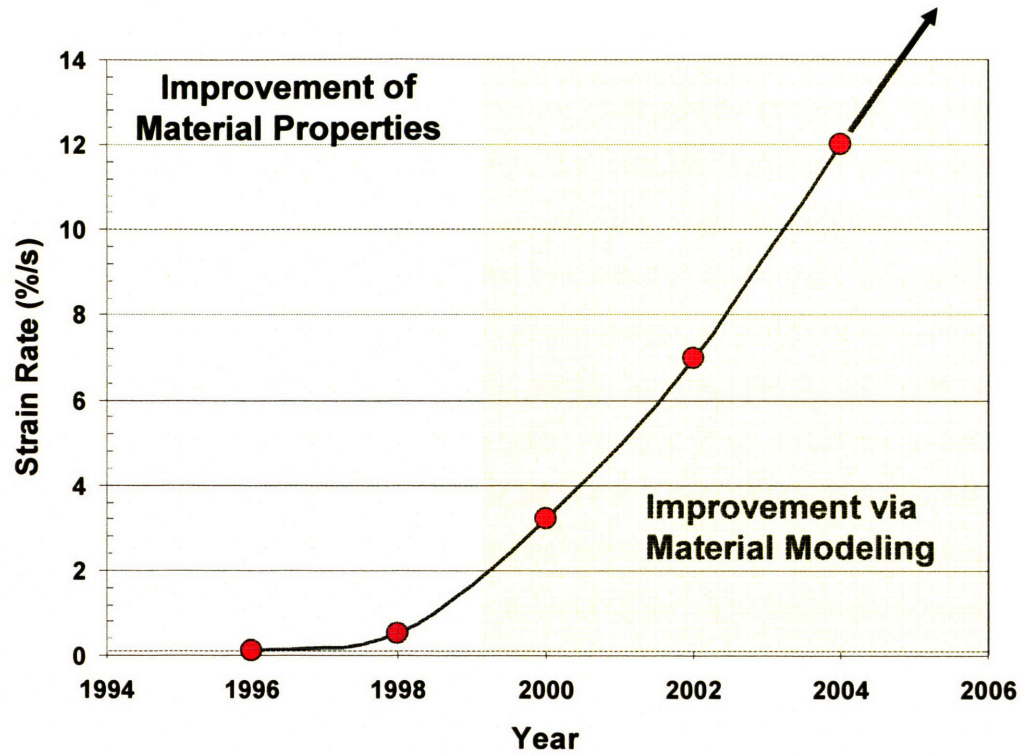


Figure 10.1: Progress of the maximum strain performance of the MIT BioInstrumentation Lab PPy conducting polymer actuator since 1996.



Strain Rate Projection for 2005: >20 %/s
Strain Rate Projection for 2006: >40 %/s

Figure 10.2: Progress of the maximum strain rate performance of the MIT BioInstrumentation Lab PPy conducting polymer actuator since 1996.

10.2 Challenges and Future work

As progress is made towards matching mammalian muscle properties we are faced by manufacturing challenges at three levels. First, the chemical synthesis of the new actuator molecules is often times difficult and time consuming. The development of streamlined synthesis techniques can only be accomplished by extensive knowledge of organic synthesis techniques and of the specific advantages and disadvantages of different synthesis pathways. Already, considerable improvements were made in the yields of new molecules. Computational simulation of the new molecular designs gives excellent insight into the mechanical behavior one might observe but as of yet, it is very difficult to properly simulate the behavior of the large numbers of molecules needed to make bulk actuators. As the available computational power grows, the usefulness of the simulations as a design tool will grow.

The second manufacturing challenge that we face is to take newly synthesized molecules and turn them into high quality polymer films. The new films must have both good electrical conductivity to ensure fast distribution of charge during oxidation and reduction and good mechanical properties to minimize creep and increase lifetime at high stresses. Monomers which include both electroactive elements and elastic elements have been synthesized to build materials that are both highly crosslinked for good mechanical properties and highly conducting.

Finally, the third manufacturing challenge that we face in the development of conducting polymer actuators is to create useable engineering devices from the technology. Conducting polymer actuators are unlike traditional actuators because they require immersion in an electrolyte solution or gel. The immersion makes the actuators similar to biological muscle, which is isolated from the body's internal environment by flexible cell walls and from the external environment by flexible skin. Flexible coatings are currently pursued as a means to encapsulate the polymer actuator.

Three fundamental directions may help in addressing these challenges. First, a good understanding of the chemistry involved helps to improve the polymer synthesis. Temperature, choice of electrolyte, chemical concentrations, and electrochemical potential or current density all affect the polymerization reaction by changing the likelihood of unwanted

side reactions that branch or terminate the growing polymer chain. Extensive experiments have been done already and are ongoing to optimize conditions for polymerization of new monomers. Third, development of electromechanically active block copolymers or self-assembly techniques could provide a route to ordered structures at the sub-micrometer level. Block copolymers via self-assembly offer a route to very anisotropic properties with expansion and contraction tailored to be in only one direction [Pytel R.Z. 2004].

Note that muscle amplifies movement by a clever hierarchical structure of the muscle cell, where material organization is achieved at different levels. In other words, muscle is not only nanostructured but it is also microstructured and macrostructured and each level of organization achieves a specific function. It is a complex and elegant mechanism that mankind has barely started to understand.

Finally, there are about 300 ionic liquids¹. Development of parallel characterization methods would enable to scan rapidly through existing ionic liquids and find the optimal ones for best contractile performance.

¹ http://www.ionicliquids-merck.de/servlet/PB/show/1368600/IL-Catalog_22.09.2004.pdf

10.3 Contributions to knowledge

- Goal of 20% actuation strain in conducting polymers reached for both PPy activated in ionic liquids as well as poly(QT) activated in 0.1 M TEAP in PC
- Complete characterization of PPy in Ionic Liquids.
- Characterized passive properties of PPy as a function of temperature.
- Discovered that the max range of operation for PPy is 150 °C.
- Developed robust synthesis process for PPy.
- Developed novel polymer mechanical enhancement processing technique based on heat and vacuum treatment.
- Synthesized and characterized the passive and active properties of five novel polymer based on molecular designs for the first time. These include poly(quarterthiophene), poly(calix[4]arene bis-bithiophene), poly(thianthrene), poly(vanadyl-EDOT), and poly(phenyleneEDOT).
- Developed synthesis protocol to produce thiophene-based novel conducting polymers.
- Developed a system to rapidly scan through synthesis parameters of novel conducting polymers, focused on conductivity and mechanical properties.
- Constructed novel instrumentation to electrochemically and mechanically characterize conducting polymer actuators.
- Developed an overall protocol to characterize polymer actuators.

This work has resulted in several publications, talks, and a patent:

10.3.1 Conference Proceedings

Anquetil Patrick A., Rinderknecht Derek, Vandesteeg Nathan A., Madden, John D., and Hunter Ian W.; “Large Strain Actuation in Polypyrrole Actuators”, *Proceedings of the SPIE 11th annual symposium on Electroactive Materials and Structures*, San Diego, CA, USA, **2004**.

Anquetil Patrick A., Yu Hsiao-hua, Madden, John D., Swager Timothy M. and Hunter Ian W.; “Recent Advances in Thiophene Based Molecular Actuators”; *Proceedings of the SPIE 10th annual symposium on Electroactive Materials and Structures*, San Diego, CA, USA, Vol. 5051, **2003**.

Anquetil Patrick A., Yu Hsiao-hua, Madden John D., Madden Peter G., Rinderknecht Derek, Swager Timothy M. and Hunter, Ian W., “Characterization of novel thiophene-based molecular actuators”, *First World Congress on Biomimetics and Artificial Muscles*, Albuquerque, NM, USA, Dec. 9-11, **2002**.

Anquetil Patrick A., Yu Hsiao-hua, Madden John D., Madden Peter G., Swager, Timothy M.; and Hunter, Ian W.; “Thiophene Based Molecular Actuators”, *Proceedings of the SPIE 10th annual symposium on Electroactive Materials and Structures*, San Diego, CA, USA, Vol. 4695, pp. 424-434, **2002**.

10.3.2 Talks

Anquetil Patrick, Madden John, Rinderknecht Derek, Vandesteeg Nate, Hunter Ian; “Large Strain Polypyrrole Actuators”; **MRS Fall Meeting**, Boston, MA, USA, December 1-5, **2003**.

Zimet Rachel, **Anquetil Patrick**, Yu Hsiao-hua, Swager Timothy, Hunter Ian; “Synthesis of Poly- β -hydroxyether Doped Polypyrrole Actuators”; Poster, **MRS Fall Meeting**, Boston, MA, USA, December 1-5, **2003**.

Anquetil Patrick A., Madden John D., Madden Peter G., Hunter Ian, “Conducting Polymer Molecular Muscles”, *New Data & Research In Applications For Nanotechnology and Nanomedicine*, **The Knowledge Foundation**, Royal Sonesta Hotel, Cambridge, MA, **2000**.

10.3.3 Patents

Anquetil Patrick A., Hunter Ian W., Madden John D., Madden Peter G., Pullen Anthony E, Swager Timothy M., Yu Hsiao-hua, Xu Bing, "Molecular Actuators", **U.S. Patent pending** (Application No. 10/392,354).



US 20040007695A1

(19) **United States**(12) **Patent Application Publication**
Anquetil et al.(10) **Pub. No.: US 2004/0007695 A1**(43) **Pub. Date: Jan. 15, 2004**(54) **MOLECULAR ACTUATORS, AND METHODS OF USE THEREOF****Related U.S. Application Data**

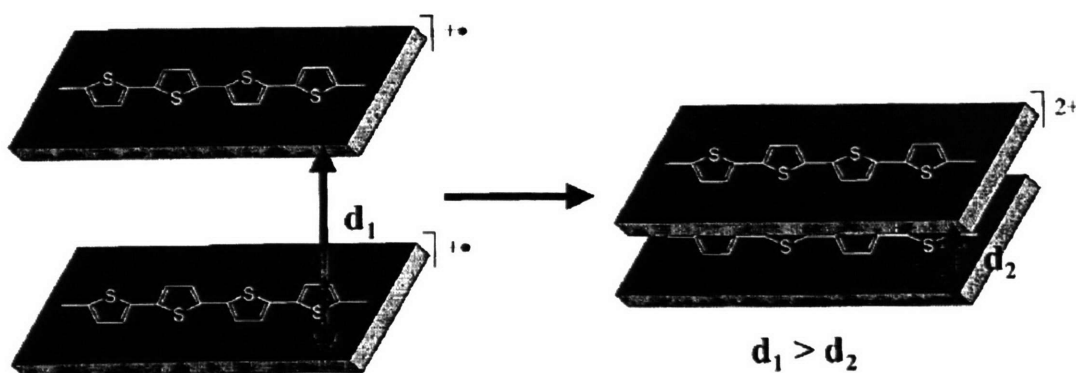
(60) Provisional application No. 60/365,889, filed on Mar. 20, 2002.

Publication Classification(51) **Int. Cl.⁷ H01B 1/00**(52) **U.S. Cl. 252/500**(76) Inventors: **Patrick A. Anquetil**, Boston, MA (US); **Ian W. Hunter**, Lincoln, MA (US); **John D. Madden**, Vancouver (CA); **Peter G. Madden**, Somerville, MA (US); **Anthony E. Pullen**, Belmont, MA (US); **Timothy M. Swager**, Newton, MA (US); **Bing Xu**, Hong Kong (HK); **Hsiao-hua Yu**, Cambridge, MA (US)**ABSTRACT**

The synthesis of thiophene based conducting polymer molecular actuators, exhibiting electrically triggered molecular conformational transitions is reported. Actuation is believed to be the result of conformational rearrangement of the polymer backbone at the molecular level, not simply ion intercalation in the bulk polymer chain upon electrochemical activation. Molecular actuation results from π - π stacking of thiophene oligomers upon oxidation, producing a reversible molecular displacement that leads to surprising material properties, such as electrically controllable porosity and large strains. The existence of active molecular conformational changes is supported by in situ electrochemical data. Single molecule techniques have been used to characterize the molecular actuators.

Correspondence Address:

FOLEY HOAG, LLP
PATENT GROUP, WORLD TRADE CENTER
WEST
155 SEAPORT BLVD
BOSTON, MA 02110 (US)

(21) Appl. No.: **10/392,354**(22) Filed: **Mar. 19, 2003**

10.3.4 Theses Co-Supervised

June 2004 - Angela Chen, “Synthesis and Characterization of Conducting Polymer Fibers”, MIT Bachelor Thesis

June 2004 - Terry Gaige, “Development of a Polypyrrole Continuous Deposition Apparatus” MIT Bachelor Thesis

April 2004 - Nick Powley, “Design of an in-situ EPR Device”, MIT Bachelor Thesis

June 2003 - Bryan Schmid, “Device Design and Mechanical Modeling of Conducting Polymer Actuators”, MIT Bachelor Thesis.

Aug. 2002 - Marie-Eve Aubin, “Nanofabrication and Self-Assembly Techniques Towards Characterizing Single Molecule Conducting Polymer Actuators”, MIT/Ecole Polytechnique de Paris Scientific Traineeship. Awarded a special distinction prize by Polytechnique’s dean of academic affairs.

July 2002 - Reed Oshel, “Characterization of Conducting Polymer Actuators utilizing Novel Ionic Liquids”, MIT Center for Materials Science & Engineering Summer Internship Thesis.

June 2002 - Derek Rinderknecht, “Development of a Dynamic Mechanical Analyzer Instrument for Active Conducting Polymer Actuator Characterization”, MIT Bachelor Thesis.

Aug. 2001 - Rachel Pytel, “Synthesis and Characterization of Conducting Polymer Composites”, MIT Center for Materials Science & Engineering Summer Internship Thesis.

10.3.5 Press Coverage

Wired Magazine, “Plastic on Steroids”, Issue 12.03, March **2004**. Available online at: <http://www.wired.com/wired/archive/12.03/start.html?pg=13>

Women’s Wear Daily (Supplement), Gilbert D., “Putting the tech into textile”. June **2003**

MIT Technology Review, “Super Soldiers”, October **2002**. Available online at: <http://www.technologyreview.com/articles/talbot1002.asp>

MIT Technology Review, “Artificial Muscles Gain Strength”, February **2002**. Available online at: <http://www.technologyreview.com/articles/cameron021502.asp>

10.4 References

Hunter I.W. and Lafontaine S., "A Comparison of Muscle with Artificial Actuators", *Technical Digest IEEE Solid State Sensors and Actuators Workshop*, pp. 178-185, (1992).

Madden J.D., Vandesteeg N., Anquetil P.A., Madden P.G., Takshi A, Pytel R., Lafontaine S.R., Wieringa P.A. and Hunter I.W., "Artificial Muscle Technology: Physical Principles and Naval Prospects", *to appear in IEEE Journal of Ocean Engineering*, (2004).

Pytel R.Z., *Private Communication, MIT BioInstrumentation Laboratory*, (2004 Sep 30).

Appendix A

Nature's Energy Sources and Methods of Manufacturing

A.1 Sources of Energy for Nature's Molecular Motors

Protein-based molecular machines are powered by chemical sources of energy such as Glucose and ATP and also by other energy sources such as light or pH/ion gradients [Mao C. et al. 1999]. At the heart of a biological motor is an allosteric pocket whose properties are comparable those of enzymes [Vale R.D. and Milligan R.A. 2000]. Motor proteins are often powered by use of the adenosine triphosphate (ATP) molecule. To achieve molecular motion, a phosphorylation reaction takes place, breaking one phosphate bond (from the ATP molecule forming adenosine diphosphate (ADP)) [Lundstrom I and Svensson S 2002]. The phosphorylated protein then exhibits a change in its molecular conformation as described by:



Such Phosphorylation typically occurs on the following amino acid residues of the “actuated” protein: serine, threonine and tyrosine. Energy is converted from Glucose to ATP, by the mitochondrion. During the molecular actuation, the high-energy density

molecule ATP is being hydrolyzed, directly transforming the released energy into movement. It is interesting to note that nature does not break the three phosphate bonds of ATP but only uses one, thus reducing the barrier of re-formation of ATP from ADP by the ATP synthase.

Nature uses widely ion gradients as source of energy. The ion pump, for example, which pushes electrically charged molecules through a cell membrane, stores energy by rectification. Ions naturally flow from higher to lower electrochemical potential. These pumps drive ions in the opposite direction, maintaining the electrochemical gradients necessary for cell survival [Astumian R.D. 2001].

Another interesting and counterintuitive view of energy driving molecular motors is also proposed by Astunian who argues that in molecular motors, energy is used to cause a cessation of motion as these motors are typically subject to thermal and quantum fluctuations [Astumian R.D. 2001]. An energy input restrains motion. Protein motors convert chemical energy into mechanical work with almost 100% efficiency. For example the efficiency of ions naturally flowing from higher to lower concentration is almost 100%. An ion channel acts as a biological rectifier, allowing electric currents to flow only in one direction. Larger ions move at lower speed than small ions.

An interesting family of molecular motors that uses diffusion as a mean of achieving molecular motion are brownian motors. Their behavior has been easily described by the Einstein relation for diffusivity of a spherical particle of radius R in a liquid of viscosity μ which is [Presson B.N.J. 1998]:

$$\langle x^2 \rangle = \frac{1}{\pi} \frac{k_B T}{R \mu} t, \quad (\text{A.2})$$

where $\langle x^2 \rangle$ is the particule's average displacement, T temperature and t the diffusion time constant. For example: Let R be 5 nm, and $\mu = 10^{-3}$ Pa·s (viscosity of water at room temperature), then the diffusion time for a molecular machine to make a displacement of 10 nm becomes $t \sim 10^{-6}$ s, which is very fast.

The maximal force that such a molecular motor can exert is the so called Einstein Force [Koza Z. 2002] :

$$F_E = 2 \frac{k_B T}{D} N, \quad (\text{A.3})$$

where N is the number of distinct internal states, D the segment length of a single step achieved by the molecular motor, and T the temperature. This Einstein force is the lower bound for the force that is exerted by the molecular motor. It is based on the assumption that a molecular motor can be modeled as diffusion of a particle in a one-dimensional lattice with periodic and asymmetric transition rates, where the lattice nodes represent different internal states and locations of the molecular motor's units.

For example, a 2 state molecular motor at generating a displacement of 10 nm at room temperature would produce at least a force of 1.62 pN.

A.2 Nature's Methods of Manufacturing

Rather than separately manufacturing and assembling parts to create devices Nature grows living systems by a 3D cofabrication process. Subsystems for sensing, movement, computation, energy storage, and energy delivery are constructed from four basic organic materials: fatty acids, sugars or carbohydrates, amino acids, and nucleotides. These subsystems are cofabricated at the same place during development from embryo through to adulthood. As a result Nature's biological systems demonstrate an incredible diversity, sophistication, and range of abilities that engineers have yet to emulate.

Another wonderful attribute of biological systems is self replication. A very central concept during replication is the use of a copy of DNA: mRNA (messenger RNA) which passes the protein's blueprint to the ribosomes (the protein assemblers) [Whitesides G.M. 2001].

Manufacturing / 3D cofabrication in cells follows a three-fold strategy:

- Polymerization: This is performed by the ribosomes, creating a long chain of amino acids (out of a library of 20 amino acids available).

- Spontaneous folding of the amino acids into 3-dimensional structures. These form complex structures that assemble into a composition of three main structures: alpha-helices, beta-sheets and linkage elements.
- Co-fabrication by means of massively parallel manufacturing. Notice that biology utilizes a linear, planar assembly strategy that then creates a 3D structure by spontaneous folding. The protein description is similar to linear code.

A.3 References

Astumian R.D., "Making Molecules into Motors", *Scientific American*, pp. 57-64, (July 2001).

Koza Z., "Maximal Forces Exerted by a Molecular Motor", *Physical Review E*, Vol. 65, (2002).

Lundstrom I. and Svensson S., "Natural Nanosystems", *Current Applied Physics*, Vol. 2, pp. 17-21, (2002).

Mao C., Sun W., Shen Z. and Seeman N., "A Nanomechanical Device Based on B-Z Transition of DNA", *Nature*, Vol. 397, pp. 144-146, (1999).

Presson B.N.J., "Sliding Friction, Physical Principles and Applications", *Springer Verlag*, Vol. ISSN 1434 4904, (1998).

Vale R.D. and Milligan R.A., "The Way Things Move: Looking Under the Hood of Molecular Motor Proteins", *Science*, Vol. 288, pp. 88-95, (2000).

Whitesides G.M., "The Once and Future Nanomachine", *Scientific American*, (Sept. 2001).

Appendix B

Theoretical Performance Estimation of poly(calix[4]arene *bis*-bithiophene)

From quantum mechanical calculations the energy for pi-pi stacking per mole of quarterthiophene molecule is 3.6 kcal/mole. It is assumed in this calculation that the pi-pi stacking energy for calix[4]arene bis-bithiophene will be the same as for the quarterthiophene molecule. As the energy to change the passive conformation of the calixarene ring is not taken into account, this energy value is thus assumed to be an upper bound of the pi-pi stacking energy of calix[4]arene bis-bithiophene.

$$E_{\text{pi_stacking}} := 3.6 \cdot 10^3 \frac{\text{cal}}{\text{mol}} \quad E_{\text{pi_stacking}} := 4.18 \cdot E_{\text{pi_stacking}} \cdot \frac{\text{J}}{\text{mol}}$$

$$E_{\text{pi_stacking}} = 1.5 \times 10^4 \frac{\text{kg m}^2}{\text{s}^2 \text{mol}} \quad \text{J per mole of Calix[4]arene bithiophene molecule}$$

$$\text{Avogadro Constant:} \quad NA := 6.022136710^{23} \cdot \text{mol}^{-1}$$

Pi-pi stacking energy for one molecule of Calix[4]arene bisquarterthiophene:

$$E_{\text{one_molecule}} := \frac{E_{\text{pi_stacking}}}{NA}$$

$$E_{\text{one_molecule}} = 2.5 \times 10^{-20} \text{ J}$$

Displacement achieved upon pi-stacking by the CalixBQT:

$$D_{\text{one_molecule}} := 3.15 \cdot 10^{-9} \cdot \text{m} - 0.34 \cdot 10^{-9} \cdot \text{m} \quad D_{\text{one_molecule}} = 2.81 \times 10^{-9} \text{ m} \\ (2.8 \text{ nm})$$

$$\text{Strain_contraction} := \frac{D_{\text{one_molecule}}}{3.15 \cdot 10^{-9} \cdot \text{m}} \quad \text{Strain_contraction} = 0.89$$

$$\text{Strain_expansion} := \frac{D_{\text{one_molecule}}}{0.4 \cdot 10^{-9} \cdot \text{m}} \quad \text{Strain_expansion} = 7.02$$

Force generated by one molecule of calix[4]arene bisbithiophene

$$F_{\text{one_molecule}} := \frac{E_{\text{one_molecule}}}{D_{\text{one_molecule}}} \quad F_{\text{one_molecule}} = 8.89 \times 10^{-12} \text{ N} \\ 8.9 \text{ pN}$$

Calculation of active stress

Assume density for the poly(calixBQT) film is same as polypyrrole:

$$d_{\text{calix}} := 1400 \cdot 10^3 \cdot \frac{\text{g}}{\text{m}^3}$$

Molecular mass of the Calix[4]arene bisbithiophene monomer $M_{\text{CalixBBT}} := 781.04 \frac{\text{g}}{\text{mol}}$

However as energy of pi-pi stacking is calculated for quarterthiophene rods, we have to add two bithiophenes to the total molecular mass of calixBBT to form calixBQT

$$M_{\text{CalixBQT}} := M_{\text{CalixBBT}} + 2 \cdot \left(166.27 \frac{\text{g}}{\text{mol}} - 2 \frac{\text{g}}{\text{mol}} \right) \rightarrow 1109.58 \frac{\text{g}}{\text{mol}}$$

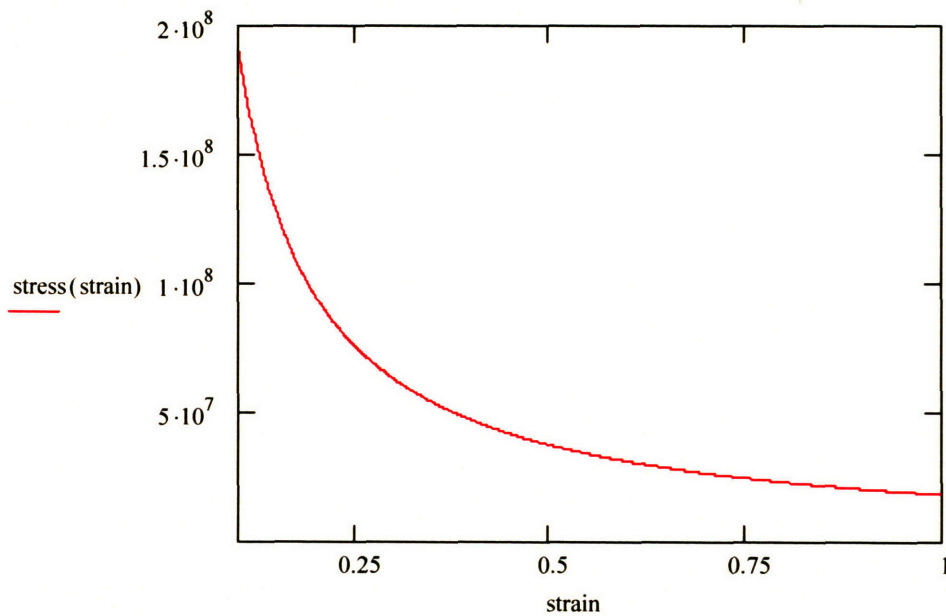
$$\text{mol_density} := \frac{d_{\text{calix}}}{M_{\text{CalixBQT}}} \quad \text{mol_density} = 1.26 \times 10^3 \frac{\text{mol}}{\text{m}^3}$$

Work per unit volume is stress * strain

$$\text{work_per_unit_volume} := E_{\pi\text{-stacking}} \cdot \text{mol_density} \quad \text{work_per_unit_volume} = 1.9 \times 10^7 \text{ Pa}$$

(J per mol * mol per m³)

$$\text{stress}(\text{strain}) := \frac{\text{work_per_unit_volume}}{\text{strain}}$$



For example let's assume a 20% contraction strain := 0.2

stress (strain) = 9.49×10^7 Pa	95 MPa
---	--------

Calculation of electrical to mechanical efficiency

$$\Delta V := 0.5 \text{ V} \quad e := 1.6021773310^{-19} \cdot \text{C}$$

$$N_{\text{electrons}} := 1$$

Input energy to contact calixBQT: $E_{\text{in}} := \Delta V \cdot N_{\text{electrons}} \cdot e$

$$E_{\text{in}} = 8.01 \times 10^{-20} \text{ J}$$

$$\text{Efficiency} := \frac{E_{\text{one molecule}}}{E_{\text{in}}}$$

Efficiency = 0.31	31 % efficiency
-------------------	-----------------

Appendix C

iLabNoteBook: A Digital Laboratory

Notebook

Part of the experimental work of this thesis was documented using the iLabNoteBook digital laboratory notebook. A brief overview of the iLabNoteBook is offered in the next pages¹. The concept of the iLabNoteBook was created by Patrick Anquetil, extending an original idea of Ian Hunter. It evolved into a project supported in part by the MIT-Microsoft iCampus alliance for which Patrick Anquetil secured the funds. Andrew Taberner and Rachel Pytel used the iLabNoteBook extensively and added novel practical thoughts to the original idea.

¹ Conference paper presented at the International Conference on Computers and Advanced Technology in Education, Kauai, Hawaii USA, August 16-18, 2004.

iLabNoteBook: A Digital Laboratory Notebook Based on the Microsoft Tablet PC Platform

Patrick A. Anquetil, Rachel Z. Pytel, Andrew Taberner and Ian W. Hunter
BioInstrumentation Laboratory, Department of Mechanical Engineering
Massachusetts Institute of Technology
77 Massachusetts Avenue, Room 3-147
Cambridge, MA 02139, U.S.A.
bioinstrumentation.mit.edu
patanq@mit.edu*, hzimet@mit.edu, taberner@mit.edu, ihunter@mit.edu

Abstract *

The iLabNoteBook is an experiment at the MIT BioInstrumentation Laboratory in which we attempt to replace traditional laboratory notebooks with Windows XP powered Tablet PCs. This new computing platform offers a multimedia environment for scientists and students to document their work and conduct scientific research. The virtual laboratory notebook empowers researchers not only to record experimental procedures digitally but also to add multiple data-format content to a lab notebook page. In addition these electronic notebooks can be easily searched, backed-up, transported and shared amongst colleagues worldwide. Evaluation of this technology was conducted for a one year period among fourteen scientists at MIT.

Key Words

Digital laboratory notebook, Tablet PC, multimedia

1. Introduction

Laboratory researchers must keep daily records of their experiments for intellectual property and preservation of knowledge purposes in a so called lab notebook. Such a lab notebook contains, for example, descriptions of experimental setups experimental data, chemical formulas, recipes, thoughts and ideas. It must contain all the information a fellow colleague would need to reproduce the documented experiments. In addition, these notes have a high value for the laboratory as they are the official record of its entire knowledge base.

Lab notebooks usually come in the form of bound paper books with a major limitation: their content is static and not adapted to the digital environment seen in a modern laboratory. Many scientific instruments are designed to produce digital output and are typically controlled by a computer, outputting data at rates sometimes exceeding

1 Gbits/s. Meanwhile, most laboratories around the world use paper-based laboratory notebooks to record details about experiments with these instruments. This irony goes even further when multimedia files such as graphs, pictures, videos and sound are to be added to the documentation. These multimedia formats are indeed readily available in a digital format, but must be printed out and manually attached to a traditional paper lab notebook. In addition, the use of email and the internet allow researchers from all over the world to communicate cheaply and easily. However, this communication is hindered when the topic of discussion (the scientific data) is not in a format that is easily searchable or shareable via computer. There is a sense in which the laboratory notebook needs to evolve and adapt to the effectiveness of the digital world [1]. Many companies, including Pfizer [2], Infinity Pharmaceuticals [3], Incyte [4], Quest International [5] and Dow AgroSciences LLC [6] have adopted a method to keep electronic scientific records [7], [8], [9]. This paper presents an experiment at MIT's multidisciplinary BioInstrumentation Laboratory which takes this concept even further, by using Tablet PCs as digital laboratory notebooks. Tablet PCs offer advantages over desktop or laptop computers in the area of scientific documentation in that researchers can input data or sketches with a pen the same way they do on paper. They get the benefits of a computerized notebook (ease of data collection and manipulation) as well those of the paper notebook (ease of data entry).

2. Requirements for the iLabNoteBook

A lab notebook typically contains descriptions of an experimental setup, experimental data, chemical formulas, recipes, calculations, graphs, and pictures, in addition to the researcher's thoughts on his experiment and results. In the past, most of the content of these laboratory notebooks were handwritten notes. Today, with the increasing adoption of digital technology, up to 80 % of a laboratory notebook may be made from pasted printouts

* To whom communication should be addressed

from computer outputs (e.g. graphs, pictures, data, etc...) [10], and researchers may spend over 20% of their time printing, cutting, pasting and transcribing results into their paper lab notebooks [9]. The purpose of the iLabNoteBook project is to evaluate a more efficient way to incorporate computer-generated information into a scientist's lab notebook. Listed below are a few key requirements for a digital laboratory notebook to be successful.

- A platform must be available for instant note taking while an experiment is being conducted
- This platform must be flexible and robust in inputting handwritten notes, text, numbers and formulas
- The tablet must be useful for performing symbolic and analytical calculations
- The platform must allow the researcher to manipulate and display of all types of experimental data, including multimedia files
- The entries must be searchable and exchangeable
- Handwritten input must be recognized and converted to text
- The platform must be able to communicate with scientific instruments, cameras, intra and internet
- The entries must be secure: they are date stamped, they are not changeable or erasable
- The platform must be programmable
- The platform should have voice to text capabilities (dictation of experimental notes) and voice recognition of commands (voice control of experiments)

In summary, we see the dynamic digital notebook as the cornerstone of the digital lab in that it enables researchers to:

- Retrieve information easily (search old entries, journal articles, the internet, etc)
- Record experimental data directly into a notebook page
- Output experimental documentation rapidly (easily create reports and publications)
- Securely archive experimental data, notes and other documentation
- Share information with colleagues

3. The Tablet PC as the iLabNoteBook platform

Tablet PCs emerged as a viable personal computing platform in the second half of 2003. A tablet PC is about the size and weight of a small laptop, but the method of input is via a stylus and not via the classical keyboard. The user writes on the screen with the stylus in the same manner as he would with pencil on paper, and can additionally use the stylus as a replacement for a mouse. The Tablet PC typically comes as a slate-like unit meant to be used flat on a desk or on one's lap like a legal pad.

(Note that some models are convertible between classical laptop and slate Tablet PC). The Tablet PC is a fully independent portable computer, with a computing power comparable to a traditional laptop.

For the iLabNoteBook experiment, it was important to us to select a Tablet PC that would feel like a notebook, not a laptop. We chose a slate-like unit: the Motion M1200 from Motion Computing [11]. This unit comprises a Pentium III processor (800 MHz), 1 GB of RAM, a 60 GB Hard Drive, a 1024 x 728 screen, FireWire, USB 1.1 and PCMCIA connections, build-in Ethernet and Wireless (Wi-Fi) adapters (Figure 1). The Motion M1200 is a pure slate that weighs only 1.51 kg. An additional keyboard can be connected to the unit via the USB port but does not attach to the computer like a laptop. This computing platform allowed us to implement the requirements of the iLabNoteBook project listed in section 2.

The Tablet PC runs a special version of the Microsoft Windows XP operating system, allowing the system to capture and recognize handwritten notes. Handwritten text can either be entered directly into applications such as MS Office (Word, PowerPoint, etc...) and MS Journal (a special application bundled with the Tablet PC that is optimized to recognize handwritten notes) or with a software utility called the Tablet Input Panel that automatically converts handwritten notes into computer text. There are a few commercially available software programs that allow you to create a digital laboratory notebook, such as the CambridgeSoft E-Notebook [12], and the GenSys Electronic Laboratory Notebook [13]. However, these programs are specifically designed for chemistry and not designed to receive handwritten input, so they were not used evaluated as part of this project. Due to the interdisciplinary nature of the BioInstrumentation lab, we needed a more flexible note-taking platform. Other interdisciplinary labs that have moved towards digital laboratory notebooks, such as the Environmental Molecular Sciences Laboratory at Pacific Northwest National Laboratory, have designed their notebook software themselves [14], [15], [16].

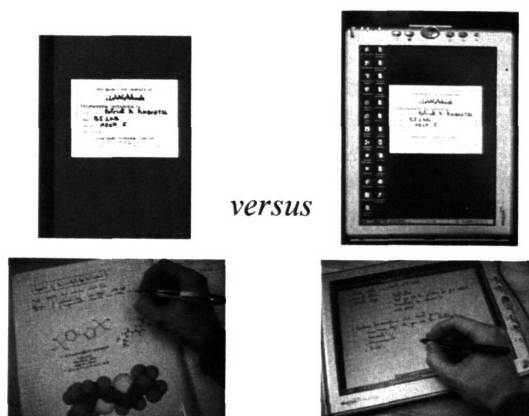


Figure 1: Analog versus Digital Laboratory notebook interface.

4. The iLabNoteBook Experiment

The vision for the iLabNoteBook project was to have students and researchers at various levels in their career use Tablet PCs as a dynamic digital laboratory notebook. Over the course of one year, fourteen researchers from the MIT BioInstrumentation Laboratory were given a Tablet PC with the requirement to use it exclusively for one month minimum to assist them in documenting their experiments digitally. Individuals varied across the seniority rank of our laboratory (from undergraduate students to the head of the laboratory) and across disciplines (mechanical engineering, materials science, chemistry, physics and biology). Usage and usability of the Tablet PC as a digital laboratory notebook was assessed on a weekly basis via a survey posted on a shared team website implemented with Microsoft SharePoint Technology [17]. This technology allows a group to create, build and manage a collaborative website in a very short amount of time (~ 30 minutes). In this environment, team members could the easily share documents, create surveys, and start discussions. It was also used as a repository for laboratory notebooks to be archived and shared amongst colleagues. The website also has a public-accessible section implemented in Microsoft SharePoint technology which serves the purpose of sharing our experience with digital laboratory notebooks with the scientific community. A screenshot of the iLabNoteBook website is presented in Figure 2 and is accessible at www.ilabnotebook.com.

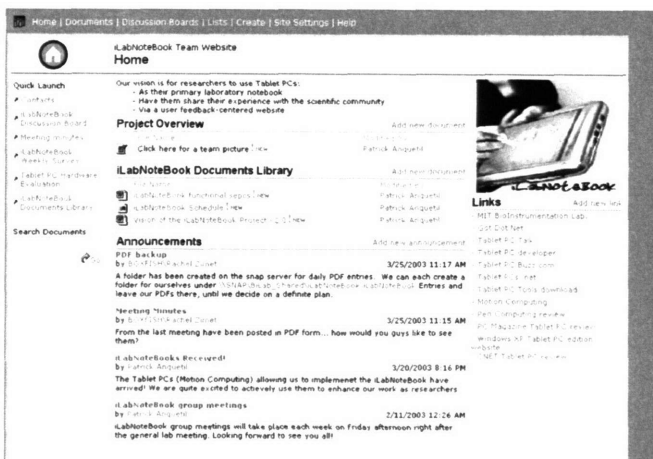


Figure 2: Screenshot of the collaborative iLabNoteBook Team website established in Microsoft Sharepoint technologies (www.ilabnotebook.com)

5. Strategies to migrate towards an electronic lab notebook

One of the difficulties in implementing a digital laboratory notebook is finding software suited for use in conjunction with the pen-input environment. For notebook entries, Microsoft Journal, Microsoft Word, and Microsoft OneNote were evaluated. In addition, typical

scientific, engineering and productivity software packages such as MathCAD, Matlab, Chemdraw, SolidEdge CAD environment, Microsoft Excel and Adobe Acrobat were used to record and analyze data. Connection to scientific instruments was made via the Agilent T&M Toolkit [18] allowing a USB to IEEE 488 computer to instrument connection. Instruments were then controlled via an interface programmed in Microsoft Visual Studio .NET [19]. For example, Figure 3 shows the iLabNoteBook tablet PC controlling three scientific instruments. Data is inserted directly into an MS Word lab notebook page via the Agilent IntuiLink connectivity.



Figure 3: Scientific instruments controlled by tablet PC (from top to bottom: Agilent 34401A Digital Multimeter, Agilent 34970A Data Acquisition Switch with 34901A multiplexer card, and Agilent E3631A Power Supply).

Much of the initial notebook testing was done using Microsoft Journal. This program accepts input in virtual ink via the stylus, and “felt like” a paper notebook. The Journal application can also turn handwritten notes into computer text, which can be very easily searched and exported to other applications. Microsoft journal was very easy to learn and excellent for handwritten notes, but it was disappointing overall because it was not easily interfaced with multimedia and OLE content.

Microsoft Word offers better compatibility with the applications used in scientific experiments. Handwritten entries in virtual ink (similar to MS Journal) can be made, but they cannot be searched or converted to text. A typical electronic laboratory notebook entry in Microsoft Word is shown in Figure 4.

Microsoft OneNote is a new program that acts as a repository for daily notes. It accepts pen as well as text input, and can add pictures and sounds to a notebook page. Entries are organized in virtual folders-tabs similar

to a real paper notebook. Although the interface is optimized for note taking, OneNote fails to produce high quality documents. In addition, OneNote, much like Microsoft Journal, is not a wide-spread format that can be read by any computer platform.

As a result, MS Word was primarily used to implement laboratory notebook pages. While this program is not optimized to implement a real laboratory notebook page, it is a wide spread standard in document authoring and it can handle dynamic as well as OLE content.

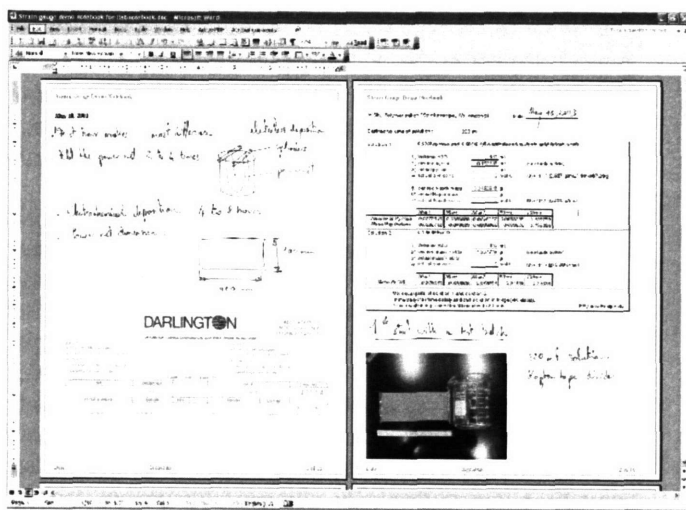


Figure 4: Template and laboratory notebook page created in Microsoft Word. Notice the multiple data types: ink, scanned picture, digital picture, and dynamic Excel worksheet.

Of great concern during the implementation of the iLabNoteBook project was the legal relevance of the digital notebook pages. Below are the strategies that were used to make sure iLabNoteBook entries agree with common legal practices of U.S. and International Patent Law:

- Save the document as a “read only” or as an adobe acrobat PDF file with a date stamp every night, such that priority of patent claims can be established.
- Print and sign the laboratory notebook documents every night.

While several chemical companies keep digital laboratory records, there is little legal precedent for electronic record keeping. Because of the uncertainty behind defending one’s IP rights with electronic records, many companies protect their knowledge by printing hard copies of their data every night [7].

6. Result of the iLabNoteBook experiment

The iLabNoteBook project received an enthusiastic adoption mainly due to its high degree of portability, and

the ability to enter pen-based inputs (annotations of existing digital media or the creation of new hand drawn sketches or notes). The iLabNoteBook concept implemented with Tablet PCs succeeded admirably here. Reasons for praise included:

- Ability to acquire data directly into the lab notebook.
- Ability to search data according to a given criteria.
- Ability to read scientific papers available online, annotate them and link them to a particular notebook daily entry.
- Large hard drive storage space, where data, manuals and notebook archives could be easily stored and transported.
- Concept of the “open lab notebook” where a given lab notebook entry/experiment be easily shared with a colleague world wide.

Figure 5 shows the overall results of our study. Criteria of grade were overall satisfaction with the iLabNotebook as a replacement for a paper lab notebook, satisfaction with hardware and software, ease of use, and quality of handwriting and speech recognition.

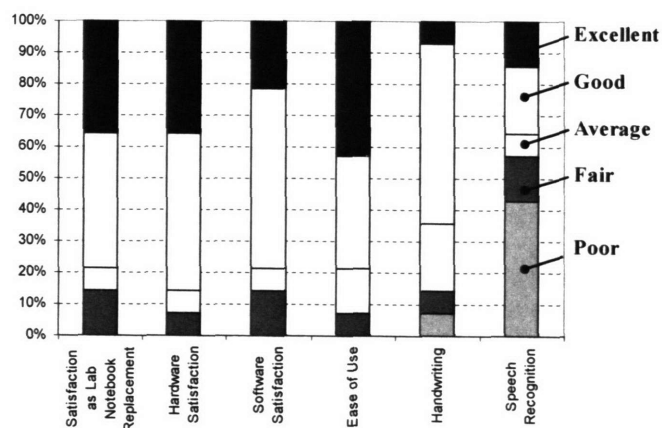


Figure 5: Compiled results of the iLabNoteBook experiment conducted with fourteen scientific researchers

In order to offer more functionality than a simple paper notebook, the iLabNoteBook needs to address the following limitations:

- It is still difficult to keep track of documents and see a clear overview of the notebook database. The chronological order of the documents (when they were created) is difficult to track. One can become quickly overwhelmed once the notebook writings grow to a certain size. This problem could in part be addressed by increasing the size and resolution of the Tablet PC screen and creating a smart folder structure.
- There is not a good way to search through visual information or scroll through notes. The brain has a much easier time finding visual information while flipping through a book than a computer does.

- It is hard to open several notebooks at the same time and lay them side by side. To prepare a summary report, it is for example easier to print out the pages and disperse them on one's desk.
- The input and interpretation of mathematical equations by computers is still at an early stage, although a company called xThink is developing an application targeting that shortcoming [20]. This is a serious limitation to the use of Tablet PCs in engineering classes [21].
- Researchers were cautious about using an expensive machine in a wet laboratory environment (chemistry or biology bench).
- The handwriting recognizer does not contain enough words for particular disciplines (for example, the chemists must be able to input the names of chemicals and not have the handwriting-to-text feature alter them).

Most of these concerns deal with the Tablet PC replacing paper altogether, while it is limited by screen size, screen resolution and smart interface. Similarly to the findings of Sellen and Harper [22] it is our belief that although the digital medium of the *iLabNoteBook* presents tremendous advantages, it will complement paper instead of replacing it all together. The *iLabNoteBook* addresses inefficiencies in handling multiple data formats and in manipulating native digital content. It offers a more efficient way to collect and record scientific information while allowing researchers to convert their work to a paper-based medium when needed.

7. Educational Significance

We foresee that the concept of the *iLabNoteBook* will have tremendous impact on both scientific and scholastic note taking, as Pen based computing extends the way many kinds of information are traditionally handled.

Implementation of interactive scientific computing in the classroom is currently being investigated in the 2.671 Instrument and Measurement [23] class taught by Professor Ian W. Hunter, as well as 2.007 Design and Manufacturing [24] class taught by Professor Alex Slocum at MIT. In 2.671, each student is given a notebook computer to use for the entire term. The class notes are MathCAD programs that the students download onto their computers and manipulate along with the lecture. The students then bring their notebooks to the 2.671 labs, collect data directly to the notebooks, and analyze the data using their notes from class. This system, which is also being investigated in other institutions [25], allows students to become comfortable doing both symbolic and numerical calculations on the same instrument they use to do their experiments. Smith et. al. conducted a similar experiment at William Jewell College, by using laptop computers in biology classes. They also found the students benefited from being able to apply the lecture concepts in real-time by using relevant computer programs, as well as the fact that they could

take use their laptops in different labs around campus. To quote Smith: "we were able to take the computers to where the action is, not the other way around" [26].

The *iLabNoteBook* project mirrors this idea of having a "mobile computational facility." The digital lab notebook allows researchers to use the same platform to collect and analyze their data. By having all of his data, data analysis programs and experimental notes on one highly portable machine, the researcher can be very organized and efficient in accessing and evaluating the results of his experiments.

In the 2.007 Design and Manufacturing class, each student is given a Tablet PC to use for the term. The students used the tablets to share ideas and design sketches with each other and experts off-campus. This gave the students the opportunity to receive valuable feedback on their ideas and progress in addition to the support of the class advisors available on campus [27]. The Tablet PC is an especially valuable tool for this use, as it allows students and off-campus experts to communicate very efficiently, but in the form with which they are the most familiar (hand sketches) [28]. In other programs, such as the community planning program at the University of Texas at Austin, it allows the students the portability to digitize and share their sketches and notes even when they are working in remote locations [29]. In fact, software is currently being developed at MIT to convert hand-drawn sketches to precise mechanical designs or simulations [30],[31],[32]. This ability to communicate in one's favorite medium is another advantage of a Tablet PC-based lab notebook. While the students of 2.007 like the tablets because they can quickly jot down design sketches and force diagrams, researchers in other fields might appreciate the ability to easily sketch organic molecules or experimental setups.

8. Conclusion

The *iLabNoteBook* experiment at the MIT BioInstrumentation Laboratory demonstrated a successful adoption of Windows XP powered Tablet PCs to replace traditional laboratory notebooks among fourteen multidisciplinary scientists. These computer-based notebooks empowered researchers not only to record experimental procedures digitally but also to add multiple data-format content to a lab notebook page. In addition the notebook entries could be easily searched, archived, transported and shared amongst colleagues worldwide.

The concept of the *iLabNoteBook* can be easily extended beyond the replacement of the traditional analog lab notebook. We foresee all the tasks required in a typical day of a laboratory researcher or student being united by a single computer that is portable, versatile and transparent to the user. Wireless communication technologies based on the IEEE 802.11 protocol (Wi-Fi) enables high speed communication between other computers and scientific

instruments, creating a truly digital laboratory environment where researchers have access to information from scientific instruments on their desk or in some cases, across the country [33].

In the meantime, however, researchers that wish to switch from a paper lab notebook to a digital one must overcome the challenges of using a new piece of equipment, as well as ensuring their notes are tamper-proof and in adherence with the intellectual property policies of their company or institution. By being aware of the limitations of the iLabNoteBook and prepared to account for them (by printing out your notes and signing them every night to insure their legality, for example), we are confident that many researchers can benefit from the additional functionality an iLabNoteBook offers when compared to a traditional paper notebook.

9. Acknowledgements

The users of the iLabNoteBook contributing to this research: Nicaulas Sabourin, Laura Proctor, Naomi Davidson, Cathy Hogan, Peter Madden, Bryan Crane, Ariel Hermann, Ben Gallup and Mike Garcia-Webb are greatly acknowledged for their enthusiasm and technology adoption.

This work was supported by the iCampus MIT-Microsoft alliance. The authors also thank the officers of iCampus: Hal Abelson, David Mitchell, Becky Bisbee and Paul Oka for their support.

10. References

-
- [1] L. Arnstein, S. Sigurdsson, & B. Franza, Ubiquitous Computing in the Biology Laboratory *Journal of the Association for Laboratory Automation* 6(1) 2001 66-70.
- [2] www.pfizer.com/main.html
- [3] www.ipi.com
- [4] www.incyte.com
- [5] www.questintl.com/home/index_02.html
- [6] www.dowagro.com/homepage/index.htm
- [7] R. Mullin, Learning to share in the lab *Chemical & Engineering News*, 81(43), 2003, 19-24.
- [8] M. B. Hentz, How we set up enterprisewide access to our laboratory notebooks. *Computers in Libraries*, 22(4), 2002, 22-28.
- [9] J. Kemsley, Enabling the 'good old scientific method,' *Chemical & Engineering News*, 81(43), 2003, 20.
- [10] M. Kihlen and M. Waligorski, Electronic lab notebooks – a crossroads is passed, *Drug Discovery Today*, 8(22), 2003, 1007-1009.
- [11] www.motincomputing.com
- [12] products.cambridgesoft.com/family.cfm?FID=7
- [13] www.gensys.com
- [14] J. D. Myers, C. Fox-Dobbs., J. Laird, D. Le, D. Reich, & T. Curtz, Electronic Laboratory Notebooks for Collaborative Research. *Proc. 5th IEEE Workshop on*
-
- Enabling Technologies: Infrastructure for Collaborative Enterprises*, 1996, 47-51.
- [15] J. D. Myers, E. Mendoza, Web-based electronic laboratory notebook developed by Battelle Pacific Northwest Laboratories. *219th American Chemical Society national meeting*, San Francisco, CA. 2001.
- [16] Stember, R. LABTrack: Introducing a legal electronic lab notebook. *221st American Chemical Society national meeting*, San Francisco, CA. 2001.
- [17] www.microsoft.com/sharepoint
- [18] www.agilent.com
- [19] www.microsoft.com
- [20] www.xthink.com/MathJournal.html
- [21] I. W. Hunter, *Thoughts on using tablet PCs in 2.671 classes and labs at MIT*. Personal communication with R. Z. Pytel, 2004.
- [22] A. J. Sellen & R. H. R. Harper, *The myth of the paperless office* (Cambridge, MA: The MIT Press, 2001).
- [23] <http://web.mit.edu/2.671/www/>
- [24] <http://pergatory.mit.edu/2.007/>
- [25] C. Mewhinney, Putting it all together: Using a laptop-based wireless network to integrate technology into both lecture and lab for general and organic chemistry. *225th ACS national meeting*, New Orleans, LA. 2003.
- [26] G. Smith, J. Dilts, P. Gabrielson, D. Heruth, J. Rettig and A. Strautman, *Bioscene*, 25(3), 1999, 11-12.
- [27] A. Slocum, Robot World – Technology infrastructure for project-based learning. Available: <http://icampus.mit.edu/projects/RobotWorld.shtml>. 2004
- [28] A Slocum, *Thoughts on using tablet PCs in 2.007 classes and labs at MIT*. Letter To: R. Z. Pytel. 2004 May.
- [29] A. Foster, Tablets sneak up on laptops *The chronicle of higher education*, 33, 2003.
- [30] T. Hammond, D. Randall, LADDER: a language to describe drawing, display and editing in sketch recognition. *Proc. Of 18th international joint conference on artificial intelligence*. Acapulco, Mexico. 2003.
- [31] Christine, A. and Randall, D. A Framework for Multi-Domain Sketch Recognition. *AAAI Spring symposium on Sketch Understanding*. Palo Alto, CA. 2002.
- [32] Y. Arar, Microsoft looks in the crystal ball, *PC World*, 2003.
- [33] K. Keating, J. D. Myers, J. G. Pelton, R. A. Bair, D. E. Wemmer, & P. D. Ellis, Development and Use of a Virtual NMR Facility. *Journal of Magnetic Resonance*, 143(1), 2000, 172-183.

Appendix D

Electrochemical Deposition Control with a Tablet PC

This program allows one to potential, deposition current and temperature via an interface programmed in Microsoft Visual Studio .NET (www.microsoft.com).

```
Imports Agilent.TMFramework
Imports Agilent.TMFramework.DataAnalysis
Imports Agilent.TMFramework.DataVisualization
Imports Agilent.TMFramework.InstrumentIO

Public Class Form1
    Inherits System.Windows.Forms.Form

    #Region " Windows Form Designer generated code "
    Public Sub New()
        MyBase.New()
        'This call is required by the Windows Form Designer.
        InitializeComponent()
        'Add any initialization after the InitializeComponent() call
    End Sub
    'Form overrides dispose to clean up the component list.

Protected Overloads Overrides Sub Dispose(ByVal disposing As Boolean)
    If disposing Then
        If Not (components Is Nothing) Then
            components.Dispose()
        End If
    End If
    MyBase.Dispose(disposing)
End Sub

    'Required by the Windows Form Designer
    Private components As System.ComponentModel.IContainer
```

```
'NOTE: The following procedure is required by the Windows Form Designer
'It can be modified using the Windows Form Designer.
'Do not modify it using the code editor.
Friend WithEvents Timer As System.Windows.Forms.Timer
Friend WithEvents savebutton As System.Windows.Forms.Button
Friend WithEvents strPath As System.Windows.Forms.TextBox
Friend WithEvents StartBtn As System.Windows.Forms.Button
<System.Diagnostics.DebuggerStepThrough> Private Sub InitializeComponent()
    Me.components = New System.ComponentModel.Container
    Me.Timer = New System.Windows.Forms.Timer(Me.components)
    Me.savebutton = New System.Windows.Forms.Button
    Me.strPath = New System.Windows.Forms.TextBox
    Me.StartBtn = New System.Windows.Forms.Button
    Me.SuspendLayout()
    '
    'Timer
    '
    Me.Timer.Interval = 1000
    '
    'savebutton
    '
    Me.savebutton.BackColor = System.Drawing.SystemColors.Control
    Me.savebutton.ForeColor = System.Drawing.Color.Black
    Me.savebutton.Location = New System.Drawing.Point(368, 232)
    Me.savebutton.Name = "savebutton"
    Me.savebutton.Size = New System.Drawing.Size(128, 23)
    Me.savebutton.TabIndex = 33
    Me.savebutton.Text = "Save"
    '
    'strPath
    '
    Me.strPath.Location = New System.Drawing.Point(16, 232)
    Me.strPath.Name = "strPath"
    Me.strPath.Size = New System.Drawing.Size(344, 20)
    Me.strPath.TabIndex = 32
    Me.strPath.Text = "C:\6 Data\test.m"
    '
    'StartBtn
    '
    Me.StartBtn.Location = New System.Drawing.Point(16, 32)
    Me.StartBtn.Name = "StartBtn"
    Me.StartBtn.Size = New System.Drawing.Size(128, 40)
    Me.StartBtn.TabIndex = 31
    Me.StartBtn.Text = "Start"
    '
    'Form1
    '
    Me.AutoScaleBaseSize = New System.Drawing.Size(5, 13)
    Me.ClientSize = New System.Drawing.Size(504, 286)
    Me.Controls.Add(Me.strPath)
    Me.Controls.Add(Me.StartBtn)
    Me.Controls.Add(Me.savebutton)
    Me.Name = "Form1"
    Me.Text = "Form1"
    Me.ResumeLayout(False)

    End Sub
#End Region

#Region "Globals definitions"
Dim AgilentDAQ As New Agilent.TMFramework.InstrumentIO.DirectIO("GPIB0::9::INSTR", False,
2000)
Dim multimeter As New Agilent.TMFramework.InstrumentIO.DirectIO("GPIB0::22::INSTR",
False, 2000)
Public count As Double
Dim temperature() As Double = New Double(999999) {}
Dim potential() As Double = New Double(999999) {}
Dim current() As Double = New Double(999999) {}
#End Region
```

```

Private Sub Form1_Load(ByVal sender As System.Object, ByVal e As System.EventArgs)
Handles MyBase.Load
    count = 0.0#
    Timer.Enabled = False

End Sub

Private Sub StartBtn_Click(ByVal sender As System.Object, ByVal e As System.EventArgs)
Handles StartBtn.Click
    Timer.Enabled = Not Timer.Enabled
    If (Timer.Enabled = True) Then
        count = 0.0#
        StartBtn.Text = "Click to Stop"
    Else
        StartBtn.Text = "Start"
    End If
End Sub

Private Sub savebutton_Click(ByVal sender As System.Object, ByVal e As System.EventArgs)
Handles savebutton.Click
    FileOpen(1, strPath.Text, OpenMode.Output)
    PrintLine(1, "Created " & System.DateTime.Now.Date.ToLongDateString & " " &
System.DateTime.Now.Date.ToLongTimeString)
    PrintLine(1, " ")
    PrintLine(1, "Time (Sec)", "Pot (V)", "Cur (A)", "Temp (C)")

    Dim x = 0
    For x = 0 To count
        Try
            PrintLine(1, x * Timer.Interval / 1000, potential(x), current(x),
temperature(x))
        Catch
            MsgBox("Alert, invalid input: " & x)
        End Try
    Next
    FileClose(1)
End Sub

Private Sub Timer_Tick(ByVal sender As System.Object, ByVal e As System.EventArgs)
Handles Timer.Tick

    multimeter.WriteLine("MEAS:CURR?")
    AgilentDAQ.WriteLine("MEAS:VOLT? (@107)")
    potential(count) = AgilentDAQ.Read()
    AgilentDAQ.WriteLine("MEAS:TEMP? TC, E, (@101)")
    temperature(count) = AgilentDAQ.Read()
    current(count) = multimeter.Read()
    count = count + 1

End Sub

Private Sub Form1_Close(ByVal sender As System.Object, ByVal e As System.EventArgs)
Handles MyBase.Closed
    Timer.Enabled = False
    AgilentDAQ.Close()
End Sub

Private Sub strPath_TextChanged(ByVal sender As System.Object, ByVal e As
System.EventArgs) Handles strPath.TextChanged

End Sub
End Class

```

Appendix E

Curriculum Vitae

Patrick A. T. ANQUETIL

Address: MIT Room 3-147
77 Massachusetts Avenue
CAMBRIDGE, MA 02139

Phone: +1-617-258-8628
e-mail: patanq@mit.edu
www: <http://bioinstrumentation.mit.edu/Projects/CP/patrick.html>

Nationality: French

GPA: 4.7 / 5.0

EDUCATION

- 1999-2004 **Massachusetts Institute of Technology (MIT), USA.**
Ph.D. in Mechanical Engineering (October 2004), Advisor: Prof. Ian HUNTER, Bio-Instrumentation Lab. Thesis on development and characterization of molecular artificial muscles based on shape changing conducting polymer materials. Minor in Business administration, including classes taken at Harvard Business School.
- 1993-98 **Swiss Federal Institute of Technology Zurich (ETH ZURICH), Switzerland.**
Master's Degree in Mechanical Engineering. Special field of study in Nano-Robotics with a minor in Business Management and Economics. Master's Thesis at Professor Tomomasa SATO's Intelligent Cooperative Systems Laboratory at the University of Tokyo (title: "Development of high resolution force sensors for micromanipulation"), sponsored by the Hubert Kudlich Fund (Switzerland).

PROFESSIONAL EXPERIENCE

- Jan. 99-Present **MIT Bio-Instrumentation Laboratory (MIT), Cambridge MA, USA**
Graduate Research Assistant. Synthesized and characterized of large strain conducting polymer-based molecular muscles. Responsibilities included: supervision and teaching of undergraduate thesis, optical instrumentation, Raman spectroscopy, materials testing instrumentation (AFM, DMA, DSC...etc.), chemistry lab area, computer systems administrator (60+ networked computers, incl. file servers, firewall, Wi-Fi wireless network). Extended experience in writing grants.
- Oct. – Dec. 98 Post Master's **The University of Tokyo, JAPAN**
Awarded a three-month, full scholarship by the Japanese Government, to continue research work on Nanotechnology at Professor Tomomasa SATO's Intelligent Cooperative Systems Laboratory at the Research Center for Advanced Science and Technology (RCAST).
- Mar.-Oct. 98 **ETH Zurich, Student's Computer Center, SWITZERLAND**
System administrator on Windows NT Server and Workstation platform.
- Apr.-July 97 **Institute for Business Management + Institute for Textile Machinery, ETH Zurich, SWITZERLAND**
Conducted a research project on "Profitability of production plant for fabrics with the revolutionary Sulzer weaving machine M8300" under the supervision of Prof. Dr. Urs MEYER.
- Feb.-May 97 **Institute for Technology Management, ETH Zurich, SWITZERLAND**
Performed research on "the role of the Japanese Ministry of International Trade and Industry (MITI) - Japan's way of managing technology at country level" under the supervision of Prof. Dr. Hugo TSCHIRKY.
- Oct.-Feb. 97 **Institute for Robotics (IFR), ETH Zurich, SWITZERLAND**
Conducted a research project at IFR laboratory on "Flexible structures for micropositioning".
- Feb.-April 96 **ABB Flexible Automation AG, Zurich, SWITZERLAND**
Six-week training in Robotics-Engineering. Member of the research team working on the integration of the ABB vision system in a new robot controller, including tests. Elaborated a feasibility study for the structure of ABB robots and developed new solutions. Several recommendations are now being implemented.
- Oct.95-July 96 **Institute for Machine Design (IKB), ETH Zurich, SWITZERLAND**
Conducted research as an undergraduate assistant on the possibility of simultaneous utilization of piezo ceramics as sensor and actuator for active structure control.
- May - July 93 **SULZER AG, Winterthur, SWITZERLAND**
Three-month technical training as part of the ETH undergraduate engineer training scheme.
- August 92 **BARMAG AG, Remscheid-Lennep, GERMANY**
Three-week basic manual training.

FOREIGN LANGUAGES

- French - Mother tongue.
German - Bilingual, gained from living and studying in Germany and in Switzerland for more than six years.
English - Excellent, TOEFL Score: 627 (August 21st, 1998). Living in the U.S. since Jan. 1999.
Japanese - Basic knowledge. Everyday practice during my nine-month stay at The University of Tokyo.

COMPUTER EXPERIENCE

- OS - Windows XP, UNIX, Solaris, Mac OS.
Tools - Microsoft Office, MathCAD, Matlab, Maple, Pro-Engineer, Solid Works, CADAM, ANSYS, Dreamweaver.
Language - Visual Basic, C/C++, C#, Java, Pascal, Modula 2.
Internet - Passionate about information technology. Followed the Internet industry since 1994. Highly interested in the latest development of the WWW and e-commerce. System administrator of the MIT Bio-Instrumentation Lab (60+ networked computers, incl. file servers, firewall, Wi-Fi wireless network), web and graphic designer.

HONORS AND AWARDS

- 2004 - Invited to the MIT-BASF Workshop on Nanotechnology in Ludwigshafen, Germany - declined
2003 - Awarded a \$30,000 grant from the Microsoft / MIT iCampus Alliance for the iLabNoteBook project (www.ilabnotebook.com); an experiment to use tablet PCs as electronic laboratory notebooks.
1998 - Awarded a scholarship from the Japanese government (Mambusho) to pursue post graduate work at the University of Tokyo, Japan.
1997 - Awarded a scholarship from the Hubert Kudlich Fund to study at the University of Tokyo, Japan.
1996 - Winner of the Swiss smartROB championships. An annual competition of mobile robots at ETH Zurich. Leader of the winning team.

EXTRACURRICULAR ACTIVITIES

- Music - Studied solfeggio and flute-playing at Academy of Music Francis Poulenc, Paris for eight years (evening classes). Performed in Symphonic Orchestras.
Sports - Basketball, tennis, squash, roller-skating, mountain biking, skiing, soccer (captain of the MIT Mechanical Engineering Department Team during the Fall 2000 and 2001 season).
General - French gourmet cooking, Connoisseur of vintage wines (especially Bordeaux wines), Arts, literature, photography and the movie industry, Executive Member of the Board of **Rotaract Club Zurich** (1996 – 1998). Elaborated partnership with IWATZ, Swiss Institution for handicapped persons. Focused attention on and motivated Rotaract members to participate in community activities.

SELECTED PUBLICATIONS

1. **Anquetil Patrick A.**, Rinderknecht Derek, Vandesteeg Nathan A., Madden, John D., and Hunter Ian W.; "Large Strain Actuation in Polypyrrole Actuators", *SPIE 11th annual symposium on electroactive materials and structures*, San Diego, CA, USA, **2004** (in press).
2. **Anquetil Patrick A.**, Brenan Colin J., Marcolli Claudia and Hunter Ian W.; "Laser Raman Spectroscopic Analysis of Polymorphic Forms in Microliter Fluid Volumes", *The Journal of Pharmaceutical Sciences*, Vol. 92, Issue 1, **2003**.
3. **Anquetil Patrick A.**, Madden John D., Madden Peter G., Hunter Ian, "Conducting Polymer Molecular Muscles", *New Data & Research In Applications For Nanotechnology and Nanomedicine*, *The Knowledge Foundation*, Royal Sonesta Hotel, Cambridge, MA, **2000**.
4. Published a total of twelve publications in refereed journals and conference proceedings.
5. Supervised ten MIT Undergraduate Theses and seven MIT undergraduate researchers supervised since January 2001.

PATENTS

- Mar. 2003 - **Anquetil Patrick A.**, Hunter Ian W., Madden John D., Madden Peter G., Pullen Anthony E, Swager Timothy M., Yu Hsiao-hua, Xu Bing, "Molecular Actuators", U.S. **Patent pending** (Application No. 10/392,354).

PRESS COVERAGE

- June 2003 - *Women's Wear Daily (Supplement)*, Gilbert D., "Putting the tech into textile".
Feb. 2002 - *MIT Technology Review*, "Artificial Muscles Gain Strength". Available online at: <http://www.technologyreview.com/articles/cameron021502.asp>
Feb. 2002 - *Swiss-up Profile* about my research activities in the U.S. Available in French and German at: http://www.swissup.com/art_content.cfm?upid=FR3220

